ENGINEERING IODOTYROSINE DEIODINASE TOWARDS BIOREMEDIATION OF HALOPHENOLS AND CHARACTERIZATION OF A UNIQUE THERMOPHILIC IODOTYROSINE DEIODINASE FROM *Thermotoga neapolitana*

by
Zuodong Sun

A dissertation submitted to Johns Hopkins University in
conformity with the requirements
for the degree of Doctor of Philosophy

Baltimore, Maryland
October 2019

Abstract

Iodotyrosine deiodinase (IYD) promotes reductive dehalogenation of chloro-, bromo-, and iodotyrosines (Cl-Tyr, Br-Tyr, and I-Tyr, respectively). This activity decreases dramatically for phenolic substrates lacking the zwitterion due to their inability to close an active site lid. Enhancing this activity will provide an attractive approach to bioremediation of halophenols. A combination of computational design with Rosetta, library construction and screening was employed to promote IYD's activity towards 2-iodophenol (2IP, a model for halophenol). The lid sequence of IYD from *Homo sapiens* (HsIYD) was redesigned by a fixed backbone approach to stabilize lid closure in the presence of 2IP. This approach successfully yielded a variant UD08 that moderately improved 2IP deiodination by 4.5-fold compared to HsIYD. UD08 expressed a disorder-to-order transition of the lid induced by 2IP as predicted by Rosetta and verified via limited proteolysis. This resembles the induced lid closure by I-Tyr in HsIYD. IYD from *Haliscomenobacter hydrossis* (HhIYD), as an easy-to-work with alternative to HsIYD, was subsequently redesigned via a fixed backbone approach and a loop remodeling approach to further improve IYD-2IP interactions. Rosetta once again demonstrated stabilization of the targeted enzyme•2IP complex with loop remodeling although an active 2IP deiodinase was not generated from these approaches.

IYD from a thermophilic bacteria *Thermotoga neapolitana* (TnIYD) was characterized for its potential to facilitate engineering and provide a crystal structure of the fully reduced IYD. TnIYD is the smallest iodotyrosine deiodinase characterized to date and therefore represents a minimal structural requirement for reductive dehalogenation. TnIYD exhibits many unique properties different from those of mesophilic IYDs such as the formation of FMN semiquinone during purification and its tight binding of tyrosine (Tyr). The oxidized FMN in crystals of I-Tyr, Tyr, and fluorotyrosine (F-Tyr) bound TnIYD was readily reduced to the FMN semiquinone, but not to the hydroquinone form upon dithionite treatment. High resolution crystal structures of I-Tyr, F-Tyr, and Tyr bound TnIYD with oxidized and semiquinone FMN suggested that no major

conformational changes from the oxidized structure were needed to support the FMN semiquinone and other radical intermediates generated during catalysis. An additional binding site for I-Tyr was identified on the surface of TnIYD and this might explain the substrate inhibition of IYDs observed under steady-state conditions. The reduction of TnIYD and HsIYD by dithionite was inhibited by both I-Tyr and Cl-Tyr and may cause the reduction of IYD to be rate-determining during steady-state catalysis.

Primary Reader and Advisor: Prof. Steven E. Rokita (Department of Chemistry)

Secondary Reader: Prof. Craig A. Townsend (Department of Chemistry)

Prof. Jeffrey J. Gray (Department of Chemical & Biomolecular Engineering)

Acknowledgement

The work presented in this dissertation was only made possible from countless help and support that I have received over the years. I would first like to thank my advisor Prof. Steve Rokita for making me the scientist who I am today by providing indispensable advising from problem solving techniques to English writing skills. He allowed me to explore my own research interest and treated me like a peer rather than a student when it came to experiment design and result analysis. This level of independence that I was able to acquire is of great value towards my long term goal of becoming an independent investigator. He has been an amazing advisor for his civility, his patience, his understanding, and his unconditional support to every one of his students. He will always be a role model for me and my future career.

I would like to thank my committee members Prof. Craig Townsend and Prof. Jeffrey Gray for reading and commenting on my thesis. In addition, I would like to thank them for their help and their recommendation letters for my postdoc application. Many thanks to Prof. Stephen Fried and Prof. Marc Ostermeier for their help with postdoc application as well. In addition, I would like to thank Prof. John Toscano for being in my GBO committee and Prof. Louise Pasternack for all great advises when I first started in the program. Also I really appreciate all the chemistry staff members for their support on research and administrative affairs.

Many of the techniques presented in this dissertation are out of the expertise of our lab and would not be possible without our wonderful collaborators in and outside The Johns Hopkins University. Prof. Jeffrey Gray's insightful course on Rosetta simulation allowed me to access the power of Rosetta as a biochemist without any experience in computational biology. In addition, his lab carried out sophisticated design simulations that are beyond my capabilities. Prof. Jennifer Kavran has offered us tremendous help with her hard work for our protein crystallography, which inspired my great interest in the area. I would also like to acknowledge our new collaborations with Prof. Squire Booker (Pennsylvania State University) on anaerobic crystallography and Prof.

Giovanni Gadda (Georgia State University) on rapid enzyme kinetics. Through these collaborations I have greatly expanded my expertise.

I would like to thank many former Rokita lab members as my mentors. Special thanks to Dr. Shalini Saha and Dr. Nattha Ingavat who helped me the most during my early and later time in the lab. Their skilled and patient demonstrations on lab techniques and always friendly advising are of great value to me. I would also like to thank Dr. Mark Hutchinson, Dr. Jimin Hu, Dr. Arnab Mukherjee, Dr. Blessing Deeyaa, Dr. Abhishek Phatarphekar, and Dr. Petrina Boucher for all the help they offered to me. Many thanks to the current members of the Rokita lab: Danielle Bautista, Shane Byrne, Harry Greenberg, Anton Kozyryev, Daniel Lemen, Ravina Moirangthem, Qi Su, and Bing Xu for their help and support and for the great time we spent together over the years. It is also a great pleasure to work with many talented undergrads and rotation graduate students: Morgan Nance (PMB), Shaun Spisak (CBI), Azam Hussain, and Gregory Berumen. I would like to thank them all for allowing me to have great experiences as a mentor myself.

I would like to thank Prof. Hsin Kuo (British Colombia Institution of Technology) for being a wonderful mentor and friend to me when he was a postdoc in our department. His friendship helped me to pass a really difficult time when I faced a major decision for my career. His kind and easygoing charisma is admired by virtually everyone who interacted with him. Many thanks to my friends Dr. Liwei Zheng and Dr. Rongfeng Li as well for their countless help and fun time.

I would like to thank the late Prof. Justine Roth for her advising of my research during the first two years of my graduate school. She was a passionate and skilled scientist of shrewd minds. Her board knowledge on many different disciplines of science is the most impressive that I have ever seen. Her great contribution to the scientific community will always be remembered.

Last but not the least, I would like to thank my parents for their unconditional love and support. It took great understanding and emotional preparation to send their only child to a foreign country for study. Their love, understanding, and support are indispensable for me to complete my

Ph. D. and explore my dream career path. Many thanks to my other beloved family members: my late grandfather, my grandmother, my aunt and uncle, and my cousins for years of priceless joy and support.

Dedication

To my father Sun, Hongyuan and my mother Liu, Guiping, for their unconditional love and countless support

Table of Contents

List of Tables

Chapter 2:

Chapter 4:

List of Figures

Chapter 1:

Chapter 2:

Chapter 3:

Chapter 4:

Chapter 5:

List of Abbreviations

Pentachlorophenol (PCP)

Iodotyrosine deiodinase (IYD)

Flavin mononucleotide (FMN)

L-Tyrosine, 3-Iodo-L-tyrosine, 3,5-Diiodo-L-tyrosine, 3-Bromo-L-tyrosine, 3-Chloro-L-tyrosine, 3-Fluoro-L-tyrosine (Tyr, I-Tyr, I_2-Tyr, Br-Tyr, Cl-Tyr, F-Tyr, respectively)

2-Iodophenol (2IP)

Oxidized, semiquinone, reduced (hydroquinone) FMN (FMN_{ox}, FMN_{sq}, FMN_{hq}, respectively)

IYDs from *Homo sapiens, Haliscomenobacter hydrossis*, *Mus musculus*, *Drosophila melanogaster*, *Pyrococcus furiosus*, *Thermotoga neapolitana* (HsIYD, HhIYD, MmIYD, DmIYD, PfIYD, TnIYD, respectively)

Solvent accessible area (SASA)

Nα-Benzoyl-DL-arginine 4-nitroanilide hydrochloride (DL-BAPNA)

Rosetta energy unit (REU)

Guided Rosetta design (GD)

Unguided Rosetta design (UD)

Root mean square deviation (RMSD)

Sodium dodecyl sulfate (SDS)-Polyacrylamide gel electrophoresis (SDS-PAGE)

Reduced nicotinamide adenine dinucleotide (phosphate) (NAD(P)H)

Isopropyl thio-β-galactoside (IPTG)

Dithiothreitol (DTT)

Tris(2-carboxyethyl)phosphine (TCEP)

Site directed mutagenesis (SDM)

Site saturation mutagenesis (SSM)

Overlap extension PCR (OEPCR)

Nickel-nitrilotriacetic acid (Ni-NTA)

Chapter 1 Introduction

1.1 Halophenols: pervasive, persist, and toxic:

The wide distribution, persistence, and toxicity of halophenols pose a great threat to the environment and human health. Halophenols such as pentachlorophenol (PCP), bromoxynil, triclosan, and tetrabromobisphenol A are widely used in agriculture and industry as pesticides, wood preservative, herbicides, antimicrobial agents, and flame retardants (Scheme 1-1). The United States import of PCP reached 14 million pounds in 2013 alone.[1] Triclosan, an antimicrobial agents banned in Europe but still used in the United States as a toothpaste additive, is now one of the most commonly detected compounds in the country's water systems.[2] Halophenols are resistant to environmental degradation and bioaccumulate in animal tissues due to their lipophilicity.[3] Bromoxynil could still be detected in the blood of 19.3% tested residents in Saskatchewan, Canada 5 months after the herbicide was applied in the region.[4] Four chlorophenols including PCP are listed as priority pollutants by the United States Environmental Protection Agency and can lead to severe health problems such as cancer, DNA damage, organ damage, or even acute death.[5–7] Structurally similar to endogenous thyroid hormones, the flame retardant tetrabromobisphenol A and polybrominated diphenyl ethers can potentially disrupt thyroid hormone homeostasis via binding and inhibition of corresponding receptors and metabolic enzymes.[8,9] Due to the negative impact of halophenols on the environment and human health, they must be properly detoxified and degraded.

1.2 Bioremediation of halophenols: a look at Nature's toolbox:

Traditional physically and chemically based pollutant remediation procedures such as landfill, soil washing and incineration may generate secondary pollutants such as waste water and toxic gas that require additional effort and cost to dispose. In contrast, bioremediation utilizes microbes and enzymes to detoxify or degrade pollutants and is environmentally friendly since the end product of bioremediation is usually less toxic and more readily degraded to non-hazardous

substances such as carbon dioxide and water.[10,11] Dehalogenation, the cleavage of carbon-halogen bond catalyzed by dehalogenases, is usually the first step towards the biodegradation of halogenated compounds.[12,13] Therefore, the search, design and improvement of dehalogenase activity towards halophenols is essential for the bioremediation of these compounds.

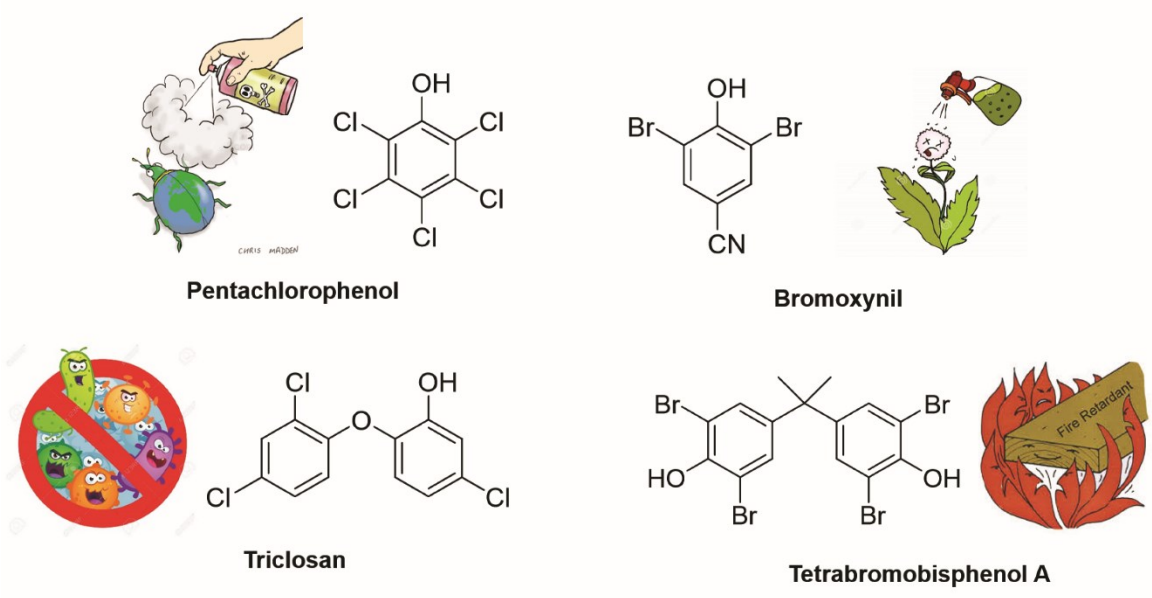

Scheme 1-1 Examples of halophenols. Pentachlorophenol, a pesticide and wood preservative; bromoxynil, an herbicide; triclosan, an antimicrobial agent; tetrabromobisphenol A, a flame retardant.

Nature has developed oxygenation, hydrolysis, and reduction-based strategies for dehalogenation (Scheme 1-2).[14] Oxygenolytic dehalogenases function by substituting the halogen in halogenated phenols with a hydroxyl group derived from molecular oxygen. These enzymes participate in the aerobic degradation of many chlorophenols.[15,16] However, many other halogenated aromatics, more heavily halogenated in particular, resist microbial degradation under aerobic conditions.[12] The requirement of oxygen also make oxygenolytic dehalogenases less suitable for applications in anaerobic environment like aquatic sediment and soil.

Hydrolytic dehalogenases substitute the halogen with a hydroxyl group derived from water. While many halogenated aliphatic compounds such as haloalkanes and haloacids are able to be dehalogenated hydrolytically,[12,17,18] examples of hydrolytic aryl halide dehalogenases are rare.[19,20]

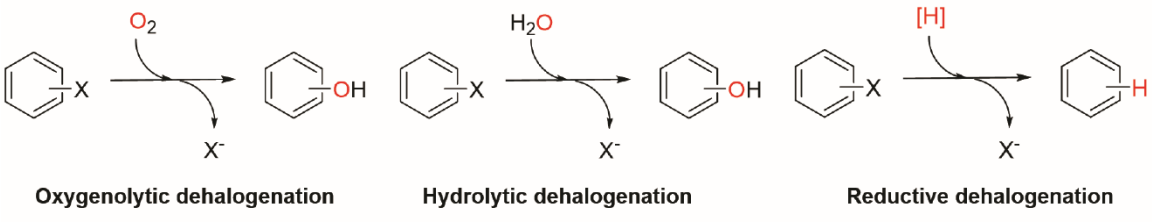

Scheme 1-2 Enzymatic dehalogenation strategies.

Reductive dehalogenases employ a two-electron reduction to substitute halides with hydrogen. An early example of this class is tetrachlorohydroquinone dehalogenase, a key enzyme in the biodegradation pathway of PCP that catalyzes two sequential reductive dechlorination of tetrachlorohydroquinone with glutathione as a cofactor.[21] Recently, dehalogenases participating in halorespiration in anaerobic bacteria have gained attention as they are able to catalyze the reductive dehalogenation of many halogenated aromatics to power cellular respiration.[22] For polyhalogenated aromatics such as polychlorinated biphenyls and hexachlorobenzene, anaerobic reductive dehalogenation is by far the most effective strategy available for their biodegradation.[12] However, dehalogenases responsible for anaerobic reductive dehalogenation are typically cobalamin and iron-sulfur cluster dependent and are therefore extremely oxygen sensitive. Despite that one oxygen tolerant example of this class was recently reported, its application in bioremediation is still hindered by the difficulty of cobalamin incorporation during its heterologous expression.[23] Therefore, an oxygen stable and easy-to-express species is still lacking from this class of reductive dehalogenase.

1.3 Iodotyrosine deiodinase (IYD): a promising candidate for bioremediation:

IYD is a flavin mononucleotide (FMN) dependent enzyme catalyzing the unusual reductive dehalogenation of 3-iodo-L-tyrosine (I-Tyr) and 3,5-diiodo-L-tyrosine (I_2-Tyr). These iodotyrosines are the byproducts of thyroid hormone biosynthesis in vertebrates and their deiodination maintains the iodine homeostasis in these organisms (Scheme 1-3).[24] IYD homologs,

however, are found in all kingdoms of life except for plants. The iodotyrosine deiodinase activity is highly conserved among homologs of IYD from different organisms despite that IYD's physiological function is unknown in organisms that do not require iodine.[25] IYD is able to act under both aerobic and anaerobic conditions and is well-expressed in *Escherichia coli* (*E. coli*). Besides deiodination, IYD also debrominates and dechlorinates 3-bromo-L-tyrosine (Br-Tyr) and 3-chloro-L-tyrosine (Cl-Tyr), respectively.[26–28]

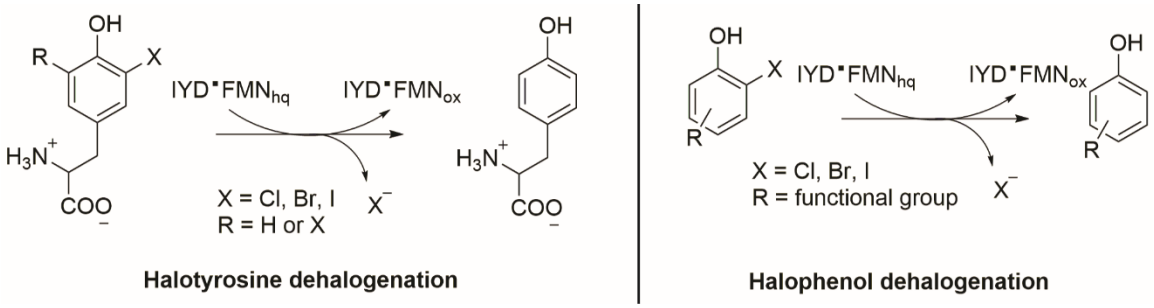

Scheme 1-3 Halotyrosine dehalogenation and proposed halophenol dehalogenation by IYD. FMN_{hq} stands for fully reduced FMN.

IYD is proposed to utilize fully reduced FMN (IYD•FMN_{hq}) to support dehalogention through a two consecutive one-electron transfer process (Figure 1-1).[26] Prior to electron transfer, the phenolic substrate tautomerizes to its keto form and the α-carbon where the halogen is attached is protonated (Step (1) in Figure 1-1). This tautomerization is believed to facilitate reduction of the substrate by switching the electron rich aromatic system to an electrophilic α-haloketone system. Evidence for this includes the nanomolar affinity of the reduced enzyme with pyridone-containing derivatives of tyrosine that mimics the keto form.[29] The α-haloketone intermediate then accepts an electron from FMN_{hq} to form an α-haloketyl radical anion intermediate (Step (2) in Figure 1-1) which subsequently eliminates halide to form a more stable phenoxy radical (Step (3) in Figure 1-1). The enzyme is half-oxidized to a transient FMN semiquinone (IYD•FMN_{sq}) intermediate which then transfers the second electron to the phenoxy radical to produce Tyr as product and oxidized FMN (FMN_{ox}) (Step (4) in Figure 1-1). This dehalogenation scheme resembles the reductive dehalogenation of α-halomethyl ketones through a ketyl anion radical intermediate in the presence

of one electron reductants.[30] The proposed mechanism is further supported by the observation of the FMN_{sq} intermediate when IYD is slowly reduced in the presence of an unreactive substrate analog 3-fluoro-L-tyrosine (F-Tyr).[31]

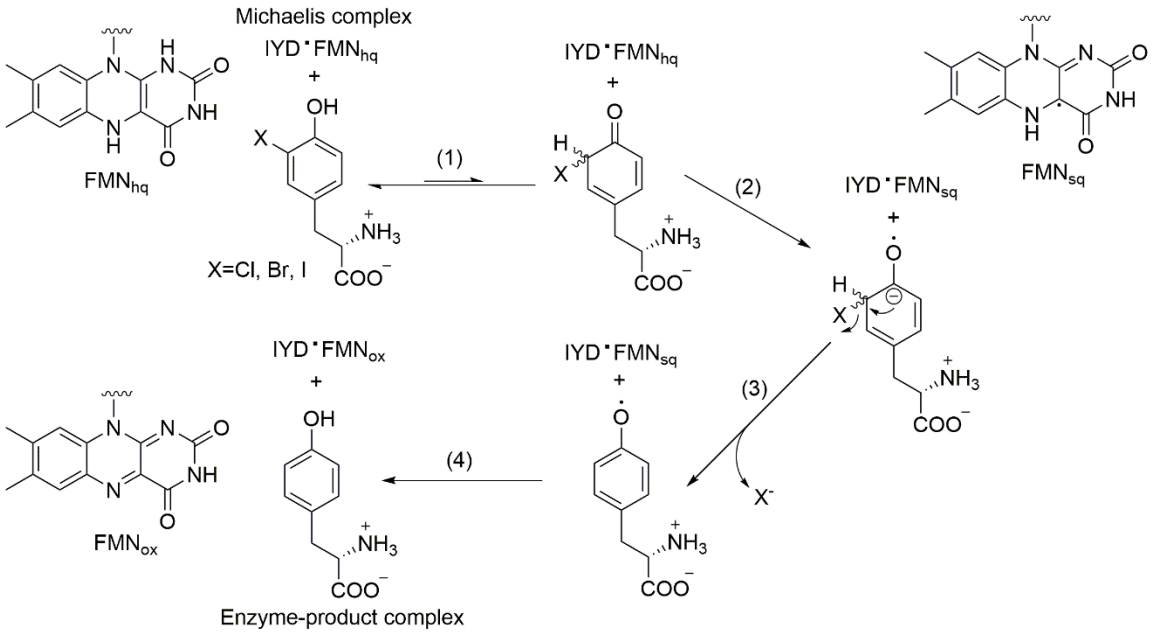

Figure 1-1 Proposed mechanism of IYD dehalogenation.

IYD seems to be a promising candidate for the bioremediation of halophenols (Scheme 1-3), due to the structural similarity between halophenols and its native substrates halotyrosines. However, the activity of native IYD towards halophenols is extremely low compared to that towards halotyrosines. 2-Iodophenol (2IP), a model compound for halophenols, binds human IYD (HsIYD) ~10^4 times less tightly and is deiodinated ~10^4 times less efficiently compared to I-Tyr.[32] Active site binding alone is not sufficient to explain IYD's low activity towards 2IP since an IYD homolog from *Haliscomenobacter hydrossis* (HhIYD) binds 2IP only 8-fold less tightly than it binds I-Tyr but still retains the 10^4 gap in catalytic activity.[32] Crystal structure of HhIYD shows that HhIYD is a homodimer with one FMN cofactor bound to each active site (Figure 1-2(A)).[32] The electron density for an active site lid of HhIYD is not observed in the crystal structure in the absence of I-Tyr, suggesting that the lid is highly flexible without substrate. However, in the co-

crystal structure of HhIYD and I-Tyr, the zwitterion of I-Tyr interacts with three residues (Glu, Lys, and Tyr) and the FMN cofactor, which induces the active site lid to form a helix-turn-helix motif that encloses the active site (blue in Figure 1-2(A) and (B)). This conformation is further stabilized by polar interactions between the hydroxyl group of I-Tyr and the ribose of FMN as well as a backbone amide of Ala 64. These structural features are also shared by HsIYD and IYD from *Mus musculus* (MmIYD).[31,33] 2IP, lacking a zwitterion, is not able to induce the lid of HhIYD to close even as it stacks below the FMN cofactor in the similar fashion as I-Tyr (Figure 1-2(C)).[32] However, no evidence suggests that the zwitterion of I-Tyr has important roles in the chemical mechanism of dehalogenation.[26] The zwitterion most likely supports efficient deiodination by stabilizing a productive conformation with the active site lid closed. Therefore, to support such a productive conformation for 2IP as substrate, the active site lid needs to be engineered to close upon 2IP binding to promote its deiodination.

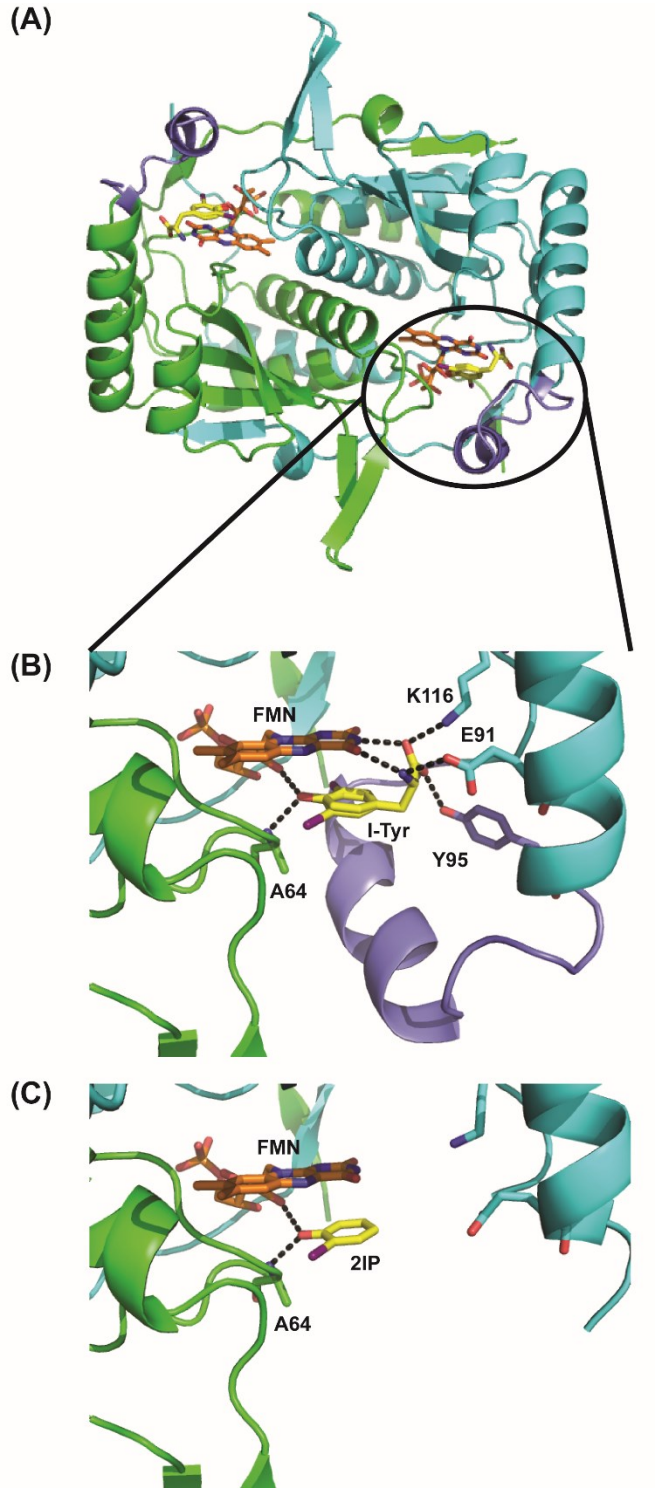

Figure 1-2 Crystal structures of HhIYD with I-Tyr and 2IP bound. (A) Overall structure of HhIYD with I-Tyr bound (PDB: 5KO8). The two monomers of HhIYD is colored with green and cyan respectively. I-Tyr and FMN are shown as yellow and orange sticks respectively. The active site lid is shown in blue. (B) The active site of HhIYD with I-Tyr bound. Protein residues are shown in sticks. Interactions between I-Tyr and HhIYD are indicated with dashed lines (within 3.5 Å). (C) The active site of HhIYD with 2IP bound (PDB: 5KRD). 2IP is shown as yellow sticks. Interactions between 2IP and HhIYD are indicated with dashed lines (within 3.5 Å).

1.4 Engineering the active site lid of IYD: a promising but challenging path:

Engineering the active site lid of IYD is a promising strategy to promote halophenol dehalogenation since the function of the lid seems to be control of substrate specificity. Furthermore, IYD belongs to the nitro-FMN reductase superfamily which catalyzes a wide range of reactions from reductive dehalogenation to nitro, quinone, flavin reduction and flavin fragmentation.[34] The enzymes within different subgroups of this superfamily all share a common core structure with an α/β fold (Figure 1-3). However, substantial variability is observed at the regions equivalent to IYD's lid.[29] These variable lids and loops surrounding the active site provide the structural basis for the great diversity of chemical functions and substrate selectivity of the superfamily. Therefore, the active site lid of IYD is likely to be evolvable for expanding its substrate specificity.[34]

Engineering flexible loops in proteins has received growing attention as the dynamic nature of such loops are often important to substrate binding and catalysis.[35] However, the exact role of loop dynamics in protein catalysis is still poorly understood and there has yet been a general approach to guide such engineering efforts.[36] Directed evolution based on error prone PCR and iterative site saturation mutagenesis is a powerful strategy to engineer enzymes.[37,38] However, the cumbersome activity assay for IYD based on radioactivity or high performance liquid chromatography (HPLC) cannot support screening of large scale libraries of enzyme variants generated by these methods. Shuffling of libraries of natural IYD variants is also not an appealing strategy since the zwitterion recognition triad (Glu, Lys, Tyr in Figure 1-2) is highly conserved in all IYD homologs and so far characterized homologs invariably exhibit specificity for halotyrosines.[29,32,39]

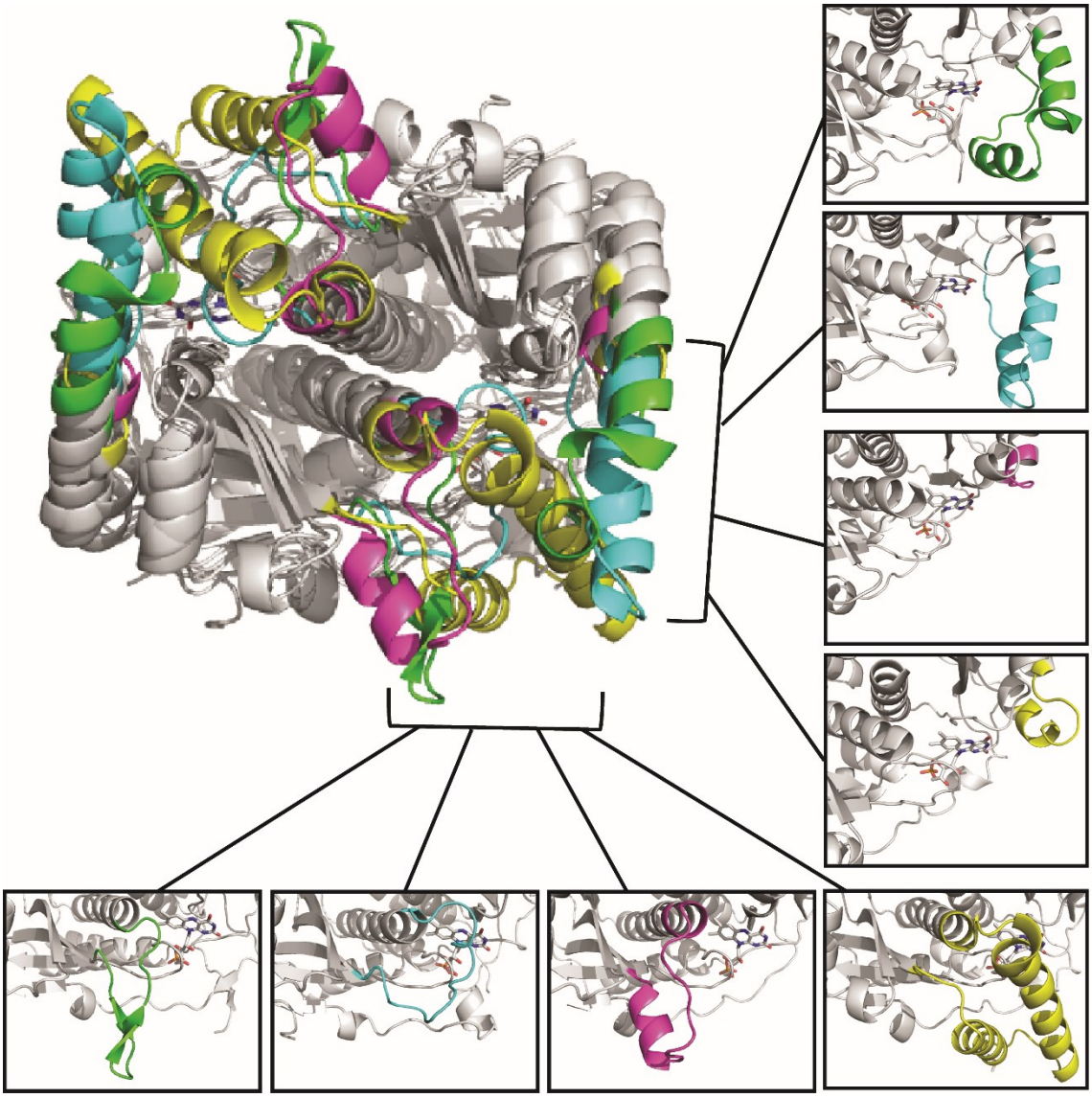

Figure 1-3 Structural diversity in the active site of the nitro-FMN superfamily. The α/β dimeric core of IYD (PDB 4TTC),[31] flavin reductase (FRP, PDB 2BKJ),[40] nitroreductase (NfsB, PDB 1YKI),[41] and flavin destructase (BluB, PDB 2ISJ)[42] are shown in gray. The variable active site regions are illustrated in green for IYD, cyan for BluB, magenta for FRP and yellow for NfsB. For simplicity, the C-terminal extension (~ 50 residues) of FRP is omitted and the carbon atoms of FMN of are shown in gray. This figure was originally published in Sun, Z.; Su, Q.; Rokita, S. E.[29]

Recently, computational design as an alternative approach to directed evolution for engineering enzymes has been rapidly gaining attention. It overcomes the bottleneck of directed evolution, the requirement of high-throughput screening, by exploring extremely large sequence spaces in silico and exporting small-sized libraries of enzyme variants for experimental

characterization.[43] Computational design is able to alter multiple amino acids simultaneously[44] and introduce sequence insertions and loop replacements[45] and has demonstrated success in increasing native activity,[46] altering substrate selectivity,[47] and even designing de novo enzymes.[48] Therefore, computational design offers an attractive approach to engineer IYD towards a halophenol dehalogenase.

However, there are a few potential obstacles for the computational design of IYD. The essence of computational design is to optimize the interactions between the enzyme and the substrate to achieve stabilization of the transition state. To date, co-crystal structures of IYD with substrate bound were only obtained with their FMN cofactor fully oxidized.[31–33,49] Therefore, the enzyme-substrate interactions from these structures may not be catalytically relevant since the FMN_{hq} is required for the dehalogenation. In addition, the rate determining step of IYD catalysis is still obscure. Neither the tautomerization step forming the unstable α-haloketone intermediate (step (1) in Figure 1-1) nor the first electron transfer step forming the reactive α-haloketyl radical anion intermediate (step (2) in Figure 1-1) seems to be the rate-determining step under steady-state condition.[50] Therefore, how IYD stabilizes the transition state of its rate-determining step remains unclear. As a result, a catalytically relevant model for the computational design of IYD to promote halophenol dehalogenation is lacking.

1.5 Specific aims:

IYD is a promising candidate for a reductive dehalogenase to remediate the widely spread and highly toxic halophenols. Its low basal activity towards halophenols needs to be improved by enzyme engineering. In this dissertation, such effort was explored by the following four aims.

Aim (1): Engineering IYD from *Homo sapiens* (HsIYD) towards a halophenol dehalogenase via computational design. To improve halophenol dehalogenation, the active site lid of HsIYD was first engineered computationally to stabilize its closed conformation in the presence

of 2IP, a model compound for halophenol. Variants of HsIYD generated by this approach were screened for tighter binding of 2IP and more efficient 2IP deiodination.

Aim (2): Engineering IYD from *Haliscomenobacter hydrossis* (HhIYD) towards a halophenol dehalogenase via computational design. After Aim (1) achieved limited success, HhIYD, an easy-to-work with alternative to HsIYD, was redesigned by two different strategies-fixed backbone design and loop replacement to further improve 2IP deiodination.

Aim (3): Charactering the structure and function of IYD from *Thermotoga neapolitana* (TnIYD). After Aim (2) failed to improve 2IP deiodination, attempts to obtain crystal structures of IYD with its FMN cofactor in the semiquinone and fully reduced states were carried out in hope to capture catalytically relevant conformations of the active site. TnIYD, a natural IYD homolog from a thermophilic bacterium, was functionally analyzed and structurally characterized with its FMN in the oxidized and semiquinone states.

Aim (4): Probing the effect of substrates and their analogs on the reduction of IYD. The reduction of HsIYD and TnIYD by sodium dithionite in the presence of substrate was monitored under steady-state conditions to reveal the basis for IYD's substrate inhibition and explore the possibility of reduction being the rate-determining step of IYD catalysis.

Chapter 2 Engineering HsIYD towards a halophenol dehalogenase via computational design

2.1 Introduction:

IYD's potential for bioremediation of halophenols is hindered by its weak activity towards substrates lacking a zwitterion. The stringent selectivity of IYD is enforced by its active site lid which is only responsive to halotyrosines. Computational design is a promising approach to engineer this active site lid to improve its recognition of halophenols and promote dehalogenation. Challenges associated with lid redesign are the inherent flexibility of the lid and the lack of structural information on catalytically active IYD•FMN_{hq}•substrate complex. However, there are several features in the co-crystal structure of IYD•FMN_{ox}•I-Tyr that could support a productive IYD•2IP complex, despite that the FMN_{ox} is catalytically inactive. The closure of the lid shields the substrate away from bulk solvent-a strategy that is common for enzymes to promote catalysis.[51] Moreover, the aromatic ring of 2IP stacks below the isoalloxazine ring of FMN, which is likely to facilitate electron transfer from reduced FMN to 2IP.[52]

As a first attempt to alter the substrate selectivity of IYD, the sequence of the active site lid was redesigned to stabilize its closed conformation in the presence of 2IP (Figure 2-1) which is analogous to the lid of oxidized native IYD in its co-crystal structure with I-Tyr (Figure 1-2(B)). 2IP is chosen as a model compound for halophenol due to its structural simplicity and similarity to I-Tyr. The sequence redesign was carried out by the program Rosetta which has demonstrated the most success in designing enzymes.[43] Rosetta is a powerful biomolecular modeling suite capable of handling a wide range of biological problems from de novo protein structure prediction to protein design and glycoengineering.[53–55] Early examples of enzyme design by Rosetta focused on the de novo design of novel enzyme activities beyond those of natural enzymes.[48,56,57] Recently, Rosetta also demonstrated success in engineering existing enzymes for improving activity and altering substrate specificity.[45,47,58] These examples are all based on template enzymes with structurally

well-defined active sites. Therefore, it is interesting to see if Rosetta is able to redesign the lid that undergoes a disorder to order transition upon 2IP binding, as in native enzyme upon I-Tyr binding.

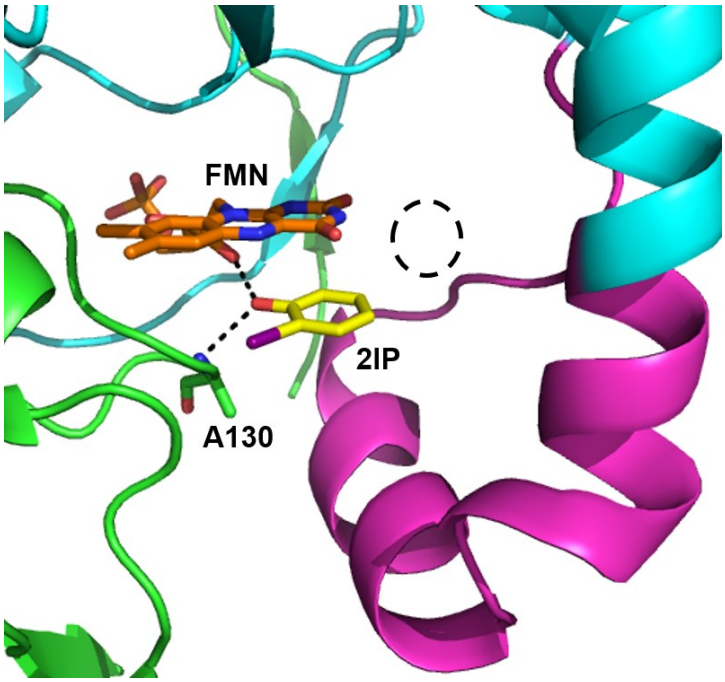

Figure 2-1 Computational model of the proposed productive complex of HsIYD and 2IP generated by PyRosetta.[59] The two monomeric polypeptides of HsIYD are colored with green and cyan respectively. 2IP and FMN are shown as yellow and orange sticks respectively. The active site lid plus three residues extended from both termini (residues 157-182, magenta) were varied by Rosetta. Polar interactions between 2IP and HsIYD are shown with dashed lines. A cavity created by the absence of the I-Tyr zwitterion is indicated by a dashed circle. For clarity, a loop on top of FMN containing residues 238-245 were hided from view.

In this chapter, the initial effort to switch HsIYD's substrate specificity from I-Tyr to 2IP was described.[60] Chemical rescue was first attempted to promote 2IP deiodination activity by using Gly and Ala as exogenous zwitterions. When such effort failed, Rosetta was used to redesign the active site lid of HsIYD to stabilize a HsIYD•2IP complex. To achieve this goal, two parallel design strategies-guided Rosetta design (GD) directed by intuitions on secondary-structure stability and unguided Rosetta design (UD) were employed. Only unguided Rosetta design generated variants that improved both the binding affinity and catalytic efficiency of HsIYD towards 2IP. The effect of mutations forming UD08 on the 2IP deiodination of HsIYD revealed the strong epistatic nature of active site lid mutations. The unguided Rosetta design further demonstrated the ability to induce

a dramatic disorder to order transition of the active site lid in the presence of 2IP as characterized by protection against trypsin proteolysis.

2.2 Materials and methods:

2.2.1 Computational design:

All Rosetta simulations were carried out via Pyrosetta 3 (an interactive Python-based interface to Rosetta).[59] The Rosetta scripts used for preparation of starting structure and lid redesign can be found in Appendix A: script A1 and A2.

(1) Preparation of the starting structure:

The crystal structure of HsIYD with I-Tyr bound (PDB 4TTC) provided a template for building the enzyme•2IP complex with the closed active site lid. The co-crystal structure was first optimized by Rosetta to eliminate structural errors in the original PDB file such as atom clashes, and unfavorable side chain rotamers.[61] A single optimization trajectory contained two stages (Appendix Figure A1(A) and Table A1). In the first stage, the side chains were allowed to repack with conformations chosen from a backbone-dependent rotamer library.[62] Hydrogens were added to the protein automatically by Rosetta. In the following minimization stage, the torsion angles of backbones and side chains and the positions of FMN and I-Tyr were optimized by gradient based minimization. The minimized structure was either accepted for next round of optimization or rejected based on the Monte Carlo Metropolis criterion.[63] The two stages were performed iteratively before the lowest energy structure encountered in the trajectory was recovered as the final output. Fifty independent structures were generated by the same protocol and ranked by their Rosetta energies. I-Tyr in the best scored structure was then substituted with 2IP by deleting the coordinates of the zwitterion and β-carbon to generate the model complex of HsIYD•2IP for lid redesign. Since IYD is a homodimer and its two active sites are functionally identical, the substrate substitution and subsequent redesign were only applied to one of the two active sites. Parameterization of small molecules-I-Tyr, 2IP, and FMN was performed following the PyRosetta user's guide.[64] The

geometries of I-Tyr and FMN were adopted from those in the co-crystal structure of HsIYD•I-Tyr (PDB 4TTC). Hydrogens and partial charges of the small molecules were added by Chem3D Pro 13.0 (Cambridgesoft) and DiscoveryStudio 4.1 (Accelrys), respectively.

(2) Fixed backbone design:

Similar to structure optimization, a two-stage protocol was used for lid redesign with fixed backbones following published procedures (Appendix Figure A1(B) and Table A1).[65] In the design stage, the side chains of the active site lid and three additional residues from both termini (residues 157-182, magenta in Figure 2-1) were varied in a random and combinatorial fashion by two different approaches. The lid, when closed, forms a helix-turn-helix motif (blue in Figure 1-1(B)). Therefore, in the first approach, the "guided Rosetta design", substitutions in the helix region of the lid were restricted to amino acids that favor α-helix formation.[66] In the loop regions of the lid, Rosetta was directed to choose amino acids frequently observed in natural IYDs at the same positions since such amino acids may stabilize the structure more than those found infrequently.[67] A detailed amino acid selection for each position is shown in Appendix Table A2. In contrast, all 20 common amino acids were allowed at all positions of the lid in the "unguided Rosetta design" approach. Sidechain rotamers of residues within 10 Å of the lid were repacked during the design stage to accommodate any potential substitutions. To reduce the computation cost, the enzyme's backbone torsion angles and small molecule (FMN and 2IP) positions were all fixed at this stage. They were, however, relaxed in the following minimization stage to optimize the structures of the variants which were then accepted or rejected by the Monte Carlo Metropolis criterion. After iterations of the two-stage algorithm, the lowest energy structure encountered in the trajectory was recovered as the final output. One hundred independent designs were calculated for both guided Rosetta design and unguided Rosetta design.

To confirm that the stabilization of the designs over the starting model was a result of mutations rather than changes of backbone and side change conformations, the starting model of

HsIYD•2IP complex was allowed to go through the same three-stage protocol except that in the design stage the active site residues were only allowed to be repacked rather than be mutated.

(3) Selection of redesigned variants for experimental characterization:

A series of filters were used to choose potential variants for characterization. A total Rosetta energy filter was first applied to select the top 20 designs in total energy. Then the solvent accessible area (SASA) of 2IP in these designs was evaluated by Pymol (education version, Schrödinger). Designs with a 2IP SASA smaller than that in the control experiment (6.4 $Å^2$) were considered for the next filter. Finally, redundant variants with the same sequences were removed from all remaining ones to give 11 total variants (2 guided designs and 9 unguided designs) for characterization.

2.2.2 Cloning:

The cloning of HsIYD was described in a previous report.[31] The vector pSMT3 contains the gene for HsIYD without the membrane anchor (residue 1-31) plus a N-terminal SUMO tag to facilitate expression of soluble proteins.[68] The SUMO tag was later removed during purification leaving a non-native serine at the N-terminal truncation of HsIYD. The construct also carries a $(His)_6$ tag at the C-terminal of IYD gene to facilitate purification.

Except for GD02 and UD01, all variants of HsIYD were generated by site directed mutagenesis.[69,70] GD02 and UD01 were constructed by sequence ligation independent cloning.[71] Briefly, the parent plasmid of HsIYD was linearized by inverse PCR. An insert containing all 9 mutations of UD01 flanked by 18 bases of homologous sequence to each end of the linearized plasmid was prepared by PCR-based DNA assembly.[72,73] The linearized plasmid and insert were digested separately by T4 DNA polymerase (New England Biolabs) at room temperature for 30 min to create 5' overhangs. The digestion reaction was stopped by addition of dCTP (Thermo Fisher Scientific) and the digestion products were purified by a cleanup kit (Thermo Fisher Scientific). The vector and insert were then mixed with a molar ratio of 1:1 and their

complementary 5' overhangs were annealed at 37 ºC for 30 min. The annealed product was transformed directly into Genehogs chemically competent cells (Invitrogen) to repair nicks.

All DNA oligonucleotides used for cloning were synthesized by IDT and are listed in Appendix Table A3. PCR was performed with Phusion High-Fidelity DNA polymerase (Thermo Fisher Scientific). The DNA sequences of all variants were verified by Sanger sequencing (Genewiz).

2.2.3 Protein expression and purification:

HsIYD and its variants were heterologously expressed in Rosetta2 chemically competent cells (Novagen). After transformation, the cells were grown in 100, 500, or 1000 mL LB media at 37 ºC with vigorous shaking (220 rpm). The cultures were cooled to 16 ºC after their $OD_{600\ nm}$ reached ~ 1. Isopropyl thio-β-galactoside (IPTG, Goldbio, 25 μM final) was then added to induce expression of IYD at 16 ºC with vigorous shaking (220 rpm) for 15 hr. Cells were harvested by centrifugation at 4 ºC and 5000×g for 10 min, flash-frozen in liquid nitrogen and stored at -80 ºC.

Enzymes with the SUMO tag removed from the prep were obtained as follows: frozen cell pellets were thawed at room temperature and resuspended in ~ 25 mL cell lysis buffer (50 mM sodium phosphate, 500 mM sodium chloride, 10% glycerol, 25 mM imidazole, 0.5 mM tris(2-carboxyethyl)phosphine (TCEP), pH 8.0) by vortex. From then on, all procedures were done at 4 ºC unless otherwise noted. FMN was added to the suspension to a final concentration of ~ 300 μM to enhance its occupancy in IYD. Cells were then lysed by an EmulsiFlex-C3 homogenizer (Avestin) with 4 passes at ~17000 psi. ULP1 protease (~ 40 μg) was then added to the cell lysate to cleave the SUMO tag off the deiodinase. Cell debris was removed by centrifugation at 45000×g for 1 hr. The ULP1 digestion was completed during this time. The supernatant was mixed with 5 mL of HispurTM nickel-nitrilotriacetic acid (Ni-NTA) resin (Thermo Fisher Scientific, pre-equilibrated with 10 column volumes of cell lysis buffer) by a bench top Econo pump (Bio-rad) at a flow rate of 1 mL/min. Since the SUMO tag also carries a N-terminal $(His)_6$ tag, both SUMO and the

deiodinase bound the resin. The SUMO tag, however, can be removed from the resin by extensive washing with 16 column volumes of cell lysis buffer and 16 colum volumes of washing buffer (50 mM sodium phosphate, 500 mM sodium chloride, 10% glycerol, 60 mM imidazole, 0.5 mM TCEP, pH 8.0) using an ÄKTA protein purification system (GE Healthcare) at 1 mL/min. Finally, the bound protein was eluted with elution buffer (50 mM sodium phosphate, 500 mM sodium chloride, 10% glycerol, 250 mM imidazole, 0.5 mM TCEP, pH 8.0). Most SUMOs were removed by one Ni-NTA column, but a second Ni-NTA column as described above was generally needed to completely remove the tag. The eluted proteins were then supplied with ~300 μM FMN and incubated on ice for 1 hr to further increase the FMN occupancy. Finally, the proteins were exchanged into storage buffer (50 mM sodium phosphate, 100 mM sodium chloride, 15% glycerol, 1 mM TCEP, pH 7.4) using a gravity driven PD-10 desalting column (GE healthcare) following manufactures' instructions. The proteins were then concentrated with a 50 kD molecular weight cut off centrifugal filter unit (Amicon), aliquoted, flash-frozen with liquid nitrogen and stored in -80 ºC.

A partial purification protocol modified from the above protocol was used to purify variants used for binding and activity screening. The SUMO tag was removed from the deiodinases after purification by the ULP1 protease but not further removed from the prep. All procedures were done at 4 ºC unless otherwise noted. Dithiothreitol (DTT) was used as the reductant in all buffers for the purification of GD01-02 and UD01-09 but switched to TCEP for all the other purifications for its greater oxygen stability. Cell lysate clarified via centrifugation was mixed with 2-3 mL Ni-NTA resin by a rotary shaker with mild agitation for 30 min. The subsequent washing (cell lysis buffer, 10 column volumes) and elution steps were driven by gravity. ULP1 protease (~ 40 μg) was then added to eluted proteins to cleave the SUMO tag overnight. The mixture of the SUMO tag and the deiodinase was directly exchanged into storage buffer by using either a centrifugal filter unit (50 kD molecular weight cut off, Amicon) or a Econo-Pac 10DG gravity desalting column (Bio-rad)

following manufactures' instructions. For purification of DM01 variants with substitutions at E157, cell pellets from 100 mL cultures were lysed with B-PER™ bacterial cell extraction reagent (Thermo Fisher Scientific) following manufacturer's instructions. Lysozyme (1 mg/mL, Thermo Fisher Scientific) and Pierce™ universal nuclease (25 unit, Thermo Fisher Scientific) were also added to the lysate to facilitate cell lysis. After elution from the nickel affinity column (200 μL), the variants were frozen directly in elution buffer without buffer exchange.

Enzymes used for limited proteolysis with trypsin required extra purification to avoid detectable contaminants on SDS-PAGE. Enzymes used in these experiments had their C-terminal $(His)_6$ tag removed by site directed mutagenesis but were still able to bind to the Ni-NTA column by $(His)_6$ tag attached to the SUMO. After elution, the SUMO together with its $(His)_6$ tag was cleaved by ULP1 protease and the deiodinase-SUMO mixture was loaded onto a second Ni-NTA column. At this point the deiodinase was free of $(His)_6$ tag and therefore would flow through the column while the SUMO tag and any non-specific Ni-NTA binding proteins were still retained on the column. The purified deiodinases were then exchanged into storage buffer and frozen as described above.

The purified enzymes were analyzed by 12% SDS-PAGE with Comassie brilliant blue staining. Enzyme concentration was determined by either UV-vis absorption of enzyme-bound FMN ($\varepsilon_{450\ nm}$=12500 $M^{-1}cm^{-1}$)[74] or quantification of FMN liberated from the enzyme by HPLC at 445 nm upon denaturation with 4.4% formic acid (see Section 2.2.5 for detailed HPLC methods). The discrepancy between the two methods was ≤ 10%. The FMN occupancy of purified deiodinases was determined by the ratio of enzyme-bound FMN (determined by UV-vis) over the total protein concentration which was calculated from UV absorption at 280 nm (extinction coefficient estimated by the ExPASy ProtParam tool)[75] after correcting for the contribution from bound FMN (A280/A450 = 1.57).[31]

2.2.4 Binding dissociation constant:

The affinity (dissociation constant, K_d) of substrates (I-Tyr and 2IP) to HsIYD and its variants was determined by measuring the quenching of enzyme-bound FMN_{ox} fluorescence upon stacking of the substrates' aromatic ring to FMN_{ox} as previously described.[27] Briefly, I-Tyr or 2IP was titrated into 4 μM enzyme in 200 mM potassium chloride, 100 mM potassium phosphate, pH 7.4 with mild stirring at 25 ± 1 °C. Quenching of FMN fluorescence upon addition of substrates was recorded at 516 nm with an excitation wavelength of 450 nm. K_d was obtained from fitting the dependence of fluorescence intensity on substrate concentration to a previously described binding isothermal.[21]

2.2.5 Deiodination activity assay:

The deiodination activity was measured by quantifying the rate of product (phenol or Tyr) formation via reverse-phase HPLC as previously described.[28,32] Briefly, 80 nM to 5 μM enzyme was incubated with 0.5-10 mM 2IP in 900 μL of 220 mM potassium chloride, 110 mM potassium phosphate, pH 7.4 at 25 ± 1 °C for 5 min. Sodium dithionite (5%, 100 μL) in 5% sodium bicarbonate was then added to initiate catalysis. For initial screening of HsIYD variants generated by Rosetta, the reactions were quenched after 30 min by 50 μL of 88% formic acid. Resorcinol (30 μM final) in the above buffer was then added as an internal standard. For all other activity measurements, the reaction was quenched after 5-30 min by addition of 100 μL of a 1:1 mixture of 88% formic acid and 0.55 μM (final) Cl-Tyr (as an internal standard) in the above buffer. The reaction was then analyzed by an Agilent 1100 series HPLC equipped with a 1200 series multiwavelength detector. The product of the reaction, Tyr or phenol, was separated on a C18 reverse phase column (Agilent, Microsorb-MV 300 C18, 250 × 4.6 mm) by a gradient of water and acetonitrile both containing 0.44% formic acid at a flow rate of 1 mL/min and detected at 271 nm. See Appendix Table A4 for the detailed solvent gradients. For steady state kinetics measurements, the rate versus substrate concentration was fitted with Michaelis-Menton equation to obtain k_{cat} and K_M.

2.2.6 Limited proteolysis:

Deiodinases (HsIYD, DM01, GD02, or UD08, 5 μg) and its corresponding substrates (100 μM I-Tyr or 10 mM 2IP) were incubated in 200 mM NaCl, 100 mM sodium phosphate pH 7.4 at 25 ± 1 °C for 5 min. When substrate was not present, the above buffer was added to maintain a constant volume. Sodium salts were used in this buffer instead of potassium salts used in binding and activity experiments to avoid precipitation of SDS involved in the later SDS-PAGE analysis. Digestion was initiated by addition of trypsin (fleshly prepared before use, Sigma-Aldrich, TPCK treated) in the same buffer. The final deiodinase to trypsin ratio was 50:1 (in μg) in all cases. Aliquots of 5 μL was removed from the digestion reaction at indicated time points and mixed immediately with an equal volume of standard SDS-PAGE loading buffer. The mixture was then heated in a boiled water bath for 5 min to ensure denaturation of all proteins. The reaction aliquots were then analyzed by 15% SDS-PAGE. After electrophoresis, the gel was mixed with 100 mL Coomassie brilliant blue staining solution, microwaved for 90 s at the highest output and then agitated mildly for 30 min. The same procedures were used to destain the gel twice with 10% (v/v) acetic acid. During the second time, agitation was reduced to 15 min to avoid over-destaining. Gel bands were then scanned and undigested proteins were quantified by densitometry (ImageQuant TL 7.0, GE Healthcare) with pre-constructed calibration curves. The consumption of undigested proteins overtime followed pseudo first order kinetics from which the digestion rate constant and half-life of undigested proteins were calculated.

2.2.7 Effect of I-Tyr and 2IP on trypsin activity:

A 1 mg/mL suspension of Nα-Benzoyl-DL-arginine 4-nitroanilide hydrochloride (DL-BAPNA) in 200 mM sodium chloride, 100 mM sodium phosphate pH 7.4 was strongly vortexed for 10 min. The DL-BAPNA did not completely dissolve and the suspension was then centrifuged at 14000×g for 5 min. The supernatant was used as the substrate stock solution whose concentration was adjusted with the above buffer to give a UV absorbance of 0.45 at 315 nm. To set up the assay,

trypsin (8 μM) and deiodinase substrates (100 μM I-Tyr or 10 mM 2IP) in the above buffer were mixed to a total volume of 65 μL and incubated at room temperature (25 ± 1°C) for 5 min. In the control, buffer was used to substitute substrates. The reaction was initiated by addition of 85 μL of DL-BAPNA stock solution and the release of proteolysis product, 4-nitro-aniline, was monitored at 405 nm (ε_{405nm}=9920 $M^{-1}cm^{-1}$)[76] every 15 seconds for 5 min. The first eight points were fit into a linear line to obtain the initial rate of the reaction.

2.2.8 Identification of trypsin digestion site on HsIYD:

The two major trypsin digestion products of HsIYD were extracted separately from the SDS-PAGE gel.[77] Briefly, the gel bands containing the digestion products were carefully excised and placed into a 2 mL centrifuge tube (USA-Scientific, 1620-2700). Destaining solution (a 1:1 mixture of 50 mM ammonium bicarbonate and acetonitrile, 200 μL) was subsequently added to the tube and the gel bands were crushed manually with a glass rod. The resulting gel particles were incubated with the destaining solution for 10 min to remove the Coomassie brilliant blue. After centrifugation at 14000×g for 5 min, the blue supernatant containing the Coomassie stain was discarded and the gel particles were washed once with another 200 μL destaining solution. The now colorless gel particles were allowed to dry in air for 10 min before incubated with 100 μL extraction solution (a mixture of 88% formic acid, water and isopropanol in 1:3:2 volume ratio). The mixture was then vortexed mildly for 7 hr during which time the digestion products were extracted into solution from the gel. After centrifuged at 14000×g for 5 min, the supernatant was transferred into a 1.5 mL centrifuge tube carefully without disturbing the pelleted gel particles. Another 100 μL of the extraction solution was used to wash the gel particles, centrifuged, and combined with the previous fraction. The combined solution was then evaporated to ~ 20 μL under vacuum (Savant Speed Vac®, SC100A) and analyzed directly by a Waters Acquity/XevoG2 UPLC-MS system to detect peptides from the trypsin digestion. Peptides were separated using an Acquity UPLC® Protein BEH C4 column (300 Å, 1.7 μm, 2.1 mm×50 mm) and a binary mobile phase of

water and acetonitrile (1% v/v formic acid in each) that remained at 100% water for 1 min and then a linear gradient of acetonitrile to 80% for the next 6.5 min and remained at this condition for another 0.9 min. The capillary voltage, sampling cone and extraction cone were set to 3 kV, 40 V, and 4 V, respectively and the source temperature was 130 ºC. The desolvation gas temperature and flow rate were 400 ºC and 400 L/hr, respectively. All data were analyzed by BiopharmaLynx (Waters). The mass of HsIYD without SDS-PAGE treatment and undigested HsIYD extracted from the gel was also obtained to check any protein modification during SDS-PAGE.

2.2.9 Rosetta simulation of DM01 variants with E157 substitutions:

(1) Preparation of a starting structure of DM01:

A protocol similar to that in Section 2.2.1 part (2) was used to generate the double mutation variant DM01. In the design stage, E158 and M162 of HsIYD were mutated to Y and A, respectively. Sidechain rotamers of residues within 10 Å of the two residues were repacked during the design stage to accommodate any potential mutations. The enzyme's backbone torsion angles and small molecule (FMN and 2IP) positions were all fixed at this stage but later relaxed in the following minimization stage to optimize the variant structure which was then accepted or rejected by the Monte Carlo Metropolis criterion. After iterations of the two-stage algorithm, the lowest energy structure encountered in the trajectory was recovered as the final output. Five independent structures were generated and the one with the lowest energy (the deviations of energy between five structures were less than 1 Rosetta energy unit (REU)) was used as the starting structure for the site saturation mutagenesis simulation.

(2) Calculation of DM01 variants with E157 substitutions:

A protocol similar to that in Section 2.2.1 part (2) was used for site saturation mutagenesis simulation calculation. In the design stage, E157 of DM01 was mutated to all other 19 canonical amino acids. Sidechain rotamers of residues within 10 Å of E157 were repacked during the design stage to accommodate any potential mutations. The enzyme's backbone torsion angles and small

molecule (FMN and 2IP) positions were all fixed at this stage but later relaxed in the following minimization stage to optimize the variant structure which was then accepted or rejected by the Monte Carlo Metropolis criterion. After iterations of the two-stage algorithm, the lowest energy structure encountered in the trajectory was recovered as the final output. Five independent structures were generated and the one with the lowest energy (in most case, the deviations of energy between 5 structures were less than 1 Rosetta energy unit (REU)) was used for subsequent analysis.

2.2.10 Additional software:

Least-square fittings were performed with Origin 2017 (Originlab). All structural illustrations were prepared by Pymol (education version, Schrödinger).

2.3 Results and discussion:

2.3.1 Exogenous zwitterions failed to rescue 2IP deiodination:

Since the presence of a zwitterion in the substrate confers the 10^4-fold higher selectivity of HsIYD towards I-Tyr over 2IP,[32] efficient deiodination of 2IP can potentially be rescued by an exogenous zwitterion. Such chemical rescue has been used to restore the activity of an inactive aspartate aminotransferase mutant K258A via exogenous amines.[78] More recently, exogenous imidazole was shown to rescue the tyrosine kinase Src R388A mutant in vivo.[79] The difference between I-Tyr and 2IP is a zwitterion and a β-carbon which altogether closely resembles Ala. Amino acids bigger than Ala may clash with 2IP in the active site once the lid closes. Therefore, Ala and Gly were chosen as the rescue compounds.

The binding affinity (K_d) and deiodination activity (V/[E]) of HsIYD with 2IP were measured in the absence and presence of 10 mM Gly and Ala (2×10^3 times HsIYD concentration). The deiodination activity was measured at two 2IP concentrations: one equal to its K_M (4 mM) and one smaller than its K_M (0.5 mM). As shown in Appendix Table A5, the presence of Gly did not affect the K_d but increased the deiodination activity by 1.3-fold at both 2IP concentrations. Ala, in contrast to Gly, decreased the K_d by 1.1-fold while left activity unchanged at both 2IP

concentrations. Therefore, simple zwitterionic compounds like Gly and Ala have no significant effects on the binding and deiodination of 2IP by HsIYD. Chemical rescue with exogenous zwitterions is not a practical solution to switch substrate specificity of HsIYD towards 2IP.

2.3.2 Computational design by Rosetta with fixed backbones stabilized a HsIYD•2IP complex with the lid closed:

Once chemical rescue failed to promote 2IP deiodination, Rosetta was used to redesign the active site lid of HsIYD to stabilize the proposed productive conformation for 2IP deiodination (Figure 2-1). This model complex of HsIYD•2IP was built by first optimizing the co-crystal structure of HsIYD•I-Tyr (PDB 4TTC)[31] in Rosetta. The zwitterion and β-carbon of I-Tyr were then deleted to generate the HsIYD•2IP complex. The Rosetta model of HsIYD•2IP differed from the co-crystal structure of HsIYD•I-Tyr only by a 0.5 Å all-atom root mean square deviation (RMSD). The sequence of the lid was then redesigned by a protocol consisting of two stages. In the design stage, the sidechains of the lid area (residues 157-182, magenta in Figure 2-1) were varied via two different strategies. Rosetta was either allowed to choose amino acid variants randomly from all 20 canonical amino acids (unguided Rosetta design, or UD) or from a limited selection of amino acids that stabilizes the helix-turn-helix motif of the closed lid (guided Rosetta design, or GD) (Appendix Table A2). The backbones of the lid were fixed during the design stage but were allowed to relax together with the side chains in a subsequent minimization stage to accommodate the incorporated substitutions. The design and minimization stages were then iteratively alternated before outputting a final design sequence. Any energy change of the redesigned enzyme•2IP complex from the starting structure could be from either changes of amino acid identity or changes of protein conformation due to the relaxation in the minimization stage. Therefore, as a control, the same protocol was used to repack rather than redesign the HsIYD•2IP complex to capture the energy change solely from conformational relaxation. Since Rosetta sampling is stochastic, multiple independent designs starting from the same starting model were needed to avoid trapping of the designs into a local energy minimum.[53] Therefore, 100 independent

designs were generated for the control as well as guided and unguided design. While 100 independent designs only explored a small fraction of the possible sequence space, a previous study showed that 100 independent designs were enough to reach convergence in sequence variability when the backbones were fixed during the design stage.[80] Indeed, ~ 85% of the redesigned positions on the lid showed less than three amino acid substitutions among all 100 sequences of both the guided and unguided design (Appendix Figure A2).

The averaged total energies of both the 100 guided and unguided Rosetta designs were lower than that of the control by 8 and 13 Rosetta energy units (REU), respectively (Table 2-1), suggesting that both strategies stabilized the enzyme•2IP complex via redesign of the lid sequence. These energy decreases are significant since a previous study showed that even a 0.8 REU decrease in Rosetta calculated binding energy was sufficient to result in a 2-fold increased binding affinity of the protease calpain to a redesigned peptide.[81] As shown in Table 2-1 by the standard deviation of Rosetta energies, the control showed the smallest variability in total energy followed by the guided design and then unguided design. This trend correlates well with the increased degree of freedom from the control to the unguided design (Appendix Table A1). The sequences of guided designs also showed less variability and therefore higher degree of convergence than those of unguided designs (Appendix Figure A2).

Table 2-1 Evaluation of designs generated by Rosetta. This table was originally published from Sun, Z.; Rokita, S. E.[60]

Criteria	Average of	Control[a,b]	Guided design[a]	Unguided design[a]
Total energy	All 100 designs	-812.7 ± 0.2	-821 ± 1	-825 ± 2
	Top 20 designs	-812.9 ± 0.1	-821.0 ± 0.1	-829 ± 1
Binding energy of 2IP[c]	Top 20 designs	-9.4 ± 0.1	-9.6 ± 0.1	-9.8 ± 0.3
Lid stabilization energy[d]	Top 20 designs	-2.4 ± 0.1	-10.4 ± 0.2	-18 ± 1
SASA of 2IP (Å^2)	Top 20 designs	6.4 ± 0.3	3.2 ± 1.3	6 ± 3

[a]The energy calculated by Rosetta is expressed in Rosetta energy units (REUs). [b]The control is repacking of the native HsIYD without varying its sequence. [c]Binding energy of 2IP is defined as the energy of the enzyme•2IP complex minus that of the ligand free enzyme. [d]Lid stabilization energy is defined as the energy of the ligand free design minus that of the ligand free starting model.

The designs were ranked based on two criteria-total energy and solvent accessible area (SASA) of 2IP. The top 20 designs in total energy were selected for further analysis. To understand how both guided and unguided design stabilized the enzyme•2IP complex over the control, the averaged total energy of the top 20 designs were broke down into two parts: (1) the interaction between 2IP and enzyme and (2) the stabilization of the lid structure. The differences in binding energy of 2IP between the control and design only accounted for ~2% of the difference in total energy (Table 2-1). In contrast, the major stabilization of the enzyme•2IP complex by the design over the control was provided by the lid stabilization energy. The control only modestly stabilized the lid over the starting model by 2.4 REU as a result of conformational relaxation (all atom RMSD < 0.1Å) introduced during the minimization stage. In contrast, both design strategies increased the lid stabilization energy by at least 4-fold compared to the control, suggesting much greater stabilization of the lid by amino acid substitutions.

The SASA of 2IP was then calculated by Pymol for the top 20 control and design structures to evaluate packing of the active site. A cavity (dashed circle in Figure 2-1) is formed in the active site when the zwitterion of I-Tyr is absent. Filling this cavity may lead to tighter packing of the active site and thus greater stability of the enzyme•2IP complex.[82,83] Although Rosetta does not specifically penalize a cavity, the van der Waals attraction energy term in Rosetta's energy function would favor more compacted structures.[84] All but one of the top 20 guided Rosetta designs decreased SASA compared to the control, indicating a tighter packing around 2IP (Table 2-1). This is expected as Rosetta was instructed to put bulky, hydrophobic residues near the void in guided Rosetta design (Appendix Table A2). In contrast, only 11 of the top 20 unguided Rosetta designs decreased SASA.

Finally, the top 20 designs with decreased SASA were checked for redundant sequences and 17 of 19 GDs and 2 of the 11 UDs were removed from the collection. The higher number of redundant sequences for guided design than unguided design is yet another sign of its higher level

of convergence. Both the 2 GDs (GD01-02, ranked by descending order in total energy) carry 9 substitutions from HsIYD in the 26-residue variable region compared to 14-18 for the 9 UDs (UD01-09, ranked by descending order in total energy) (Figure 2-2). It is not a surprise that residues of the zwitterion recognition triad (E157, Y161, and K182) were not retained in any final variants, except for K182 in GD01 and GD02.

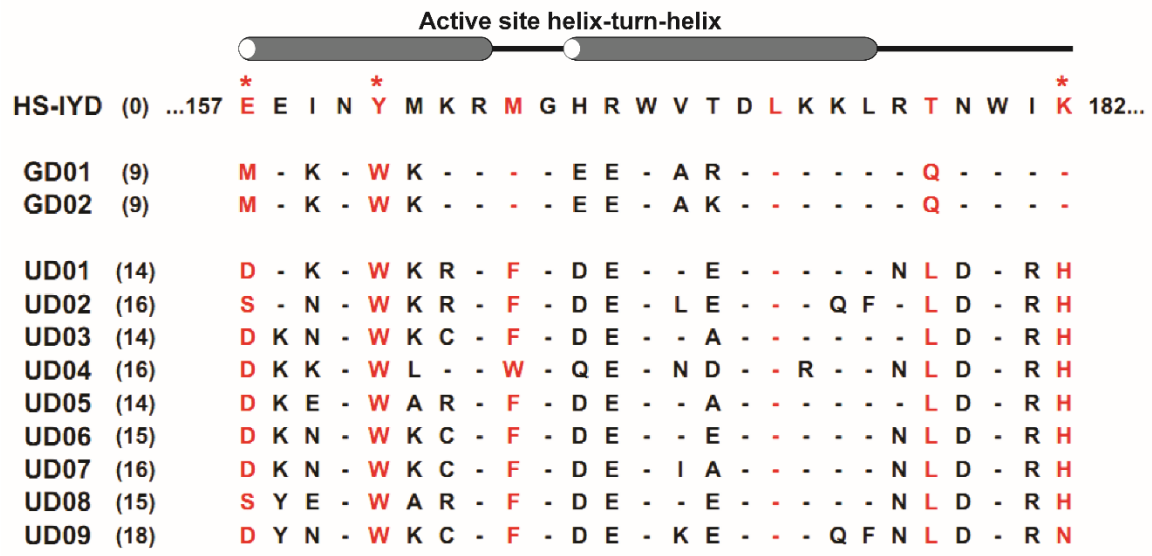

Figure 2-2 Lid sequence of HsIYD and redesigned variants. Conserved residues are labeled with dash (-). Residues with their side chains within 5 Å of the zwitterion of I-Tyr are colored in red. The ones forming polar interactions with the zwitterion of I-Tyr are indicated by star (*). Total number of mutations that each designed enzyme carries are listed in parenthesis following the enzyme labels. The lid sequence of HsIYD is flanked by its residue numbers. Secondary structures of the lid are shown on top of the alignment (α-helix as gray cylinders and loop as black lines). This figure is modified from Sun, Z.; Rokita, S. E.[60]

2.3.3 Variants generated by Rosetta improved binding, catalytic efficiency and substrate selectivity of HsIYD towards 2IP:

The 11 selected variants were constructed from HsIYD by sequence-ligation independent cloning and site-directed mutagenesis.[69–71] The mutant enzymes were then expressed in *E. coli* with a N-terminal SUMO tag[68] and a C-terminal $(His)_6$ tag to facilitate solubility and purification via Ni-NTA affinity chromatography, respectively. All 11 variant enzymes were expressed as soluble proteins (Appendix Figure A3) despite containing large number of mutations (at least 9) from HsIYD. The SUMO tag was released from the variants by ULP1 protease post Ni-NTA

chromatography but was not further removed from the enzyme preparation. The presence of the SUMO tag did not affect the initial binding and activity screening (data not shown) or measurement of enzyme concentration since the enzymes were quantified based on bound FMN rather than total protein.

The binding affinity of variants towards 2IP was measured by a FMN fluorescence quenching assay as previously reported.[27] While both GDs bound 2IP at least 2-fold weaker than HsIYD, the 9 UDs invariably bound 2IP tighter (Figure 2-3(A)). The 2IP deiodination activity of the variants was measured with 0.5 mM and 1 mM 2IP (Figure 2-3(B) and Appendix Table A6). For all enzymes with detectable activity, the activity at 0.5 mM 2IP was 2-fold smaller than that at 1 mM 2IP. This indicates that the activity measurements were all performed under conditions where the enzyme was not saturated with substrate and there was no significant decrease in K_M for any variants compared to HsIYD. Three of the nine UDs improved the 2IP deiodination activity by at least 1.5-fold where two GDs had no detectable activity. Clearly, variants generated by the guided and unguided design provided a sharp contrast even though they share ~ 50% similar or identical mutations. Restricting amino acid substitution limited the sequence space relative to that explored under unrestricted conditions and in return prevented identification of beneficial mutations. For the unguided Rosetta design, there is a discrepancy between the 100% successful rate in binding affinity improvement and the 30% successful rate in activity improvement. This is consistent with the previous report that active site binding is not sufficient to drive 2IP deiodination.[32]

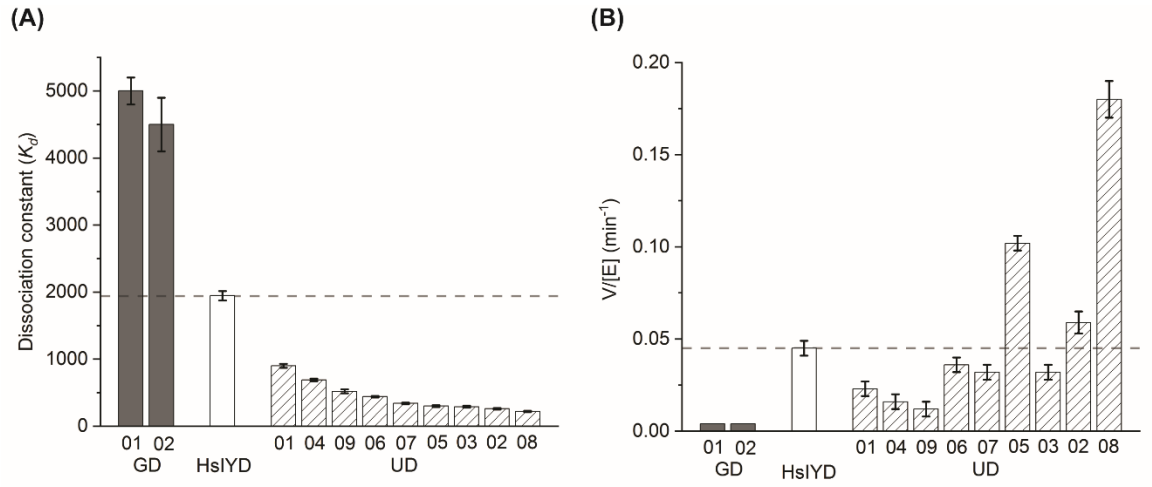

Figure 2-3 Characterization of HsIYD and its variants. (A) Affinity of 2IP to HsIYD and its variants. Two independent measurements were fitted as one curve to obtain the K_d and associated error from the fitting. (B) Deiodination activity of HsIYD and its variants with 1 mM 2IP. The V/[E] represent the average of two independent measurements. The error is either the range of two independent measurements or three times the background of the assay (0.004 min^{-1}), whichever is larger. This figure was originally published in Sun, Z.; Rokita, S. E.[60]

The unguided Rosetta design UD08 has both the largest increase in 2IP binding affinity (10-fold) and deiodination activity (4.5-fold). Its binding and steady-state kinetics with both I-Tyr and 2IP were characterized in detail (Table 2-2). The enzymes used in these studies were purified further to remove the SUMO tag from the enzyme preparation by extensive washing of Ni-NTA column (Appendix Figure A4). The FMN occupancy of the enzymes was estimated to be at least 90%. Although UD08 bound 2IP 10-fold tighter than HsIYD, the K_M only decreased by 1.3-fold. The 4.5-fold increase in k_{cat}/K_M, therefore, was mainly a result of a 3.5-fold increased k_{cat}. This is comparable or approaching the levels of activity boost in some previously published efforts of enzyme engineering by rational or computational design and directed evolution.[45,85–88] With I-Tyr as substrate, UD08 increased both the K_d and K_M by ~10^3-fold compared to HsIYD while left k_{cat} unchanged (Table 2-2). Therefore, UD08 decreased the catalytic efficiency of I-Tyr deiodination by three orders of magnitude compared to that of HsIYD. Such an effect can be explained by disruption of interactions between the zwitterion of I-Tyr and the zwitterion recognition triad of HsIYD with mutations E157S, Y161W, and K182H. Overall, UD08 increased the substrate

selectivity towards 2IP by 10^4-fold compared to that of HsIYD by improving 2IP deiodination and suppressing I-Tyr deiodination (Table 2-3). Therefore, the unguided Rosetta design with fixed backbones has demonstrated the ability to promote 2IP deiodination with relatively small computational and experimental cost.

Table 2-2 The dissociation constants and steady-state kinetics of HsIYD, UD08, DM01, and TM01 with 2IP and I-Tyr. This table was originally published in Sun, Z.; Rokita, S. E.[60]

Substrate	Enzyme[a]	K_d (μM)[b]	k_{cat} (min^{-1})[c]	K_M (μM)[c]	k_{cat}/K_M ($min^{-1}\times\mu M^{-1}$)[c]	Activity change[d]
2IP	HsIYD	$(2.4 \pm 0.1)\times10^3$	0.26 ± 0.01[e]	$(4.4 \pm 0.4)\times10^3$ [e]	$(6.0 \pm 0.6)\times10^{-5}$ [e]	1
	UD08	230 ± 6	0.92 ± 0.05	$(3.4 \pm 0.4)\times10^3$	$(2.7 \pm 0.4)\times10^{-4}$	4.5 ± 0.8
	DM01	$(1.57 \pm 0.03)\times10^3$	1.03 ± 0.07	$(5.0 \pm 0.7)\times10^3$	$(2.1 \pm 0.3)\times10^{-4}$	3.5 ± 0.7
	TM01	$(1.31 \pm 0.04)\times10^3$	0.96 ± 0.05	$(2.9 \pm 0.4)\times10^3$	$(3.3 \pm 0.5)\times10^{-4}$	5.5 ± 1.0
I-Tyr	HsIYD	0.14 ± 0.03	6.1 ± 0.4[b]	7.3 ± 0.8[b]	0.8 ± 0.1[b]	1
	UD08	470 ± 10	5.7 ± 0.2	$(1.5 \pm 0.1)\times10^4$	$(3.9 \pm 0.4)\times10^{-4}$	$(4.6 \pm 0.8)\times10^{-4}$
	DM01	0.042 ± 0.008	4.4 ± 0.2	1.4 ± 0.4	3.1 ± 0.9	4 ± 1
	TM01	10.0 ± 0.3	32 ± 3	130 ± 30	0.25 ± 0.06	0.30 ± 0.08

[a]Enzymes used in these studies are purified from SUMO contamination. [b]Three independent measurements were fitted as one curve to obtain the K_d and associated error. [c]All the data and error bars were obtained by fitting of three independent measurements as one curve. [d]Activity change is defined as the ratio of the k_{cat}/K_M of the variants to that of the HsIYD. [e]Data from Ingavat, N.; et, al.[32]

Table 2-3 The substrate selectivity of HsIYD, UD08, DM01, TM01 towards 2IP. This table was originally published in Sun, Z.; Rokita, S. E.[60]

Enzyme	2IP selectivity[a]	Relative 2IP selectivity[b]
HsIYD	$(7.14 \pm 0.12)\times10^{-5}$	1
UD08	0.69 ± 0.11	1×10^4
DM01	$(7 \pm 2)\times10^{-5}$	1
TM01	$(1.3 \pm 0.4)\times10^{-3}$	18

[a]2IP selectivity is defined as the ratio of the k_{cat}/K_M for 2IP to that for I-Tyr. [b]Relative 2IP selectivity is the 2IP selectivity of variant enzymes relative to that of HsIYD.

2.3.4 Amino acids responsible for the improved 2IP deiodination by UD08 were highly epistatic:

UD08 contains 15 mutations from HsIYD (Figure 2-2) and it is unlikely that all of them contribute to promote 2IP deiodination. To identify mutations that can increase 2IP deiodination

activity as potential "hot spots" for further activity improvements, 15 separate variants were constructed by introducing these mutations individually to HsIYD via site directed mutagenesis. Their effects on the 2IP deiodination activity were evaluated by the activity screening assay described in the above section (Appendix Figure A5). As shown in Figure 2-4, the mutational effects can be divided into three categories. Two of the 15 mutations (E158Y and M162A) increased the activity of HsIYD with 2IP by more than 1.5-fold and are therefore beneficial mutations. Seven of the 15 mutations are deleterious as they decreased the activity by more than 1.5-fold. The remaining 6 changed the activity by less than 50% and thus are classified as neutral. The beneficial mutations discovered by computational design in this case occurred in a much higher rate (~ 13%) than those typically from directed evolution (0.01-1%).[89]

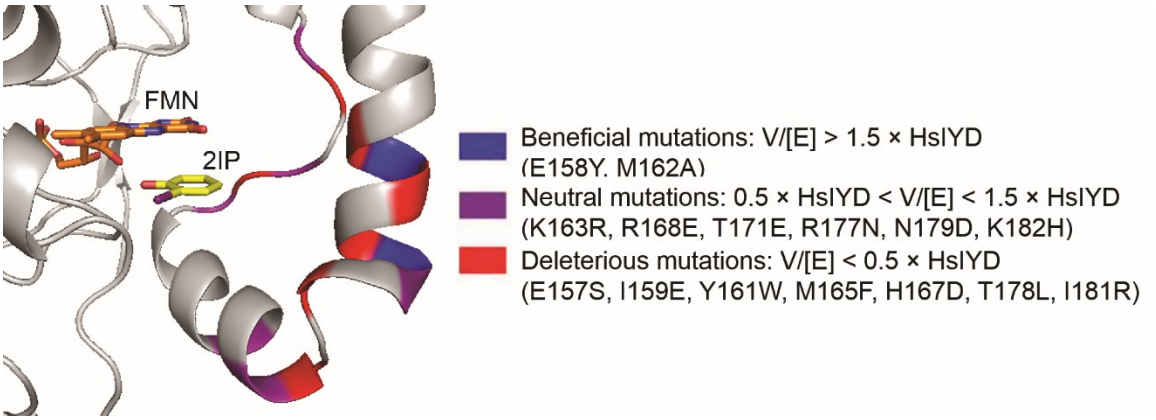

Figure 2-4 Effects of individual substitutions on HsIYD that combine to form UD08 mapped onto the model complex of HsIYD•2IP. See Appendix Table A7 for details. This figure was modified from Sun, Z.; Rokita, S. E.[60]

Interestingly, summing the effects of all 15 mutations (V/[E] measured with 0.5 and 1 mM 2IP) would generate a variant that decreased the 2IP deiodination activity of HsIYD by 25-fold. Defying this prediction, the activity of UD08 (V/[E] measured with 0.5 and 1 mM 2IP) actually increased 4.5-fold experimentally compared to the wildtype enzyme. This non-additivity shows that the effects of these mutations are dependent on the specific protein environment-a phenomenon known as epistasis.[90] Although the exact molecular basis of epistasis is still not fully understood, mutations interacting with each other, either directly or indirectly, tend to be epistatic.[90,91] The 15

mutations of UD08 are all confined locally within the lid and as a result interactions between mutations are highly likely. Epistasis could greatly frustrate protein engineering by accumulation of single mutations since the fitness landscape becomes rugged and the outcome of combining mutations would not be predictable.[89] In contrast, Rosetta is able to offer multiple mutations simultaneously (as in the case of UD08) and may serve as a more efficient strategy to explore a rugged fitness landscape of active site lids like that of HsIYD.

A variant DM01 combining the two beneficial mutations, E158Y and M162A, was generated from HsIYD. These two mutations individually increased the 2IP deiodination activity of HsIYD by 3.0- and 2.7-fold, respectively and a simple addition of the two implied an 8-fold increase. However, the DM01 just increased the activity by 3.5-fold and again demonstrated epistasis. With 2IP as substrate, the k_{cat} of UD08 and DM01 was nearly the same and K_M differed only by 1.5-fold (Table 2-2). Therefore, the two beneficial mutations together are responsible for nearly 80% of the rate increase of 2IP deiodination by UD08 compared to HsIYD. Interestingly, DM01 binds I-Tyr even 3-fold tighter and deiodinates I-Tyr 3.7-fold more efficiently than HsIYD, resulting in no net change in the substrate selectivity from HsIYD (Table 2-3). Interestingly, these two mutations (M162A more frequently) are observed among natural IYD homologs (Appendix Figure A2). E158Y could possibly stabilize the α-helix by participating in a π-π interaction with a nearby W180 (within 4.5 Å) and M162A could potentially decrease the solvent exposed hydrophobic area of the sidechain (Appendix Figure A6(A)). Since the two mutations are surface exposed and away from the zwitterion recognition site, their beneficial effects are likely independent of the presence of either substrate.

2.3.5 Extremely low evolvability of E157 in DM01 highlighted the importance of side chain interactions:

The two beneficial mutations (E158Y and M162A) in UD08 are both located more than 5 Å away from 2IP in the model structure. In contrasts, none of the five mutations in UD08 within 5 Å of 2IP are beneficial on the context of HsIYD. This is surprising since residues near the substrate

binding site are intuitively "hot spots" for designing productive enzyme-substrate interactions. E157 is one of the three zwitterion recognition triad and is strictly conserved in all IYD homologs (Appendix Figure A2).[29] Previous study showed that even a similar substitution of Glu to Gln at this position in IYD from *Drosophila melanogaster* (DmIYD) decreased the k_{cat}/K_M of I-Tyr deiodination by at least three orders of magnitude.[28] However, with 2IP as substrate, this position is facing hydrophobic aromatic ring of 2IP and should favor hydrophobic substitutions than charged residues. Therefore, E157 could potentially be evolvable as a "hot spot" to improve 2IP deiodination. To evaluate the evolvability of E157, site saturation mutagenesis was performed at this position on the context of DM01. DM01 was chosen as the parent enzyme so that any potential activity increase can be made on top of previously identified beneficial mutations. The evolvability here is defined as the ability to promote 2IP deiodination via mutagenesis.

Nineteen common amino acid substitutions at E157 of DM01 were constructed by site directed mutagenesis and expressed and purified similarly with the variants generated by Rosetta design (Appendix Figure A7). The yield of the E157K variants was 3-4 times less compared to the rest variants including the E157R as judges by SDS-PAGE and UV-vis spectroscopy. The activity of the site saturation mutations was again assayed with 0.5 mM and 1 mM 2IP as described in section 2.3.3 (Figure 2-5 and Table A8). Defying our expectation, E157 in DM01 had extremely low evolvability as only E157D slightly increased the activity by 1.3-fold. All the other mutations are deleterious with at least 2-fold activity decrease. The importance of a small, negatively charged residue at this position to 2IP deiodination is quite counterintuitive. Asp is typically an α-helix "breaker"[66] and its small size is not expected to facilitate tight packing around 2IP. In addition, a negatively charged residue would not promote interactions with the hydrophobic ring of 2IP. Further defying expectations, large, hydrophobic substitutions at E157 generally conferred lower activity than polar substitutions. This might partly explain the failure of guided design approach in which Rosetta was specifically instructed to install large, hydrophobic substitutions at or near E157.

To check if Rosetta simulation can reproduce the experimentally observed effects of E157 mutations, the stability of the DM01•2IP complex with E157 substitutions was evaluated by Rosetta (Appendix Figure A8**)**. Although the stability of these variants calculated by Rosetta did not precisely agree with the experimental activity profile, Rosetta still favored a negatively charged residue at this position over other substitutions and performed far better at predicting the deleterious effects of bulky, hydrophobic substitutions than intuition.

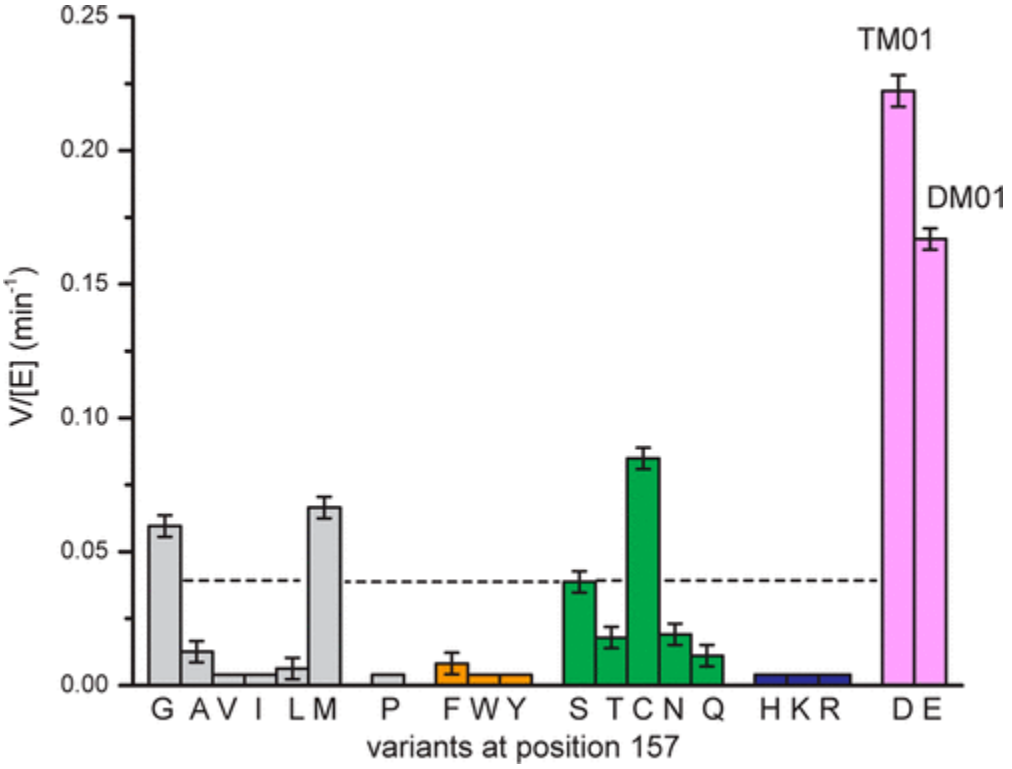

Figure 2-5 Deiodination activity of DM01 variants with substitutions at E157. Bars were colored by the chemical properties of the amino acid side chains with gray as non-polor, orange as aromatics, green as polar, blue as positively charged, and pink as negatively charged. The dashed line represents the activity level of HsIYD. The values of V/[E] were measured with 1 mM 2IP and represent the average of two independent trials. The error bar represents either the range of two independent measurements or three times the background of the assay (0.004 min^{-1}), whichever one is larger. This figure was originally published in Sun, Z.; Rokita, S. E.[60]

The substrate binding and steady state kinetics were then evaluated for a triple mutation variant TM01 combining DM01 and the only more beneficial substitution at E157 (E157D/E158Y/M162A on the context of HsIYD). With 2IP as substrate, TM01 mildly increased

the k_{cat}/K_M by 1.6-fold compared to that of DM01 (Table 2-2), which was mainly contributed to a decrease in K_M. The response of TM01 to I-Tyr is more dramatically changed compared to that of DM01. TM01 binds I-Tyr 240-fold less tightly and deiodinates I-Tyr 12-fold less efficiently. The magnitude of the activity decrease is, however, not as significant as the 10^3-fold activity drop with the Glu to Gln mutation in DmIYD.[28]

The extremely constrained evolvability of E157 may originate from its extensive interactions with nearby residues. E157 could potentially interact with N160 and K182 as shown in the model structure of HsIYD•2IP (Appendix Figure A6(B)). The salt bridge between K182 and E157 could shield the charges of both residues facing the hydrophobic ring of 2IP. The hydrogen bonding between E157 and N160 could also prevent the Asn from interacting with the helix backbone and cause its destabilization.[66] The unguided designs preserved these interactions by coevolution of E157D/S and K182H (Figure 2-2). In contrast, K182 was fixed in the guided design and E157 was restricted to hydrophobic substitutions and thereby disrupting the interactions between E157, N169, and K182. Again, the results demonstrated that the effect of single mutations on the active site lid is strongly dependent on the context. It has been shown that the rate of amino-acid substitution though out the evolution of natural enzymes is an order of magnitude slower compared to what is expected without epistasis.[92] Therefore, epistasis is likely a common feature for protein evolution. While it is difficult to bypass the effect of epistasis by rational design, Rosetta is able to overcome such limitation by exploring a much bigger sequence space with coordinated substitutions.

2.3.6 Unguided Rosetta design changed the responsiveness of the active site lid towards 2IP:

Rosetta was employed to stabilize the active site lid of HsIYD in its closed conformation with 2IP bound in hope to increase its activity towards 2IP. To verify if Rosetta indeed generated variants that stabilized the active site lid in response to 2IP, the conformation of the active site lids of HsIYD and its variants UD08, GD02, and DM01 was probed by limited proteolysis. The

resistance to proteolysis can be used to probe flexible regions of proteins since such regions are more accessible to the active site of proteases and thus are preferentially digested over more compact and structured regions.[93] To prove the principle, if the active site lid of HsIYD is closed into a compact and structured conformation by binding of a substrate, the resulting enzyme•substrate complex should confer more proteolytic resistance than the substrate free enzyme.

In the absence of substrates, HsIYD was digested into two major digestion products, a ~16 kD peptide and a ~13 kD peptide, as separated and shown by SDS-PAGE (Figure 2-6). To identify the site of proteolysis, the two digestion products were extracted from the gel and analyzed by mass spectrometry. Characterization of the ~13 kD digestion product was not successful due to low signal-to-noise ratio. However, the ~16 kD digestion product was identified as three similar but distinct peptide fragments whose masses correspond to those produced by alternative cleavage at positions K163 and R164 (Appendix Figure A9, Figure A10 and Table A9). These two residues are in the middle of the active site lid which is expected to undergo a disorder to order transition responding to I-Tyr binding (Figure 2-7).

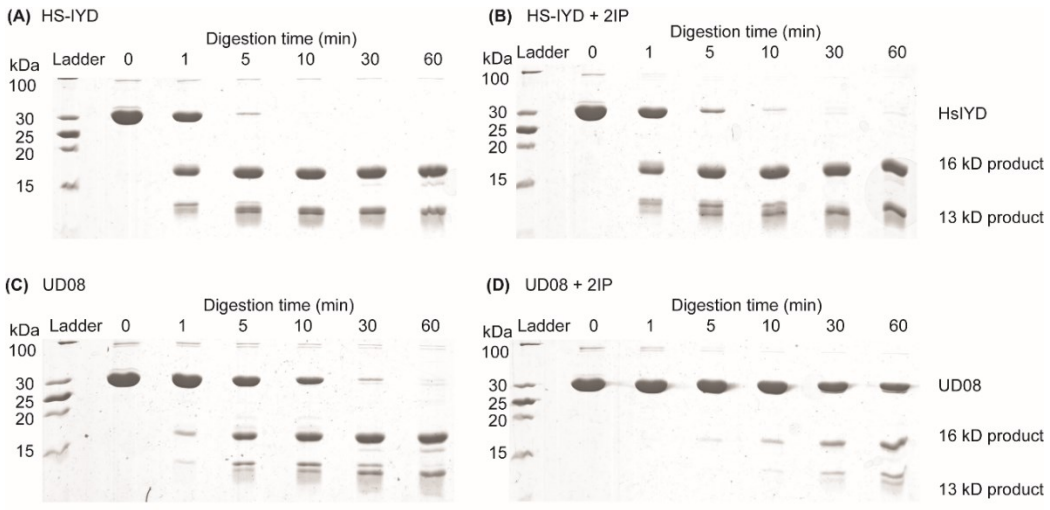

Figure 2-6 Limited proteolysis of HsIYD and UD08 in the absence and presence of 2IP analyzed by SDS-PAGE. (A) substrate-free HsIYD; (B) HsIYD in the presence of 10 mM 2IP; (C) substrate-free UD08; (D) UD08 in the presence of 10 mM 2IP. This figure was originally published in Sun, Z.; Rokita, S. E.[60]

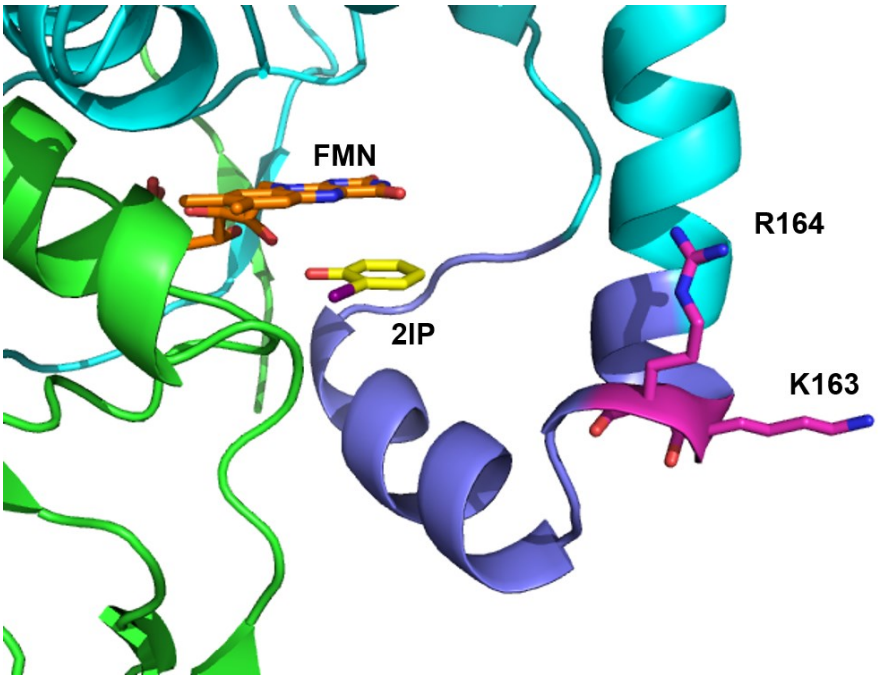

Figure 2-7 Sites of trypsin proteolysis on HsIYD. The digestion sites K163 and R164 are shown in magenta. Green and cyan represent the two identical polypeptides of the homo dimer. The active site lid is colored in blue. FMN and 2IP are shown by orange and yellow sticks. This figure was modified from Sun, Z.; Rokita, S. E.[60]

The remaining undigested HsIYD over time was quantified by densitometry and fitted into a first-order decay to obtain the half-life of HsIYD in limited proteolysis (Appendix Figure A11). In the absence of substrates, 50% of HsIYD was digested in as short as 1.5 min (Figure 2-8). The presence of I-Tyr greatly increased the resistance of HsIYD towards trypsin digestion by at least 160-fold, as expected by the ability to induce the closure of the active site lid (Figure 2-8). In contrast, addition of 2IP to the digestion reaction only marginally protected HsIYD by 1.2-fold (Figure 2-6 and Figure 2-8). Control experiments showed that 100 μM I-Tyr had no effect on the innate proteolytic activity of trypsin while 10 mM 2IP suppressed its activity by only approximately 1.3-fold (Appendix Figure A12). Therefore, the 1.2-fold protection 2IP afforded to HsIYD is merely a result of inhibition of trypsin rather than 2IP induced conformational change of the lid. The results are consistent with the previous crystallographic studies showing that binding of I-Tyr but not 2IP induces the disordered lid of IYD to form the ordered helix-turn-helix motif.[31,32]

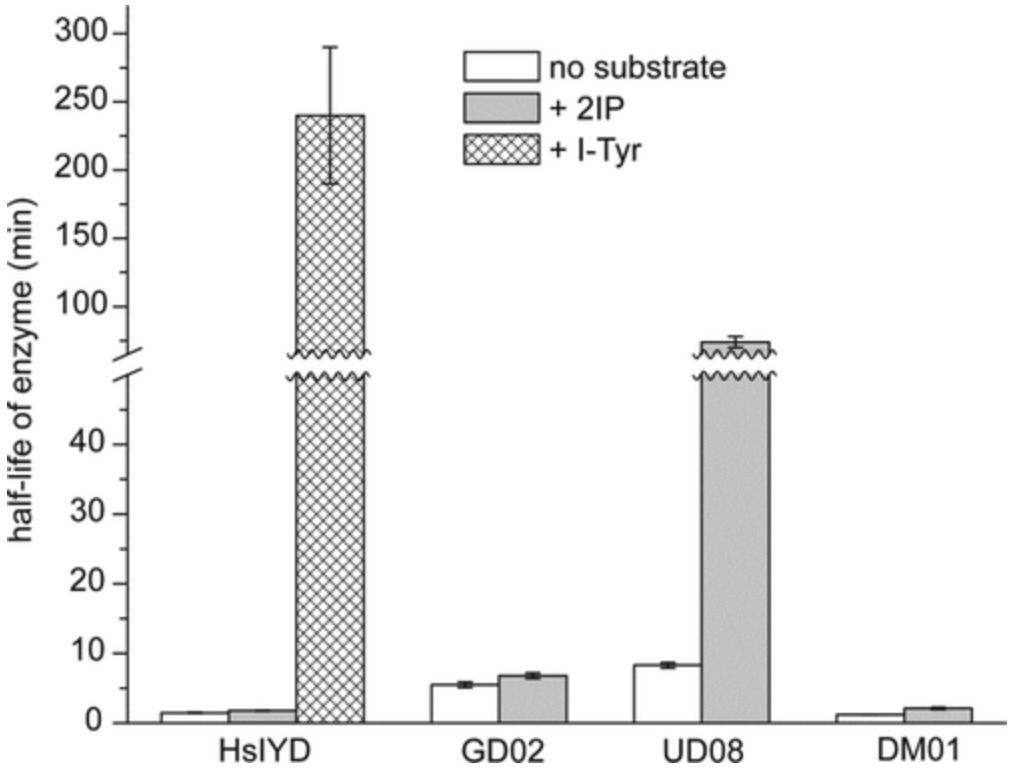

Figure 2-8 Half-life of HsIYD and its variants in limited proteolysis. These values and error bars were obtained from fitting two independent measurements as one curve. This figure was originally published in Sun, Z.; Rokita, S. E.[60]

The accessibility of the active site lids of HsIYD variants was then evaluated similarly as the wildtype enzyme. Even in the absence of ligand, UD08, the variant with the largest improvement of binding affinity and deiodination efficiency towards 2IP, was already more protected against trypsin digestion by 5.6-fold than HsIYD (Figure 2-8**)**. The gain in resistance to proteolysis for UD08 is not a result of a shift in the indicated digestion sites since one of the digest sites of HsIYD R164 was retained in UD08 while the other one K163 was mutated to an Arg which was still a preferred site for trypsin. Moreover, the size of the digestion products of UD08 was comparable to that of HsIYD (Figure 2-6). Therefore, the gain in resistance to proteolysis for UD08 is more likely a gain in structure for the lid of UD08 in the absence of ligand. More importantly, the presence of 2IP further increased the resistance of UD08 to trypsin by 9-fold (Figure 2-6 and Figure 2-8), which is far greater than the inhibitory effect of 2IP on the trypsin activity. These

results are best explained by the ability of the active site lid of UD08 to interact with 2IP and be stabilized it into a more structured conformation as predicted by Rosetta.

The guided design GD02 which had no measurable activity towards 2IP also showed similar protection from trypsin direction by 3.7-fold compared to HsIYD in the absence of 2IP (Figure 2-8). Both trypsin digestion sites in HsIYD are also present in GD02. Therefore, the lid of GD02 likely also gained structure compared to that of HsIYD in the absence of 2IP. However, unlike the case of UD08, the presence of 2IP did not increase the trypsin resistance of GD02 to a significant extent. This is consistent with the fact that GD02 decreased the binding affinity towards 2IP by 2-fold compared to that of HsIYD. Therefore, the lid of GD02 is not able to respond to 2IP and be stabilized further, despite gaining structure mildly in the absence of 2IP.

The double mutation variant DM01 accounts for nearly 80% of UD08's 2IP deiodination activity increase. Yet, the trypsin digestion patterns of DM01 were nearly identical to that of HsIYD both in the absence and presence of 2IP (Figure 2-8**)**. Therefore, DM01 did not show any protection against trypsin despite improved 2IP deiodination relative to HsIYD. In contrast to the 15 substitutions in UD08 that induced a drastic change in the responsiveness of the lid from I-Tyr to 2IP, the double mutation in DM01 most likely stabilized the lid in a more subtle fashion which is beneficial to both 2IP and I-Tyr deiodination as discussed in Section 2-3-4.

Overall, only the unguided Rosetta design demonstrated the ability to change substrate selectivity of HsIYD and trigger a disorder to order transition of the active site lid responding to 2IP. Since the protection of UD08 from trypsin digestion by 2IP is already approaching the level demonstrated by HsIYD and the native substrate I-Tyr, further stabilization of the lid with 2IP bound is unlikely to significantly improve the activity. This might be more successfully approached by focusing on subtle optimization of the active site just as the two mutations forming DM01 improved activity without a conformational change of lid in response to 2IP.[94,95]

2.4 Summary:

To generate an efficient dehalogenase to remediate toxic halophenols, substrate specificity of HsIYD was challenged by computational design to accept an unnatural substrate 2IP. The intrinsically disordered lid of HsIYD was redesigned by Rosetta's fixed backbone design to induce a disorder-to-order transition of the lid responding to the presence of 2IP rather than the natural substrate I-Tyr. While a guided approach based on stabilizing the secondary structures of the closed lid failed to improve 2IP deiodination, success was obtained when Rosetta was allowed to sample all amino acids without restriction. This unguided approach successfully identified three variants promoting 2IP deiodination, the best of which exhibited a k_{cat}/K_M that was 4.5-fold than that of HsIYD. The native activity of HsIYD on I-Tyr was simultaneously suppressed 10^4-fold by this variant UD08. Furthermore, only the unguided design demonstrated the ability to change the responsiveness of the active site lid from I-Tyr to 2IP. When rational based engineering of the lid is frustrated by the strong epistasis of lid mutations resulting from extensive side-chain interactions, Rosetta is able to overcome such limitation by offering coordinated mutations simultaneously.

Chapter 3 Engineering IYD from *Haliscomenobactor hydrossis* towards a halophenol dehalogenase via computational design

3.1 Introduction:

The attempt to engineer HsIYD via computational design to detoxify halophenols was mildly successful. Redesigning the active site lid of HsIYD which controls the substrate selectivity using Rosetta improved the deiodination efficiency of a model halophenol-2IP by 4.5-fold while diminishing the activity towards the native substrate I-Tyr by 2×10^3-fold. Moreover, Rosetta demonstrated the ability to change the responsiveness of the active site lid towards 2IP and induce a disorder-to-order transition of the lid in the presence of 2IP. Despite the success, the 2IP deiodination activity of the best performing variant is still three orders of magnitude lower than the native activity of HsIYD with I-Tyr and is far from practically applicable. Thus, more active variants towards halophenols are required.

As mentioned in Chapter 2, the advantage of Rosetta over rational design or accumulation of random mutations is the ability to explore a much larger sequence space by offering many coordinated mutations simultaneously. Two different approaches to further enlarge the sequence space Rosetta can navigate were described in this chapter. In the first approach, instead of sampling every position on the active site lid, the design was focused on a few "hot spots" that are typically responsible for catalysis and substrate recognition. Despite that the degree of freedom is narrowed, the number of possible variants Rosetta can evaluate with the same computational cost will be greatly increased. Rosetta has been used to successfully improve enzyme selectivity towards non-native substrates by redesigning substrate-enzyme interactions at restricted positions.[58,96] In a different approach, the sampling space of Rosetta was broaden by relaxing constrains on backbone conformation of the lid. When HsIYD was engineered as described in Chapter 2, Rosetta was restricted to explore sequences that could stabilize the lid in a closed conformation in the presence of 2IP. This conformation, however, is evolutionarily optimized to specifically support

haloptyrosine dehalogenation. It is possible that alternative compact conformations of the lid are able to or even better to support halophenol dehalogenation. Rosetta has also demonstrated success with such a loop remodeling approach to switch substrate selectivity of human guanine deaminase or improve activity of a de novo designed Diels-Alderase.[45,47]

In this chapter, both approaches described above were utilized to engineering a new parent sequence HhIYD in collaboration with Prof. Jeffrey Gray (Johns Hopkins University). HhIYD is from the bacterium *Haliscomenobacter hydrossis*, a species commonly found in water after sewage treatment and possibly involved in the degradation of water pollutants.[97] The structural and functional analysis of HhIYD recently became available.[32] Similar to HsIYD, HhIYD also favors I-Tyr as a substrate over 2IP by 10^4-fold. However, HhIYD is much easier to express and purify as it does not need a SUMO tag to be expressed in soluble form. Although 2IP still cannot induce the lid of HhIYD to close, it binds HhIYD ~ 20-fold tighter than it binds to HsIYD. As a result, it might be easier to improve the interactions between HhIYD and 2IP. HhIYD was first redesigned at nine residues near the hydrophobic edge of 2IP to improve enzyme-2IP interaction. This approach obtained limited success by increasing the 2IP deiodination activity of HhIYD by only 2-fold. To further improve 2IP deiodination, the lid of HhIYD was substituted by shorter loops from PDB that can potentially form a more structured lid with 2IP bound. Remodeled lids of 15 and 16 amino acids long all failed to support 2IP deiodination. Despite such failure, Rosetta again demonstrated its ability to stabilize more structured lids of alternative backbone conformations from the native lid in the presence of 2IP as shown by limited proteolysis.

3.2 Materials and methods:

3.2.1 Computational design:

All Rosetta simulations were carried out via Rosetta 3 with REF15 as the default energy function by the lab of Prof. Gray.[53,84]

(1) Preparation of the starting structure:

The starting structure of HhIYD•2IP was prepared with the Fastrelax method by Morgan Nance of the Gray lab.[98] Briefly, the coordinates of the β-carbon and zwitterion of I-Tyr in the co-crystal structure of HhIYD and I-Tyr (PDB 5KO8) were deleted to generate an initial model of the HhIYD•2IP complex.[32] This initial model was then optimized by Rosetta's Fastrelax protocol with rounds of sidechain repacking and minimization. The final output (see Figure 3-1) was used as the starting structure of HhIYD•2IP for lid redesign. Parameterization of I-Tyr, 2IP, and FMN was performed following the Rosetta user's guide as described in Section 2.2.1.[99] The geometries of these small molecules were calculated by Gaussian 09 with the basis set 6-311+g(d).[100] The iodine atom was calculated by a separate basis set-LanL2DZ aug-cc-pVTZ-PP. Population analysis of geometry optimized small molecules was performed in Gaussian 09 with the CM05 method to obtain partial charges.[101]

(2) Redesign of HhIYD at selected positions with limited backbone freedom:

Briefly, nine residues in HhIYD within 5 Å of the zwitterion of I-Tyr in the co-crystal structure of HhIYD and I-Tyr (PDB 5KO8)[32] were varied by Rosetta with a protocol modified from the Fastrelax used to prepare the starting structure (Figure 3-1) by Morgan Nance of the Gray lab. In the original Fastrelax protocol, side chains were repacked while the backbones were minimized. For redesigning HhIYD, the nine residues were allowed to mutate while all other side chains were repacked and the backbones were minimized. This protocol offered some backbone freedom during design. However, the backbone movement provided by minimization was very subtle. The RMSD between the starting model and the designs was generally less than 0.5 Å which was very similar to those of the previous fixed backbone designs. A total of 10,000 independent designs were generated by this protocol. These designs were first evaluated by two in silico analyses: forward folding and ligand docking. The forward folding experiment checks the ability of the new sequences to refold to the desired structure by Rosetta's de novo loop-modeling methods when the constraints of backbone conformation are removed.[47,102] Ligand docking predicts the ability of the

redesigned active site to bind 2IP in the desired conformation.[103] Variants succeeded in both experiments were ranked by total Rosetta energy and Fpocket score which is an algorithm detecting cavities in the active site to evaluate atom packing around 2IP.[104] Finally, the top five designs by total Rosetta energy and by Fpocket score were manually evaluated for sequence redundancy. Seven designs with the most sequence diversity were selected for experimental characterization.

(3) Loop remodeling of the lid:

Loop remodeling of the lid was performed by a loop hash method by Drew Morley and Dr. Shourya Burman of Gray lab.[98] Briefly, a library of loop segments containing 15 amino acids was derived from PDB. This libraries was queried to find loops with terminal coordinates matching those of the N- and C-terminal of HhIYD's lid in the HhIYD•2IP complex (20 amino acid, S94-D113). The backbone of the lid was then substituted by those of the matching loops identified. Kinematic closure (KIC) protocol was used to ensure the closure of the loop termini onto the rest of the protein.[105] The sequences of the new lids were subsequently redesigned using the Fastrelax protocol described in the part (2) to optimize interactions with 2IP and the rest of the protein. Finally, 50000 independent structures generated by this approach were filtered by SASA of the protein and 2IP, forward folding and ligand docking as described before. Only 1 variant passed all tests and was selected for experimental characterization.

Variants containing 16 amino acid lids were remodeled in a similar fashion. However, one residue in the middle of the newly substituted loops was mistakenly fixed during the design and therefore still retained the amino acid from the wildtype sequences. Moreover, a residue from the native enzyme immediately after the C-terminus of the loop was subjected to the sequence redesign even through it was not a part of the new loop. As a result, 17 amino acids in total were actually mutated during the sequence redesign stage. Six variants was selected as described before for experimental characterization.

3.2.2 Cloning:

The sequences encoding the active site lid (residues 161-177) and a nearby flexible loop (residues 200-208) of HsIYD were deleted via sequence ligation independent cloning and the termini from both deletions were linked together respectively to generate the HsIYD_Δlid/loop variant.[71] The plasmid pET24a carrying HhIYD with a C-terminal $(His)_6$ tag was described previously.[32] All variants of HhIYD redesigned at selected positions were generated by site directed mutagenesis.[69,70] The 15-mer loop remodeling design J3736 was constructed by sequence ligation independent cloning as described in 2.2.2.[71] The 16-mer loop remodeling designs were generated by site directed mutagenesis,[69,70] overlap extension PCR,[106] and Q5® site-directed mutagenesis (New England Biolabs).

All DNA oligonucleotides used for cloning were synthesized by IDT and Sigma (see Appendix Table B1 for a list of oligonucleotides). PCR was performed with Phusion High-Fidelity DNA polymerase (Thermo Fisher Scientific). The DNA sequences of all variants were verified by Sanger sequencing (Genewiz).

3.2.3 Protein expression and purification:

All variants were heterologously expressed as described in 2.2.3. The HsIYD_Δlid/loop variant was purified as follows. Frozen cell pellets (from 500 mL culture, ~ 4 g) were thawed at room temperature and resuspended in ~ 25 mL cell lysis buffer (50 mM sodium phosphate, 500 mM sodium chloride, 10% glycerol, 25 mM imidazole, 0.5 mM TCEP, pH 8.0) by vortex. From then on, all procedures were done at 4 ºC unless otherwise noted. Cells were lysed by an EmulsiFlex-C3 homogenizer (Avestin) with 4 passes at ~17000 psi. FMN was added to the lysate to a final concentration of ~ 300 μM to enhance the occupancy of the cofactor in the protein. Cell debris was removed by centrifugation at 45000×g for 1 hour. The supernatant was mixed with 3 mL Ni-NTA resin (Thermo Fisher Scientific, pre-washed with 5 volumes of cell lysis buffer) on a rotary shaker for 30 min. The resin with His-tagged protein bound was loaded onto a column and

cell lysate was allowed to flow through. The column was then washed with 10 column volumes of cell lysis buffer and 5 column volumes of washing buffer (50 mM sodium phosphate, 500 mM sodium chloride, 10% glycerol, 60 mM imidazole, 0.5 mM TCEP, pH 8.0). Proteins were finally eluted from the column with 4 column volumes of elution buffer (500 mM sodium chloride, 50 mM sodium phosphate, pH 8.0, 10% glycerol, 250 mM imidazole, 0.5 mM TCEP). ULP1 protease (40 μg) was then added to eluted proteins to cleave the SUMO tag overnight. The next day proteins were concentrated with a 50 kD molecular weight cut off spin filter (Amicon) and passed through a gel filtration column (Sephacryl S-200HR, GE Healthcare) equilibrated with 100 mM sodium chloride, 50 mM sodium phosphate, pH 7.4, 1 mM TCEP, and 10% glycerol to remove the cleaved SUMO tag. The purified enzymes were then concentrated, aliquoted, flash-frozen with liquid nitrogen, and stored at -80 °C.

Variants redesigned at selected positions and the 16-mer loop remodeling designs were purified similarly as the DM01 variants with substitutions at E157 as described in Section 2.2.3. The 15-mer loop remodeling design J3736 and enzymes used for limited proteolysis studies were purified to homogenous similarly as the HsIYD_Δlid/loop variant with the following modification. Proteins eluted from the Ni-NTA column were supplied with ~300 μM FMN and incubated on ice for 1 hour to further increase the FMN occupancy in the enzyme. The proteins were subsequently exchanged into storage buffer (50 mM sodium phosphate, 100 mM sodium chloride, 15% glycerol, 1 mM TCEP, pH 7.4) using a gravity driven PD-10 desalting column (GE healthcare) following manufactures' instructions. The proteins were then concentrated, aliquoted, stored in -80 ºC as described in the previous protocol.

Purified enzymes were analyzed by 12% SDS-PAGE with Comassie brilliant blue staining. Enzyme concentration was determined by either UV-vis absorption of enzyme-bound FMN ($\varepsilon_{450\ nm}$=12500 $M^{-1}cm^{-1}$)[74] or quantification of FMN liberated from the enzyme by HPLC (see deiodination activity assay for details) at 445 nm upon denaturation with 4.4% formic acid. The

discrepancy between the two methods was ≤ 10%. The FMN occupancy of highly purified variants was determined by the ratio of enzyme-bond FMN over the total protein concentration as calculated from UV absorption at 280 nm (extinction coefficient estimated by the ExPASy ProtParam tool)[75] after correcting the contribution of A280 from bound FMN (A280/A450 = 1.57).[31]

3.2.4 Binding dissociation constant:

The affinity (dissociation constant) of 2IP to HhIYD and its variants was determined as described in Section 2.2.4.

3.2.5 Deiodination activity assay:

The deiodination activity was measured as described in Section 2.2.5 by quantifying phenol formation by HPLC with Cl-Tyr as an internal strandard.

3.2.6 Limited proteolysis:

Trypsin proteolysis of HhIYD and its variants was performed as described in Section 2.2.6.

3.2.7 Additional software:

Least-square fittings were performed with Origin 2017 (Originlab). All structural illustrations were prepared by Pymol (education version, Schrödinger).

3.3 Results and discussion:

3.3.1 Redesign of HhIYD at selected positions with limited backbone freedom only marginally improved 2IP deiodination:

When HsIYD was engineered, the sequence of the entire active site lid, regardless of active site residues or surface residues, was sampled to stabilize the desired structure. While mutations on the enzyme surface can promote catalysis like the two beneficial mutations in UD08, active site mutations are more likely to support the binding of 2IP by directly interacting with the substrate. Since 2IP and I-Tyr differ by a zwitterion, active site residues around the zwitterion are the potential "hot spots" for switching substrate selectivity. Therefore, nine residues within 5 Å of the zwitterion of I-Tyr in its co-crystal structure with HhIYD (PDB: 5KO8)[32] were redesigned to stabilize a target

model of HhIYD•2IP (Figure 3-1). The number of independent designs was increased from 100 used in HsIYD redesign to 10000 for HhIYD redesign as an attempt to further enlarge the sequence space for Rosetta to sample.

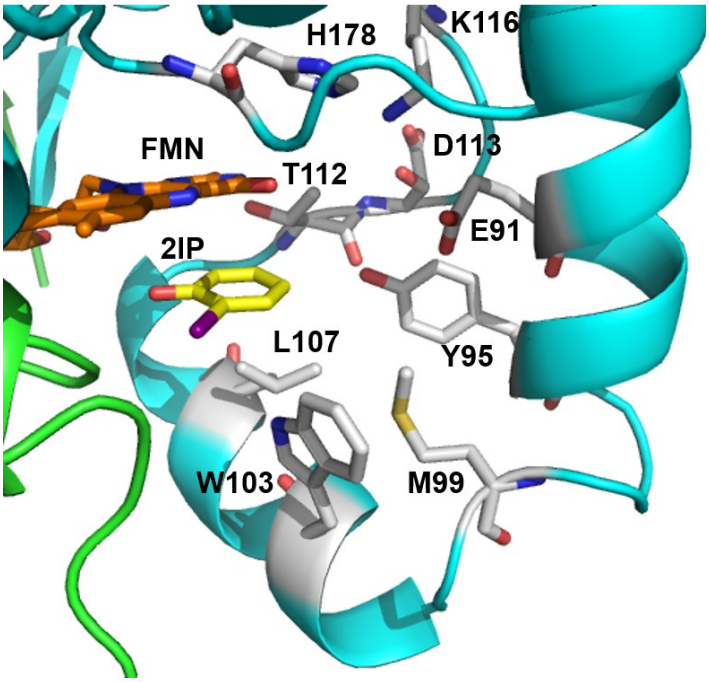

Figure 3-1 Computational model of HhIYD and 2IP with the active site lid closed generated by Rosetta.[53] The two monomers of HhIYD is colored with green and cyan respectively. 2IP and FMN are shown as yellow and orange sticks respectively. Residues (gray) within 5 Å of the zwitterion of I-Tyr in its co-crystal structure with HhIYD were varied by Rosetta.

Such effort, however, did not seem to greatly increase the variability in the designed sequences. Except for M99 and W103, sequences at other seven positions of the total 10000 independent designs converged into one or two amino acid substitutions (Appendix Figure B1). Such high level of convergence still holds when the 10000 designs were narrowed down to ten after applying filters based on the ability of the lid to refold into the desired structure and to stabilize 2IP binding (forward folding and ligand docking simulations, see Materials and Methods for details), total Rosetta energy and packing around 2IP (Figure 3-2). Interestingly, bulky, hydrophobic substitutions were overwhelmingly favored in both top five designs with the highest total energy (BS1-5, ranked by descending order in total energy) and the top five designs with the tightest

packing around 2IP (BF1-5, ranked by descending order in total energy). Such a bias towards large hydrophobic amino acids is expected as they can favorably interact with 2IP's hydrophobic edge and fill the cavity in the active site created by the absence of the zwitterion of I-Tyr (Figure 3-1). However, this contradicts the results of the previous redesign of HsIYD (Section 2.3.5). Hydrophobic substitutions were exclusively disfavored at position E157 (E91 in HhIYD) of the HsIYD variant DM01 due to the disruption of polar interactions between E157 and nearby N160 and K180 (N94 and K116 in HhIYD).[60] While N94 in HhIYD was not subject to redesign, E94 and K116 were always co-mutated in HhIYD variants. Therefore, the polar interaction network in the active site of wildtype enzyme could be substituted with a hydrophobic interaction network in the variants to achieve stabilization of the lid structure and favor the binding of substrates more hydrophobic than I-Tyr. Three of the top five designs in total energy and four of the top five designs in active site packing represented the greatest sequence variability among each group and were selected for experimental characterization.

		91	95	99	103	107	112	113	116	172
HhIYD	(0)	E	Y	M	W	L	T	D	K	H
BS1	(9)	A	V	L	T	W	Y	N	F	M
BS2	(9)	-	F	-	A	F	A	-	-	-
BS3	(9)	-	T	-	T	W	Y	-	-	-
BS4	(9)	-	N	-	T	W	Y	-	-	-
BS5	(9)	-	V	-	T	W	Y	-	-	-
BF1	(9)	F	F	W	W	V	A	N	H	M
BF2	(9)	W	-	M	L	L	-	N	H	-
BF3	(9)	L	-	W	W	L	-	N	N	-
BF4	(9)	L	-	W	W	L	-	T	A	-
BF5	(9)	L	-	Y	F	L	-	N	N	-

Figure 3-2 Sequence of HhIYD and its variants generated by redesigning selected positions. Conserved residues within the subgroup of best total energy (BS1-5) and best packing around 2IP (BF1-5) are labeled with dash (-).Designs selected for experimental characterization are highlighted in red. Total number of mutations that each variant carries are listed in parenthesis.

The seven selected variants were all successfully expressed and purified as soluble proteins with a yield ~2-fold less than that of HhIYD (~15 mg/L culture) (Appendix Figure B2). The enzymes were partially purified for the purpose of initial activity screening and the presence of contaminating proteins would not interfere with quantification of IYD since its concentration was determined by enzyme-bound FMN. Deiodination of 2IP was measured by the same HPLC assay described in Section2.2.5 with 25 μM and 250 μM 2IP. Neither the variants nor HhIYD had measurable activity with 25 μM 2IP (no larger than 0.004 min^{-1}-the detection limit which is three time the background of the assay). With 250 μM 2IP, only BF4 showed 2-fold higher deiodination activity compared to that of HhIYD while all the other designs failed to improve the activity (Figure 3-3). The largest activity increase with these variants is still ~2.5-fold smaller than that of the most activity HsIYD variants (UD08 and TM01).[60] Therefore, redesign of HhIYD residues near the hydrophobic edge of 2IP is not a robust approach to enhance the 2IP deiodination of HhIYD.

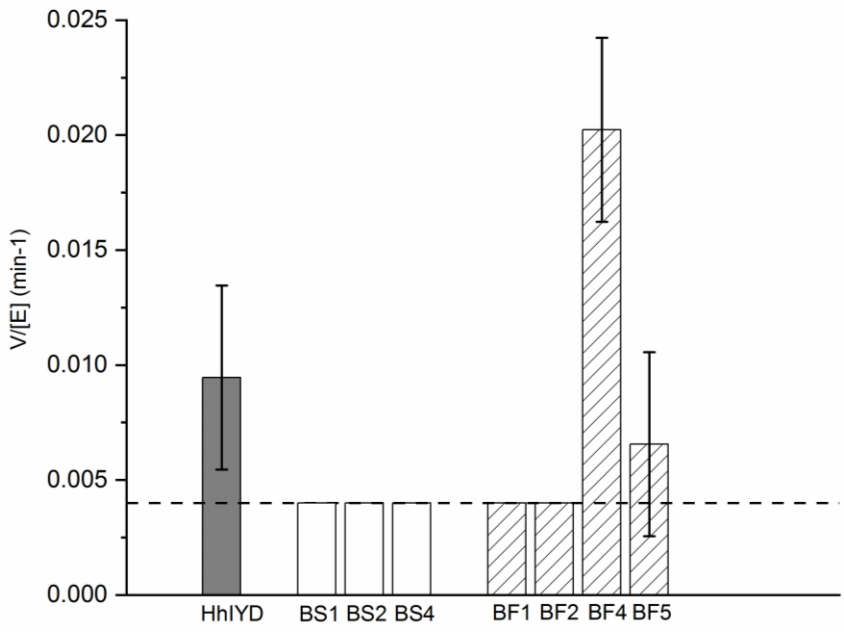

Figure 3-3 2IP deiodination activity of HhIYD and its variants generated by redesign at 9 selected positions. The activity was measured with 250 μM 2IP. The V/[E] represent the average of two independent measurements. The error is either the range of two independent measurements or three times the background of the assay (0.004 min^{-1}, indicated by the dashed line), whichever is larger.

The result of fixed backbone design of HhIYD again contradicted our intuition of promoting enzyme•2IP interactions and stabilizing the closed lid with hydrophobic force. Without I-Tyr, the lid of HhIYD is highly flexible as indicated by the lack of electron density for the lid in the crystal structure.[32] The closed conformation of the lid, despite being highly structured, is actually not a thermodynamically favorable conformation in the absence of ligand. The interactions between the zwitterion and the recognition triad (Glu, Tyr, Lys) likely overcome the thermodynamic barrier of the open-to-close transition of the lid. Hydrophobic interactions, on the other hand, may not be strong enough to support such transition. Since the intrinsic disorder of the wildtype lid is difficult to maneuver, it might be easier to redesign sequences stabilizing a shorter and more rigid loop that can also hold 2IP in the desired conformation in the active site.

3.3.2 HhIYD variants with remodeled lids failed to support 2IP deiodination:[1]

Removing restrictions on backbone conformation allows Rosetta to sample a substantially larger sequence and conformation space and generate alternative loops that may confer the desired non-native activity.[45,47] On the other hand, such an approach is more risky than fixed backbone design since it might induce large conformational changes of the protein and as a result destabilize the enzyme as a whole. Remodeling the lid of HhIYD seems promising since members of the nitro-FMN reductase superfamily including IYD all share a structurally similar dimeric core but have different loops around their active sites to confer diverse catalytic activity and substrate selectivity (Section 1.4 and Figure 1-2).[29,34] In addition, a variant of HsIYD with the active site lid and a nearby flexible loop truncated was successfully expressed as soluble protein (Appendix Figure B3). The yield of this variant was ~ 4-fold less than that of the wildtype enzyme (typically ~ 9 mg/L culture) and its FMN occupancy was only ~ 50% (typically ~ 100% for the wildtype enzyme). The variant showed no quenching of its fluorescence with up to 10 mM 2IP and no deiodination activity with

[1] The cloning and characterization of the 15-mer loop remodeling design J3736 were performed by Shaun Spisak (Johns Hopkins University) and Zuodong Sun.

2IP between 20 μM and 5 mM (no larger than 0.004 min^{-1}-the detection limit which is three time the background of the assay). Despite that this variant is a totally inactive 2IP deiodinase, it demonstrated the stability of the dimeric core of IYD on its own without the presence of the active site lid. Therefore, the active site lid of structurally similar HhIYD is likely to be remodeled without necessarily impairing the overall stability of the enzyme.

The remodeling of the lid started with substituting the entire lid with loop segments of different sizes from PDB via a loophash method.[98] Only loops shorter than the original lid (20 amino acids) were considered since a shorter loop is likely to be more rigid and generally easier to be modeled accurately.[102] However, the loop must be long enough to form a lid which can position 2IP in the active site and exclude bulk solvent. Therefore, loops of 15 and 16 amino acids were chosen as initial attempts to balance these factors. The sequence of the remodeled lid was then optimized by the standard Rosetta Design protocol.[65] The final outputs were filtered by the ability of the lid to refold into the desired structure and to stabilize 2IP binding (forward folding and ligand docking simulations) and by the solvent accessible area of the overall protein and 2IP to assess packing of the lid. Of the 50,000 independent 15-mer loop remodeling variants generated, only one survived all the filtering criteria. Therefore, more non-optimized solutions than the fixed backbone approach might be sampled by the loop remodeling approach, despite that it allows Rosetta to sample a much larger sequence and conformational space.

The new lid of this sole 15-mer variant J3736 is predicted to have a helix-loop structure as shown in Figure 3-4 (see Appendix Figure B4 for sequences). The residues of J3736 near the non-polar edge of 2IP are more hydrophobic compared to those in HsIYD. Such a preference for hydrophobic residues again makes intuitive sense but failed to promote 2IP deiodination when applied on the backbone of the native lid. The variant expressed and generated soluble proteins with a yield (~ 10 mg/L culture) comparable to that of the HhIYD and a FMN occupancy of ~ 96%, which demonstrated that the lid remodeling did not affect the global stability of the enzyme nor the

binding of FMN. The binding affinity of 2IP to J3736 was measured by the same fluorescence quenching assay. The dissociation constant K_d of 2IP to J3736 was estimated to be 149 ± 9 μM and represented a 2.2-fold increase compared to that to HhIYD (67 ± 2 μM).[32] Despite that J3736 is able to bind 2IP tighter than any of the previously studied HsIYD variants in Chapter 2, it did not exhibit any deiodination activity (no larger than the detection limit of the assay, 0.004 min^{-1}) with 2IP concentrations from 25 μM to 5 mM. The result again echoes the previous finding that binding is not sufficient to support deiodination.[32]

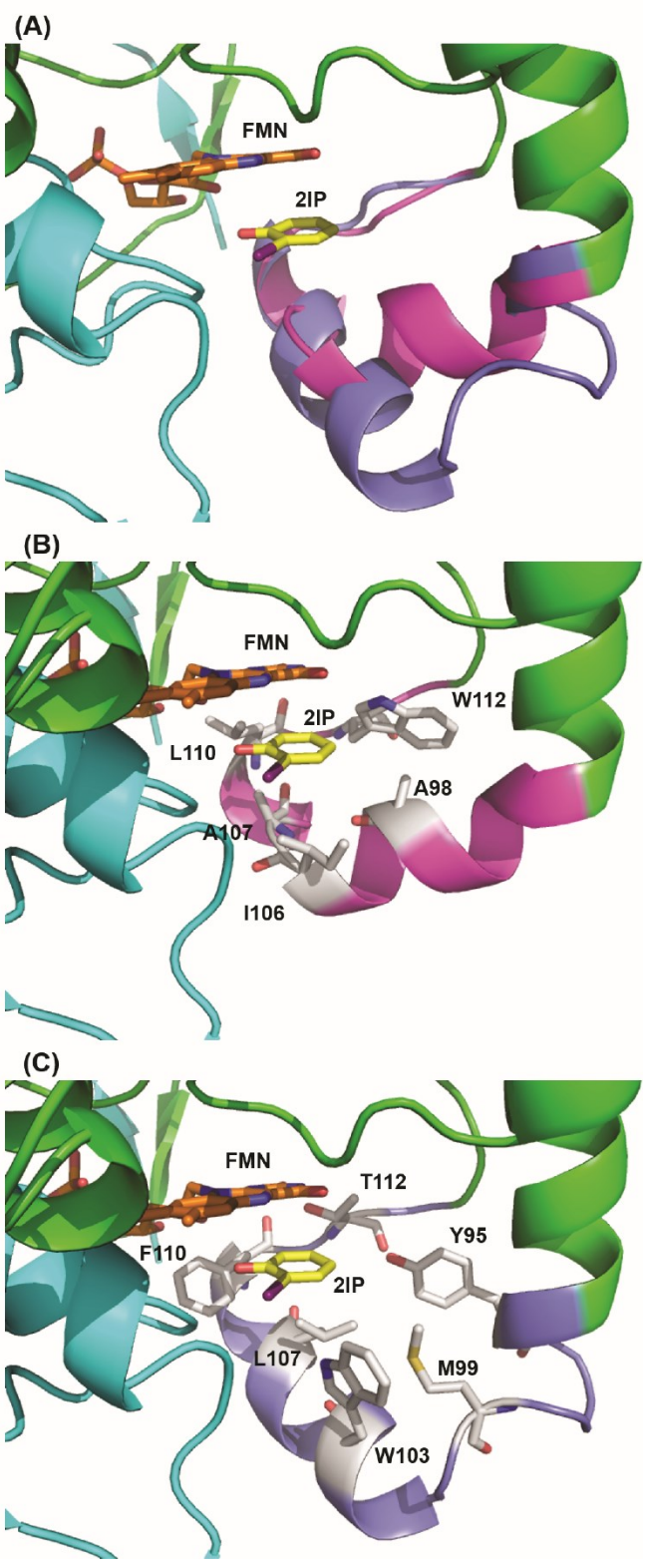

Figure 3-4 Computational models of HhIYD•2IP and the 15-mer loop remodeling variant J3736•2IP generated by Rosetta. (A) Overlay of the two models. The monomeric units of the enzyme were colored with green and cyan. FMN and 2IP are shown in orange and yellow, respectively. The active site lid of HhIYD and the remodeled lid of J3736 were shown in blue and magenta, respectively. (B) Residues (gray) surrounding 2IP's hydrophobic aromatic ring in J3736. (C) Residues (gray) surrounding 2IP's hydrophobic aromatic ring in HhIYD.

Six 16-mer loop remodeling designs were subsequently selected from 50,000 independent designs by criteria similar to those for the 15-mer designs. The six designs can be categorized into three groups based on their predicted structures. Designs 0609, 0479, and 4354 are all predicted to fold into the same conformation (Figure 3-5(A)). Design 0039 has a unique structure that packs most tightly around 2IP by visual inspection (Figure 3-5(B), also Appendix Figure B6). Designs 1719 and 3654 are structurally very similar to the 15-mer design J3736 (Figure 3-5(C) and (D)). All six variants were expressed well as soluble proteins with yields between 10 and 20 mg/L culture. FMN was invariably incorporated into the variants but the occupancy could not be determined since the variants were only partially purified and their 280 nm absorption would be biased by contaminating proteins. Unfortunately no measurable deiodination activity (no larger than 0.004 min^{-1}, the detection limit) was found for any of the 16-mer variants with both 250 μM and 2.5 mM 2IP. The effort of redesigning the lid of HhIYD via loop remodeling so far failed to improve 2IP deiodination.

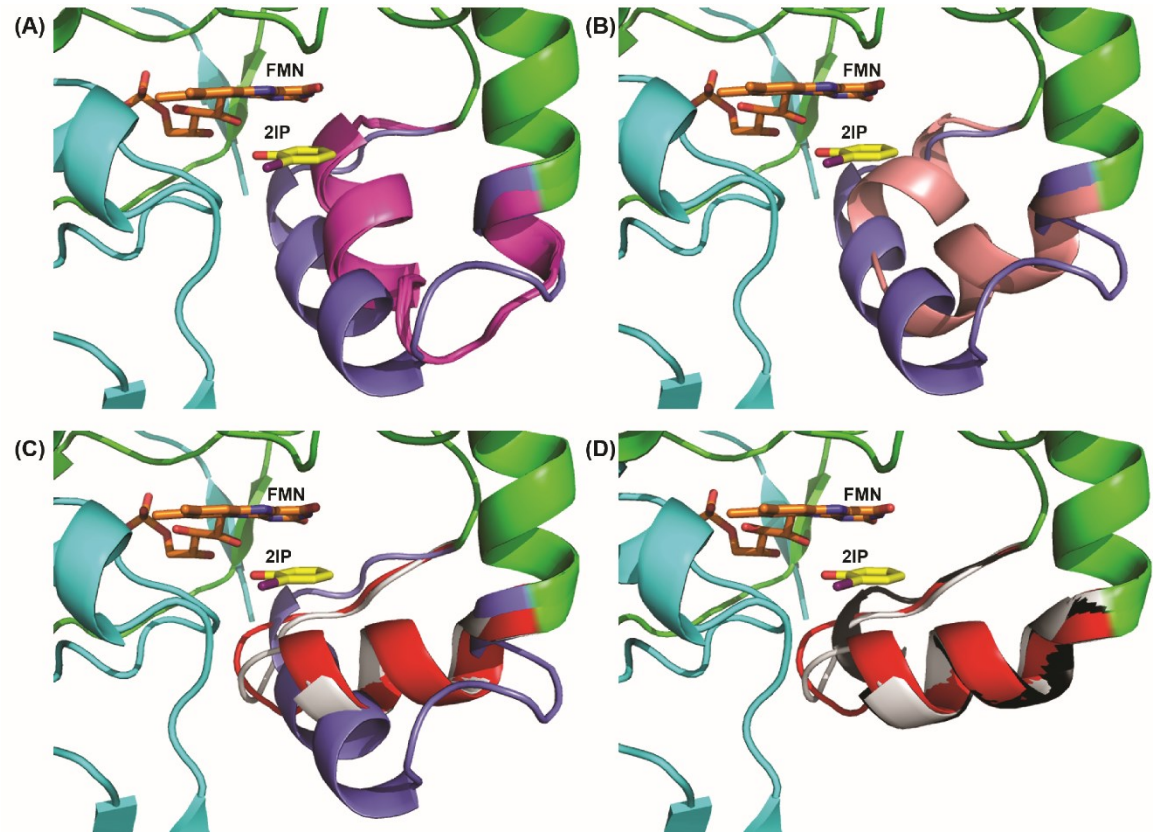

Figure 3-5 Computational models of HhIYD•2IP and the 16-mer loop remodeling variants generated by Rosetta.[53] (A) Overlay of HhIYD•2IP and designs 0609, 0479, and 4354 with 2IP. The monomeric units of the enzyme were colored with green and cyan. FMN and 2IP are shown in orange and yellow, respectively. The active site lid of HhIYD and the remodeled lids of 0609, 0479, and 4354 were shown in blue and magenta, respectively. (B) Overlay of HhIYD•2IP and design 0039•2IP. The active site lid of HhIYD and the remodeled lids of 0039 were shown in blue and pink, respectively. (C) Overlay of HhIYD•2IP and designs 1719 and 3654 with 2IP. The active site lid of HhIYD and the remodeled lids of 1719 and 3654 were shown in blue, red, and gray, respectively. (D) Overlay of designs 1719, 3654, and J3736 with 2IP. The remodeled lids of 1719, 3654, and J3736 were shown in red, gray, and black, respectively.

3.3.3 The remodeled lids of HhIYD variants were more structured than the native lid in the absence or presence of 2IP:

As shown in Section 2.3.6, the lid of UD08, a successful design of HsIYD improved 2IP deiodination, demonstrated a disorder-to-order transition upon 2IP binding.[60] In contrast, the lid of a failed design GD02 was not responsive to 2IP. The lids of selected loop remodeling variants were analyzed similarly to probe whether or not the conformations of their remodeled lids are responsible for the impaired activity of the variants. In the absence of 2IP, more than 90% of HhIYD (5 μg)

was digested within 30 min by 50 ng of trypsin (Figure 3-6(A)) into two major and many minor peptides (shown as two discrete bands in a smear less than 15 kD on SDS-PAGE). However, even ten times more trypsin failed to cleave 5 μg J3736 after 1 hour of digestion (Figure 3-6(B)). Increasing trypsin concentration further by 100 and 1000 times only resulted in minor digestion of J3736. HhIYD and J3736 only differ by their lids and both of their lids have one trypsin digestion site (an Arg, Appendix Figure B5(A) and (B)). Therefore, the ultra-stability of J3736 over HhIYD cannot be explained by a lack of trypsin digestion site. The lid of J3736 most likely has a very rigid conformation that resists trypsin digestion even in the absence of 2IP.[60,93]

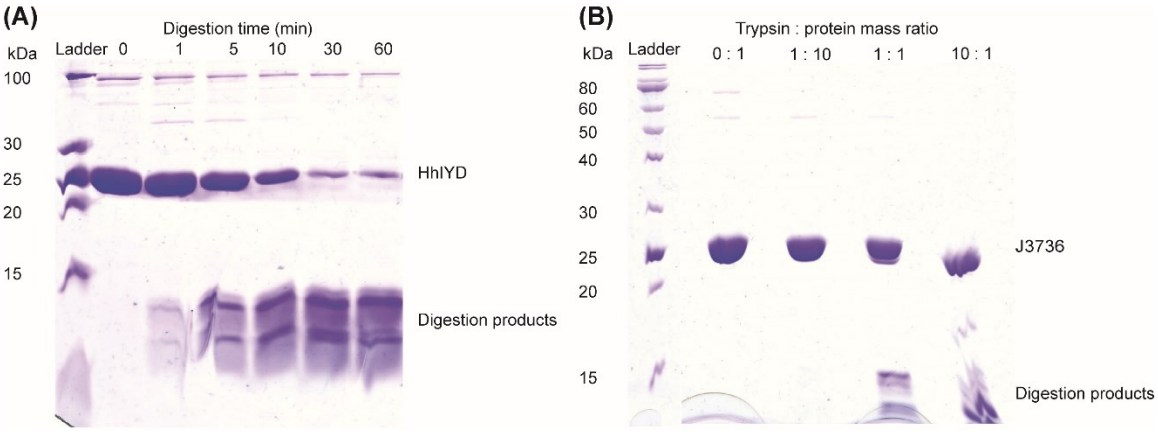

Figure 3-6 Trypsin digestion of HhIYD and J3736 in the absence of 2IP analyzed by SDS-PAGE. (A) Trypsin digestion of HhIYD overtime. The mass ratio of HhIYD to trypsin was 50:1. (B) J3736 digested by different amounts of trypsin. The digestion time in all cases were 1 hour.

Design 0039, the 16-mer loop remodeling variant with the tightest packing around 2IP by visual inspection (Appendix Figure B6), was then digested by trypsin with HhIYD as a control in the absence and presence of 2IP (Appendix Figure B7). The remaining parent protein overtime was fit into a first-order decay from which the half-life of the parent protein was derived (Figure 3-7). The half-life of ligand free 0039 was ~ 2-fold smaller than that of HhIYD, which suggested that the new lid in 0039 was actually more accessible to trypsin than the native lid in HhIYD. This could be a result of greater conformational flexibility of the new lid in the absence of 2IP. However, the greater accessibility of 0039 to trypsin can also be explained by the increased number of digestion

sites from 1 in the lid of HhIYD to 3 in the lid of 0039 (Appendix Figure B5(C)). The presence of 2IP slowed the trypsin digestion of HhIYD by ~ 2-fold (Figure 3-7). This decrease in digestion rate is just a bit more than the inhibitory effect of 2IP on the innate proteolytic activity of trypsin (1.3-fold, Appendix Figure A12). Therefore, 2IP did not significantly increased the trypsin resistance of HhIYD by inducing its active site lid to be more structured. This is also consistent with the lack of electron density for the lid of HhIYD in the co-crystal structure with 2IP.[32] The new lid of 0039, however, gained 5-fold more protection in the presence of 2IP (Figure 3-7), which is significant compared to the simple inhibitory effect of 2IP on trypsin. Therefore, such a gain in protection for 0039 indicates that its lid is induced by 2IP to gain more structure and as a result is less accessible to trypsin.

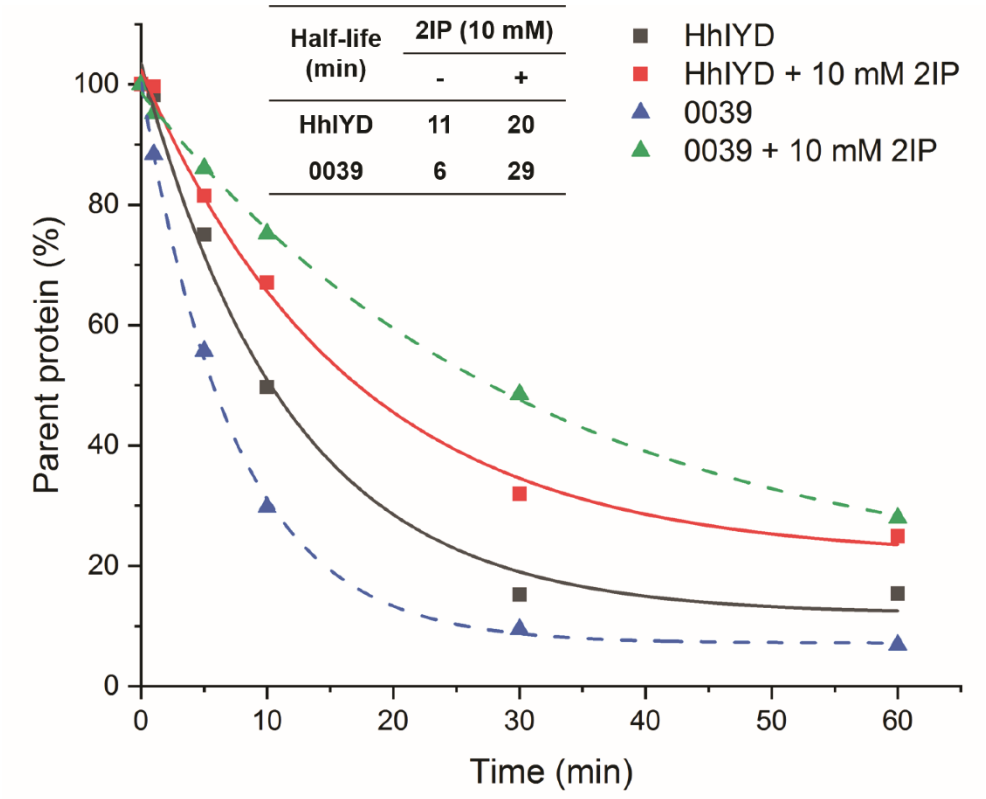

Figure 3-7 The first order decay of the undigested protein in limited proteolysis. The solid lines represent the fitting of remaining HhIYD over time by first order decay kinetics. The dashed lines represent the fitting of remaining 0039 over time by first order decay kinetics. Each data point is a single determination.

In the lid remodeling approach, Rosetta was instructed to replace the native lid of HhIYD with a shorter loop in hope to gain more structure to support 2IP binding. The remodeled lid of the 15-mer design J3736 is indeed much more rigid even in the absence of 2IP. Such structural rigidity, however, did not block the entrance of 2IP to the active site since 2IP can still bind to J3736, albeit ~3-fold less tightly than to HhIYD. Moreover, the remodeled lid of the 16-mer design 0039 is able to gain structure in response to 2IP, resembling the lid of native HsIYD responding to I-Tyr and the redesigned lid of HsIYD variant UD08 responding to 2IP.[60] The gain in trypsin protection of 0039's lid with 2IP is only 2-fold less than that of UD08's lid with 2IP. Yet 0039 has no measurable activity with 2IP while UD08 improved 2IP deiodination of HsIYD by 4.5-fold. Therefore, the result again highlight the ability of Rosetta to create a lid that undergoes a disorder-to-order transition in the presence of 2IP even when the conformation of the new lid is completely different from that of the native lid. The failure of the loop remodeling designs to promote 2IP deiodination is likely not due to a lack of responsiveness to 2IP for the remodeled lids. When the 15-mer loop remodeling variant J3736 was analyzed by ligand docking for its ability to bind 2IP in the target conformation expected for catalysis, multiple alternative conformations of 2IP which deviated from the target conformation were stabilized in low energy enzyme•2IP complexes (Figure 3-8). The result might suggest that the remodeled lid was able to stabilize 2IP conformations that were not productive. This phenomenon is not specific to this one variant but is ubiquitous to all variants generated by fixed backbone design and loop remodeling of HhIYD, which may again explain the low activity of HhIYD variants towards 2IP. It is possible to promote the dehalogenation of halophenols by creating specific enzyme-substrate interactions to stabilize the productive conformation. Since the results of HsIYD and HhIYD engineering demonstrated ineffectiveness of hydrophobic interactions to promote enzyme•2IP interactions, future design should focus on designing polar enzyme-substrate interactions to stabilize the productive conformation. This is difficult for 2IP which does not have many functional groups to support polar interactions.

Bromohydroquinone, the brominated analog of 2IP with a hydroxyl group at the para-position, is potentially a better model compound than 2IP to facilitate the design of more efficient substrate recognition via its additional hydroxyl group.

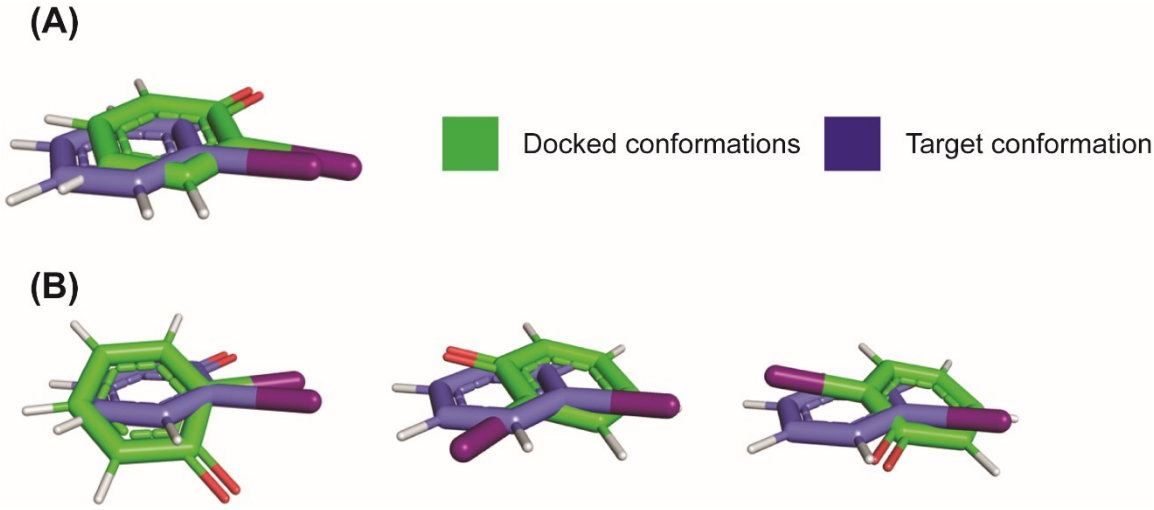

Figure 3-8 Deviation of alternative conformations of 2IP from the target conformation detected in ligand docking of the 15-mer loop remodeling variant J3736. (A) Conformation of 2IP in J3736 and target conformation of 2IP in the starting HhIYD•2IP complex superimposes with each other. (B) Alternative conformations of 2IP in J3736 deviates from the target conformation of 2IP in the starting HhIYD•2IP complex. The carbons in 2IP in the target conformation is colored blue while those in the alternative conformations are colored green. Oxygen and iodine atoms were colored red and purple, respectively.

3.4 Summary:

In this chapter, HhIYD was redesigned to support 2IP deiodination by two computational approaches. These approaches aimed at enlarging the sequence and conformational space compared to that used in the redesign HsIYD described in Chapter 2. The first approach focused on just 9 residues around the zwitterion of I-Tyr in its co-crystal structure with HhIYD. The number of independent designs were also increased by 100-fold compared to that in the fixed backbone design of HsIYD to further increase sampling of the sequence space. The most active variant towards 2IP generated by this approach, however, was only 2-fold faster than the HhIYD. The second design approach was subsequently explored to replace the native lid with shorter loops from the PDB that can potentially form a more structured lid upon binding of 2IP. Variants with remodeled lids of 15

and 16 amino acids rather than the native length of 20 showed many desired properties such as the ability to bind 2IP (despite weaker than the wildtype), to form a much more rigid lid than that of the native enzyme in the absence of 2IP, and to form a lid that can gain structure upon 2IP binding. However, none of the loop remodeling variants exhibited measurable activity towards 2IP. Similarly as in engineering of HsIYD (Section 2.3.6), Rosetta once again demonstrated success in altering the responsiveness of the active site lid of IYD from I-Tyr to 2IP via the lid remodeling approach. However, the target model of IYD•2IP stabilized by Rosetta was derived from the crystal structure of catalytically inactive oxidized IYD and might not lead to productive deiodination as expected. Better guidance for designing a halophenol dehalogenase from IYD might be obtained from the structure of the catalytically active reduced IYD.

Chapter 4 Structural and functional analysis of IYD from *Thermotoga neapolitana*: a thermophilic IYD with unique properties

4.1 Introduction:

The efforts of engineering IYD towards a halophenol dehalogenase via computational design so far produced limited success in improving IYD's activity with the model compound 2IP. However, computational design via Rosetta did demonstrated the ability to stabilize a compact conformation of IYD's active site lid with 2IP bound. This active site conformation is derived from the co-crystal structure of IYD with fully oxidized FMN and I-Tyr and is the best model available. However, it is the fully reduced, not the oxidized, FMN cofactor that supports deiodination. Therefore, the model used previously for IYD•2IP complex might not be productive. The structural information of the fully reduced IYD is needed to uncover possible enzyme-substrate interactions that support active deiodination.

Obtaining such structural information is challenging since the fully reduced FMN is very sensitive to oxygen. As a result, crystals containing fully reduced FMN need to be generated and handled under absolutely anaerobic environments. Previous efforts using sodium dithionite to reduce the pre-grown co-crystals of HsIYD or HhIYD containing the oxidized FMN and an inactive substrate analog F-Tyr failed as the crystals quickly melted.[50] One additional disadvantage of using previously crystallized IYDs to obtain the reduced structure is that all structures of oxidized IYD obtained so far are mid-resolution (2-3 Å). Although pronounced conformational differences have been observed between oxidized flavoproteins and their fully reduced counterparts,[107,108] in many other cases reduction of the flavin cofactor does not change the conformation of the flavoprotein to a significant extent.[109,110] If the differences between the oxidized and reduced structures of IYD are subtle, mid-resolution structures will likely not be able to capture them.

One way to potentially improve the quality of protein crystals is to increase the thermostability of the protein being crystallized.[111] Certain thermophilic bacteria and archaea were found to contain IYD homologs in their genome.[29] Representatives from the themophilic bacteria *Thermotoga neapolitana* (TnIYD) and archaea *Pyrococcus furiosus* (PfIYD) were characterized preliminarily and the results suggested that they could indeed deiodinate I_2-Tyr at 25 °C and, with a higher activity, at 60 °C.[112,113] While most signature residues conserved in mesophilic IYDs are also present in thermophilic IYDs such as the zwitterion recognition triad and a threonine hydrogen bonding to the N5 of FMN modulating its one-electron chemistry, there are marked differences between the two groups (Figure 4-1(A)).[29] First, the active site lid of thermophilic IYDs is one amino acid short than that of mesophilic IYDs, suggesting that the conformation of the lid might be slightly different in thermophilic IYDs. In addition, a loop near the active site (Appendix Figure B3(A)) where the halogen atom of the substrate is positioned in all mesophilic IYDs are completely missing for thermophilic IYDs. This loop is unstructured in ligand free HsIYD and MmIYD but folds into a hairpin like structure when I-Tyr is bound.[31,33] In HhIYD, the loop is structured even in the absence of ligand.[32] Finally, all mesophilic IYDs have N- or C-terminal extensions of various lengths (Figure 4-1(B)) compared to thermophilic IYDs. These N-terminal extensions typically include a membrane association domain (not present in certain invertebrates and lower organisms) and an intermediate domain.[29] Although the functions of the loop near the active site and the intermediate domain are still not clear, they are not absolute requirements for catalysis as thermophilic IYDs can still function as deiodinases without them. Therefore, thermophilic IYDs form a unique subgroup of IYD that represents the minimal structural requirement for the reductive dehalogenation.

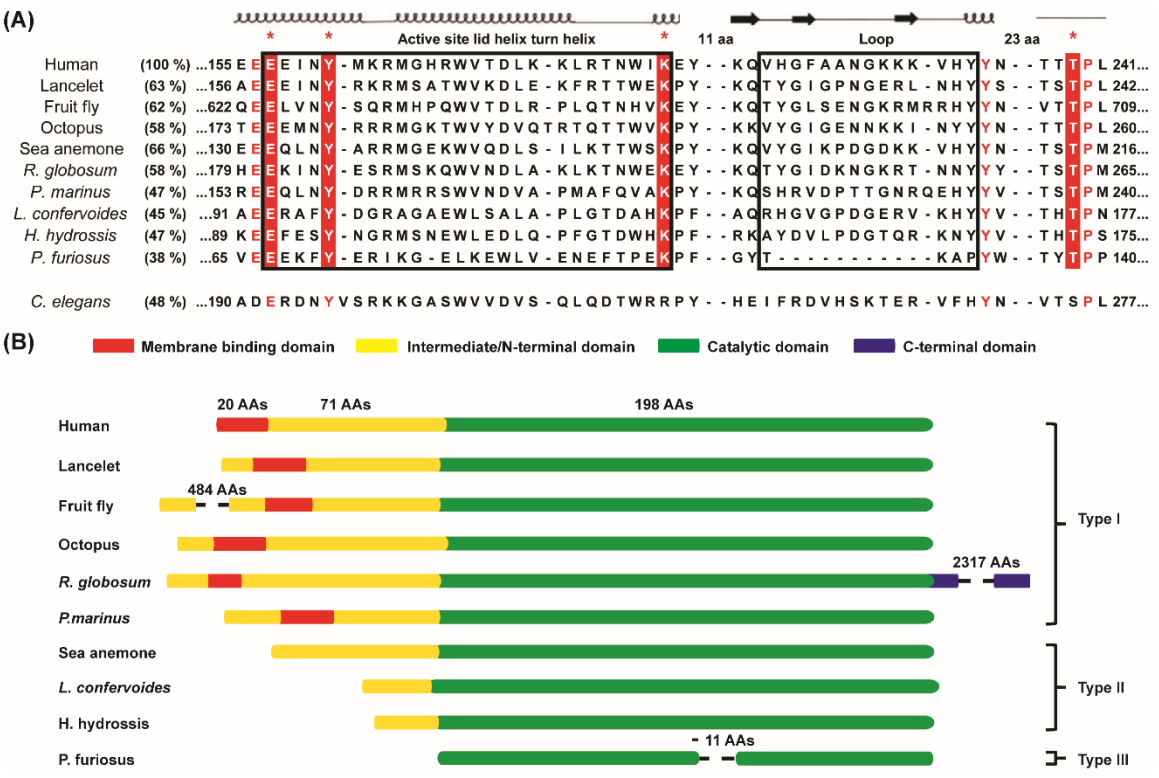

Figure 4-1 Sequence comparison of IYD homologs. (A) Sequence alignment of the catalytic domains of IYD homologs. The percent amino acid identical to human IYD is indicated in parenthesis following the name of the organism. Sequence numbers of each homologs are given on both sides of the alignment. Secondary structure elements (on top of the sequences) are derived from the co-crystal structure of HsIYD and I-Tyr bound (PDB ID: 4TTC).[31] The active site lid and the nearby flexible loop are enclosed by solid squares. Conserved residues are colored red. IYD's signature sequence elements, Glu157, Y161, K182, and T239, are indicated by red sharing and a star on top of the sequence. (B) The domain representation of IYD homologs. The membrane association of lancelet IYDs is species dependent as a homolog from *Branchiostoma belcheri* is predicted to have a membrane anchor but one from *Branchiostoma floridae* is not. Both figures are originally published in Sun, Z,; Su, Q.; Rokita, S. E.[29]

Thermophilic IYDs are also good starting points for engineering IYD towards a halophenol dehalogenase. The thermostability of thermophilic IYDs may tolerate more structurally deleterious but functionally beneficial mutations than their mesophilic counterparts.[114] In addition, thermophilic enzymes are typically more stable to proteolysis and organic solvents, which may allow thermophilic IYDs to better tolerant the harsh environment at contaminated sites of halophenols when used as extra-celluar enzymes.[115] Detailed structural and functional analysis of

thermophilic IYDs was the first step towards utilization of their potentials for the bioremediation of halophenols.

In this chapter, the characterization of TnIYD as a representative of thermophilic IYDs was described. Overexpressed TnIYD was purified from *E. coli* cells in its semiquinone form. Free Tyr was discovered to bind TnIYD tightly and stabilize its semiquinone form. The activity of TnIYD at 25 °C already rivaled that of mesophilic IYDs and increased further at 60 ºC as expected. Co-crystal structures of oxidized and semiquinone TnIYD with I-Tyr, F-Tyr, and Tyr were determined and the results suggested overall similarity in the enzyme architecture and the active site binding of the ligands between TnIYD and mesophilic IYDs. An additional binding site for I-Tyr besides the two active sites was observed on the surface of TnIYD. This additional binding of I-Tyr to the enzyme-substrate complex is likely to be the molecular basis for its severe substrate inhibition of activity.

4.2 Materials and methods:

4.2.1 Cloning:

The original plasmid pET28 encoding TnIYD was a generous gift from Dr. Janine Copp (University of British Columbia, Vancouver). TnIYD from this plasmid was then subcloned into a pET24(a) vector (Novagen) via restriction sites NdeI and XhoI introduced by PCR. Both restriction enzymes were purchased from New England Biolabs. A C-terminal $(His)_6$ tag was then added to the TnIYD sequence by site directed mutagenesis to facilitate purification.[69,70] The resulting construct encoding TnIYD with the C-terminal $(His)_6$ tag was used for all subsequent studies. The TnIYD variant Y112A was constructed via site directed mutagenesis.[69,70] The flavin reductase Fre from *E. coli* was amplified from *E. coli* genome (Genehogs, Invitrogen) with a C-terminal $(His)_6$ tag and cloned into pET24a vector via overlap extension PCR.[106]

All DNA oligonucleotides used for cloning were synthesized by IDT and Sigma (see Appendix Table C1 for a list of oligonucleotides). PCR was performed with Phusion High-Fidelity

DNA polymerase (Thermo Fisher Scientific). The DNA sequences of all variants were verified by Sanger sequencing (Genewiz).

4.2.2 Protein expression and purification:

TnIYD, its variant Y112A, and flavin reductase Fre from *E. coli* were heterologously expressed as described in 2.2.3. TnIYD with Tyr bound (greenish yellow TnIYD) was purified as follows. Frozen cell pellets from 500 mL culture (~ 4g) were thawed at room temperature and resuspended in ~ 25 mL cell lysis buffer (50 mM sodium phosphate, 500 mM sodium chloride, 10% glycerol, 25 mM imidazole, 0.5 mM TCEP, pH 8.0) by vortex. From then on, all procedures were done at 4 ºC unless otherwise noted. FMN was added to the suspension to a final concentration of ~ 300 μM to enhance the occupancy of the cofactor. Cells were then lysed by an EmulsiFlex-C3 homogenizer (Avestin) with 3 passes at ~17000 psi. Cell debris was removed by centrifugation at 45000×g for 30 min. The supernatant was mixed with 3 mL of Ni-NTA resin (Thermo Fisher Scientific, pre-equilibrated with 10 column volumes of cell lysis buffer) in a gravity column by a rotary shaker for 30 min. The column was then washed with 10 column volume of cell lysis buffer. Finally, the His-tagged protein was eluted with 4 column volumes of elution buffer (50 mM sodium phosphate, 500 mM sodium chloride, 10% glycerol, 250 mM imidazole, 0.5 mM TCEP, pH 8.0). The eluted proteins were then supplied with ~300 μM FMN and incubated on ice overnight to further increase the FMN occupancy. The proteins were further purified by a gel filtration column (Sephacryl S-200HR, GE Healthcare) equilibrated with storage buffer (100 mM sodium chloride, 50 mM sodium phosphate, pH 7.4, 1mM TCEP, and 10% glycerol). The purified enzymes were then concentrated with a 30 kD molecular weight cut off centrifugal filter unit (Amicon), aliquoted, flash-frozen with liquid nitrogen, and stored at -80 °C.

TnIYD and the Y112A variant free of bound Tyr were purified similarly as Tyr bound proteins except for the following modifications. After centrifugation of cell lysate, the supernatant was mixed with 5 mL of Ni-NTA resin (Thermo Fisher Scientific, pre-equilibrated with 10 column

volumes of cell lysis buffer) by a bench top Econo pump (Bio-rad) at a flow rate of 1 mL/min. The column was then washed with 1 column volume of cell lysis buffer followed by 4 column volumes of cell lysis buffer supplemented with sodium dithionite (2% final, technical grade, Sigma-Aldrich) with the same Econo pump and flow rate. The column was then washed extensively with 16 column volumes of air saturated washing buffer (50 mM sodium phosphate, 500 mM sodium chloride, 10% glycerol, 60 mM imidazole, 0.5 mM TCEP, pH 8.0) using an ÄKTA protein purification system (GE Healthcare) at 1 mL/min before elution. After supplemented with ~300 μM FMN on ice for 1 hr, the proteins were exchanged into storage buffer using a gravity driven PD-10 desalting column (GE healthcare) following manufactures' instructions.

TnIYD used for crystallography was purified similarly as the Tyr free enzyme except for the following modifications. Once the cell lysate were loaded onto the Ni-NTA column, no dithionite treatment was applied. Instead, the column was directly washed with 16 column volumes of cell lysis buffer and 16 column volumes of washing buffer by the same ÄKTA protein purification system at 1 mL/min. The proteins eluted from the Ni-NTA column was concentrated to 1 mL and incubated with ~300 μM FMN on ice overnight before further purified by a gel filtration column similarly as above. The proteins eluted from the gel filtration column were then supplemented with ~300 μM FMN on ice for 1 hr before exchanged into crystallization buffer (10 mM Tris, 100 mM sodium chloride, pH 7.4). This protein was then concentrated to ~ 20 mg/mL and stored on ice without freezing.

The flavin reductase Fre was purified similarly as TnIYD used for crystallography. However, no FMN was added to the lysate since Fre does not use flavin as a cofactor. In addition, a gel filtration column was not performed for Fre purification and Fre eluted from Ni-NTA column was directly buffer exchanged into storage buffer via a gravity driven PD-10 desalting column (GE healthcare) following manufactures' instructions.

The purified enzymes were analyzed by 12% SDS-PAGE with Comassie brilliant blue staining. Protein concentration and FMN occupancy were determined similarly via UV-vis as described in Section 3.2.3.

4.2.3 Identification of the ligand in TnIYD expressed and purified from *E. coli*:

The greenish yellow form of TnIYD (40 μM) was prepared in a 1:1 solution of water and storage buffer (as mentioned above) supplemented with 4.4% formic acid. This solution was incubated at room temperature for 5 min before centrifugation at 14000×g for 5 min. The supernatant (200 μL) was analyzed by a Jasco HPLC system with two PU-980 Intelligent pumps and a MD-1510 photo-diode array detector. The solvent gradient used was listed in Appendix Table C2. The same HPLC protocol was used to analyze the ligand free enzyme as well. A hydrophilic species identified from the analysis of the greenish yellow form of TnIYD was collected from HPLC and evaporated to dryness under vacuum (Savant Speed Vac, SC100A). The residues were reconstituted with 120 μL water and the sample was analyzed by a Waters Acquity/XevoG2 UHPLC-MS system. Small molecules were separated using an Acquity UPLC® HSS T3 column (100 Å, 1.8 μm, 2.1 mm×100 mm) and a binary mobile phase of water (A) and acetonitrile (B) with 0.1% v/v formic acid in each at a flow rate of 0.3 mL/min. The 10 min separation gradient started with mobile phase B at 0% (0 min) which was then increased to 5% B (0-1 min), then 60% B (1-7 min), then 95% B (7-7.1 min), then held at 95% (7.1-9 min), then decreased to 0% (9-9.1 min), and finally re-equilibrated with system at 0% (9.1-10 min). The column was held at 35 ºC. The positive electrospray ionization mode was used for the MS detection of small molecules. The capillary voltage, sampling cone and extraction cone were set to 3 kV, 40 V, and 4 V, respectively and the source temperature was 130 ºC. The desolvation gas tempearature and flow rate were 400 ºC and 400 L/hr, respectively. All data were analyzed by Masslynx v4.1 (Waters).

4.2.4 Reduction of TnIYD and air re-oxidation monitored by UV-vis spectroscopy:

All reduction and re-oxidation assays were performed under aerobic conditions and room temperature (25 ± 1 °C) unless otherwise stated. Ligand free TnIYD (40 μM) and Tyr (68 μM) were incubated in 110 mM potassium phosphate, 220 mM potassium chloride, pH 7.4 for 5 min in an UV-vis cuvette at room temperature. Sodium dithionite (1%) in 5% sodium bicarbonate was then added to the cuvette to reach a final concentration of 3.3 mM (estimated from the weighed mass). The subsequent air re-oxidation was performed by pipetting the solution in the cuvette up and down until the colorless solution turned purple (in the presence of Tyr) or yellow (in the absence of Tyr). Reduction and re-oxidation of TnIYD in the absence of Tyr was performed similarly. The UV-vis spectra of the oxidized, fully reduced, and the re-oxidized TnIYD were recorded by a Hewlett Packard 8453 Diode-Array Spectrophotometer.

Reduction of TnIYD by free reduced FMN generated by *E. coli* flavin reductase Fre was carried out by adding 10 μM Fre to a mixture of 25 μM TnIYD, 60 μM Tyr, 300 μM FMN, and 1 mM NADH in 100 mM potassium phosphate, 200 mM potassium chloride, pH 7.4. The reduction of TnIYD was monitored by following the absorbance increase at 590 nm for TnIYD semiquinone.

Anaerobic reduction of TnIYD by free reduced FMN generated by dithionite was carried out in a gas tight cuvette sealed with a septum. A solution of 90 μM FMN and 60 μM Tyr in 100 mM potassium phosphate, 200 mM potassium chloride, pH 7.4 was deoxygenated by bubbling Ar for 20 min. The FMN was then quantitatively reduced by 5% dithionite in 5% sodium bicarbonate introduced with a gas tight syringe. The reduction of FMN was monitored by the decrease of absorbance of oxidized FMN at 450 nm. To ensure that there was no excess dithionite, oxygenated buffer was added to the cuvette to oxidize ~ 20 μM FMN. TnIYD (30 μM, oxygenated) was then added to the cuvette and the absorbance at 590 nm for TnIYD semiquinone was monitored by UV-vis.

4.2.5 Deiodination activity assay:

The deiodination activity of *E. coli* cell lysate containing overexpressed TnIYD was measured as follows. A cell pellet from 500 mL culture was resuspended in ~ 25 mL cell lysis buffer (50 mM sodium phosphate, 500 mM sodium chloride, 10% glycerol, 25 mM imidazole, 0.5 mM TCEP, pH 8.0) by vortex. Cells were then lysed by an EmulsiFlex-C3 homogenizer (Avestin) with 3 passes at ~17000 psi. Cell debris was removed by centrifugation at 45000×g for 30 min. 100 μL of the supernatant was added to 900 μL 220 mM potassium chloride, 110 mM potassium phosphate, pH 7.4 containing 20 μM I-Tyr and 300 μM FMN (not included when dithionite was used as the reductant). The concentration of TnIYD in the final mixture was estimated to be ~ 1 μM based on the typical yield of TnIYD after purification. The reaction was incubated at 25ºC for 5 min and subsequently initiated by 100 μL of 1 mM NADH or 100 μL of 5% sodium dithionite in 5% sodium bicarbonate. After 1 hour, the reaction was quenched by 100 uL of a 1:1 mixture of 88% formic acid and 0.55 μM Cl-Tyr (as an internal standard) in the above pH 7.4 buffer. The reaction was heated at 60 ºC for 2 min and centrifuged at 14000×g for 5 min to pellet precipitated proteins. The supernatant was then analyzed by HPLC with the same protocol described in Section 2.2.5. Instead of the formation of Tyr, however, the activity was monitored by the consumption of the substrate I-Tyr since unknown species derived from NADH co-elutes with Tyr.

The deiodination activity of purified TnIYD with I-Tyr and Cl-Tyr at 25 ºC was performed as follows: I-Tyr or Cl-Tyr (0.5-100 μM) in 900 μL of 220 mM potassium chloride, 110 mM potassium phosphate, pH 7.4 was incubated at 25 ± 1 °C for 5 min. Sodium dithionite (5%, 100 μL) in 5% sodium bicarbonate containing TnIYD (25 to 200 nM in 1 mL final reaction) was then added to the I-Tyr solution to initiate catalysis. The reaction was quenched by 50 μL 0.44% formic acid and then incubated at 60 ºC for 2 min to ensure the decomposition of dithionite (white precipitations were generated from the decomposition which is likely elemental sulfur).[116] Cl-Tyr (when I-Tyr as substrate) or I-Tyr (when Cl-Tyr as substrate) as an internal standard (50 μL of 0.1 mM in 10 M

sodium hydroxide) was added to the reaction to neutralize the formic acid. The neutralized reaction was then centrifuged at 14000×g for 5 min and the supernatant was analyzed by a Jasco HPLC system with two PU-980 Intelligent pumps and a multiwavelength detector. The product of the reaction-Tyr was separated on a C18 reverse phase column (Agilent, Microsorb-MV 300 C18, 250 × 4.6 mm) by a gradient of 10 mM potassium phosphate pH 6.6 and acetonitrile at a flow rate of 1 mL/min and detected at 275 nm. See Appendix Table C3 for the detailed solvent gradients. Rates with ≤ 2 μM I-Tyr were measured via following substrate consumption at 280 nm which was ~5 fold more sensitive than following product formation at 275 nm. The deiodination activity of purified TnIYD with I-Tyr at 60 ºC was measured with the same protocol above with the following modifications. The formation of Tyr was detected via fluorescence on an Agilent 1100 series HPLC equipped with a 1200 series fluorescence detector (λ_{ex} = 275 nm and λ_{em} = 312 nm). Since TnIYD exhibited severe substrate inhibition with I-Tyr and Cl-Tyr, the trace of activity verses substrate concentration was fitted into Equation 4-1 for substrate inhibition kinetics to obtain k_{cat}, K_M, and K_i.[117]

$$\frac{V}{[E]} = \frac{k_{cat}[S]}{K_M + [S]\left(1 + \frac{[S]}{K_i}\right)} \quad \text{(Equation 4-1)}$$

2IP deiodination at both 25 and 60 ºC was measured with the same protocol in Section 2.2.5. V/[E] versus substrate concentration was fitted with Michaelis-Menton equation to obtain k_{cat} and K_M.

4.2.6 Crystallization and structure determination:

Crystallization and structure determination of TnIYD with various ligands were performed in collaboration with Prof. Jennifer Kavran (Johns Hopkins University). Crystallization conditions were determined using commercially available screens with a Phoenix robot. CrystalMation Intelli-Plate 96-3 low-profile plates (Hampton research) were used for initial screening and EasyXtal 15-Well Tool X-Seal plates were used for optimization. Complexes between TnIYD and ligands

were formed by incubating approximately 10 mg/mL of purified TnIYD with 2-3-fold molar excess of either I-Tyr, Tyr, or F-Tyr in 10 mM Tris, 100 mM sodium chloride, pH 7.4 for three hours at 4 °C. Crystals were grown by hanging-drop vapor diffusion by mixing a 1:1 or 2:1 ratio of complex to well solution containing 100 mM sodium citrate, 3 M NaCl, pH 4.5 at 20 °C. Bright yellow plate shaped crystals appeared after 1 day and grown to their maximum sizes in a week with approximate dimensions 400×150×40 μm. For the oxidized form, crystals were transferred directly from the drop into a cryo-stabilization buffer containing 100 mM citric acid, ~2 mM of ligand, 3 M sodium chloride, pH 4.5 and 30% PEG400 and flash frozen in liquid nitrogen. For the semiquinone form, the drop containing the crystals was exchanged into well solution supplemented with 0.5% sodium dithionite and incubated for ~5 minutes until the crystals visibly changed from yellow to purple, indicating the presence of the flavin semiquinone. Crystals were then transferred to cryo-stabilization buffer and flash frozen in liquid nitrogen.

Diffraction data were collected at beamline 12-2 at the Stanford Synchrotron Radiation Lightsource (SSRL) and processed with XDS/Aimless.[118] For the initial structure, phases were determined by iterative rounds of molecular replacement with a search model corresponding to a ligand free, trimmed, poly-alanine monomeric model of HhIYD (PDB ID: 5KO8)[32] in Phaser.[119] Initial electron-density maps were improved by Prime-and-switch density modification.[120] Subsequent structures were determined by difference Fourier. Models were built by iterative rounds of manual-building in Coot[121] and refinement in Phenix[122].

4.3 Results and discussion:

4.3.1 TnIYD was purified in its semiquinone form stabilized by bound Tyr:

Mesophilic IYDs, when released from *E. coli* cells during purification and bound to the Ni-NTA column, were bright yellow due to the color of their oxidized FMN cofactors. The cell lysate and Ni-NTA column containing TnIYD, however, were dark purple. When directed eluted from a gravity Ni-NTA column without extensive washing, the resulting protein carried the purple color

for at least a few hours before turning into greenish-yellow after overnight incubation on ice under aerobic conditions (Appendix Figure C1). The UV-vis spectrum of the purple protein showed a broad peak between 500 nm and 700 nm (Figure 4-2(A)). The intensity of this peak gradually decreased over the course of 30 min under aerobic conditions while the absorbance at 450 nm increased concomitantly to restore the signature absorption band at 450 nm for oxidized flavin. The result suggested that the purple color and its corresponding absorption at 500-700 nm belong to a neutral blue FMN semiquinone species which overtime oxidized by air to generate the fully oxidized FMN. It is unprecedented that IYD was purified in its semiquinone form. TnIYD must somehow be reduced to at least the semiquinone within the *E. coli* cells or upon the cell lysis. This is very interesting since to date an in vivo reducing system for IYD has never been characterized. Activity assays for IYD mostly were powered either by the artificial reducing reagent sodium dithionite or by NADPH and unidentified electron transfer systems in thyroid or human embryonic kidney (HEK) 293 cells.[8,123] TnIYD must also be able to stabilize the usually highly oxygen sensitive semiquinone sufficiently for it to be observed on the time scale of the purification.

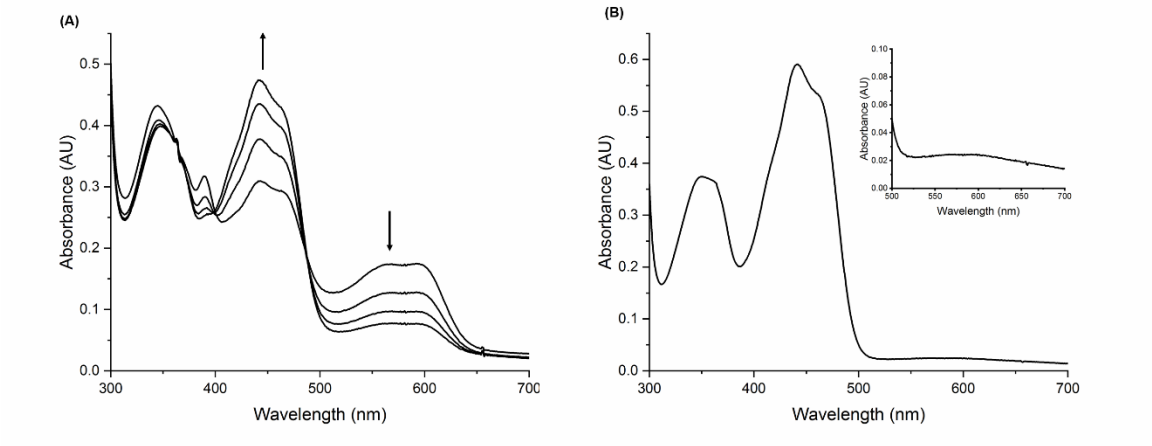

Figure 4-2 UV-vis spectrum of TnIYD at various stages of purification. (A) Spectrum of purple TnIYD eluted from a gravity Ni-NTA column. Spectrum was recorded every 10 min for 30 min. (B) Spectrum of the greenish yellow form of TnIYD obtained from overnight incubation of the purple TnIYD on ice under aerobic conditions. The insert is an enlarged view of the spectrum between 500 nm and 700 nm.

Once the purple TnIYD was oxidized to greenish yellow, no further change was observed towards the bright yellow color of a typical oxidized mesophilic IYD. The UV-vis spectrum of this greenish yellow TnIYD was very similar to that of oxidized mesophilic IYDs except for the presence of a broad band of absorbance between 500 nm and 700 nm (Figure 4-2). This band was not observed for mesophilic IYDs and might be responsible for the greenish yellow color of TnIYD. A similar greenish yellow color and spectroscopic feature were reported for the old yellow enzyme isolated from *Saccharomyces cerevisiae*[124] and attributed to a charge transfer complex between the oxidized enzyme bound FMN and 4-hydroxybenzaldehyde.[125] It is then possible that the greenish yellow color of TnIYD was also a result of a charge transfer interaction between its oxidized FMN and an aromatic small molecule. Previous studies showed that a FMN semiquinone species was observed during the slow anaerobic reduction of HsIYD and HhIYD by a reducing system of xanthine/xanthine oxidase/methyl viologen in the presence of the substrate analog F-Tyr.[31,32] This substrate analog stabilized the FMN semiquinone of mesophilic IYDs by inducing the closure of the active site lid and the concomitant formation of a hydrogen bond between the side chain of a threonine and the N5 of FMN. It is then likely that the semiquinone of TnIYD observed during its purification is also stabilized by the binding of the same small molecule that possibly forms the charge transfer band to create the greenish yellow TnIYD.

4.3.2 Identification of Tyr as the ligand in TnIYD expressed and purified from *E. coli*:

A sample of the greenish yellow TnIYD was first denatured by formic acid and then analyzed by HPLC in attempt to identify the small molecule bound to the enzyme isolated from *E. coli*. Besides FMN and the polypeptide of TnIYD, a hydrophilic species with an absorption maxima around 275 nm was also identified from this sample (Figure 4-3(A)). The retention time of this species is very close to that of Tyr analyzed as the product of the deiodination assay of I-Tyr. Comparison of HPLC retention time (Figure 4-3(A)) and mass spectra (Figure 4-3(B)) between a

Tyr standard and the hydrophilic species suggested that Tyr was the ligand in TnIYD expressed and purified from *E. coli*.

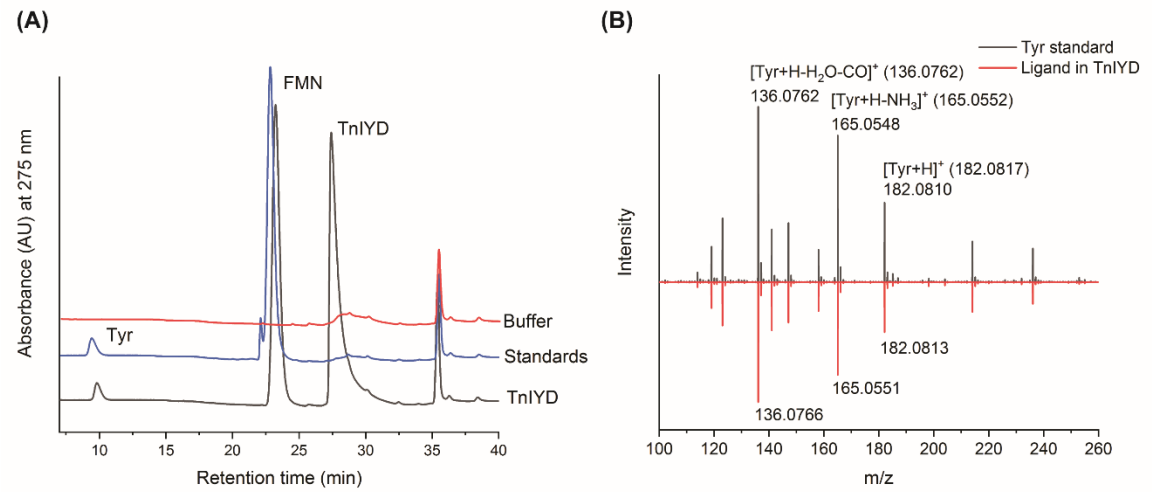

Figure 4-3 Identification of Tyr as the ligand in the greenish yellow form of TnIYD. (A) HPLC chromatograms of 40 μM greenish yellow form of TnIYD (black), 40 μM of FMN and Tyr each (blue), and a buffer black (red). (B) Comparison of mass spectra of a Tyr standard (black) and the ligand in the greenish yellow form of TnIYD isolated by HPLC. The mass fragments of the Tyr standard is assigned based on a published report.[126] The calculated exact mass for each fragment is shown in parenthesis following the assignment.

Binding of Tyr to TnIYD is surprising since none of the previously characterized mesophilic IYDs were co-purified with Tyr bound and the K_d of Tyr with mesophilic IYDs is at least 100 μM.[27,31] The Tyr that co-purified with the enzyme first needed to be removed in order to evaluate the ability of Tyr to form a charge transfer complex with oxidized TnIYD and to stabilize the semiquinone form of TnIYD. The previously mentioned 4-hydroxybenzaldehyde co-purified with old yellow enzyme from *Saccharomyces cerevisiae* was removed by anaerobic dialysis of the reduced enzyme since 4-hydroxybenzaldehyde only binds to the oxidized, not the reduced enzyme.[124] Therefore, TnIYD was reduced and washed with 2% dithionite supplemented buffer during Ni-NTA purification to learn if this treatment can remove Tyr from TnIYD as well. When washed with dithionite supplemented buffer, the purple TnIYD semiquinone quickly disappeared, indicating reduction of the purple FMN semiquinone to the colorless hydroquinone (Appendix Figure C2). The 2% dithionite in the buffer is enough to keep the system oxygen free as TnIYD

stayed colorless throughout the washing procedure under aerobic conditions. Once the column was washed with air saturated buffer, the colorless TnIYD quickly turned to bright yellow (Appendix Figure C2). Tyr was no longer detected in the HPLC analysis of this bright yellow form of TnIYD after formic acid denaturation (Appendix Figure C3). Therefore, Tyr does not seem to bind the reduced TnIYD and can be removed from oxidized TnIYD via dithionite treatment.

As expected, the charge transfer band between 500 nm and 700 nm was not observed for the ligand free TnIYD (Figure 4-4). However, this band was restored after addition of Tyr to the ligand free TnIYD. In addition, a TnIYD semiquinone species mimicking that isolated directly from *E. coli* was generated by reducing TnIYD by dithionite and then re-oxidizing by air in the presence of Tyr and was stable for at least 15 min as indicated by UV-vis spectra (Figure 4-4(A)) under aerobic conditions. In contrast, the semiquinone was not observed for the ligand free TnIYD that was similarly reduced by dithionite and re-oxidized by air (Figure 4-4(B)). The fully oxidized TnIYD was instead obtained in the absence of Tyr. These results demonstrated the ability of Tyr to stabilize TnIYD semiquione and form a charge transfer complex with fully oxidized TnIYD. The stabilization of the semiquinone by Tyr explains the persistence of the purple color of TnIYD during purification. However, a physiological reducing source must have presented in *E. coli* cells in order to generate the purple TnIYD semiquinone.

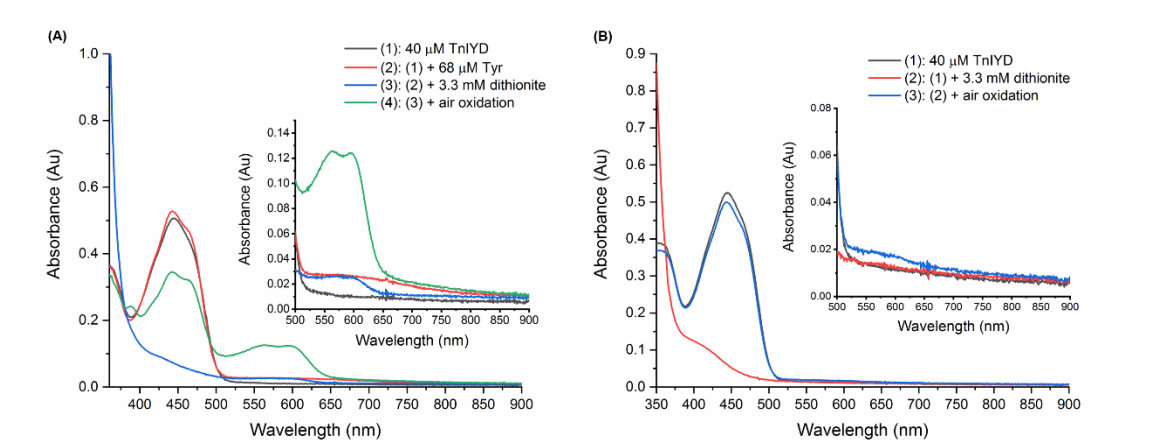

Figure 4-4 Reduction and re-oxidation of TnIYD with and without Tyr. (A) In the presence of Tyr, TnIYD forms a charge transfer band and stabilizes its semiquinone form upon reduction with dithionite followed by air re-oxidation. (B) In the absence of Tyr, no charge transfer band wasbserved for TnIYD and fully oxidized TnIYD instead of its semiquinone form was obtained upon reduction with dithionite followed by air re-oxidation. The inserts in both (A) and (B) are enlarged views of the corresponding spectrum between 500 nm and 900 nm.

4.3.3 TnIYD can be reduced by free reduced flavins generated by a flavin reductase from *E. coli*:

A reducing source for IYD from *E. coli* has never been reported. Its identification is of great interest since it will allow the bioremediation of halophenols with TnIYD or its variants in intact cells. In the standard purification of TnIYD, free FMN (~ 300 μM) is always added to the cell lysate to increase the FMN occupancy in the enzyme. However, when exogenous FMN was omitted, the Ni-NTA column was mostly greenish yellow instead of purple after loading of the cell lysate. This seems to suggest that free FMN is required for the in vivo reduction of TnIYD. The role of free FMN is most likely an electron shuttle that passes electrons to TnIYD from other reducing sources. In *E. coli*, reduced FMN can be generated by multiple NAD(P)H dependent flavin reductases.[127,128]

E. coli cell lysate containing overexpressed TnIYD was first tested for I-Tyr deiodination in the presence of FMN and NADH to see if the endogenous *E. coli* reducing system can support the catalysis of TnIYD. Since species derived from NADH co-eluted with Tyr on HPLC, the deiodination reaction was followed by the consumption of I-Tyr. As a control, when dithionite was

used as reductant, all 20 μM I-Tyr in the reaction was consumed within 1 hr. When 1 mM NADH and 300 μM exogenous FMN were used as reductant, about 10 μM I-Tyr was depleted in 1 hr. The result suggested that the endogenous reducing system in *E. coli* is capable of supporting the deiodination acitivity of TnIYD. Without FMN, NADH alone with the cell lysate containing TnIYD was not reactive towards I-Tyr, again demonstrated the requirement of free FMN in the reducing system.

The well-studied Flavin:NAD(P)H reductase Fre from *E. coli* was then overexpressed and purified to reconstitute this reducing system in vitro. Fre utilizes both NADH and NADPH to reduce FMN, FAD, and riboflavin and has been suggested to provide reducing equivalence to ribonucleotide reductase in *E. coli*.[127] When Fre was added to a mixture of TnIYD, Tyr, FMN, and NADH under aerobic conditions, a flavin semiquinone was formed as monitored by UV-vis (Figure 4-5(A)). This semiquinone species is most likely formed from reduction of TnIYD by reduced FMN since Fre reduces free FMN directly to its hydroquinone state. The full reduction of TnIYD to the hydroquinone was not observed under aerobic conditions since the fully reduced TnIYD could rapidly react with oxygen and re-oxidized to the semiquinone state which in the presence of Tyr was much slower oxidized (Figure 4-4(A)).

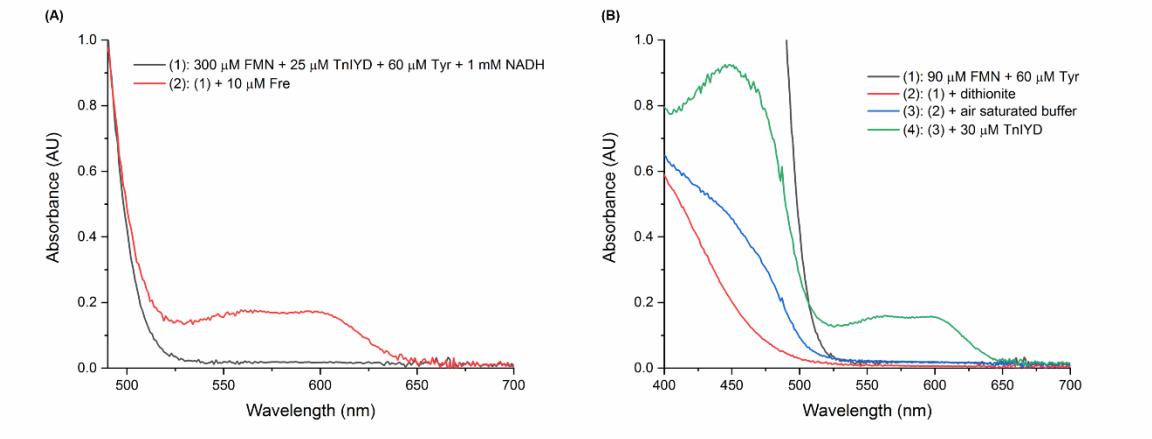

Figure 4-5 Reduction of TnIYD with free FMN. (A) TnIYD was reduced to the semiquinone form by free reduced FMN generated with a NADH/flavin reductase Fre system. (B) TnIYD was reduced to the semiquinone form by free reduced FMN generated with dithionite.

The role of Fre in this system could either be providing a source of reduced flavin that then diffuses to the proximity of TnIYD[129] or delivering reduced flavin to TnIYD via a transient complex between the two enzymes.[130] When TnIYD was added to a solution of excess Tyr and free reduced FMN generated by dithionite under anaerobic conditions, the TnIYD semiquinone was formed without Fre (Figure 4-5(B)). The absorbance of the semiquinone at ~ 590 nm reached its maximum in ~ 5 min and stayed unchanged for another 5 min. This result suggested that reduced flavin alone is capable of reducing TnIYD to its semiquinone form. It is still not clear whether the failure to observe the fully reduced TnIYD is a result of its rapid re-oxidation to the semiquinone by residual oxygen since the system was not absolutely anaerobic (the TnIYD was not deoxygenated when introduced into the Ar purged cuvette and the cuvette itself slowly leaked air into the cuvette as slow increase in 450 nm absorbance was observed overtime). However, this does not necessarily conflict with the ability of free FMN dependent endogenous reducing system in *E. coli* to support deiodination of TnIYD which requires the fully reduced enzyme bound FMN. In the presence of substrate, the re-oxidation of the fully reduced TnIYD may compete by oxygen and the substrate. Closure of the active site lid induced by substrate binding may hinder the re-oxidation by oxygen and favor catalytic deiodination.

The ability of TnIYD to bind Tyr and be reduced by free flavin may not be specific to TnIYD but rather a common feature of thermophilic IYDs since another thermophilic IYD-PfIYD was also purified from E. coli as a purple semiquinone.[112] It is possible that free flavins can also reduce mesophilic IYDs. More detailed spectroscopic and kinetic studies are needed to see if such a system has a physiological relevance and can power the bioremediation of halophenols.

4.3.4 TnIYD is a functional thermophilic iodotyrosine deiodinase with severe substrate inhibition:

TnIYD demonstrated its uniqueness compared to mesophilic IYDs with the ability to bind Tyr in a redox dependent manner and stabilize its semiquinone state during purification. Its ligand

binding and catalytic properties were subsequently evaluated to reveal the functional similarities and differences between meso- and thermophilic IYDs. Tyr free TnIYDs used in these studies were purified with a yield of ~ 15 mg/L culture and a FMN occupancy of ~90-95% (Appendix Figure C4). The binding of various ligands to TnIYD was measured via the previously described FMN fluorescence quenching assay (Section 2.2.4). At 25 ºC, halotyrosines (I-Tyr and F-Tyr) bound TnIYD tightly with sub-micromolar dissociation constants, which is consistent with the conservation of the zwitterion recognition triad (E68, Y72, and K92) in TnIYD (Table 4-1). The 50 nM K_d of TnIYD with I-Tyr is the smallest of all IYDs with halotyrosines measured to date. The K_d of F-Tyr with TnIYD is only ~2-fold larger than I-Tyr, while K_d of F-Tyr with mesophilic IYDs were at least 5-fold larger than that of I-Tyr.[27,28,31,32] Results described in Section 4.3.2 already showed that oxidized TnIYD bound Tyr and formed a charge transfer complex. The K_d of 0.5 μM for Tyr at 25 ºC is consistent the ability of Tyr to co-purify with TnIYD (Table 4-1). The affinity between Tyr and oxidized TnIYD was similar or even tighter than that between I-Tyr and DmIYD (K_d 0.62 μM) and HhIYD (K_d 8.2 μM).[28,32] The 10-fold difference in K_d between Tyr and I-Tyr with TnIYD was surprisingly small given that such a difference in mesophilic IYDs are at least 1000-fold.[27,31] The affinity of halotyrosines and Tyr with HsIYD has been correlated with the pKa of the hydroxyl group in the ligands. HsIYD preferred to bind the phenolate form of halotyrosines presumably due to its strong interactions with the 2`-hydroxyl group of FMN's ribose tail and a backbone amide of Ala 130.[31] The pKa of the hydroxyl group in Tyr (pKa 10.05) is more than one pH unit higher than halotyrosines and nearly three pH unit above the pH of the buffer (pH 7.4) used in affinity determination.[131] Tyr in the affinity assays is overwhelmingly in its phenol form and as a result does not bind mesophilic IYDs tightly. The tight binding of Tyr to TnIYD suggested that pKa of the hydroxyl group might not be a dominate factor contributing to the affinity of Tyr and halotyrosines with TnIYD. This was further demonstrated by tight binding of 3-methoxy-L-Tyrosine (MeO-Tyr) to TnIYD at 25 ºC (K_d 0.54 μM, Table 4-1) despite a high pKa of the hydroxyl

group for MeO-Tyr (pKa 10.01).[131] On the other hand, the presence of a zwitterion has a bigger effect on ligand binding than pKa of the hydroxyl group. 2IP bound to oxidized TnIYD at least 300-fold less tightly than halotyrosines and 50-fold less tightly than Tyr (Table 4-1). However, compared to mesophilic IYDs, the 26.4 μM K_d is already the smallest measured to date and is only ~ 3-fold larger than the K_d of I-Tyr with HhIYD.[32] Therefore, high affinity with TnIYD likely dependents on many factors and TnIYD may have structural features different from mesophilic IYDs to support binding of phenolic compounds.

Table 4-1 Affinity and steady-state kinetics of TnIYD with various ligands and substrates.[2]

Substrate/Ligand	K_d (μM)[a]	k_{cat} (min^{-1})[b]	K_M (μM)[b]	k_{cat}/K_M ($min^{-1}\times \mu M^{-1}$)	K_i (μM)
	TnIYD (25 ºC)				
I-Tyr	0.05 ± 0.02	5.4 ± 0.9	0.02 ± 0.10	270 ± 1000	5 ± 2
Cl-Tyr	N. D.	0.9 ± 0.1	1.3 ± 0.4	0.7 ± 0.3	18 ± 6
F-Tyr	0.08 ± 0.03	-	-	-	-
Tyr	0.49 ± 0.04	-	-	-	-
MeO-Tyr	0.54 ± 0.07	-	-	-	-
2IP	26.4 ± 0.5	0.84 ± 0.06	(4.2 ± 0.7) × 10^3	(2.0 ± 0.4) × 10^{-4}	N. D.
	TnIYD (60 ºC)				
I-Tyr	≤ 0.05	29 ± 4	0.8 ± 0.2	36 ± 10	9 ± 2
Cl-Tyr	N. D.	N. D.	N. D.	N. D.	N. D.
F-Tyr	N. D.	-	-	-	-
Tyr	0.74 ± 0.05	-	-	-	-
MeO-Tyr	N. D.	-	-	-	-
2IP	N. D.	6.5 ± 0.3	(6.6 ± 0.5) × 10^3	(9.8 ± 0.9) × 10^{-4}	N. D.

[a] The K_d and associated were obtained from nonlinear fitting of one determination to the previously published equation.[21]
[b] All the data and error bars were obtained by fitting of two independent measurements as one curve to substrate inhibition kinetics.

The activity of TnIYD with I-Tyr at 25 ºC was then measured by the previously described HPLC assay (Section 2.2.5). Substrate inhibition kinetics (Equation 4-1 in section 4.2.5) was used to describe the severe substrate inhibition of TnIYD with I-Tyr and Cl-Tyr (Appendix Figure C5).[117] Thermophilic enzymes typically have little to no activity near room temperature.[132]

[2] The kinetic parameters of TnIYD with 2IP were measured by Shaun Spisak (Johns Hopkins University).

However, TnIYD is a noticeable exception. At 25 ºC, the k_{cat} of TnIYD with I-Tyr was well within the same magnitude with the range of k_{cat} measured for mesophilic IYDs with I-Tyr.[28,31,32] Its K_M with I-Tyr, though, was 100-fold smaller than that of mesophilic IYDs. However, this K_M was subject to high error due to the lack of a sensitive enough method to measure rates with less than 0.5 μM I-Tyr. Overall, the k_{cat}/K_M of I-Tyr suggested that TnIYD catalyzed I-Tyr deiodination at least one order of magnitude more efficiently (assuming K_M is actually 0.5 μM) than mesophilic IYDs even at 25 ºC.[28,31,32] However, TnIYD exhibited severe substrate inhibition starting with I-Tyr concentration as low as 0.5 μM. Substrate inhibition is not specific to TnIYD but commonly observed for IYDs in general. The K_i of I-Tyr for TnIYD was estimated to be 5 μM which is similar in magnitude to the K_M of mesophilic IYDs with I-Tyr. Therefore, the substrate inhibition seemed to be more severe in TnIYD than mesophilic IYDs. The k_{cat}/K_M of TnIYD with 2IP was ~ 4-fold higher than mesophilic IYDs at 25 °C.[32,60] However, this is mainly a contribution of increased k_{cat} but not decreased K_M, consistent with previous findings that tight binding with the oxidized enzyme does not guarantee efficient deiodination.[32] TnIYD does not defluorinate F-Tyr even at 77 ºC (the optimum growth temperature of *Thermotoga neapolitana*) despite binds F-Tyr only 2-fold less tightly than I-Tyr.

The ligand binding and kinetic properties of TnIYD were then measured under higher temperature to evaluate the thermoadaptation of TnIYD. The optimum temperature of TnIYD should be close to the optimum growth temperature of *Thermotoga neapolitana* (77 ºC).[133] However, at 77 ºC the initial rate of TnIYD with I-Tyr was too fast to be measured accurately by the standard HPLC assay. Therefore, the binding and activity of TnIYD was instead measured at 60 ºC. An accurate dissociation constant of I-Tyr to TnIYD could not be obtained since fitting of the measurement generated a negative value for K_d. However, the traces of fluorescence quenching of TnIYD upon addition of I-Tyr measured under 25 ºC and 60 ºC overlapped with each other well (Appendix Figure C6). Therefore, the K_d of I-Tyr to TnIYD at 60 ºC was estimated to be close to

that at 25 ºC (Table 4-1). For Tyr, the K_d with TnIYD at 60 ºC was only 1.5-fold larger than that measured at 25 ºC (Table 4-1). The increased temperature did not drastically affect the binding of Tyr to TnIYD. The activity of TnIYD with I-Tyr at 60 ºC was measured by quantifying the fluorescence of the product Tyr with HPLC. The fluorescence detection of Tyr on HPLC was 100-fold more sensitive than the corresponding UV detection and therefore permits rate measurement with sub-micromolar I-Tyr. The k_{cat} of TnIYD with I-Tyr was 5.4-fold more active at 60 ºC than at 25 ºC, consistent with its thermophilic nature (Table 4-1). The K_M, though, was also 40-fold larger, although this could again be an artifact due to the high uncertainty of K_M at 25 ºC. The k_{cat}/K_M of I-Tyr with TnIYD at 60 ºC was at least 30-fold higher than mesophilic IYDs at 25 ºC.[28,31,32] This may suggest a partial loss of activity when IYD was adopted to a cold environment. However, the substrate inhibition of TnIYD with I-Tyr was still severe at 60 ºC with a K_i only 2-fold higher than that at 25 °C (Table 4-1). Mesophilic IYDs likely sacrificed some activity compared to thermophilic IYDs to partially relieve substrate inhibition. The k_{cat} and K_M of TnIYD with 2IP at 60 ºC was 8-fold and 1.5-fold higher than at 25 ºC, respectively (Table 4-1). The k_{cat}/K_M of TnIYD with 2IP at 60 ºC is at least 3-fold higher than any mesophilic IYDs and their variants, which might make TnIYD a better parent enzyme for engineering a halophenol dehalogenase.

4.3.5 Crystal structures of oxidized TnIYD in complex with I-Tyr, F-Tyr, and Tyr are similar to those of mesophilic IYDs:[3]

Crystallographic studies of TnIYD are of great interest since the structure of TnIYD represents a minimal scaffold required for reductive dehalogenation (Section 4.1). Comparison of structures of TnIYD with mesophilic IYDs may also reveal the structural basis for the tight binding of Tyr with thermophilic but not mesophilic IYDs. In addition, the presumably decreased flexibility of TnIYD at room temperature may result in crystals with better quality than mesophilic IYDs and

[3] Looping and freezing of the crystals, data collection, and structure determination were performed by Prof. Jennifer Kavran (Johns Hopkins University).

may in return yield high-resolution structures which are potentially useful in revealing subtle differences between the oxidized and reduced structures.[111]

Indeed, co-crystals of oxidized TnIYD with I-Tyr, F-Tyr, and Tyr all yielded high-resolution structures (1.8 Å, 1.6Å, 1.6Å, respectively). The data collection and structure refinement statistics are listed in Table 4-2. In the co-crystal structure of TnIYD and I-Tyr, the two subunits of TnIYD form a homodimer contains the same α/β core with other members of the nitro-FMN reductase superfamily (Figure 1-2 and Figure 4-6(A)). The two active sites at the dimer interface are identical and each active site contains a FMN cofactor. Despite sharing only 37% identity (based on the length of TnIYD, 186 amino acids), there is no major conformational changes between HsIYD and TnIYD as evident from an RMSD of 1.48 Å for 269 Cα atoms (Figure 4-6(B)). The active site lid of TnIYD shares the helix-turn-helix motif of the lids in mesophilic IYDs (Figure 4-6(C)).[31–33] The lid of TnIYD is one amino acid shorter than HsIYD and only minor conformational differences between the lids of two enzymes were observed at the "turn" region between two helixes of the lid (Figure 4-6(C) and (D)). Consistent with prediction by sequence alignment, a loop near the active site of mesophilic IYDs is truncated in TnIYD (Figure 4-6(C)). This loop interacts with the lid in mesophilic IYDs via π-π interaction between a Tyr on the loop and a Trp on the lid (Figure 4-6(D)). However, in TnIYD these residues were substituted with a Pro and a Leu respectively and are not in apparent contact distance (≥ 3.5 Å, Figure 4-6(C)). Since TnIYD is even more active than all mesophilic IYDs characterized at 25 ºC, this loop is not absolutely needed for the catalytic deiodination.

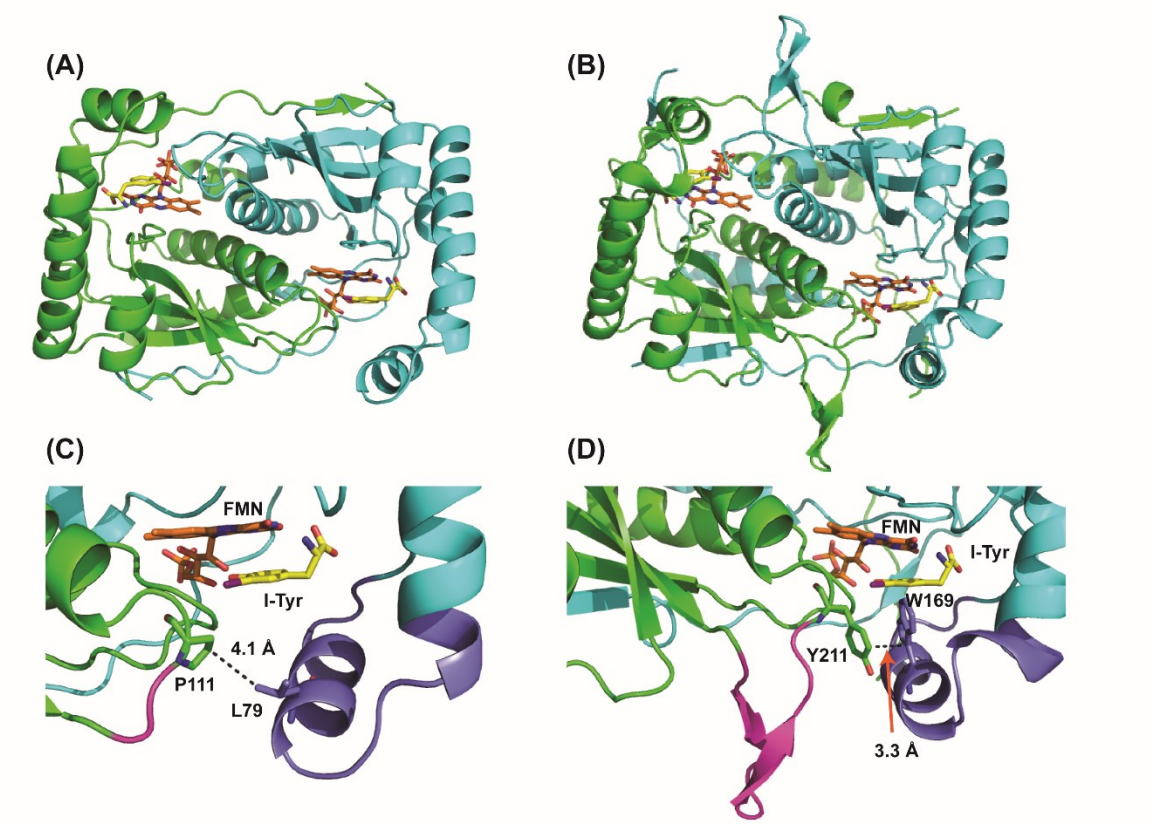

Figure 4-6 Crystal structures of I-Tyr bound to TnIYD and HsIYD.Co-crystal structure of TnIYD with I-Tyr (PDB 6Q1L). The monomeric units of the enzyme are colored with green and cyan. FMN and 2IP are shown in orange and yellow, respectively. (B) Co-crystal structure of HsIYD with I-Tyr (PDB 4TTC).[31] (C) Active site of TnIYD with I-Tyr bound. The active site lid and the truncated loop relative to HsIYD are shown in blue and magenta, respectively. Shortest distance between P111 and L79 is indicated by a dashed line. (D) Active site of HsIYD with I-Tyr bound. The active site lid and the loop are shown in blue and magenta, respectively. Shortest distance between Y211 and W169 is indicated by a dashed line and an orange arrow.

Table 4-2 Data Collection and Refinement Statistics of the oxidized TnIYD structures.[4]

PDB ID	6PZ0	6Q1L	6Q1B
Protein	TnIYD	TnIYD	TnIYD
Ligand	Tyr	I-Tyr	F-Tyr
Oxidation state	oxidized	oxidized	oxidized
Data Collection			
Space group	$P2_12_12_1$	$P2_12_12_1$	$P2_12_12_1$
Unit Cell			
a,b,c (Å)	42.88, 81.82, 103.75	42.86, 81.23, 103.90	42.31, 80.77, 102.08
α=β=γ (°)	90	90	90
Number of unique reflections[a]	34678 (1965)	47126 (2264)	47253 (2162)
Number of observed reflections[a]	225230 (11584)	211852 (9484)	1234895 (49162)
Resolution (Å)[a]	35.67-1.80 (1.84-1.80)	37.91-1.60 (1.63-1.60)	39.08-1.60 (1.62-1.60
Rpim (%)[a,b]	4.3(13.8)	3.9 (38.0)	2.6 (33.2)
I/σ[a]	15.1(5.1)	10.7 (2.1)	17.0 (2.1)
Completeness (%)[a]	99.8 (97.7)	96.9 (95.5)	99.6 (93.2)
Redundancy[a]	6.5 (5.9)	4.5 (4.2)	26.1 (22.7)
Refinement			
Rcryst(%)[a,c]	15.83 (16.63)	16.51 (22.82)	16.57 (40.12)
Rfree(%)[a,c]	20.10 (21.59)	19.60 (26.28)	20.32 (45.43)
Ramachandran analysis			
Favored (%)	97.85	98.65	98.11
Allowed (%)	2.15	1.35	1.89
rmsd bonds	0.007	0.011	0.015
rmsd angles	1.051	1.286	1.393
Average B-factor for protein (Å^2)	23.55	25.49	26.35
Average B-factor for water (Å^2)	31.15	31.15	13.59
Average B-factor for ligands (Å^2)	15.21	16.35	14.00

[a]The values in parentheses are for the highest resolution shell. [b]$R_{pim} = \Sigma hkl \sqrt{((1/(n-1))}\ \Sigma i\ |Ii - \langle I \rangle| / \Sigma hkl \Sigma i Ii$, where Ii is the intensity of an individual reflection and <I> is the mean intensity obtained from multiple observations of symmetry related reflections. [c]R_{cryst} is $\Sigma||F_o - F_c||/\Sigma F_o$, where F_o is an observed amplitude and F_c a calculated amplitude; R_{free} is the same statistic calculated over a subset of the data that has not been used for refinement.

The binding of I-Tyr to TnIYD is stabilized by multiple interactions between I-Tyr, FMN, and the protein that are well conserved in mesophilic IYDs (Figure 4-7(A) and (B)).[31–33] The

[4] This table was compiled by Prof. Jennifer Kavran (Johns Hopkins University).

zwitterion of I-Tyr forms contacts with the zwitterion recognition triad (E68, Y72, and K92) and the isoalloxazine ring of FMN (Figure 4-7(A)). The enzyme-substrate interactions are also stabilized by: (1) hydrogen bonding interactions between the hydroxyl group of I-Tyr and the backbone amide of Met 41 (Ala in mesophilic IYDs) as well as the 2`-hydroxyl group of FMN's ribose tail, and (2) π-π interaction between the aromatic ring of I-Tyr and the isoalloxazine ring of FMN. F-Tyr binds TnIYD similarly as I-Tyr which is expected from the similar structures of both ligands with HsIYD. [31,134] Interestly, Tyr binds TnIYD in an almost identical fashion to I-Tyr with both TnIYD and HsIYD (Figure 4-7(C)). Therefore, the much tighter binding of Tyr to TnIYD than HsIYD is not a result of an alternative binding mode in the active site. The only noticeable difference between the structures of TnIYD with I-Tyr and Tyr is the conformation of a Tyr (Y112) near the iodine of I-Tyr. When Tyr binds the active site, the ring of Y112 points towards the ring of Tyr (the "in" conformation of Y112) and the two may potentially engage in hydrophobic interactions (closest distance 3.8 Å) to stabilize Tyr binding. The ring of Y112 points away from I-Tyr (the "out" conformation of Y112A) in the structure of TnIYD and I-Tyr possibly due to repulsion between the two (closest distance 2.2Å if the "in" conformation is retained). The affinity of Tyr was, therefore, measured with the TnIYD Y112A variant. The K_d of Tyr with TnIYD Y112A (0.9 μM) was only 2-fold greater than that of the wildtype enzyme and is still at least two orders of magnitude smaller than mesophilic IYDs. Therefore, Y112 is not a major contributor to the tight binding of Tyr to TnIYD.

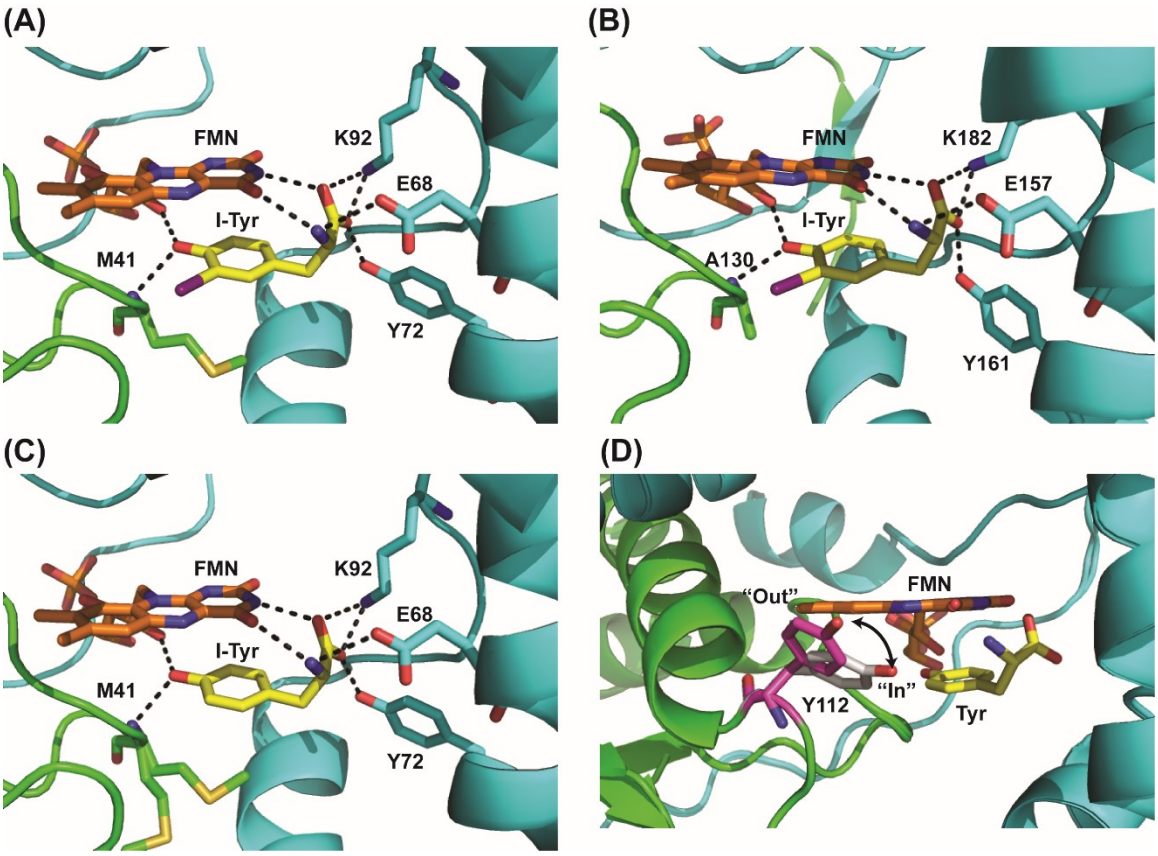

Figure 4-7 Active sites of TnIYD and HsIYD. (A) Active site structure of TnIYD with I-Tyr (PDB: 6Q1L). The monomeric units of the enzyme were colored with green and cyan. FMN and I-Tyr are shown in orange and yellow, respectively. Interactions between the substrate and TnIYD are shown in dashes (≤ 3.5 Å). (B) Active site structure of HsIYD with I-Tyr (PDB 4TTC).[31] (C) Active site structure of TnIYD with Tyr (PDB 6PZ0). M41 displays two conformations in this structure. (D) Overlay of active site of TnIYD with I-Tyr amd Tyr bound. For clarity, only Tyr (yellow) is shown as ligand and I-Tyr is omitted from the view. Y112 is colored magenta (the "out" conformation) and gray (the "in" conformation) in the structures with I-Tyr and Tyr bound, respectively.

4.3.6 Co-crystal structures of TnIYD in its semiquinone form and I-Tyr, F-Tyr, and Tyr are similar to those of oxidized TnIYD:[5]

The co-crystals of oxidized TnIYD with I-Tyr, F-Tyr, and Tyr were soaked into crystallization buffer supplemented with 0.5% dithionite in hope to obtain crystals of fully reduce TnIYD with ligand bound. The co-crystals of TnIYD with ligands upon dithionite treatment changed color from bright yellow to purple in ~ 10 s for F-Tyr and Tyr as ligand and in ~ 5 min for

[5] Looping and freezing of the crystals, data collection, and structure determination were performed by Prof. Jennifer Kavran (Johns Hopkins University).

I-Tyr as ligand. The purple color of the crystal indicating formation of TnIYD semiquinone (Figure 4-2(A)) and prolonged incubation with dithionite did not reduce the crystals of TnIYD semiquinone further to the fully reduced TnIYD which is expected to have a light yellow color or be colorless. The structure of the TnIYD semiquinone is still very interesting as very few crystal structures of flavoproteins in the semiquine form are available due to the difficulty in its formation and stabilization.[135–137] In addition, the co-crystal structures of I-Tyr and Tyr with TnIYD semiquinone can mimic the complexes between TnIYD semiquinone and the proposed halotyroxyl radical anion intermediate (Intermediate 2 in Figure 1-1) and tyroxyl radical intermediate (Intermediate 3 in Figure 1-1), respectively. Therefore, these structures may reveal the molecular basis by which TnIYD stabilizes these highly reactive intermediates during catalysis. The co-crystal structures of the semiquinone form of TnIYD with I-Tyr, F-Tyr, and Tyr were solved to 1.35 Å, 1.5 Å, and 1.5 Å, respectively. The data collection and structure refinement statistics are listed in Table 4-3. There is no visible conformational changes for TnIYD when these structures were compared to each other and to the corresponding oxidized co-crystal structures (Figure 4-8(A)). Previous studies reported subtle changes in the conformation of the isoalloxazine ring (2-5 ° bending) and the ribityl chain of protein bound flavin semiquinone compared to its oxidized counterpart.[135,137] However, no changes in FMN conformation were observed in the co-crystal structures of oxidized TnIYD and semiquinone TnIYD with I-Tyr bound (Figure 4-8(B)). The results seemed to suggest that the active site arrangement in the oxidized structures are sufficient to stabilize the proposed radical intermediates and the semiquinone of the FMN cofactor during catalysis. The formation of the active site lid in particular excludes bulk solvents from the active site (although there are specific water molecules in the active site whose roles are not clear) and creates a relative hydrophobic environment around I-Tyr which is a general strategy used by enzymes to stabilize highly reactive radical species.[138] Finally, it has been shown that flavoproteins can be reduced by X-ray.[135,139] It is always possible that the crystal of oxidized TnIYD was reduced by the X-ray beam to semiquinone

TnIYD or both the oxidized and semiquinone TnIYD were reduced to fully reduced TnIYD. Therefore, the fact that no structural differences were observed between the oxidized and semiquinone TnIYD could be an artifact.

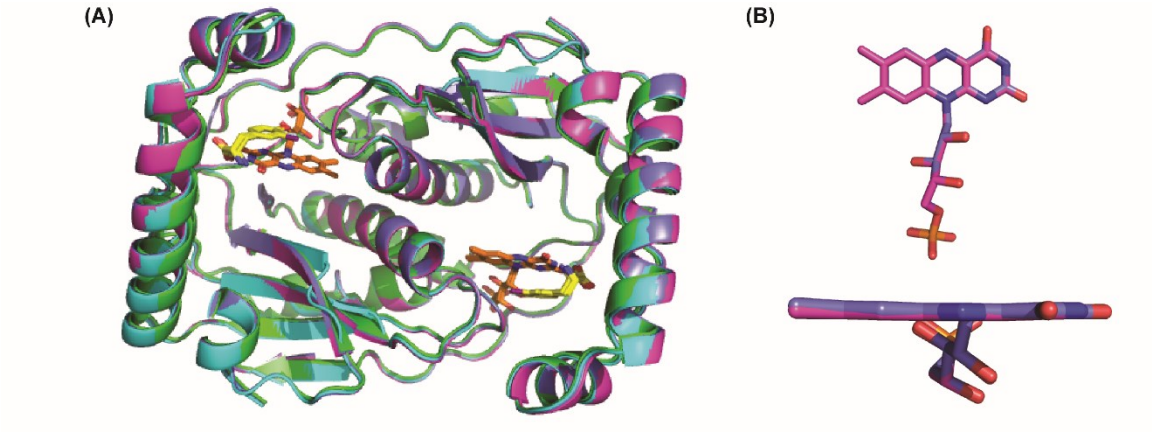

Figure 4-8 Crystal structures of TnIYD in its semiquinone form. (A) Overlay of co-crystal structures of TnIYD semiquinone and I-Tyr (magenta), F-Tyr (cyan), Tyr (green) with co-crystal structure of oxidized TnIYD and I-Tyr (blue). FMN and I-Tyr are shown in orange and yellow, respectively. (B) Overlay of oxidized FMN (blue) and FMN semiquinone (purple) in the corresponding co-crystal structures of TnIYD and I-Tyr.

Table 4-3 Data Collection and Refinement Statistics of the TnIYD semiquinone structures.[6]

PDB ID	n/a	6Q1L	n/a
Protein	TnIYD	TnIYD	TnIYD
Ligand	Tyr	I-Tyr	F-Tyr
Oxidation state	semiquinone	semiquinone	semiquinone
Data Collection			
Space group	P212121	P212121	P212121
Unit Cell			
a,b,c (Å)	42.91, 81.87, 103.74	42.86, 81.23, 103.90	42.31, 80.50, 101.79
α=β=γ (°)	90	90	90
Number of unique reflections[a]	86499 (3948)	47126 (2264)	46581 (2076)
Number of observed reflections[a]	1173112 (48215)	211852 (9484)	1219785 (48821)
Resolution (Å)[a]	39.65-1.3 (1.32-1.30)	37.91-1.60 (1.63-1.60)	38.93-1.60 (1.62-1.60)
Rpim (%)[a,b]	4.5 (191.7)	3.9 (38.0)	4.8 (81.6)
I/σ[a]	10.5 (1.2)	10.7 (2.1)	16.8 (2.9)
Completeness (%)[a]	95.2 (88.7)	96.9 (95.5)	99.2 (89.2)
Redundancy[a]	13.6 (12.2)	4.5 (4.2)	26.2 (23.5)
Refinement			
Rcryst(%)[a,c]	19.08 (31.17)	16.51 (22.82)	16.46 (32.89)
Rfree(%)[a,c]	20.87 (32.85)	19.60 (26.28)	19.77 (35.56
Ramachandran analysis			
Favored (%)	98.10	98.65	97.58
Allowed (%)	1.9	1.35	2.15
rmsd bonds	0.006	0.011	0.016
rmsd angles	1.053	1.286	1.441
Average B-factor for protein (Å^2)	16.48	25.49	14.90
Average B-factor for water (Å^2)		31.15	
Average B-factor for ligands (Å^2)		16.35	

[a]The values in parentheses are for the highest resolution shell. [b]R_{pim} =Σhkl√((1/(n-1)) Σi |Ii - <I>| / ΣhklΣiIi, where Ii is the intensity of an individual reflection and <I> is the mean intensity obtained from multiple observations of symmetry related reflections. [c]R_{cryst} is $\Sigma||F_o - F_c||/\Sigma F_o$, where F_o is an observed amplitude and F_c a calculated amplitude; R_{free} is the same statistic calculated over a subset of the data that has not been used for refinement.

4.3.7 An additional binding mode of I-Tyr in the structures with oxidized and semiquinone TnIYD is possibly the structural basis for the severe substrate inhibition of TnIYD:

As described in the last section, no major changes of TnIYD were induced by reduction of its oxidized FMN to the semiquinone form. However, an alternative binding site for I-Tyr besides

[6] This table was compiled by Prof. Jennifer Kavran (Johns Hopkins University).

the two active sites was discovered in the structure of TnIYD semiquinone with I-Tyr (Figure 4-9(A)). Full electron density for the iodine and phenol ring of I-Tyr can be detected at this alternative binding site. Careful inspections of the electron density map of the oxidized TnIYD with I-Tyr also revealed extra electron density corresponding to the iodine atom of I-Tyr. However, no extra electron density at this site was displayed for the structures with F-Tyr and Tyr, regardless of the oxidization state of FMN. This alternative binding of I-Tyr is most likely mediated by van der Walls interactions between the iodine and the backbone and Cα atoms of R114 and E115 (between 4.0 Å and 4.5 Å, Figure 4-9(B)). The smaller fluoride and hydrogen atoms provide much weaker van der Walls interactions compared to iodine and therefore F-Tyr and Tyr are not seen at this alternative binding site.

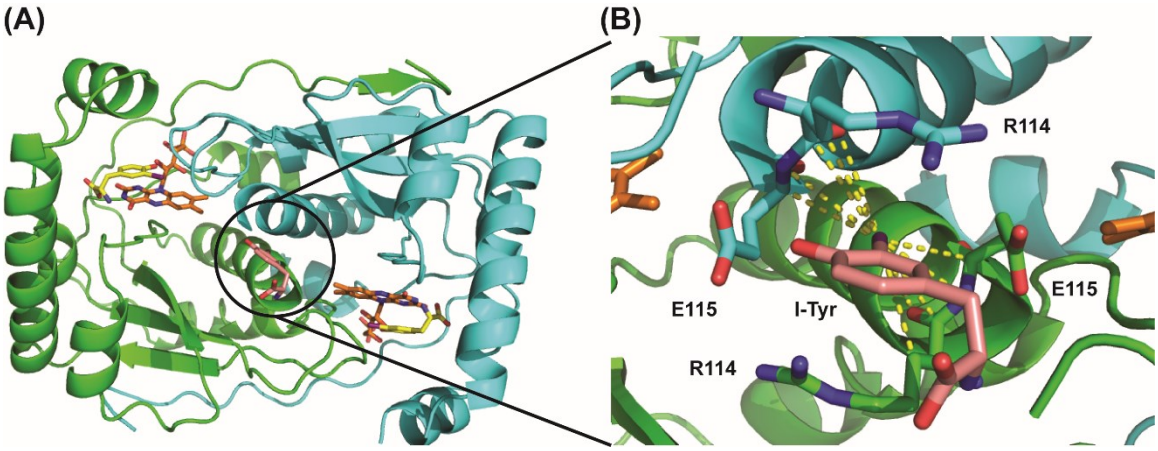

Figure 4-9 Additional binding site of I-Tyr in the structure of TnIYD semiquinone with I-Tyr. (A) An overall view of the alternative binding site on the context of the whole protein. The monomeric units of the enzyme are colored with green and cyan. FMN and I-Tyr in the active sites are shown in orange and yellow, respectively. I-Tyr occupies the alternative site is colored in pink. (B) Interactions (yellow dashes, 4.0-4.5 Å) between the iodine of I-Tyr and R114 and E115.

The biophysical basis of substrate inhibition on enzyme kinetics is proposed to involve the binding and subsequent inhibition of the enzyme-substrate complex by a second molecule of substrate.[117] Therefore, the alternative binding observed for TnIYD with I-Tyr might be the molecular basis for its severe substrate inhibition. As stated above, the van der Walls interactions likely responsible for the binding of I-Tyr will be weaker once iodine is substituted with smaller

atoms and potentially result in weaker substrate inhibition. The 4-fold larger K_i of Cl-Tyr TnIYD relative to that of I-Tyr is consistent with this hypothesis (Table 4-1). The substrate inhibition is generally weaker in mesophilic IYDs which likely explains the absence of I-Tyr occupying similar alternative binding sites in the structures of oxidized mesophilic IYDs.

4.4 Summary:

In this chapter, the structural and functional analysis of a thermophilic IYD-TnIYD was described. TnIYD was purified from *E. coli* cells in its semiquinone form. This semiquinone species was formed via reduction of the oxidized enzyme by free flavin generated by *E. coli* flavin reductases. Binding of Tyr further stabilized the TnIYD semiquinone. TnIYD is a functional thermophilic deiodinase that exhibits higher activity with increased temperature. Even at 25 °C the activity of TnIYD was already higher than mesophilic IYDs, albeit with more severe substrate inhibition. TnIYD represents the minimal structural requirement for reductive dehalogenation as it lacks the N-terminal extensions and a flexible loop near the active site typically in mesophilic IYDs. The binding mode of I-Tyr and Tyr to the active site of oxidized TnIYD is identical to oxidized HsIYD, even though TnIYD binds Tyr at least two orders of magnitude tigher than mesophilic IYDs. Tyr, however, does not bind to fully reduced TnIYD and therefore avoids inducing severe product inhibition. The co-crystals of oxidized TnIYD with I-Tyr, Tyr, F-Tyr were readily reduced to the semiquinone form by dithionite but were not able to undergo further reduction to the hydroquinone. Reduction of the FMN cofactor from oxidized to semiquinone did not change the overall structure of TnIYD, the conformation of FMN, and the active site binding of ligands, suggesting that the active site conformation and binding mode of the substrate observed with the oxidized structures are sufficient to stabilize intermediates involving TnIYD semiquinone during catalysis. An alternative binding mode for I-Tyr was observed with both oxidized and the semiquinone TnIYD. This binding is mainly mediated by the van der Walls interaction between the halogen atom of the ligand and protein atoms surrounding the binding site and is likely the

molecular basis for the severe substrate inhibition of TnIYD. The results established that TnIYD is a functional thermophilic dehalogenase but represents a unique subgroup of IYDs as it exhibits many differences from previously characterized mesophilic IYDs. Further structural and mechanistic studies are needed to reveal the productive substrate-enzyme interactions with fully reduced TnIYD and the rate-determining step of its catalysis to facilitate the engineering of TnIYD towards the bioremediation of halophenols. Since the reduction of the crystals of TnIYD•FMN_{ox} by dithionite only resulted in crystals of TnIYD•FMN_{sq} but not TnIYD•FMN_{hq}, two parallel alternative approaches to obtain the crystals of TnIYD•FMN_{hq} are currently under investigation. In the first approach, TnIYD•FMN_{hq} will be generated by dithionite reduction of TnIYD•FMN_{ox} prior to crystallization. TnIYD•FMN_{hq} will then be mixed with F-Tyr and crystallized in an anaerobic glovebox. Access to the glovebox is kindly provided by Prof. Squire Booker (Pennsylvania State University). Alternatively, the crystal of ligand free TnIYD•FMN_{ox} might be reduced to TnIYD•FMN_{hq} by dithionite. F-Tyr can then be soaked into crystal of ligand free TnIYD•FMN_{hq} to generate the co-crystal of TnIYD•FMN_{hq} and F-Tyr.

Chapter 5 Effect of substrates and substrate analogs on the reduction of iodotyrosine deiodinase: cofactor regeneration as a possible rate-determining step for dehalogenation

5.1 Introduction:

Over the years, IYD enzymology has been advanced via identification of IYD's sequence in mammals, its heterologous expression and purification, discovery of its wide distribution in all domains of life, and determination of its crystal structures.[24,29] However, one important question still remains unanswered: what is the rate-determining step for the reductive dehalogenation catalyzed by IYD?

As mentioned in Chapter 1, the proposed mechanism for the reductive dehalogenation of IYD proceeds by two sequential one electron transfer steps from the reduced FMN cofactor of IYD (IYD•FMN_{hq}) to the halogenated substrates.[29] Redox titration and mutational analysis have demonstrated the likely involvement of a FMN semiquinone intermediate (IYD•FMN_{sq}) in IYD catalysis under steady-state conditions.[31] However, the IYD•FMN_{sq} intermediate was not observed in a significant quantity during the re-oxidation of HsIYD•FMN_{hq} by I-Tyr under pre-steady state conditions.[26] Therefore, any steps that may involve accumulation of the FMN semiquinone such as halide release and the second electron transfer (Figure 1-1, step (3) and (4), respectively) are not likely to be rate-determining. Other possible slow steps along the reaction coordinate are the tautomerization of substrate and the first electron transfer (Figure 1-1, step (1) and (2), respectively) since they both involve formation of unstable substrate and/or FMN intermediates. However, the lack of a solvent isotope effect suggested that protonation of the carbon with iodine attached during the tautomerizaiton of I-Tyr is not the rate-determining step for HhIYD.[50,140] In addition, reconstitution of FMN by analogs with varied redox potentials did not significantly affect the activity of I-Tyr deiodination of HhIYD, which then suggested that electron transfer was also not

rate-determining.[50,141] There seems to be no other steps from the oxidative half reaction of IYD•FMN_{hq} that can be rate-determining.

The first order rate constants for the re-oxidation of HsIYD•FMN_{hq} measured under pre-steady state conditions showed a linear response to I-Tyr concentration up to 25-fold higher than the enzyme concentration (8 μM) (Figure 5-1).[26] In addition, the second order rate constant of HsIYD•FMN_{hq} re-oxidation by I-Tyr correlates well with the k_{cat}/K_M value obtained under steady-state condition. This implies that the re-oxidation is rate-determining when HsIYD is not saturated with I-Tyr. However, the first order rate constants of HsIYD•FMN_{hq} re-oxidation observed at all I-Tyr concentrations were invariably higher (up to 17-fold) than the k_{cat} value measured under steady-state conditions. Thus, the first order rate constant of HsIYD•FMN_{hq} re-oxidation with saturation levels of I-Tyr is higher than the k_{cat}. This suggests that the dehalogenation reaction will no longer be rate-determining as the concentration of I-Tyr increases towards saturation level. Therefore, the rate-determining step under such conditions may be associated with the reductive half reaction of IYD catalysis.

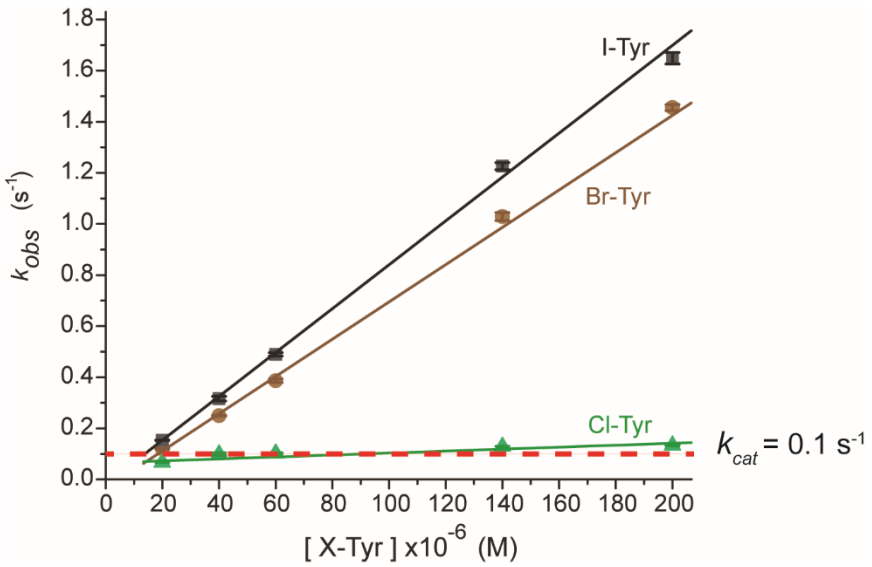

Figure 5-1 Oxidation of HsIYD•FMN_{hq} (8 μM) by halotyrosines as a function of concentration under pre-steady state conditions. Oxidation of HsIYD•FMN_{hq} was monitored by absorbance at 446 nm. Values and error bars were the average and standard deviation of three independent measurements. The solid lines were generated by linear best fits to the data. The red dashed line represented the k_{cat} value of HsIYD with I-Tyr under steady-state conditions. This figure was modified from Bobyk, K. D.; Ballou, D. P., Rokita, S. E.[26]

The reductive half reaction for IYD is the reduction of its oxidized FMN cofactor (IYD•FMN_{ox}) to HsIYD•FMN_{hq}. As mentioned in Chapter 4, the physiological reducing equivalent for IYD is NADPH but sodium dithionite is used instead in most enzymological studies since the electron transfer system proposed to shuttle electrons between NADPH and IYD has not yet been identified.[29] Dithionite reduction of IYD was not expected to be rate-determining since dithionite is strongly reducing ($E_{0.5}$ = -660 mV, pH 7) and is the most versatile and widely used reducing agent in biochemistry.[142,143] Flavin reduction by NAD(P)H can be rate-determining in some reductases and monooxygenases.[144,145] However, these past investigations have not determined if reduction by dithionite can be rate-determining in these systems. In one example where the dithionite reduction and the NADH reduction of the FMN dependent type 2 isopentenyl diphosphate:dimethylallyl diphosphate isomerase was compared, dithionite was able to reduce the enzyme at least 50-fold faster than NADH.[146,147]

In this chapter, the effect of substrates and substrate analogs on the reduction of HsIYD and TnIYD by excess dithionite was studied to determine its contribution to the rate-determining step of steady-state catalysis. The reduction of HsIYD and TnIYD was monitored by the decrease in 450 nm absorbance in the presence of I-Tyr, Cl-Tyr, F-Tyr, and Tyr at 25 °C. While all four ligands were found to inhibit the reduction of TnIYD as described below, only I-Tyr and Cl-Tyr inhibited HsIYD. The inhibition of enzyme reduction by substrates was more pronounced at higher substrate concentrations. As a result, reduction of enzyme under such conditions can be rate-limiting for the turnover of both enzymes. The inhibition of TnIYD reduction by I-Tyr and F-Tyr was partially relieved by an Y112A mutation. At 60 °C, the rate of TnIYD reduction in the presence of I-Tyr was much faster than that at 25 °C, which is consistent to the thermophilic nature of *Thermotoga neapolitana*.

5.2 Materials and methods:

5.2.1 Protein expression and purification:

HsIYD, TnIYD, TnIYD Y112A were expressed in E. coli as previously described (Section 2.2.3). HsIYD was purified with the same protocol in Section 2.2.3 in which the SUMO tag was removed from the preparation after cleaved off from HsIYD by ULP1 protease. TnIYD and TnIYD Y112A free of Tyr were purified as described in Section 4.2.2.

5.2.2 Reduction of IYD in the absence and presence of Tyr and halotyrosines:

Reduction of IYD in the absence and presence of substrates and substrate analogs were monitored by UV-vis spectroscopy aerobic conditions. TnIYD, TnIYD Y112A and HsIYD (15 μM) was alternatively incubated with 1 to 100 equivalent of I-Tyr, Cl-Tyr, F-Tyr, or Tyr relative to enzyme in 180 μL of 110 mM potassium phosphate, 220 mM potassium chloride, pH 7.4 in a cuvette at room temperature (25 ± 1 ºC with a thermometer) for 5 min. Sodium dithionite (20 μL of 0.5% in 5% sodium bicarbonate) was then added to the cuvette and vigorously mixed by pipetting for 6 s to initiate the reduction. The spectrum from 200 to 900 nm was monitored with a

Hewlett Packard 8453 Diode-Array Spectrophotometer every 5 s for 15 min. Reduction of TnIYD in the presence of 1 and 100 equivalent of I-Tyr was repeated at 60 ± 2 ºC (the actual temperature in the cuvette holder was measured by a thermometer and maintained by a circulating bath).

In cases when I-Tyr were added after the reduction of IYD, the enzyme was first incubated with sodium dithionite at room temperature for 5 min. The reaction was initiated by addition of I-Tyr (1 equivalent to enzyme), mixed and monitored similarly as described above.

5.2.3 HPLC analysis of the dithionite reduction of IYD in the presence of I-Tyr:

Reduction of HsIYD and TnIYD in the presence of I-Tyr described in the last section was quenched by 10 μL 44% formic acid. The cuvette was then incubated at 60 ºC for 2 min to ensure the decomposition of dithionite (white precipitations were generated from the decomposition which is likely elemental sulfur).[116] Phenol as an internal standard (10 μL of 0.1 mM in 10 M sodium hydroxide) was added to the reaction to neutralize the formic acid. The neutralized reaction was then transferred to a microcentrifuge tube and centrifuged at 14000×g for 5 min. The supernatant (10-100 μL) was diluted by 110 mM potassium phosphate, 220 mM potassium chloride, pH 7.4 to a final volume of 1100 μL. This sample (900 μL) was then analyzed by HPLC and the deiodination product Tyr was detected via fluorescence as described in Section 4.2.5.

5.2.4 Deiodination assay with different methods of reaction initiation:

Deiodination by TnIYD with I-Tyr was measured after two alternative methods of reaction initiation. The TnIYD•FMN_{hq} initiation method (reaction initiated by adding TnIYD reduced by excess dithionite to a solution of I-Tyr) is same as the deiodination assay with I-Tyr described in Section 4.2.5 in which Tyr was detected by HPLC by monitoring fluorescence. The dithionite initiation method (reaction initiated by adding dithionite to a solution of TnIYD pre-incubated I-Tyr) is same as the deiodination assay with 2IP as substrate described in Section 4.2.5.

5.3 Results and discussion:

5.3.1 Reduction of HsIYD by dithionite is inhibited by I-Tyr:

Dithionite reduction of HsIYD•FMN_{ox} was monitored by the decrease of 450 nm absorbance in the absence and presence of I-Tyr to investigate the effect of substrate on the reduction of HsIYD•FMN_{ox}. In the absence of I-Tyr, 0.05% dithionite (~ 24 mM) fully reduced HsIYD•FMN_{ox} (15 μM) within the mixing time of the assay (≤ 6 s) (Figure 5-2(A), red). However, when the same experiment was repeated in the presence of 15 μM I-Tyr, the reduction of HsIYD•FMN_{ox} slowed by at least 5-fold as reduction required 30 s to complete (Figure 5-2(A), blue). The observed change in absorbance at 450 nm is a combined effect of HsIYD•FMN_{ox} reduction by dithionite (decreased 450 nm absorbance) and HsIYD•FMN_{hq} oxidation by I-Tyr (increased 450 nm absorbance). The delay in full reduction observed in the presence of I-Tyr is not solely a result of the re-oxidation of HsIYD•FMN_{hq}. When 15 μM I-Tyr was added to HsIYD•FMN_{hq} in the presence of excess dithionite (0.05%), re-oxidation (up to 10% of total HsIYD•FMN_{ox}) was observed within the first 10 s (Figure 5-2(A), black). However, within the same time period ~ 40% of total HsIYD•FMN_{ox} remained in the oxidized form when reduced in the presence of I-Tyr. The slower reduction is also not caused by the accumulation of Tyr-the deiodination product of I-Tyr since the presence of up to 100 equivalent of Tyr to enzyme had no effect on the reduction of HsIYD•FMN_{ox} (Figure 5-2(B)), consistent with the weak binding of Tyr to HsIYD (K_d > 1 mM).[31] Therefore, the binding of I-Tyr inhibits the reduction of HsIYD. It is possibly that the closure of the active site lid induced by I-Tyr blocks entrance of dithionite into the active site.

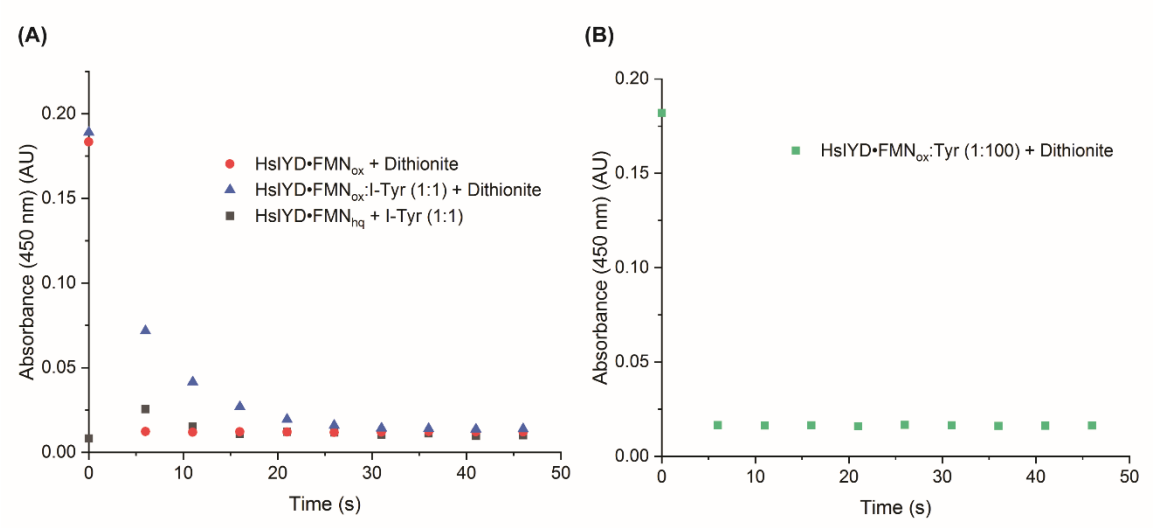

Figure 5-2 Reduction of HsIYD•FMN_{ox} in the absence and presence of I-Tyr and Tyr. (A) Solutions (180 µL) of HsIYD•FMN_{ox} (15 µM final) and I-Tyr (0 µM (red) and 15 µM final (blue)) in 220 mM potassium chloride, 110 mM potassium phosphate, pH 7.4 were mixed with 20 µL 0.5% sodium dithionite in 5% sodium bicarbonate at t = 0 s. Reduction of HsIYD•FMN_{ox} was monitored by decrease of absorbance at 450 nm. For the re-oxidation of HsIYD•FMN_{hq} by I-Tyr (black), solutions (160 µL) of HsIYD•FMN_{ox} (15 µM final) in the above buffer was mixed with 20 µL 0.5% sodium dithionite in 5% sodium bicarbonate prior to addition of 20 µL I-Tyr (15 µM final) at t = 0 s. Re-oxidation of HsIYD•FMN_{hq} was monitored by increase of absorbance at 450 nm. (B) Reduction of HsIYD•FMN_{ox} in the presence of 100 equivalent of Tyr to enzyme was performed similarly as described in (A).

Dithionite reduction of HsIYD in the presence of 5-100 equivalent of I-Tyr was subsequently investigated to study the effect of I-Tyr concentration on the reduction of HsIYD. The decrease of absorbance at 450 nm slowed as the concentration of I-Tyr increased (Figure 5-3). With I-Tyr concentrations between 7.5 and 20 equivalent to HsIYD, the decrease of 450 nm absorbance with a slow phase followed by a fast phase (Figure 5-3, green, purple, yellow). The slow phase is most likely a steady-state during which the reduction of HsIYD•FMN_{ox} by excess dithionite was inhibited by the rapid re-oxidation of HsIYD•FMN_{hq} by I-Tyr. As I-Tyr was consumed overtime, the rate of reduction began to outcompete the rate of re-oxidation and the 450 nm absorbance started to decrease rapidly due to the fast buildup of HsIYD•FMN_{hq}. Such hypothesis was confirmed by HPLC analysis of the reduction reaction in the presence of 20 equivalent I-Tyr to HsIYD. At this I-Tyr concentration, the phase where reduction of

HsIYD•FMN_{ox} was slower than the re-oxidation of HsIYD•FMN_{hq} lasted about 370 s (Figure 5-3, yellow). Roughly 210 µM deiodination product Tyr (70% of total I-Tyr) was produced during this phase. The remaining I-Tyr represented approximately 6 equivalent to HsIYD at the beginning of the next phase where reduction outcompetes re-oxidation. This is in good agreement with the fact that the first phase was not observed with I-Tyr less than 7.5 equivalent to HsIYD (Figure 5-3, green) likely due to much slower re-oxidation of HsIYD•FMN_{hq} compared to the reduction of HsIYD•FMN_{hq} at low I-Tyr concentrations (Figure 5-2 (B)). The results suggested that the reduction of HsIYD•FMN_{ox} was inhibited by I-Tyr in a concentration dependent manner and was slower than the re-oxidation of HsIYD•FMN_{hq} at high I-Tyr concentrations.

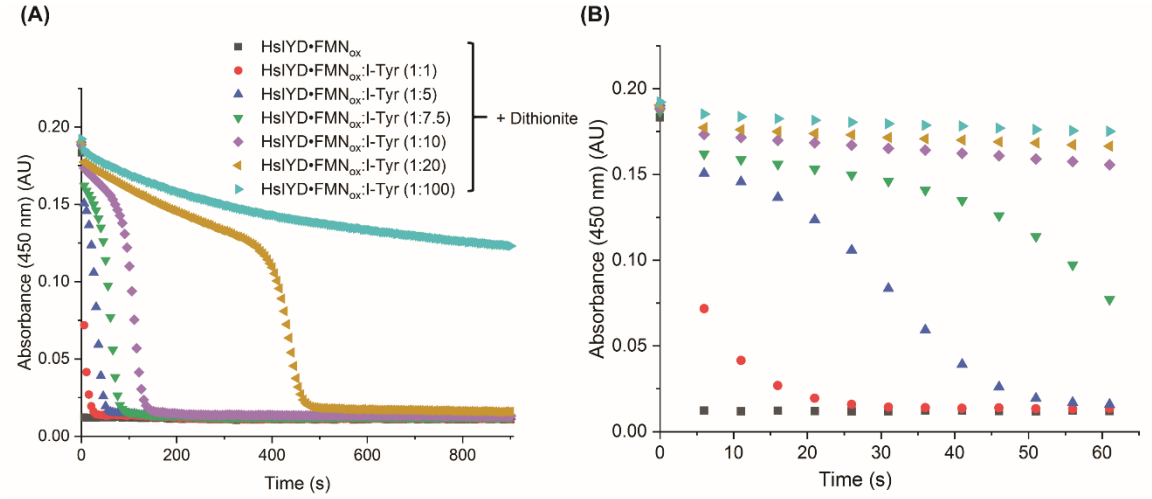

Figure 5-3 Effect of I-Tyr concentration on reduction of HsIYD•FMN_{ox}. (A) Solutions (180 µL) of HsIYD•FMN_{ox} (15 µM final) and I-Tyr (5-100 equivalent to HsIYD) in 220 mM potassium chloride, 110 mM potassium phosphate, pH 7.4 were mixed with 20 µL 0.5% sodium dithionite in 5% sodium bicarbonate at t = 0 s. Reduction of HsIYD•FMN_{ox} was monitored by decrease of absorbance at 450 nm. The data with 0 and 1 equivalent were the same with those shown in Figure 5-2(A). (B) The same data in (A) within the first 60 s of reduction. The conditions are color-code as described in (A).

5.3.2 A HsIYD semiquinone species is detected during the reduction of HsIYD:

During the reduction of HsIYD in the presence of high concentrations of I-Tyr (10-100 equivalents), an absorption band around 590 nm corresponding to a FMN semiquinone (FMN_{sq}) species was observed during the phase where reduction is slower than re-oxidation (Figure 5-4).[148]

A similar HsIYD•FMN_{sq} species was also observed during the re-oxidation of HsIYD•FMN_{hq} by I-Tyr under pre-steady-state conditions at a very low level that did not correlate to an on-pathway intermediate.[26] A FMN_{sq} species was also observed with MmIYD during its re-oxidation with I-Tyr under single turnover conditions and was stable under aerobic conditions for days (post turnover).[27] Therefore, the HsIYD•FMN_{sq} species observed during the reduction is most likely an off pathway species different from the catalytically active HsIYD•FMN_{sq} during catalysis. This species is most likely stabilized by the binding of substrates since the ligand free enzyme is readily reduced. The formation of this HsIYD•FMN_{sq} species might be an additional source for the overall decrease of 450 nm absorbance besides the slowly increasing population of HsIYD•FMN_{hq}.

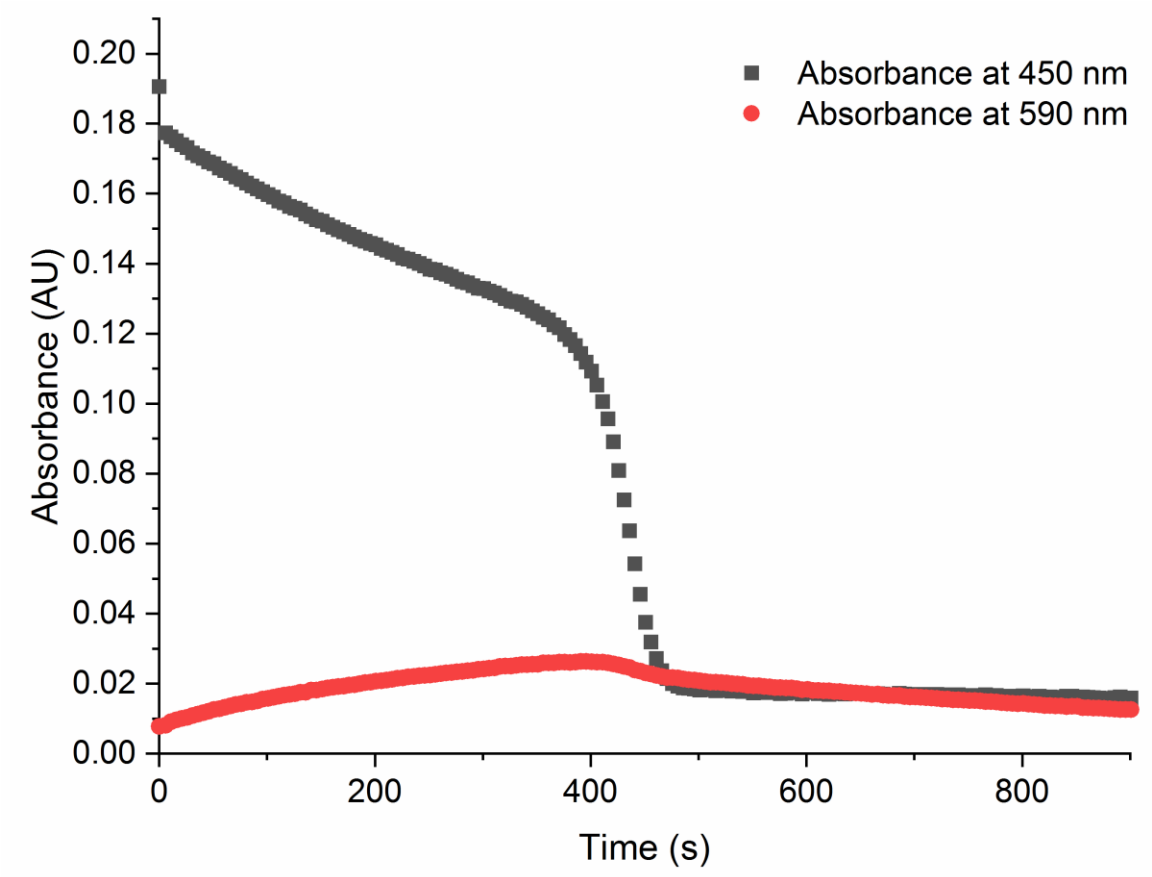

Figure 5-4 Formation and decay of a HsIYD•FMN_{sq} species during the dithionite reduction of HsIYD in the presence of I-Tyr (20 equivalent to enzyme). The data shown in this figure were from the same reduction assay of HsIYD in the presence of I-Tyr (20 equivalent to enzyme) as shown in Figure 5-2(A).

5.3.3 Reduction of HsIYD by dithionite is inhibited by Cl-Tyr in addition to I-Tyr:

The effect of Cl-Tyr on the ditionite reduction of HsIYD was studied similarly as I-Tyr (Figure 5-5(A)). The reduction of HsIYD•FMN_{ox} in the presence of 1 equivalent of Cl-Tyr occurred similarly to that observed with 1 equivalent I-Tyr. Therefore, both Cl-Tyr and I-Tyr inhibit the reduction of HsIYD•FMN_{ox} relative to the ligand free enzyme under single turnover conditions. Interestingly, no significant inhibition of HsIYD•FMN_{ox} reduction in the presence of as much as 100 equivalent of F-Tyr to enzyme was observed despite that F-Tyr binds to HsIYD•FMN_{ox} only 10-fold less tightly than I-Tyr and Cl-Tyr.[31] In the presence of more than 5 equivalent of I-Tyr, the reduction of HsIYD started with a slow phase where the rate of re-oxidation outcompetes the rate of reduction followed by a fast phase where the re-oxidation becomes rate-limiting due to depletion of substrates. However, the decrease in 450 nm absorbance with high concentrations of Cl-Tyr started with a fast phase for a few seconds before entering a slow steady phase (Figure 5-5(B)). The re-oxidation rate of HsIYD•FMN_{hq} by Cl-Tyr was much slower than I-Tyr (Figure 5-1).[26] Therefore, if the slow phase is where the re-oxidation and reduction reaches an equilibrium, the fast phase proceeding this equilibrium is probably the pre-steady-state phase before the slow re-oxidation of HsIYD•FMN_{hq} started competing with the reduction. However, when the concentration of Cl-Tyr is smaller than 100 equivalent to enzyme, the re-oxidation is still rate-determining so that the accumulation of HsIYD•FMN_{hq} dominates. The HsIYD•FMN_{sq} species also formed during turnover of HsIYD•FMN_{ox} in the presence of more than 5 equivalent of Cl-Tyr to enzyme) in a higher concentration than that was observed in the presence of I-Tyr at similar concentrations. Higher concentrations of HsIYD•FMN_{sq} were similarly observed during the re-oxidation of HsIYD•FMN_{hq} by Cl-Tyr than by I-Tyr under previous pre-steady-state investigations.[26] Based on results obtained here, the rate-determining step for Cl-Tyr turnover is likely the re-oxidation of HsIYD•FMN_{hq} under low Cl-Tyr concentrations since the reduction of HsIYD•FMN_{hq} was much less inhibited by re-oxidation for Cl-Tyr compared to I-Tyr. Under high Cl-Tyr concentrations, the

rates of re-oxidation are comparable to the k_{cat} of I-Tyr deiodination (Figure 5-1). The steady-state kinetics of HsIYD with Cl-Tyr has not been reported. However, the k_{cat} for Cl-Tyr was 3-fold and 6-fold less than I-Tyr for DmIYD and TnIYD (25 °C, Table 4-1), respectively.[28] The re-oxidation rates of HsIYD under high Cl-Tyr concentrations are likely to be higher than its steady-state k_{cat} and therefore the reduction of HsIYD could still be at least partially rate-determining at high Cl-Tyr concentrations.

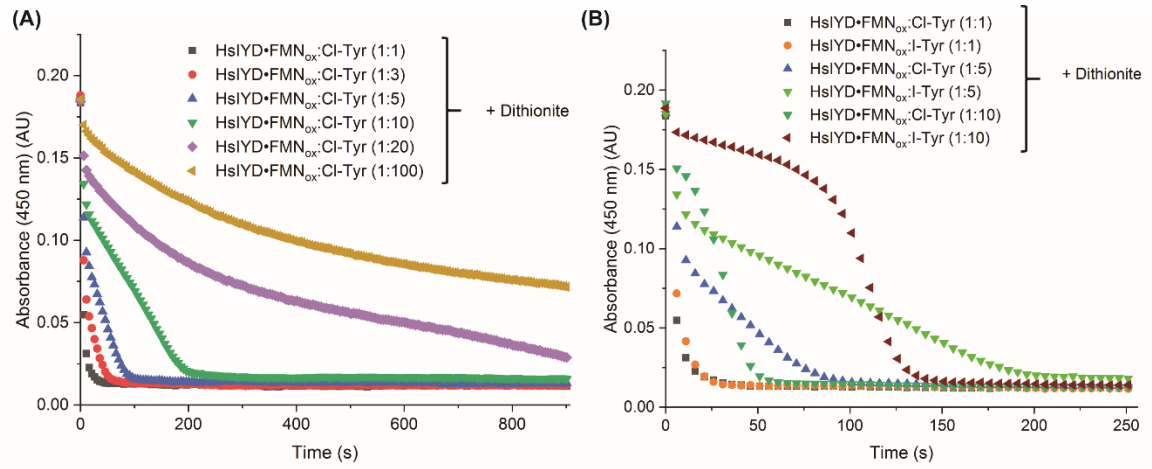

Figure 5-5 Effect of Cl-Tyr concentration on reduction of HsIYD•FMN_{ox}. (A) Solutions of HsIYD•FMN_{ox} (15 μM final) and Cl-Tyr (1-100 equivalent to HsIYD) were mixed with dithionite same as decribed in Figure 5-2(A). Reduction of HsIYD•FMN_{ox} was monitored by decrease of absorbance at 450 nm. (B) Comparison of reduction of HsIYD•FMN_{ox} in the presence of 1, 5, and 10 equivalent of I-Tyr and Cl-Tyr. The data for I-Tyr were the same with those shown in Figure 5-2(A).

5.3.4 Reduction of TnIYD by dithionite is severely inhibited by I-Tyr:

The effect of I-Tyr on the dithionite reduction of oxidized TnIYD (TnIYD•FMN_{ox}) was then studied similarly to that with HsIYD by monitoring the decrease of 450 nm absorbance. In the absence of I-Tyr, TnIYD•FMN_{ox} (15 μM) was fully reduced by dithionite (0.05%) within the mixing time of the assay (≤ 6 s) similar to HsIYD (Figure 5-6(A), black). Strikingly, even just 1 equivalent of I-Tyr to TnIYD severely slowed the decrease of 450 nm absorbance by at least 500-fold (~ 4.2 μM reduced in 15 min) compared to ligand free TnIYD (Figure 5-6(A), red). This inhibition is 100-fold more severe than that observed for HsIYD with 1 equivalent of I-Tyr. The

inhibition is not a result of rapid re-oxidation since re-oxidation of pre-reduced TnIYD•FMN_{hq} by 1 equivalent I-Tyr in the presence of excess dithionite was only observed during the first 60 s (Figure 5-6(B), red). The inhibition is also not caused by accumulation of Tyr since 1 equivalent of Tyr only marginally inhibited the reduction for less than 60 s (Figure 5-6(B), green). However, Tyr inhibited TnIYD reduction much more efficient than HsIYD reduction since no inhibition of HsIYD reduction was observed in the presence of up to 100 equivalent of Tyr to enzyme (Figure 5-2(B)). This is consistent with 10^4-fold tighter binding of Tyr to TnIYD•FMN_{ox} than to HsIYD•FMN_{ox}. The results demonstrated that the reduction of TnIYD was severely inhibited by binding of 1 equivalent of I-Tyr. Similarily as for HsIYD, such inhibition is likely due to the closure of TnIYD's active site lid induced by I-Tyr.

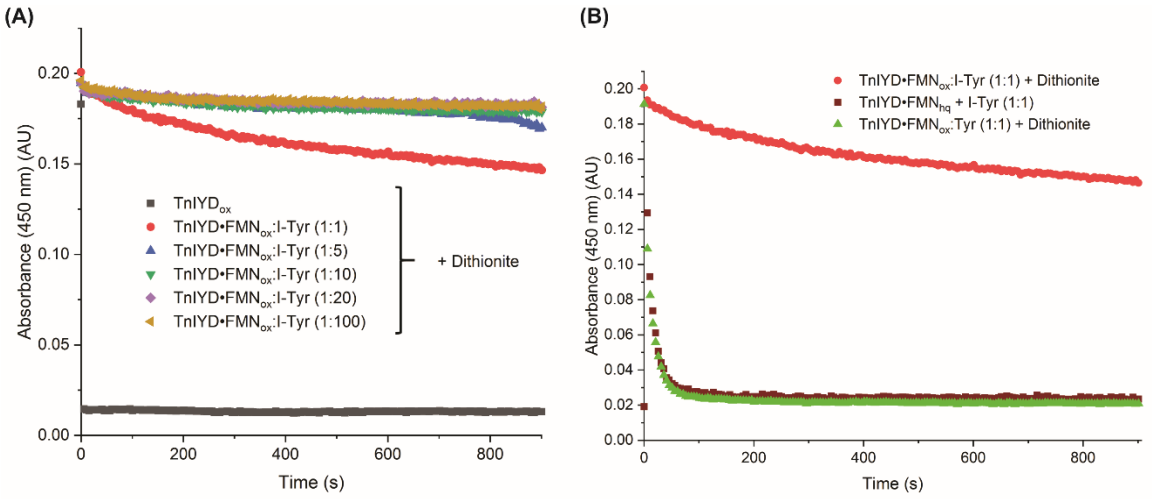

Figure 5-6 Effect of I-Tyr and Tyr on reduction of TnIYD•FMN_{ox}.(A) Solutions of TnIYD•FMN_{ox} (15 µM final) and I-Tyr (1-100 equvalent to enzyme) were mixed with dithionite similarly as described in Figure 5-2(A). Reduction of TnIYD•FMN_{ox} was monitored by decrease of absorbance at 450 nm. (B) For reduction of TnIYD in the presence of Tyr, a solution of TnIYD•FMN_{ox} (15 µM final) and Tyr (1 equvalent to enzyme, green) was mixed with dithionite similarly as described in Figure 5-2(A). For the re-oxidation of TnIYD•FMN_{hq} by I-Tyr (dark red), a solution of TnIYD•FMN_{ox} (15 µM final) was mixed with sodium dithionite prior to addition of I-Tyr (15 µM final) as described in Figure 5-2(A). Re-oxidation of TnIYD•FMN_{hq} was monitored by increase of absorbance at 450 nm.

Inhibition of TnIYD reduction was even more pronounced as I-Tyr concentration increased (Figure 5-6(A)). With more than 5 equivalent of I-Tyr, the decrease of 450 nm absorbance in the

presence of excess dithionite nearly stalled (only 1.3 μM TnIYD•FMN_{ox} (less than 10%) reduced in 15 min). Detection of Tyr after15 min of TnIYD reduction reaction with 10, 20, 100 equivalent of I-Tyr showed that TnIYD in these reactions were still actively producing Tyr with V/[E]s of 0.17, 0.21, and 0.08 min^{-1}, respectively. The results suggested that at high I-Tyr concentrations, the reduction of TnIYD was also slower than re-oxidation of TnIYD•FMN_{hq} by I-Tyr in addition to the already severe inhibition by binding of I-Tyr as demonstrated under single turnover conditions. The magnitude of V/[E]s of Tyr formation described above were about 10-fold smaller than the k_{cat} of TnIYD with I-Tyr at 25 °C (Table 4-1). This discrepancy is a result of different reaction initiation method being used. The reactions for steady-state kinetics of TnIYD with I-Tyr described in Section 4.3.4 were initiated by adding TnIYD•FMN_{hq} pre-reduced with dithionite to a solution of I-Tyr (TnIYD•FMN_{hq} initiation). However, when the reactions were initiated by adding dithionite to pre-incubated TnIYD and I-Tyr like in the reduction assays (dithionite initiation), the measured k_{cat} (0.42 ± 0.07 min^{-1}) was 10-fold smaller than that obtained by the TnIYD•FMN_{hq} initiation method and is within the same order of magnitude with the V/[E]s measured in the reduction assay (Appendix Table D1).[7] Two initiation methods only have different impacts on the first turnover after which the next turnover starts with the TnIYD•Tyr complex for both methods. Therefore, the much slower activity measured by the dithionite initiation method compared to the TnIYD•FMN_{hq} initiation method was most likely due to inhibition of TnIYD reduction by pre-incubation with I-Tyr in the first turnover. A TnIYD semiquinone species (TnIYD•FMN_{sq}) was also detected during the reduction of TnIYD in the presence of I-Tyr, but in much smaller quantity compared to HsIYD.

5.3.5 Reduction of TnIYD by dithionite was inhibited by Cl-Tyr and F-Tyr as well:

The effect of Cl-Tyr on the reduction of TnIYD•FMN_{ox} by dithionite was studied similarly as that described above with I-Tyr (Figure 5-7). Cl-Tyr also inhibited the reduction of TnIYD at both low (1 equivalence) and high (100 equivalence) concentrations. TnIYD reduction inhibited by

[7] This measurement were performed by Shaun Spisak (Johns Hopkins University).

Cl-Tyr was somewhat less compared to that produced by I-Tyr. This might be a result of slower re-oxidation of TnIYD•FMN_{hq} by Cl-Tyr (Table 4-1). However, unlike in the case of HsIYD for which 100 equivalent of F-Tyr did not show any inhibition of reduction, F-Tyr significantly slowed reduction of TnIYD with just 1 equivalent (Figure 5-7). Increase the concentration of F-Tyr to 100 equivalence to TnIYD further inhibited its reduction by 2-fold. Since F-Tyr was not able to re-oxidize TnIYD•FMN_{hq} (Section 4.3.4), this provided direct evidence that reduction of TnIYD•FMN_{ox} is inhibited by binding of halotyrosines alone. Inhibition of the reduction of TnIYD by F-Tyr was still much less compared to I-Tyr and Cl-Tyr as 100 equivalent of F-Tyr to TnIYD inhibits the reduction to a similar degree as observed with 1 equivalent of I-Tyr and Cl-Tyr. This is inconsistent with similar affinity of I-Tyr and F-Tyr to TnIYD (Table 4-1).

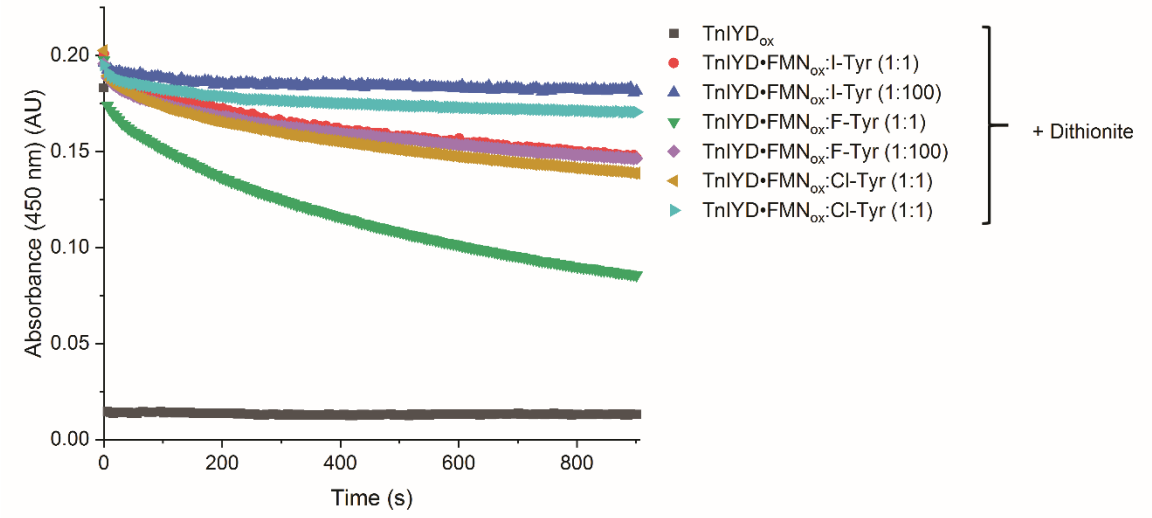

Figure 5-7 Effect of F-Tyr and Cl-Tyr on reduction of TnIYD•FMN_{ox}. Solutions of TnIYD•FMN_{ox} (15 μM final) and F-Tyr or Cl-Tyr (1 and 100 equvalent to enzyme) were mixed with dithionite as described in Figure 5-2(A). Reduction of TnIYD•FMN_{ox} was monitored by decrease of absorbance at 450 nm. The data for reduction of TnIYD in the presence of 1 and 100 equivalent of I-Tyr were the same as shown in Figure 5-6.

5.3.6 A TnIYD variant partially relieved the inhibition of TnIYD reduction by I-Tyr and F-Tyr:

As described in Section 4.3.5, residue Y112 of TnIYD is the only residue near the active site that exhibited a conformational difference between the co-crystal structures of

TnIYD•FMN_{ox}•I-Tyr and TnIYD•FMN_{ox}•Tyr (Figure 4-7(D)). This residue was suspected to be responsible for the tight binding of Tyr to TnIYD•FMN_{ox} but later proven not to be the case by an Y112A mutation. Since Y112 is also close to the FMN cofactor, substitutions of this residue may affect the reduction of TnIYD. Therefore, the reduction of TnIYD Y112A (Section 4.3.5) was studied similarly to the wildtype enzyme in the presence of I-Tyr and F-Tyr (Figure 5-8). The reduction of TnIYD Y112A in the presence of I-Tyr (1 and 100 equivalents) was only mildly faster than TnIYD with I-Tyr (Figure 5-8(A)). However, 1 equivalent of F-Tyr inhibited the reduction of the mutant much more weakly than that with TnIYD (Figure 5-8(B)). This effect was even more pronounced with 100 equivalent F-Tyr so that the reduction rate difference between with 1 and 100 equivalent of F-Tyr was smaller for the Y112A variant (1.2-fold) than for TnIYD (2-fold). A possible explanation for this observation is that Y112A could create a path for dithionite to access the FMN cofactor (Appendix Figure D1) when the lid is closed in the presence of I-Tyr and F-Tyr. The reason why the inhibition of reduction was relieved to a greater degree for F-Tyr than for I-Tyr might be a result of stronger repulsion of negatively charged dithionite ion by the much bigger iodine compared to fluorine, at least in the case of 1 equivalent of both ligands.

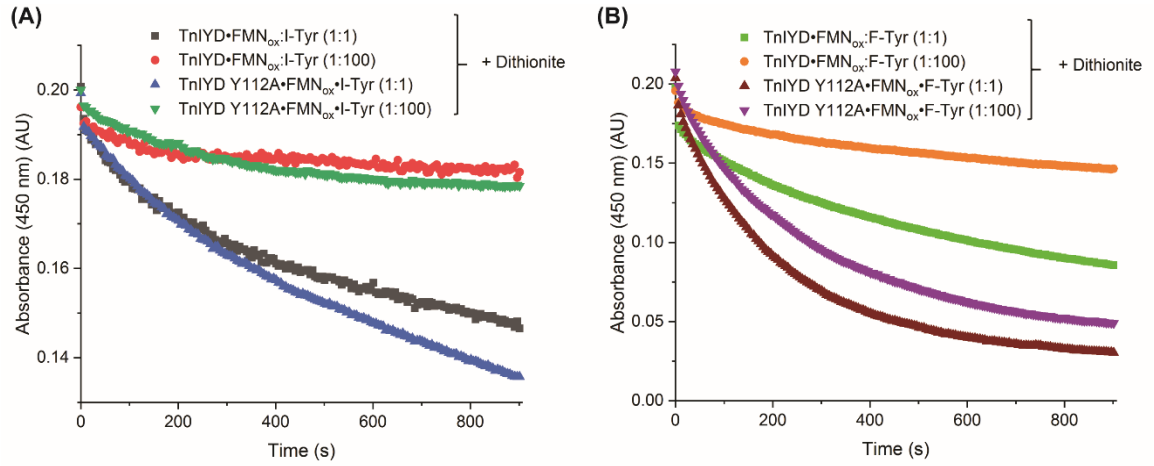

Figure 5-8 Effect of Y112A mutation on the inhibition of reduction of TnIYD•FMN_{ox} by I-Tyr and F-Tyr. (A) Solutions of TnIYD Y112A•FMN_{ox} (15 μM final) and I-Tyr (1 and 100 equvalent to enzyme) were mixed with dithionite as described in Figure 5-2(A). Reduction of TnIYD•FMN_{ox} was monitored by decrease of absorbance at 450 nm. The data for reduction of TnIYD in the presence of 1 and 100 equivalent of I-Tyr were the same as shown in Figure 5-6. (B) Solutions of TnIYD Y112A•FMN_{ox} (15 μM final) and F-Tyr (1 and 100 equvalent to enzyme) were mixed with dithionite as described in Figure 5-2(A). The data for reduction of TnIYD in the presence of 1 and 100 equivalent of F-Tyr were the same as shown in Figure 5-7.

5.3.7 The reduction of TnIYD in the presence of I-Tyr was significantly faster at 60 °C:

Since TnIYD is a thermophilic enzyme, its reduction in the presence of substrate is expected to be faster at elevated temperatures. If the reduction is rate-determining at 25 °C, the higher activity of TnIYD measured at 60 °C compared to at 25 °C would also suggest faster reduction rates at 60°C. Therefore, the reduction of TnIYD in the presence of I-Tyr was studied at 60 °C similarly to that as 25 °C. Indeed, the reduction of TnIYD in the presence of 1 equivalent of I-Tyr was much faster at 60 °C compared to that at 25 °C (Figure 5-9). Almost full reduction was achieved within the first 120 s after which the 450 nm absorption started to increase. Since there is no excess I-Tyr, this increase cannot be attributed to the re-oxidation of TnIYD•FMN_{hq} by I-Tyr. Re-oxidation of TnIYD•FMN_{hq} by oxygen was also not likely because the system was essentially anaerobic in the presence of excess dithionite. Instead, it is likely an effect of evaporation despite that the cuvette was capped with a stopper. This hypothesis is supported by the higher initial absorbance at 450 nm before addition of dithionite at 60 °C compared to that at 25 °C despite

having the same amount of enzyme in each case. About 7% of the solvent was evaporated during the 5 min incubation time of TnIYD and I-Tyr before introducing dithionite. Therefore, 21% of the solvent should be evaporated in the 15 min of the assay. This agrees well with the observed 22% increase in 450 nm absorbance during the same period. The faster reduction at 60 °C could be a thermodynamics effect as dithionite is more reducing at higher temperatures[142] or a simple kinetic effect. However, TnIYD could also exhibit greater conformational flexibility at higher temperatures which might provide an easier access to the FMN cofactor for dithionite.

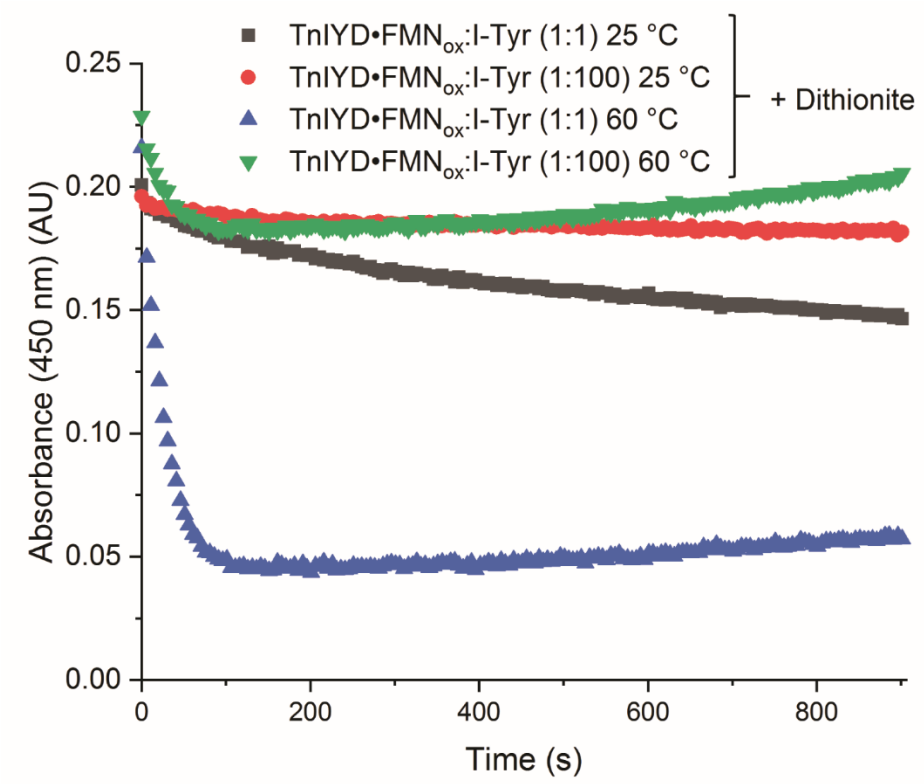

Figure 5-9 Effect of temperature on the reduction of TnIYD•FMN_{ox} in the presence of I-Tyr. Solutions of TnIYD•FMN_{ox} (15 µM final) and I-Tyr (1 and 100 equvalent to enzyme) were mixed with dithionite as described in Figure 5-2(A) under 60 °C. Reduction of TnIYD•FMN_{ox} was monitored by decrease of absorbance at 450 nm. The data for reduction of TnIYD in the presence of 1 and 100 equivalent of I-Tyr at 25 °C were the same as shown in Figure 5-6.

The reduction of TnIYD was still much faster in the presence of 100 equivalent of I-Tyr at 60 °C compared to at 25 °C as indicated by the ~ 20% decrease in 450 nm absorbance in the first 120 s °C compared to ~ 1.3% at 25 °C. After this initial reduction period the absorbance started to

increase again in a rate similarly as in the presence of 1 equivalent I-Tyr. Therefore, this increase is again an effect of solvent evaporation overtime. The maximum 20% reduction with 100 equivalent I-Tyr compared to almost full reduction with 1 equivalent I-Tyr is likely again due to the rapid re-oxidation of TnIYD•FMN_{hq} being rate-determining.

5.3.8 A note on the biological implication of the slow reduction of IYD by dithionite in the presence of substrate:

Inhibition on reduction of IYD by dithionite in the presence of substrates and substrate analogs suggested that reduction of the enzyme (regeneration of IYD•FMN_{hq}) could be rate-determining when substrate concentration is high. However, does this effect observed with an artificial reductant applies to the physiological reduction of IYD as well? It is beneficial for IYD to be reduced after the substrate is bound and the active site lid is closed so that the reduced FMN will transfer electrons to substrates rather than to oxygen that would generate reactive oxygen species. However, the closure of the active site lid also shields FMN from solvent and therefore potentially hinders the reduction of the enzyme. Some flavoenzymes evolved mechanisms using substrate binding to greatly increase the rate of reduction by NAD(P)H.[147,149,150] In some of these cases conformational changes induced by substrate binding have been suggested to expose the N5 of FMN to the NAD(P)H binding site and facilitate the reduction of the cofactor.[151,152] Therefore, it is possible that the physiological reducing system of IYD which shuttles electrons between NADPH and IYD can induce a conformational change of substrate-bound IYD to facilitate reduction. However, there are no conserved residues on the surface of IYD homologs from bacterial to mammalian near the N5 of FMN to support the recognition of an electron transfer protein. In addition, no conserved reductases have been found to cluster with the gene of IYD in genomes of bacteria and archaea that containing IYD homologs. An IYD reductase was also never co-purified with IYD isolated from thyroid issues.[123] Therefore, the physiological reducing partner of IYD might not be a reductase that specifically recognizes IYD but may act as a general reducing system that non-specifically interacts with IYD. The NADPH responsive activity of IYD has been

supported by the following reducing systems: (1) thyroid issue homogenates containing the physiological IYD reducing sytem;[123] (2) a HEK 293 cell homogenate;[153] (3) and reducing systems such as spinach ferredoxin reductase/ferredoxin from *Clostridium pasteurianum*, bovine ferredoxin/ferredoxin reductase, and cytochrome c reductase/methyl viologen.[154,155] However, in none of these cases did the NADPH responsive activity of IYD support faster deiodination than the dithionite responsive activity measured under similar conditions. It is possible that the NADPH responsive activity can be increase by increasing concentrations of NADPH and the reducing system. However, at least in the thyroid tissue homogenate the ratio of IYD versus its physiological reducing system should be similar to that in vivo. The reduction of IYD could potentially be rate-determining for I-Tyr deiodination in vivo as well. Such a hypothesis might be tested once the physiological reducing system is identified.

5.4 Summary:

In this chapter, the reduction of HsIYD and TnIYD by excess dithionite was studied by monitoring the decrease in 450 nm absorbance in the absence and presence of substrates and substrate analogs. A single equivalent of I-Tyr and Cl-Tyr inhibited reduction of HsIYD•FMN_{ox} by ~ 5-fold while F-Tyr and Tyr did not. In the presence of excess I-Tyr, reduction of HsIYD•FMN_{ox} was slow compared to re-oxidation of HsIYD•FMN_{hq} and therefore might be rate-determining for IYD turnover. In the presence of Cl-Tyr, the reduction of HsIYD was faster than the re-oxidation of HsIYD•FMN_{hq} and therefore the reduction of HsIYD might not be rate-determinging except at high Cl-Tyr concentrations. A likely off pathway HsIYD•FMN_{sq} species was also detected during the enzyme turnover. A single equivalent of I-Tyr, Cl-Tyr, and F-Tyr all severely inhibited reduction of TnIYD•FMN_{ox} by at least 250-fold while Tyr more mildly inhibited the reduction by 10-fold at 25 °C. Higher concentrations of I-Tyr, Cl-Tyr, and F-Tyr further inhibited reduction of TnIYD at 25 °C. For F-Tyr, this inhibition was simply due to binding of F-Tyr to the enzyme while with I-Tyr and Cl-Tyr rapid re-oxidation also slowed reduction.. Reduction of TnIYD inhibited by

I-Tyr and F-Tyr can be partially relieved by an Y112A mutation. The mutation likely created a path for dithionite to access the FMN cofactor more readily. At 60 °C, the reduction of TnIYD in the presence of 1 and 100 equivalent of I-Tyr was much faster than that at 25 °C. Despite the faster reduction, TnIYD•FMN_{hq} regeneration could still be rate-determining at 60 °C since the reduction of TnIYD•FMN_{hq} in the presence of 100 equivalent of I-Tyr was still slower than re-oxidation TnIYD•FMN_{ox}. The reduction of IYD monitored in the UV-vis assay with substrate concentrations higher than 1 equivalence to enzyme was complicated by the intertwining of reduction and re-oxidation. Therefore, to obtain the true reduction rates of IYD in the presence of higher concentrations of substrate, rapid kinetics will be used to capture the pre-steady-state phase of the reduction reaction before re-oxidation in collaboration with Prof. Giovanni Gadda (Georgia State University). The rate constants obtained will then determine whether or not reduction of the enzyme is the true rate-determining step with dithionite as the reductant.

Chapter 6 Conclusion

IYD provides a rare aerobic strategy for the bioremediation of halophenols by reductive dehalogenation. However, its weak native activity towards halophenols needs to be first improved before its full potential can be utilized for this application. To generate an efficient halophenol dehalogenase, HsIYD was first redesigned by Rosetta to accept 2IP, a model for halophenols, as an efficient substrate. The sequence of the active site lid of HsIYD was varied by Rosetta's fixed backbone design protocol to stabilize the closed lid in the presence of 2IP. This approach successfully improved 2IP deiodination of HsIYD by 4.5-fold only when Rosetta was allowed to sample all amino acids without restrictions. In contrast, a parallel approach guiding Rosetta via intuition to stabilize secondary structures of the lid failed to generate active variants towards 2IP. Attempts to further improve 2IP deiodination by accumulation of single mutations were frustrated by the strong epistatic nature of lid mutations possibly resulting from extensive side-chain interactions. Rosetta can overcame such epistasis with coordinated mutations introduced simultaneously. While as little as 2 mutations were able to improve 2IP deiodination, only a sum of 15 mutations generated by the unguided Rosetta design demonstrated success in changing the responsiveness of the active site lid from I-Tyr to 2IP with.

Further attempts to improve the computational design were focused on enlarging the sequence space for Rosetta to explore. First, fixed backbone design was performed on nine residues around the zwitterion of I-Tyr in its co-crystal structure with HhIYD, an easy-to-work with alternative to HsIYD. Focusing the design effort on these nine residues near the substrate over the entire lid increased sampling of mutations that could potentially interact with the substrate. However, this approach only improved 2IP deiodination by 2-fold compared to HhIYD. Subsequently, the native lid of HhIYD was remodeled by replacing the lid with shorter loops (15 and 16 amino acid long) from the PDB that can potentially form a more structured lid upon binding of 2IP. This approach again failed to generate active variants towards 2IP. Nevertheless, Rosetta

once again demonstrated the ability to alter the stability and responsiveness of an active site lid with the loop replacement protocol. The results demonstrated Rosetta as a great tool for stabilizing the targeted enzyme•2IP complex. But the failure to obtain an efficient 2IP deiodinase might suggest the incorrectness of the target model which was proposed from the crystal structures of catalytically inactive oxidized IYD. The crystal structure of the catalytically active reduced IYD might instead reveal productive enzyme-substrate interactions for catalysis to guide future designs.

IYD from a thermophilic bacteria *Thermotoga neapolitana* (TnIYD) was characterized for its potential to gain a high resolution crystal structure of the fully reduced IYD. Previously, the crystals of oxidized mesophilic IYDs were unstable to reduction by dithionite. The possibly low conformational flexibility of a thermophilic IYD at room temperature might improve the quality of crystals. In addition, its thermostability might also facilitate IYD engineering by the ability to incorporate more structurally deleterious but functionally beneficial mutations than mesophilic IYDs. Surprisingly, TnIYD was purified containing an FMN semiquinone species which was generated via reduction of TnIYD•FMN_{ox} in the presence of Tyr. This reduction was supported by free reduced flavins generated from the endogenous *E. coli* flavin reducing systems. TnIYD was demonstrated to be a functional halotyrosine dehalogenase with severe substrate inhibition at both 25 and 60 °C. The k_{cat} of TnIYD with 2IP at 60 °C already rivals those of mesophilic IYDs with I-Tyr at 25 °C, making it a potentially good parent enzyme for designing a halophenol dehalogenase. High resolution crystal structure of TnIYD•FMN_{ox} with I-Tyr, F-Tyr, or Tyr bound showed overall similarity to mesophilic IYDs but demonstrated TnIYD as a structurally minimal halotyrosine dehalogenase. TnIYD•FMN_{ox} was able to bind Tyr two orders of magnitude more tightly than mesophilic IYDs. Yet the crystal structure of TnIYD•FMN_{ox} with Tyr resembles mesophilic IYDs with I-Tyr and therefore did not suggest the structural basis for its tight binding of Tyr. The crystals of TnIYD•FMN_{ox} with I-Tyr, Tyr, F-Tyr bound were readily reduced to TnIYD•FMN_{sq} by dithionite in less than 5 min but further reduction did not lead to the crystals containing FMN

hydroquinone. There is no significant conformational change for TnIYD in the crystal structure upon reduction from TnIYD•FMN_{ox} to TnIYD•FMN_{sq}, suggesting that the active site of oxidized structures are sufficient to stabilize intermediates involving TnIYD semiquinone during catalysis. The discovery of an additional binding site for I-Tyr at the dimer interface of TnIYD likely offers an explanation for the substrate inhibition of IYDs.

The re-oxidation rates of HsIYD•FMN_{hq} by I-Tyr measured under pre-steady-state conditions were much faster than the k_{cat} of HsIYD with I-Tyr under steady-state conditions. The result suggested that the re-oxidation of HsIYD was not rate-determining under steady-state conditions. The reduction half of the catalysis therefore could be rate-determining. Single equivalents of I-Tyr and Cl-Tyr, but not F-Tyr and Tyr, were indeed found to inhibit the dithionite reduction of HsIYD•FMN_{ox} by about 5-fold compared to ligand free enzyme. In the presence of higher concentrations of I-Tyr (> 1 equivalent to enzyme), reduction of HsIYD•FMN_{ox} was slower than with re-oxidation of HsIYD•FMN_{hq} and thus is possibly rate-determining. However, in the presence of higher concentrations of Cl-Tyr (> 1 equivalent to enzyme), reduction of HsIYD•FMN_{ox} outcompeted re-oxidation of HsIYD•FMN_{hq} except at very high concentrations of Cl-Tyr (100 equivalent). Reduction inhibited by substrates and substrate analogs was much more pronounced for TnIYD as single equivalents of I-Tyr, Cl-Tyr, and F-Tyr all severely inhibited the reduction of TnIYD•FMN_{ox} by at least 250-fold while Tyr more mildly inhibited reaction by 10-fold at 25 °C. Higher concentrations of I-Tyr, Cl-Tyr, and F-Tyr (100 equivalent) further slowed the reduction of TnIYD. While for the catalytically inactive F-Tyr this is most likely an effect of F-Tyr binding, for I-Tyr and Cl-Tyr the reduction of TnIYD•FMN_{ox} was further inhibited by the faster re-oxidation of TnIYD•$FMN_{hq,}$ which makes reduction a possible rate-determining step for TnIYD catalysis as well. At 60 °C, the reduction of TnIYD in the presence of 1 equivalent I-Tyr was much faster than that at 25 °C, which is likely the basis for the thermoactivation of TnIYD.

Appendices

Appendix A: Supporting information for Chapter 2

Table A1 Degree of freedom allowed at each calculation stage. This table was originally published in Sun, Z.; Rokita, S. E.[60]

	Side chain torsion angle	Side chain identity	Backbone torsion angle	FMN position	2IP position	Dimer interface
Repacking stage	Relaxed, all AAs[a]	Fixed	Fixed	Fixed	Fixed	Fixed
Design stage	Relaxed, AAs of the lid and of 10 Å within the lid	Relaxed, AAs of the lid	Fixed	Fixed	Fixed	Fixed
Local minimization stage	Relaxed, AAs of the lid	Fixed	Relaxed, AAs of the lid	Fixed	Fixed	Fixed
Global minimization stage	Relaxed, all AAs	Fixed	Relaxed, all AAs	Relaxed	Relaxed	Relaxed

[a]AA stands for amino acid.

Table A2 Constrains at each position of the active site lid for the guided Rosetta design approach. This table was originally published in Sun, Z.; Rokita, S. E.[60]

AA in HsIYD	Residue number	Mutation library	Rationale[a]
E	157	A, F, L, M, W	Non-polar facing protein interior; A, L, and M favor α-helix formation; Except for A, bulky to fill up the void
E	158	Not changed	Charged on protein surface; Favor α-helix formation
I	159	E, Q, K, R	Polar on protein surface; Except for Q, favor α-helix formation
N	160	Not changed	Conserved in all IYD homologs; Interacts with a few nearby residues; Despite disfavors α-helix formation and being a polar residue facing protein interior
Y	161	A, F, L, M, W	Same as residue 157
M	162	K, R	Charged on protein surface; Favor α-helix formation; Positive charge stabilizes helix dipole at the C-terminus
K	163	G, K	K is charged on protein surface and presents a positive charge stabilizes helix dipole at the C-terminus; G stabilizes the α-helix at C-cap position.
R	164	Not changed	Conserved in all IYD homologs; Interacts with a few nearby residues; Charged on protein surface
M	165	Not changed	Conserved in all IYD homologs
G	166	G, D, N, S	Stabilize the α-helix at N-cap position
H	167	E, P	Stabilize the α-helix at N+1 position; E presents a negative stabilizes helix dipole at the N-terminus
R	168	E	Charged on protein surface; Negative charge stabilizes helix dipole at the N-terminus
W	169	Not changed	Conserved in all IYD homologs; π-stacked with Y211
V	170	A, L, M, Q	No clear polarity preferences; A, L, M favor α-helix formation
T	171	E, Q, K, R	Charged/polar on protein surface; E, K, R favor α-helix
D	172	Not changed	Conserved in all IYD homologs; Interacts with a few nearby residues; Charged on protein surface; Despite disfavors α-helix formation
L	173	Not changed	Conserved in all IYD homologs; Non-polar underneath 2IP; Favor α-helix formation
K	174	Not changed	Charged on protein surface; Positive charge stabilizes helix dipole at the C-terminus; Favor α-helix formation"
K	175	Not changed	Same as residue 174
L	176	Not changed	Non-polar facing protein interior; Favors α-helix
R	177	Q, K, R, G	No clear preference, naturally occurred in IYD homologs
T	178	E, D, N, T, Q	Same as residue 177
N	179	D, N, T	Same as residue 177
W	180	Conserved	Conserved in all IYD homologs
I	181	I, V, E, S, H	Same as residue 177
K	182	M, K	K may interact with a few nearby residues; M is a bulky non-polar residue facing protein interior and may fill up the void

[a]Factors stabilizing α-helix were based on published studies.[66,156,157]

Table A3 DNA oligonucleotides used for cloning. This table was originally published in Sun, Z.; Rokita, S. E.[60]

		DNA oligonucleotides[a]	PCR Template
Vector linearization	F[g]	AACTGGATTAAAGAGTACTTGG	HsIYD[c]
	R[g]	TTCCTCCTCAATGATCTTTC	
GD02 DNA assembly	1	AAGATCATTGAGGAGGAAATGGAGAAAAACTGGAAAAAAAGGATGGGAGAAGAATGGGCG	-
	2	GTACTCTTTAATCCAGTTCTGTCTCAGTTTCTTGAGGTCTTTCGCCCATTCTTCTCCCAT	
GD01 SDM[b]	F	TGGGAGAAGAATGGGCGAGAGACCTCAAGAAACTG	GD02
	R	CAGTTTCTTGAGGTCTCTCGCCCATTCTTCTCCCA	
UD01 DNA assembly	1	GATGAGAAAAACTGGAAAAGAAGGTT	-
	2	AGGTCTTCGACCCATTCATCTCCAAACCTTCTTTTCCAGTTTTTCTCAT	
	3	GATGAATGGGTCGAAGACCTCAAGAAACTGAACCTGGATTGG	
	4	ATGACGCCAATCCAGGTTCAGTTTCTTG	
	F	GAAAGATCATTGAGGAGGAAGATGAGAAAAACTGGAAAAG	Assembled UD01
	R	GGCAGTATCCAAGTACTCATGACGCCAATCCAGGTTC	
UD06 SDM	F	AGATAAGAACAACTGGAAATGCAGGTTTGGAGATGAATG	UD01
	R	TTTCCAGTTGTTCTTATCTTCCTCCTCAATGATCTTTCG	
UD07 SDM	F	ATGGATCGCAGACCTCAAGAAACTGAACCTGGATTGGC	UD06
	R	CTTGAGGTCTGCGATCCATTCATCTCCAAACCTGCATTTC	
UD08 SDM	F	GGAATCTTATGAAAACTGGGCAAGAAGGTTTGGAGATGAATG	UD01
	R	GCCCAGTTTTCATAAGATTCCTCCTCAATGATCTTTCGAATC	
UD03 SDM	F	ATGGGTCGCAGACCTCAAGAAACTGCGCCTGGATTGGCG	UD07
	R	TTGAGGTCTGCGACCCATTCATCTCCAAACCTGCATTTC	
UD05 SDM	F	TAAGGAAAACTGGGCACGCAGGTTTGGAGATGAATGGGTC	UD03
	R	GCGTGCCCAGTTTTCCTTATCTTCCTCCTCAATGATCTTTC	
UD02 SDM[d]	F (1)	GGAATCTGAGAACAACTGGAAAAGAAGGTTTGGAGATG	UD01
	R (1)	CCAGTTGTTCTCAGATTCCTCCTCAATGATCTTTCGAATC	
	F (2)	ATGGCTGGAAGACCTCAAGCAATTTCGCCTGGATTGGCGTCATG	UD02 (1)[e]
	R (2)	ATTGCTTGAGGTCTTCCAGCCATTCATCTCCAAACCTTCTTTTCCAG	
UD09 SDM[d]	F (1)	GGAAGATTATAACAACTGGAAATGTAGGTTTGGAGATGAATGG	UD02
	R (1)	ACATTTCCAGTTGTTATAATCTTCCTCCTCAATGATCTTTCGAATC	
	F (2)	ATGGAAAGAAGACCTCAAGCAATTTAACCTGGATTGGCGTAATGAG	UD09 (1)[e]
	R (2)	GCTTGAGGTCTTCTTTCCATTCATCTCCAAACCTACATTTCC	
UD04 SDM[d]	F (1)	AGAAAAACTGGCTGAAAAGGTGGGGAGATGAATGGATCGCAGAC	UD07

	R (1)	CCACCTTTTCAGCCAGTTTTTCTTATCTTCCTCCTCAATGATCTTTCG	
	F (2)	GGGACAGGAATGGAACGATGACCTCAGGAAACTGAACCTGG	UD04 (1)[e]
	R (2)	CATCGTTCCATTCCTGTCCCCACCTTTTCAGCCAGTTTTTC	
UD08 IM[e] E157S	F	AGGAGGAAAGCGAGATCAACTACATGAAAAGGATGGGACATC	HsIYD
	R	GTTGATCTCGCTTTCCTCCTCAATGATCTTTCGAATCTTG	
UD08 IM E158Y	F	AGGAGGAAGAGTACATCAACTACATGAAAAGGATGGGACATC	HsIYD
	R	GTTGATGTACTCTTCCTCCTCAATGATCTTTCGAATCTTG	
UD08 IM I159E	F	AGGAGGAAGAGGAGGAAAACTACATGAAAAGGATGGGACATC	HsIYD
	R	GTTTTCCTCCTCTTCCTCCTCAATGATCTTTCGAATCTTG	
UD08 IM Y161W	F	AGATCAACTGGATGAAAAGGATGGGACATCGCTGGGTCACAG	HsIYD
	R	CATCCTTTTCATCCAGTTGATCTCCTCTTCCTCCTCAATGATC	
UD08 IM M162A	F	AGATCAACTACGCGAAAAGGATGGGACATCGCTGGGTCACAG	HsIYD
	R	CATCCTTTTCGCGTAGTTGATCTCCTCTTCCTCCTCAATGATC	
UD08 IM K163R	F	AGATCAACTACATGCGTAGGATGGGACATCGCTGGGTCACAG	HsIYD
	R	CATCCTACGCATGTAGTTGATCTCCTCTTCCTCCTCAATGATC	
UD08 IM M165F	F	AGATCAACTACATGAAAAGGTTTGGACATCGCTGGGTCACAG	HsIYD
	R	AAACCTTTTCATGTAGTTGATCTCCTCTTCCTCCTCAATGATC	
UD08 IM H167D	F	GGATGGGAGATCGCTGGGTCACAGACCTCAAGAAACTGAG	HsIYD
	R	GACCCAGCGATCTCCCATCCTTTTCATGTAGTTGATCTCC	
UD08 IM R178E	F	GGATGGGACATGAATGGGTCACAGACCTCAAGAAACTGAG	HsIYD
	R	GACCCATTCATGTCCCATCCTTTTCATGTAGTTGATCTCC	
UD08 IM T171E	F	TGGGACATCGCTGGGTCGAAGACCTCAAGAAACTGAGAACC	HsIYD
	R	TTCGACCCAGCGATGTCCCATCCTTTTCATGTAGTTGATC	
UD08 IM R177N	F	AAACTGAACACCAACTGGATTAAAGAGTACTTGGATACTGCC	HsIYD
	R	CCAGTTGGTGTTCAGTTTCTTGAGGTCTGTGACCCAG	
UD08 IM T178L	F	AAACTGAGACTGAACTGGATTAAAGAGTACTTGGATACTGCC	HsIYD
	R	CCAGTTCAGTCTCAGTTTCTTGAGGTCTGTGACCCAG	
UD08 IM N179D	F	AAACTGAGAACCGATTGGATTAAAGAGTACTTGGATACTGCC	HsIYD
	R	CCAATCGGTTCTCAGTTTCTTGAGGTCTGTGACCCAG	
GD08 IM I181R	F	AACTGGCGCAAAGAGTACTTGGATACTGCCCCTATTTTG	HsIYD
	R	GTACTCTTTGCGCCAGTTGGTTCTCAGTTTCTTGAGGTC	
GD08 IM K182H	F	AACTGGATTCACGAGTACTTGGATACTGCCCCTATTTTG	HsIYD
	R	GTACTCGTGAATCCAGTTGGTTCTCAGTTTCTTGAGGTC	
DM01 (E158Y/M162A)	F	AGAGTACATCAACTACGCGAAAAGGATGGGACATCGCTGG	HsIYD
	R	TCGCGTAGTTGATGTACTCTTCCTCCTCAATGATCTTTCG	
His-tag deletion	F	AGATCATGGTGACAGTATAACACCATCACCATCACCATTAG	HsIYD and variants
	R	TTATACTGTCACCATGATCTGGTCCAGAGGTTTGCGCTTG	
	F	AGGAGGAAGCGTACATCAACTACGCGAAAAGGATGGGACATC	DM01

DM01 SSM[f] E157A	R	GTTGATGTACGCTTCCTCCTCAATGATCTTTCGAATCTTG	
DM01 SSM E157C	F	AGGAGGAATGCTACATCAACTACGCGAAAAGGATGGGACATC	DM01
	R	GTTGATGTAGCATTCCTCCTCAATGATCTTTCGAATCTTG	
DM01 SSM E157D	F	AGGAGGAAGATTACATCAACTACGCGAAAAGGATGGGACATC	DM01
	R	GTTGATGTAATCTTCCTCCTCAATGATCTTTCGAATCTTG	
DM01 SSM E157F	F	AGGAGGAATTTTACATCAACTACGCGAAAAGGATGGGACATC	DM01
	R	GTTGATGTAAAATTCCTCCTCAATGATCTTTCGAATCTTG	
DM01 SSM E157G	F	AGGAGGAAGGCTACATCAACTACGCGAAAAGGATGGGACATC	DM01
	R	GTTGATGTAGCCTTCCTCCTCAATGATCTTTCGAATCTTG	
DM01 SSM E157H	F	AGGAGGAACATTACATCAACTACGCGAAAAGGATGGGACATC	DM01
	R	GTTGATGTAATGTTCCTCCTCAATGATCTTTCGAATCTTG	
DM01 SSM E157I	F	AGGAGGAAATTTACATCAACTACGCGAAAAGGATGGGACATC	DM01
	R	GTTGATGTAAATTTCCTCCTCAATGATCTTTCGAATCTTG	
DM01 SSM E157K	F	AGGAGGAAAAATACATCAACTACGCGAAAAGGATGGGACATC	DM01
	R	GTTGATGTATTTTTCCTCCTCAATGATCTTTCGAATCTTG	
DM01 SSM E157L	F	AGGAGGAACTGTACATCAACTACGCGAAAAGGATGGGACATC	DM01
	R	GTTGATGTACAGTTCCTCCTCAATGATCTTTCGAATCTTG	
DM01 SSM E157M	F	AGGAGGAAATGTACATCAACTACGCGAAAAGGATGGGACATC	DM01
	R	GTTGATGTACATTTCCTCCTCAATGATCTTTCGAATCTTG	
DM01 SSM E157N	F	AGGAGGAAAACTACATCAACTACGCGAAAAGGATGGGACATC	DM01
	R	GTTGATGTAGTTTTCCTCCTCAATGATCTTTCGAATCTTG	
DM01 SSM E157P	F	AGGAGGAACCGTACATCAACTACGCGAAAAGGATGGGACATC	DM01
	R	GTTGATGTACGGTTCCTCCTCAATGATCTTTCGAATCTTG	
DM01 SSM E157Q	F	AGGAGGAACAGTACATCAACTACGCGAAAAGGATGGGACATC	DM01
	R	GTTGATGTACTGTTCCTCCTCAATGATCTTTCGAATCTTG	
DM01 SSM E157R	F	AGGAGGAACGTTACATCAACTACGCGAAAAGGATGGGACATC	DM01
	R	GTTGATGTAACGTTCCTCCTCAATGATCTTTCGAATCTTG	
DM01 SSM E157S	F	AGGAGGAAAGCTACATCAACTACGCGAAAAGGATGGGACATC	DM01
	R	GTTGATGTAGCTTTCCTCCTCAATGATCTTTCGAATCTTG	
DM01 SSM E157T	F	AGGAGGAAACCTACATCAACTACGCGAAAAGGATGGGACATC	DM01
	R	GTTGATGTAGGTTTCCTCCTCAATGATCTTTCGAATCTTG	
DM01 SSM E157V	F	AGGAGGAAGTGTACATCAACTACGCGAAAAGGATGGGACATC	DM01
	R	GTTGATGTACACTTCCTCCTCAATGATCTTTCGAATCTTG	
DM01 SSM E157W	F	AGGAGGAATGGTACATCAACTACGCGAAAAGGATGGGACATC	DM01
	R	GTTGATGTACCATTCCTCCTCAATGATCTTTCGAATCTTG	
DM01 SSM E157Y	F	AGGAGGAATATTACATCAACTACGCGAAAAGGATGGGACATC	DM01
	R	GTTGATGTAATATTCCTCCTCAATGATCTTTCGAATCTTG	

[a]All DNA oligonucleotides are from 5' end to 3' end from left to right. [b]SDM, site directed mutagenesis; [c]Template here is the pSMT3 plasmid carrying the indicated enzyme; [d]GD02, 04, 09 were constructed by two rounds of SDM; [e]The template for second round SDM is the PCR product of first round SDM as indicated by the number in parenthesis; [f]SSM, site saturation mutagenesis; [g]F, forward; R, reverse.

Table A4 HPLC solvent programs for Tyr, phenol and FMN analysis. This table was originally published in Sun, Z.; Rokita, S. E.[60]

Program 1: resorcinol as internal standard:

Time (min)	% Solvent B[a]
0	0
10	7
25	35
30	95
40	95
45	0
55	0

Program 2: Cl-Tyr as internal standard:

Time (min)	% Solvent B[a]
0	0
10	7
25	7
30	95
40	95
45	0
55	0

[a]Solvent A is 0.44% formic acid in water and solvent B is 0.44% formic acid in acetonitrile.

Table A5 The binding affinity and deiodination activity of HsIYD towards 2IP in the absence and presence of Gly or Ala. This table was originally published in Sun, Z.; Rokita, S. E.[60]

	K_d[a] ($\times 10^3$, μM)	V/[E] (min^{-1})[b]	
		0.5 mM 2IP	**4 mM 2IP**
No Amino acid	2.4 ± 0.1	0.020 ± 0.004	0.121 ± 0.004
+ 10 mM Gly	2.42 ± 0.08	0.026 ± 0.004	0.164 ± 0.004
+ 10 mM Ala	2.12 ± 0.07	0.019 ± 0.004	0.119 ± 0.005

[a]Three independent measurements were fitted as one curve to obtain the K_d and associated error. [b]The V/[E] represent the average of three independent measurements. The error is either the standard deviation of three independent measurements or three times the background of the assay (0.004 min^{-1}), whichever is larger.

Table A6 2IP deiodination activity of HsIYD and its variants generated by Rosetta with 0.5 mM 2IP. This table was originally published in Sun, Z.; Rokita, S. E.[60]

	V/[E] (min^{-1})[a]		V/[E] (min^{-1})[a]
HsIYD	0.024 ± 0.004[b]	UD04	0.008 ± 0.004
GD01	≤ 0.004[c]	UD05	0.055 ± 0.004
GD02	≤ 0.004[c]	UD06	0.017 ± 0.004
UD01	0.012 ± 0.004	UD07	0.016 ± 0.004
UD02	0.028 ± 0.004	UD08	0.094 ± 0.006
UD03	0.016 ± 0.004	UD09	0.007 ± 0.004

[a]The V/[E] represent the average of three independent measurements. The error is either the standard deviation of three independent measurements or three times the background of the assay (0.004 min^{-1}), whichever is larger. [b]Data from Ingavat, N.; et, al.[32]

Table A7 2IP deiodination activity of HsIYD variants containing individual mutations that combine to generate UD08. This table was originally published in Sun, Z.; Rokita, S. E.[60]

	V/[E] (min^{-1})[a]			V/[E] (min^{-1})[a]	
	0.5 mM 2IP	**1 mM 2IP**		**0.5 mM 2IP**	**1 mM 2IP**
HsIYD	0.019 ± 0.004[b]	0.040 ± 0.004[b]	H167D	0.010 ± 0.004	0.021 ± 0.004
E157S	0.005 ± 0.004	0.011 ± 0.004	R168E	0.022 ± 0.004	0.043 ± 0.004
E158Y	0.059 ± 0.004	0.117 ± 0.004	T171E	0.017 ± 0.004	0.033 ± 0.004
I159E	0.012 ± 0.004	0.026 ± 0.004	R177N	0.020 ± 0.004	0.042 ± 0.004
Y161W	0.011 ± 0.004	0.019 ± 0.004	T178L	0.010 ± 0.004	0.018 ± 0.004
M162A	0.056 ± 0.004	0.100 ± 0.004	N179D	0.016 ± 0.004	0.031 ± 0.004
K163R	0.018 ± 0.004	0.034 ± 0.004	I181R	0.011 ± 0.004	0.020 ± 0.004
M165F	0.006 ± 0.004	0.010 ± 0.004	K182H	0.013 ± 0.004	0.026 ± 0.004

[a]The values of V/[E] represent the average of two independent measurements. The error is either the standard deviation of two independent measurements or three times the background of the assay (0.004 min^{-1}), whichever is larger. [b]Data from Ingavat, N.; et, al.[32]

Table A8 2IP deiodination activity of E157 substituted DM01 variants measured with 0.5 mM 2IP. This table was originally published in Sun, Z.; Rokita, S. E.[60]

	V/[E] (min^{-1})[a]		V/[E] (min^{-1})[a]
DM01	0.088 ± 0.004	DM01-E157M	0.033 ± 0.004
DM01-E157A	0.006 ± 0.004	DM01-E157N	0.009 ± 0.004
DM01-E157C	0.037 ± 0.006	DM01-E157P	≤ 0.004
DM01-E157D	0.116 ± 0.004	DM01-E157Q	0.006 ± 0.004
DM01-E157F	0.004 ± 0.004	DM01-E157R	≤ 0.004
DM01-E157G	0.031 ± 0.004	DM01-E157S	0.021 ± 0.004
DM01-E157H	≤ 0.004	DM01-E157T	0.010 ± 0.004
DM01-E157I	≤ 0.004	DM01-E157V	≤ 0.004
DM01-E157K	≤ 0.004	DM01-E157W	≤ 0.004
DM01-E157L	≤ 0.004	DM01-E157Y	≤ 0.004

[a]The values of V/[E] represent the average of two independent measurements. The error is either the standard deviation of two independent measurements or three times the background of the assay (0.004 min^{-1}), whichever is larger.

Table A9 Characterization of the trypsin digestion products of HsIYD. This table was originally published in Sun, Z.; Rokita, S. E.[60]

		Calculated MW (Da)[a]	Detected MW (Da)[a]	Modifications[a]	# of Met in sequence[a]
Undigested HsIYD		29780.21	29779.66	None	6
	post SDS-PAGE	29780.21	29875.32	+ 95.11 6 oxygens	6
~16 kD digestion product	Fragment 1	15316.93	15364.69	+ 47.76 3 oxygens	3
	Fragment 2	15059.64	15107.41	+ 47.77 3 oxygens	3
	Fragment 3	14903.45	14951.08	+ 47.63 3 oxygens	3
~ 13 kD digestion product		No fragments detected[b]			

[a]Experimental and calculated masses of undigested peptide and digested peptide fragments extracted from gel differ by integer numbers of oxygens. This number equals to the number of methionines present in the sequence. Therefore, such a discrepancy is a result of oxidation of methionines during SDS-PAGE.[158] [b]The signal to noise ratio for the mass spectrometry analysis of this digestion product is very low. This product showed on the gel as a concentrated band followed by lots of smears (Figure 2-6), it is possible that this band contains multiple peptide fragments with similar molecular weights.

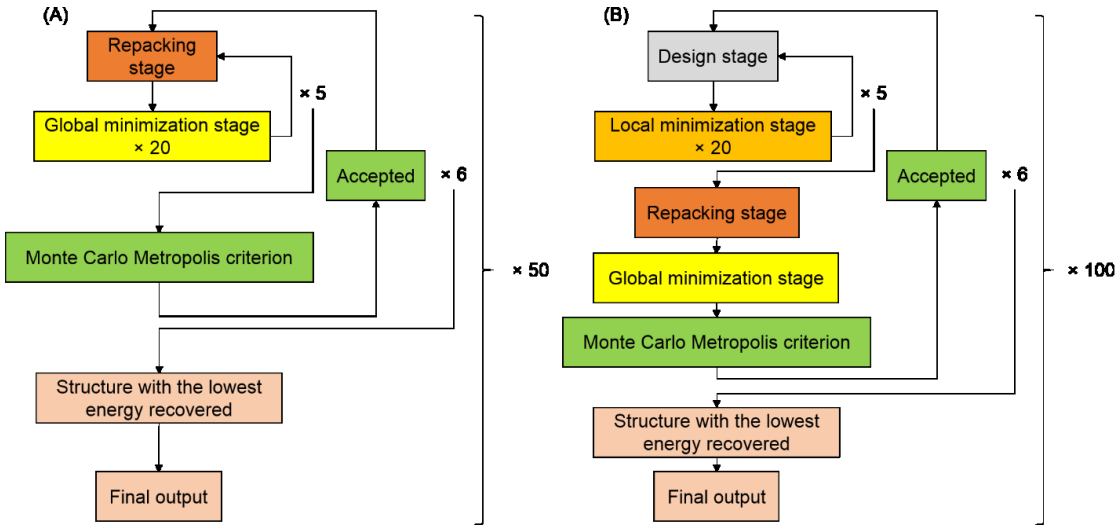

Figure A1 Overview of computational simulation protocols. (A) Preparation of the starting model (B) Fixed backbone design. Numbers in boxes and by arrows indicate dependent repeats-the output of last round calculation enters the next round as the starting structure. Numbers by the parenthesis represent independent repeats-the same initial starting structure is used for every individual repeat. The local minimization differs from the global minimization by the degree of freedom allowed (see Appendix **Table A1** for details). This figure was originally published in Sun, Z.; Rokita, S. E.[60]

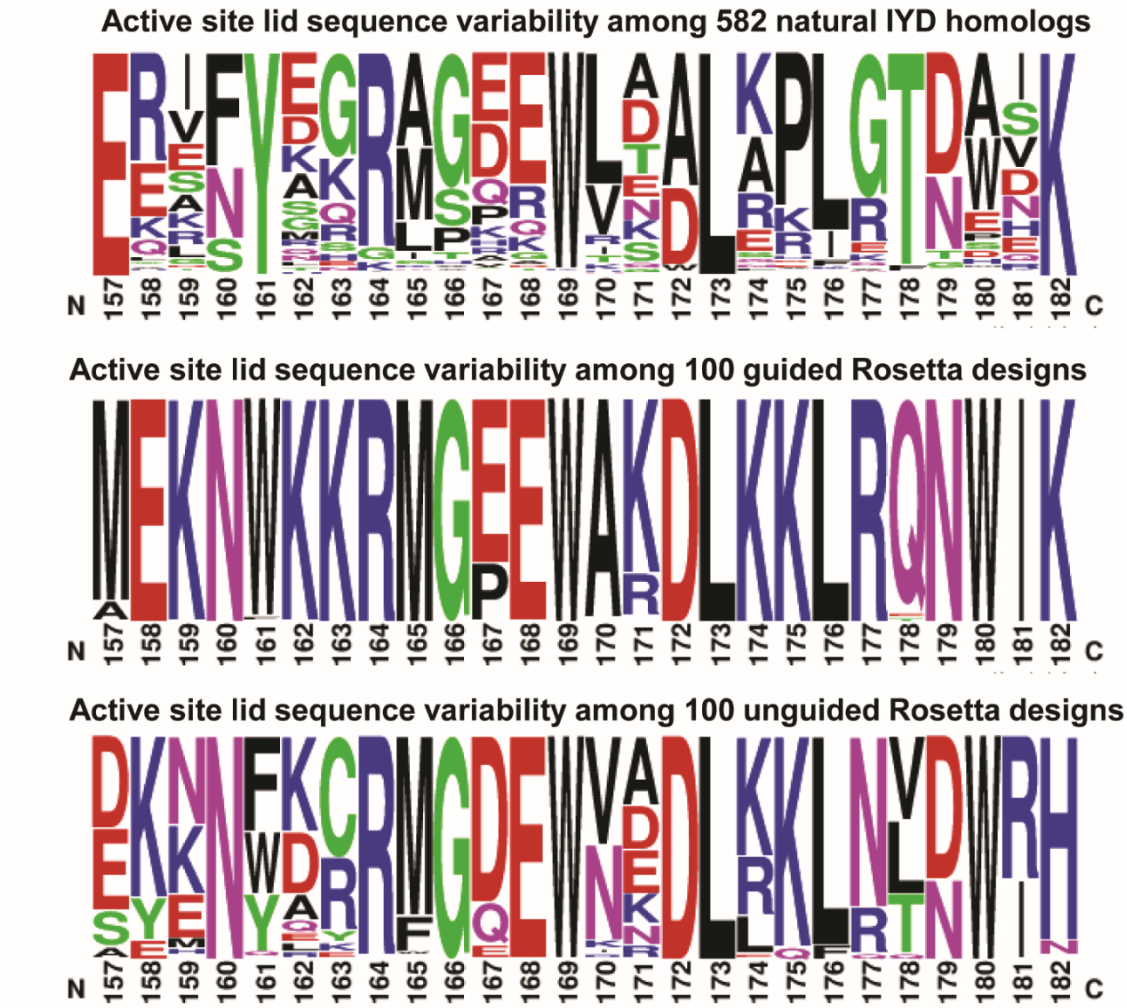

Figure A2 Sequence logo displaying variability of amino acid in the active site lid of natural IYD homologs[34] (top), guided Rosetta designs (middle), and unguided Rosetta designs (bottom). The sequence alignment was generated with Clustal Omega.[159] The sequence logo was constructed by WebLogo.[160] This figure is modified from Sun, Z.; Rokita, S. E.[60]

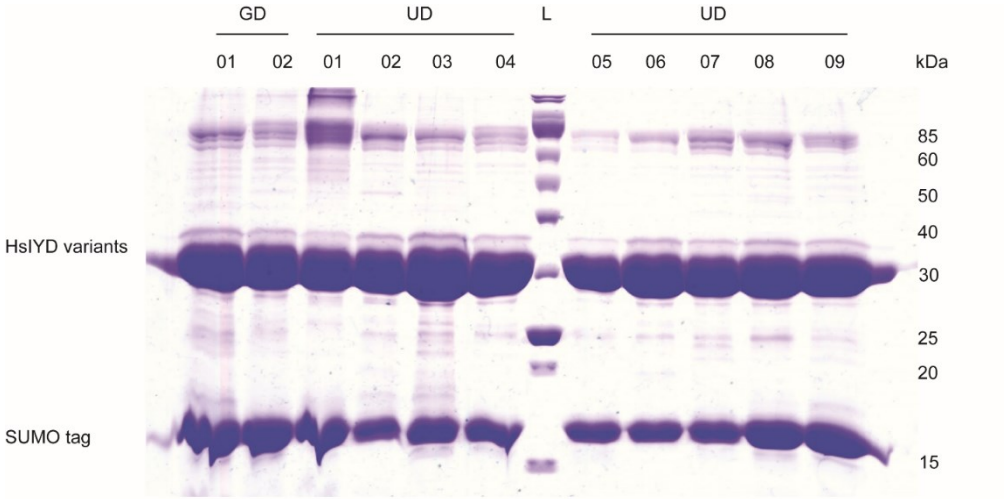

Figure A3 SDS-PAGE of Rosetta designed enzymes. L represents protein ladder. This figure was originally published in Sun, Z.; Rokita, S. E.[60]

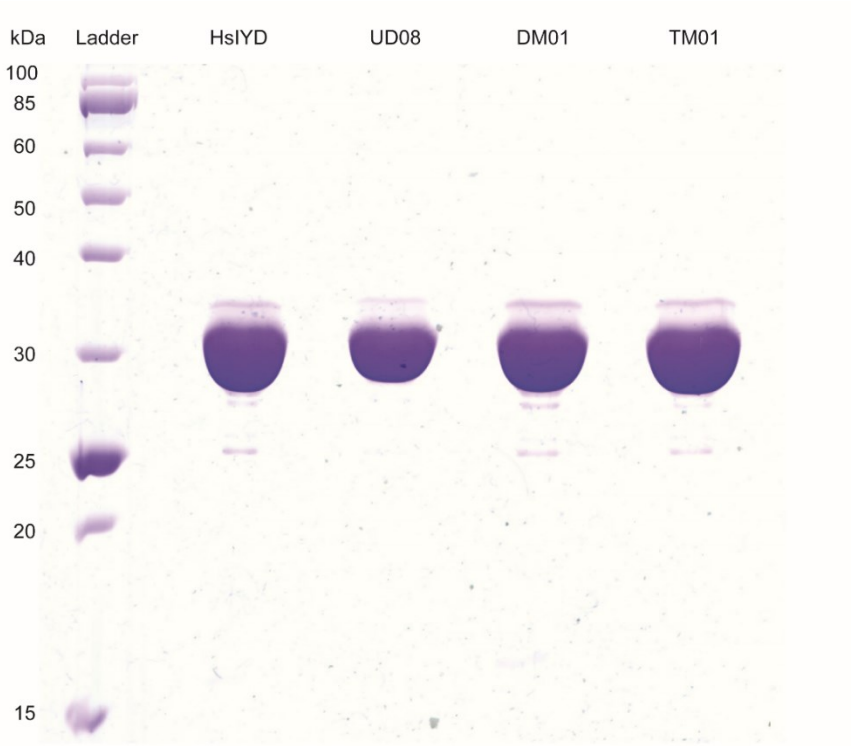

Figure A4 SDS-PAGE of highly purified enzymes for substrate binding and Michaelis-Menton kinetics characterization. SUMO tag in these enzymes was removed by first cleavage with ULP1 protease before Ni-NTA affinity column. Despite that the SUMO tag also carries a $(His)_6$ tag, it does not bind the nickel resin as strongly as His-tagged HsIYD and its variants. Therefore, SUMO can be removed by extensive washing of the Ni-NTA column. This figure was originally published in Sun, Z.; Rokita, S. E.[60]

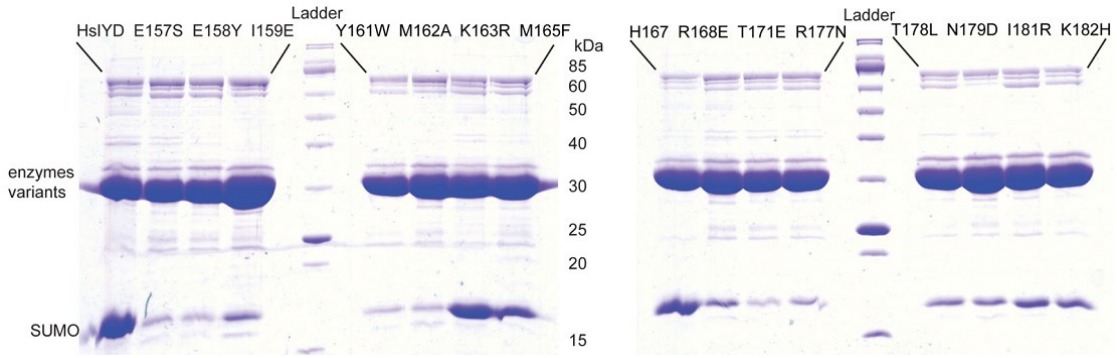

Figure A5 SDS-PAGE of HsIYD variants containing individual mutations that combine to generate UD08. The intensity of the SUMO bands for HsIYD, K163R, M165F, and H167D are higher than those of the other lanes as a result of different buffer exchange methods used in purification. Enzymes in these lanes were buffer-exchanged with a desalting column which does not differentiate SUMO from mutant enzymes. All the other enzymes were buffer-exchanged with a spin concentrator with a 50kD molecular weight cutoff. SUMO is less than 50kD and passes through the concentrator together with small molecules. This figure was originally published in Sun, Z.; Rokita, S. E.[60]

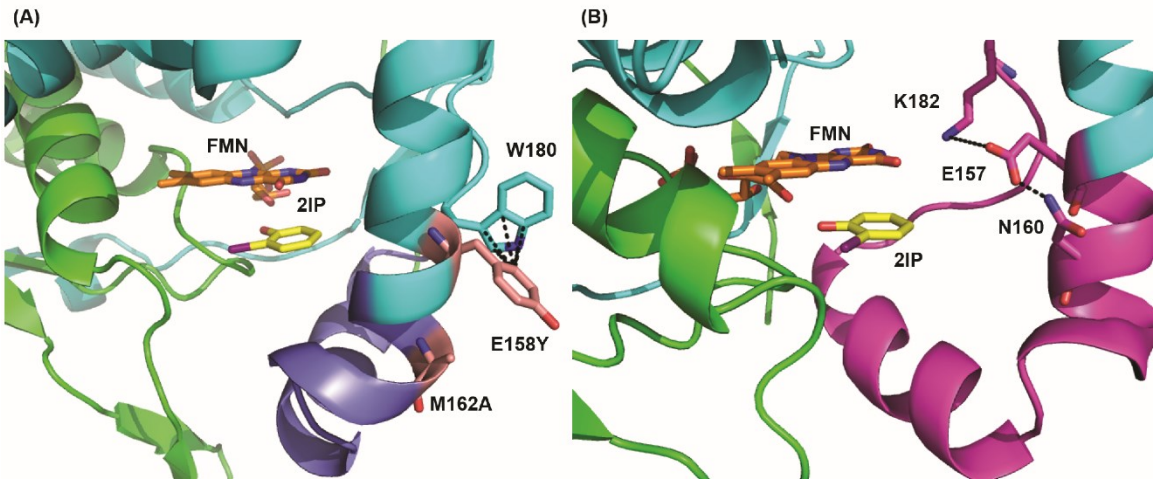

Figure A6 Model structures of DM01 and HsIYD in complex with 2IP generated by PyRosetta.[59] The backbones of the homodimer are colored as green and cyan. FMN and 2IP are shown in orange and yellow sticks, respectively. (A) Model structure of DM01•2IP complex. The active site lid is shown in blue. The double mutations E158Y and M162A are shown in pink. Interactions between E158Y and W180 are shown by dashed lines. (B) Model structure of HsIYD•2IP complex. The lid area subjected to redesign by Rosetta is shown in magenta. Interactions between active site residues E157, K182, and N160 are shown by dashed lines. For clarity, a loop on top of FMN containing residues 235-243 was omitted for both figures. This figure was modified from Sun, Z.; Rokita, S. E.[60]

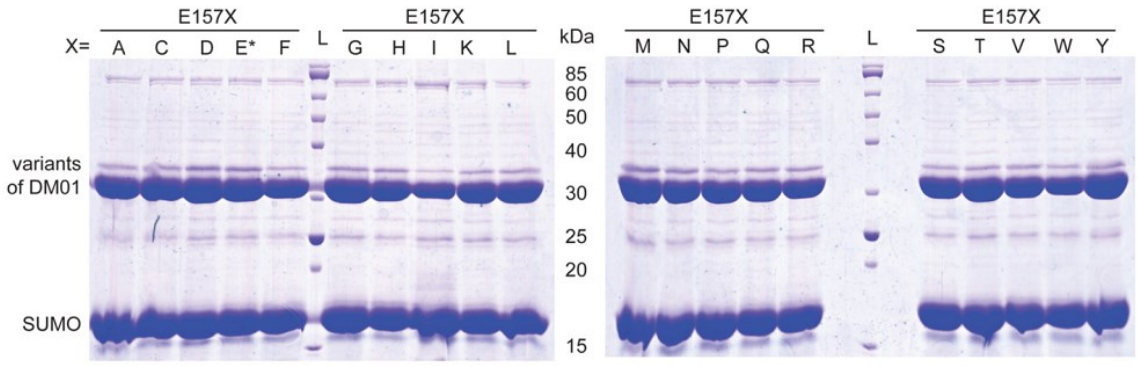

Figure A7 SDS-PAGE of E157 substituted DM01 variants. L represents protein ladder. E157K was loaded three times more than other variants. This figure was originally published in Sun, Z.; Rokita, S. E.[60]

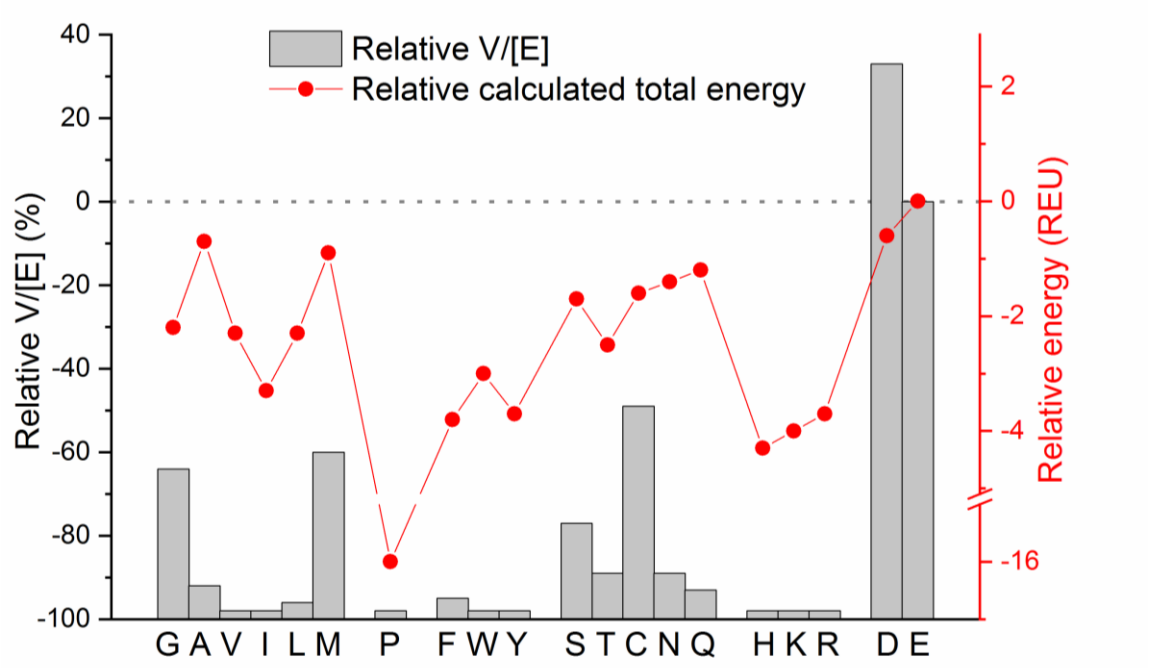

Figure A8 Comparison between the effect of E157 substitution on the 2IP deiodination activity of DM01 and the stability of corresponding variants calculated by Rosetta. Gray bars: relative 2IP deiodination activity to that of DM01. The negative sign represents decrease of activity. Red dots: relative total energy to that of DM01 calculated by Rosetta. The negative sign represents destabilization of enzyme•2IP complex. The energies are in Rosetta energy units (REU). This figure was originally published in Sun, Z.; Rokita, S. E.[60]

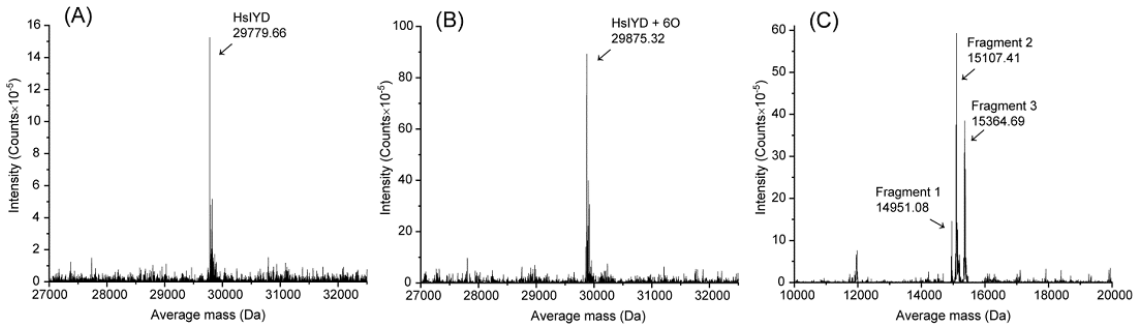

Figure A9 Intact protein mass spectra of HsIYD and its ~ 16kD trypsin digestion product. (A) HsIYD (B) HsIYD extracted from SDS-PAGE. (C) The ~ 16 kD trypsin digestion product of extracted from SDS-PAGE. This figure was originally published in Sun, Z.; Rokita, S. E.[60]

Figure A10 Sequences of HsIYD and its ~ 16 kD digestion products identified by mass spectrometry (**Table A9**). The methionines subjected to oxidation were bolded and italicized. This figure was originally published in Sun, Z.; Rokita, S. E.[60]

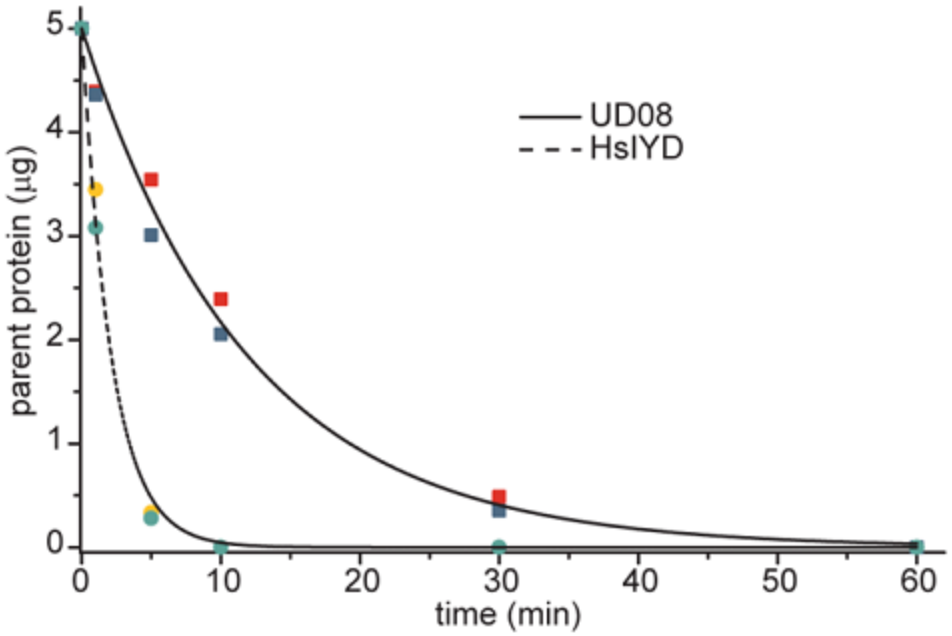

Figure A11 The first order decay of the undigested protein in limited proteolysis. Blue and red squares represent two independent measurements for HsIYD. Dashed line is the fitting of remaining HsIYD over time with first order decay kinetics. The two independent measurements were fitted as one curve. Yellow and green circles represent two independent measurements for UD08. Solid line is the fitting of remaining UD08 over time with first order decay kinetics. As in the case of HsIYD, the two independent measurements were fitted as one curve. This figure was originally published in Sun, Z.; Rokita, S. E.[60]

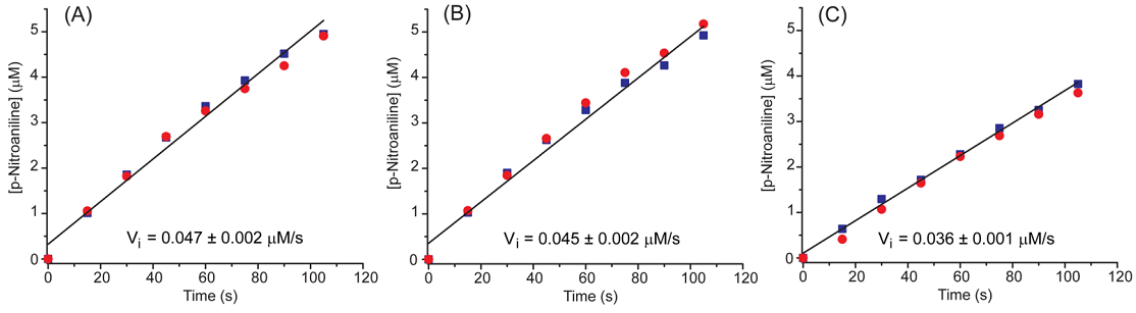

Figure A12 Trypsin digestion of Nα-Benzoyl-DL-arginine 4-nitroanilide hydrochloride (DL-BAPNA). (A) No deiodination substrates present. (B) In the presence of 100 μM I-Tyr. (C) In the presence of 10 mM 2IP. Red and blue data sets are two independent measures and are fitted as one curve. This figure was originally published in Sun, Z.; Rokita, S. E.[60]

Script A1 Python scripts for preparation of starting structure.

```
# Set working directory
import os
os.chdir('Insert directory')

# Import Rosetta
from rosetta import *
init()

# Initialize PyMOL Mover
pmm = PyMOL_Mover()
pmm.keep_history(True)

# Pose IYD complex
IYD_FMN_MIT_m3 = pose_from_pdb('4TTC.pdb')
IYD_FMN_MIT_m3.pdb_info().name('IYD_FMN_MIT_m3')
pmm.apply(IYD_FMN_MIT_m3)

scorefxn_fa = get_fa_scorefxn()

print scorefxn_fa(IYD_FMN_MIT_m3)
print 'Original IYD_FMN_MIT_m3 complex score is:',scorefxn_fa(IYD_FMN_MIT_m3)
scorefxn_fa.show(IYD_FMN_MIT_m3)

from toolbox import get_hbonds
hbond_set = get_hbonds(IYD_FMN_MIT_m3)
hbond_set.show(IYD_FMN_MIT_m3,443)
hbond_set.show(IYD_FMN_MIT_m3,444)

# Set up the fold tree
ft = FoldTree()
ft.add_edge(1,152,-1)
ft.add_edge(152,169,-1)
ft.add_edge(169,220,-1)
ft.add_edge(221,221,-1)
ft.add_edge(222,222,-1)
ft.add_edge(152,374,1)
ft.add_edge(169,221,2)
ft.add_edge(221,222,3)
ft.add_edge(374,223,-1)
ft.add_edge(374,391,-1)
ft.add_edge(391,442,-1)
ft.add_edge(443,443,-1)
ft.add_edge(444,444,-1)
ft.add_edge(391,443,4)
ft.add_edge(443,444,5)
print ft
ft.check_fold_tree()
IYD_FMN_MIT_m3.fold_tree(ft)
```

```
# Build working pose
rp_mi_ful = Pose()
rp_mi_ful.assign(IYD_FMN_MIT_m3)
print rp_mi_ful.fold_tree()
print 'Check pose energy:',scorefxn_fa(rp_mi_ful)

# Build minimization mover
movemap = MoveMap() # Build movemap for the minimization mover
movemap.set_bb(True)
movemap.set_chi(True)
movemap.set_jump(1,True)
movemap.set_jump(4,True) # Allow ligand in chain B to move
movemap.show() # Check the movemap

min_mover = MinMover()
min_mover.movemap(movemap)
min_mover.score_function(scorefxn_fa)
min_mover.min_type("dfpmin_atol")
min_mover.tolerance(0.00001)
print min_mover

# Set up job distributor
jd1 = PyJobDistributor('minimized',50,scorefxn_fa)
jd1.native_pose = IYD_FMN_MIT_m3

# Set up Monte Carlo Object
kT = 1.0
mc = MonteCarlo(rp_mi_ful,scorefxn_fa,kT)

# Repack and minimize IYD_FMN_MIT_m3 complex

for l in range (1,51):
   rp_mi_ful.assign(IYD_FMN_MIT_m3)
   mc.reset(rp_mi_ful)
   for k in range (1,7):
      for i in range(1,6):
         print 'Check pose energy:',scorefxn_fa(rp_mi_ful)
         task_pack = standard_packer_task(rp_mi_ful)
         task_pack.restrict_to_repacking()
         task_pack.or_include_current(True)
         pack_mover = PackRotamersMover(scorefxn_fa,task_pack)
         pack_mover.apply(rp_mi_ful)
         print 'For structure',l,'round:',k,'iteration:',i,'Repacked IYD_FMN_MIT_m3 complex score
is:',scorefxn_fa(rp_mi_ful)
         for j in range(1,21):
            min_mover.apply(rp_mi_ful)
            print 'For structure',l,'round:',k,'iteration:',i,'Minimized repacked IYD_FMN_MIT_m3
complex score for interation',j,'is:',scorefxn_fa(rp_mi_ful)
      mc.boltzmann(rp_mi_ful)
```

```
            mc.show_scores()
            mc.show_counters()
            mc.show_state()
        mc.recover_low(rp_mi_ful)
        print 'For structure',l,'the lowest energy is:',scorefxn_fa(rp_mi_ful)
        rp_mi_ful.pdb_info().name('minimized')
        pmm.apply(rp_mi_ful)
        scorefxn_fa.show(rp_mi_ful)
        hbond_set = get_hbonds(rp_mi_ful)
        hbond_set.show(rp_mi_ful,443)
        hbond_set.show(rp_mi_ful,444)
        jd1.output_decoy(rp_mi_ful)

print 'Job is done!'
```

Script A2 Python scripts for unguided Rosetta design, guided Rosetta design and wildtype control. The script for all three protocols were same, except for three different resfiles being used for corresponding protocol to guide action on individual residues"

```
# Set working directory
import os
os.chdir('Insert directory')

# Import Rosetta
from rosetta import *
init()

# Initialize PyMOL Mover
pmm = PyMOL_Mover()
pmm.keep_history(True)

# Pose IYD complex
IYD_FMN_2IP_m13 = pose_from_pdb('IYD_FMN_2IP_m13.pdb')
IYD_FMN_2IP_m13.pdb_info().name('IYD_FMN_2IP_m13')
pmm.apply(IYD_FMN_2IP_m13)
print IYD_FMN_2IP_m13.sequence()

scorefxn_fa = get_fa_scorefxn()

print scorefxn_fa(IYD_FMN_2IP_m13)
print 'Original IYD_FMN_2IP_m13 complex score is:',scorefxn_fa(IYD_FMN_2IP_m13)
scorefxn_fa.show(IYD_FMN_2IP_m13)

from toolbox import get_hbonds
hbond_set = get_hbonds(IYD_FMN_2IP_m13)
hbond_set.show(IYD_FMN_2IP_m13,443)
hbond_set.show(IYD_FMN_2IP_m13,444)

# Set up the fold tree
ft = FoldTree()
ft.add_edge(1,152,-1)
ft.add_edge(152,169,-1)
ft.add_edge(169,220,-1)
ft.add_edge(221,221,-1)
ft.add_edge(222,222,-1)
ft.add_edge(152,374,1)
ft.add_edge(169,221,2)
ft.add_edge(221,222,3)
ft.add_edge(374,223,-1)
ft.add_edge(374,391,-1)
ft.add_edge(391,442,-1)
ft.add_edge(443,443,-1)
ft.add_edge(444,444,-1)
ft.add_edge(391,443,4)
ft.add_edge(443,444,5)
```

```
print ft
ft.check_fold_tree()
IYD_FMN_2IP_m13.fold_tree(ft)

# Build working pose
design = Pose()
design.assign(IYD_FMN_2IP_m13)
print design.fold_tree()
print 'Check pose energy:',scorefxn_fa(design)

# Build minimization mover
movemap_1 = MoveMap() # Build movemap for the minimization mover
movemap_1.set_bb(True)
movemap_1.set_chi(True)
movemap_1.set_jump(1,True)
movemap_1.set_jump(4,True) # Allow ligand in chain B to move
movemap_1.show() # Check the movemap

min_mover_1 = MinMover()
min_mover_1.movemap(movemap_1)
min_mover_1.score_function(scorefxn_fa)
min_mover_1.min_type("dfpmin_atol")
min_mover_1.tolerance(0.00001)
print min_mover_1

movemap_2 = MoveMap() # Build movemap for the minimization mover
movemap_2.set_bb_true_range(309,334) # Only allow lid rigion to move
movemap_2.set_chi_true_range(309,334)
movemap_2.show() # Check the movemap

min_mover_2 = MinMover()
min_mover_2.movemap(movemap_2)
min_mover_2.score_function(scorefxn_fa)
min_mover_2.min_type("dfpmin_atol")
min_mover_2.tolerance(0.00001)
print min_mover_2

# Set up job distributor
jd1 = PyJobDistributor('Final',100,scorefxn_fa)
jd1.native_pose = IYD_FMN_2IP_m13

jd4 = PyJobDistributor('mc',600,scorefxn_fa)
jd4.native_pose = IYD_FMN_2IP_m13

# Set up Monte Carlo Object
kT = 1.0
mc = MonteCarlo(design,scorefxn_fa,kT)

# Repack and minimize IYD_FMN_2IP_m13 complex
```

```
for l in range (1,101):
   design.assign(IYD_FMN_2IP_m13)
   mc.reset(design)
   for k in range (1,7):
      for i in range(1,6):
         print 'Check pose energy:',scorefxn_fa(design)
         task_pack_2 = standard_packer_task(design)
         parse_resfile(design,task_pack_2,"X.resfile")
         "Insert the coresponidng resfile listed below for each protocol"
         task_pack_2.or_include_current(True)
         pack_mover_2 = PackRotamersMover(scorefxn_fa,task_pack_2)
         pack_mover_2.apply(design)
         print 'For structure',l,'round:',k,'iteration:',i,'Repacked IYD_FMN_2IP_m13 complex
sequence is:',design.sequence()
         print 'For structure',l,'round:',k,'iteration:',i,'Repacked IYD_FMN_2IP_m13 complex score
is:',scorefxn_fa(design)
         for j in range(1,21):
            min_mover_2.apply(design)
            print 'For structure',l,'round:',k,'iteration:',i,'Minimized repacked IYD_FMN_2IP_m13
complex score for interation',j,'is:',scorefxn_fa(design)
      task_pack_1 = standard_packer_task(design)
      task_pack_1.restrict_to_repacking()
      task_pack_1.or_include_current(True)
      pack_mover_1 = PackRotamersMover(scorefxn_fa,task_pack_1)
      pack_mover_1.apply(design)
      print 'For structure',l,'mc round:',k,'Repacked IYD_FMN_2IP_m13 complex score
is:',scorefxn_fa(design)
      for m in range(1,21):
         min_mover_1.apply(design)
         print 'For structure',l,'mc round:',k,'Minimized repacked IYD_FMN_2IP_m13 complex
score for interation',m,'is:',scorefxn_fa(design)
      mc.boltzmann(design)
      mc.show_scores()
      mc.show_counters()
      mc.show_state()
      design.pdb_info().name('mc')
      pmm.apply(design)
      jd4.output_decoy(design)
   mc.recover_low(design)
   print 'For structure',l,'the lowest energy is:',scorefxn_fa(design)
   print 'For structure',l,'the sequence is:',design.sequence()
   design.pdb_info().name('Final')
   pmm.apply(design)
   scorefxn_fa.show(design)
   hbond_set = get_hbonds(design)
   hbond_set.show(design,443)
   hbond_set.show(design,444)
   jd1.output_decoy(design)

print 'Job is done!'
```

Appendix B: Supporting information for Chapter 3

Table B1 DNA oligonucleotides used for cloning.

		DNA oligonucleotides[a]	PCR Template
Vector linearization	F[b]	TGGCATAAACCATTTTTGG	HhIYD[c]
	R[b]	TTCAAATTCCTCTTTTTCAGC	
J3736 DNA assembly	F	AAAGAGGAATTTGAACGTGCGGAAGAGGCGCTGCAGATTGCGCCG TTTCTGAACTGGGTG	-
	R	AAATGGTTTATGCCACACCCAGTTCAGAAACGGCGCAATCTGCAG CGCCTCTTCCGCACG	
0039 SDM[d]	F1	GCTGAAAAAGAGGAATTTGAAAAAGGCGAATATTGGGCACAGATT GCGCCGTTTCTGAAC	HhIYD
	R1	TTCAAATTCCTCTTTTTCAGCAGCTTGTCGGATTTTCGCTTTG	
	F2	GAAAAAGGCGAATATTGGGCAGAAATTATCAAAATTGCGAACTGG GTGTGGCATAAACC	0039 (1)[e]
	R2	TGCCCAATATTCGCCTTTTTCAAATTCCTCTTTTTCAGCAGC	
	F3	CAGAAATTATCAAAATTGCGCGTGATATGGGCGGTCATAAACCAT TTTTGGAAATTG	0039 (2)[e]
	R3	CGCAATTTTGATAATTTCTGCCCAATATTCGCCTTTTTC	
1719 SDM[d]	F1	GCTGAAAAAGAGGAATTTGAACGCTATGATGAAGCGAAACAGATT GCGCCGTTTCTGAAC	HhIYD
	R1	TTCAAATTCCTCTTTTTCAGCAGCTTGTCGGATTTTCGCTTTG	
	F2	GAAAGCGCTGGCGAAAGGCGCGCATAGCTGGGTGCCGCATAAACC ATTTTTGGAAATTG	1719 (1)[e]
	R2	GCCTTTCGCCAGCGCTTTCGCTTCATCATAGCGTTCAAATTC	
0479 Q5[f]	F	GCTGACCAAACGCGCAGGTGGCCCGCATAAACCATTTTTGGAAAT TG	HhIYD
	R	TCTTCATTGCCCGGATCAGAGCTCGCTTCAAATTCCTCTTTTTCAGC	
0609 OEPCR[g]	F	GCTGAAAAAGAGGAATTTGAAGCGAGCTCTGATCCGCGTAATGAA GAGCTGTTAAAACTGGCGGGTGGCTATCATAAACCATTTTTGGAA ATTG	HhIYD
	R	TTCAAATTCCTCTTTTTCAGCAGCTTGTCGGATTTTCGCTTTG	
4354 SDM	F	GCTCTAACCCGGAAAATAAAGAGCTGACCAGCCGCGCAGG	0479
	R	TTTATTTTCCGGGTTAGAGCTCGCTTCAAATTCCTCTTTTTCAGCAG C	
3654 SDM[d]	F1	GCTGAAAAAGAGGAATTTGAACGCTATGAGGAAGCACAGCAGATT GCGCCGTTTCTGAAC	HhIYD
	R1	TTCAAATTCCTCTTTTTCAGCAGCTTGTCGGATTTTCGCTTTG	
	F2	GAACGCTATGAGGAAGCACAGGCATCTGCAGGTCCGGGTAACTGG GTGTGGCATAAACC	3654 (1)[e]
	R2	CTGTGCTTCCTCATAGCGTTCAAATTCCTCTTTTTCAGCAGC	
	F3	AGGCATCTGCAGGTCCGGGTGTGGAAATTGTGTATCATAAACCAT TTTTGGAAATTG	3654 (2)[e]
	R3	ACCCGGACCTGCAGATGCCTGCGCTTCCTCATAGCGTTC	

[a]All DNA oligonucleotides are from 5' end to 3' end from left to right. [b]F, forward; R, reverse. [c]Template here is the pSMT3 plasmid carrying the indicated enzyme. [d]SDM, site directed mutagenesis. 0039, 1719, 3654 were constructed by two or three rounds of SDM. [e]The template for the next round SDM is the PCR product of the previous round of SDM indicated by the number in parenthesis. [f]Q5, Q5® site-directed mutagenesis. [e]OEPCR, overlap extension PCR.

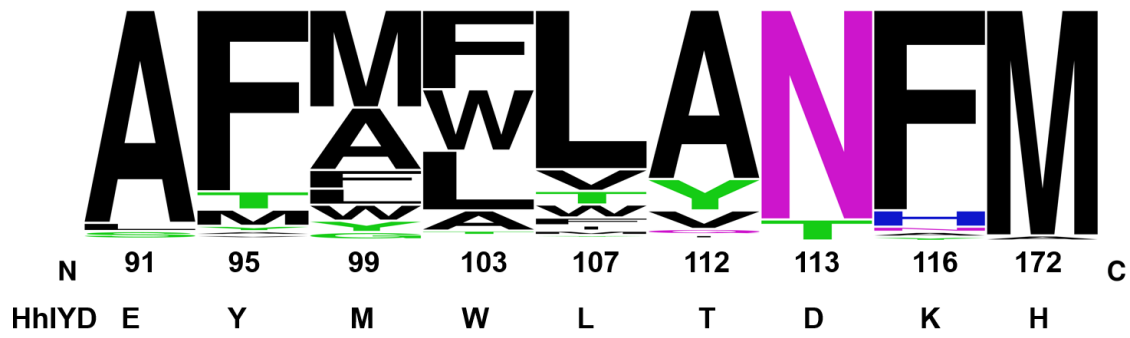

Figure B1 Sequence logo displaying variability of nine redesigned residues in 10000 independent designs of HhIYD. This figure was provided by Morgan Nance of the Gray lab (Johns Hopkins University).

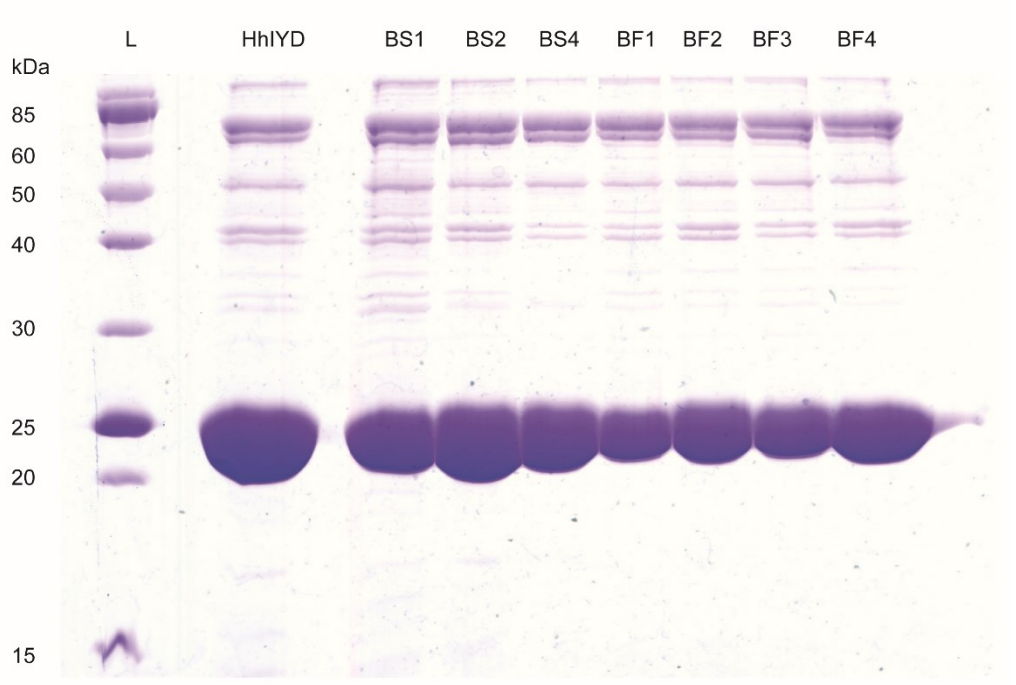

Figure B2 SDS-PAGE of HhIYD after the Ni-NTA column and its variants generated by redesign at selected positions. L represents protein ladder.

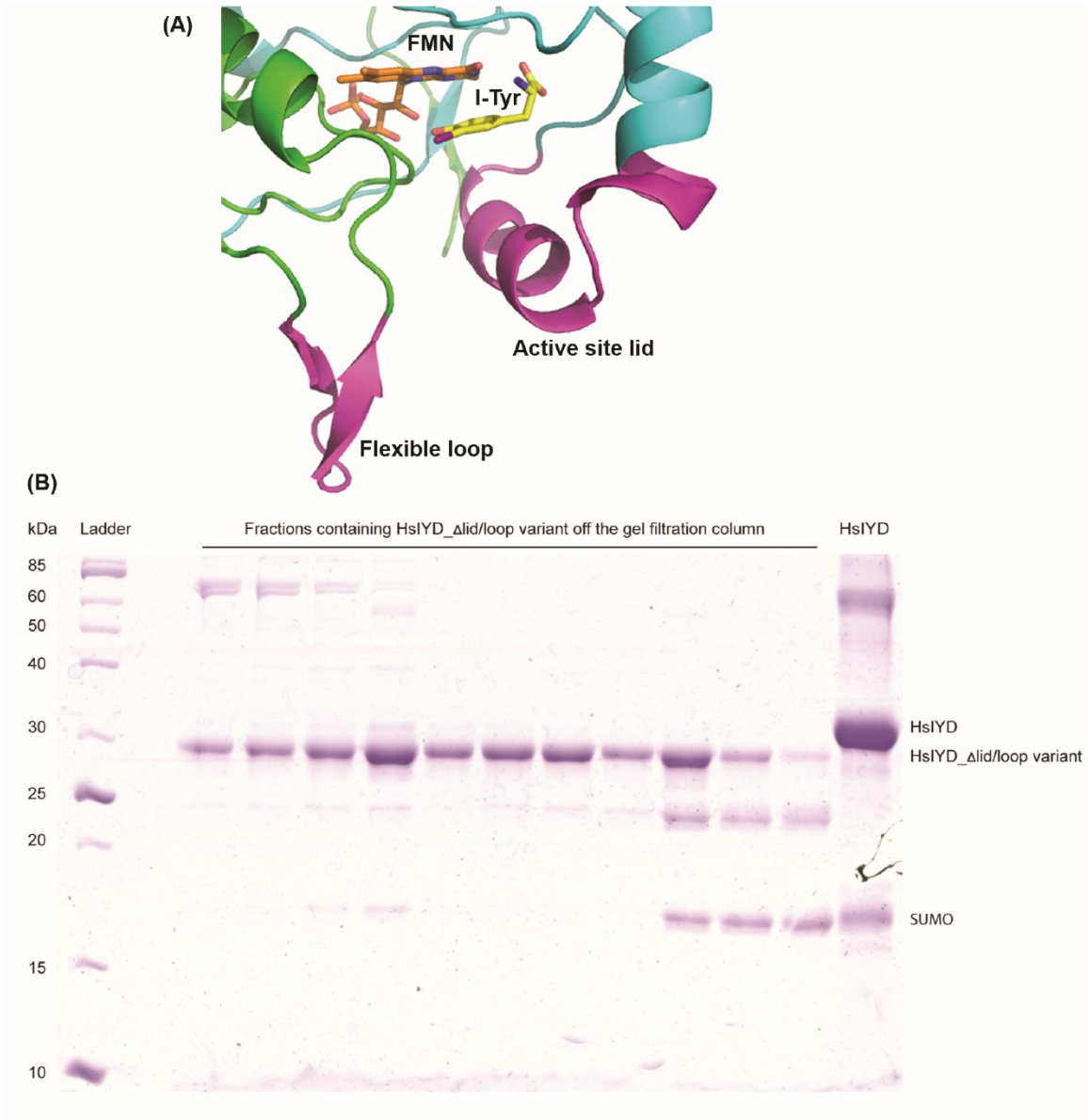

Figure B3 Construction and purification of HsIYD_Δlid/loop variant. (A) Co-crystal structure of HsIYD and I-Tyr (PDB 4TTC).[31] Green and cyan represents two monomeric units of HsIYD. FMN and I-Tyr are shown in orange and yellow, respectively. The active site lid (residues 161-177, magenta) and a flexible loop nearby (residues 200-208, magenta) were deleted to form the HsIYD_Δlid/loop variant. The N- and C-termini of both deletion were linked together without further modification, respectively. (B) SDS-PAGE of purified HsIYD_Δlid/loop variant and partially purified HsIYD. The variant which is 26 amino acid shorter than HsIYD run visibly further down on the gel than HsIYD.

J3736	**(15)**	**… 93**	**R**	**A**	**E**	**E**	**A**	**L**	**Q**	**I**	**A**	**P**	**F**	**L**	**N**	**W**	**V**		**114…**
1719	**(17)**		**R**	**Y**	**D**	**E**	**A**	**K**	**A**	**L**	**A**	**K**	**G**	**A**	**H**	**S**	**W**	**V**	**P**
3654	**(17)**		**R**	**Y**	**E**	**E**	**A**	**Q**	**A**	**S**	**A**	**G**	**P**	**G**	**V**	**E**	**I**	**V**	**Y**
0039	**(17)**		**K**	**G**	**E**	**Y**	**W**	**A**	**E**	**I**	**I**	**K**	**I**	**A**	**R**	**D**	**M**	**G**	**G**
4354	**(17)**		**A**	**S**	**S**	**N**	**P**	**E**	**N**	**K**	**E**	**L**	**T**	**S**	**R**	**A**	**G**	**G**	**P**
0479	**(17)**		**A**	**S**	**S**	**D**	**P**	**G**	**N**	**E**	**E**	**L**	**T**	**K**	**R**	**A**	**G**	**G**	**P**
0609	**(17)**		**A**	**S**	**S**	**D**	**P**	**R**	**N**	**E**	**E**	**L**	**L**	**K**	**L**	**A**	**G**	**G**	**Y**

Figure B4 Lid sequence of HhIYD loop remodeling variants. Total number of amino acids allowed to mutate are listed in parenthesis following the enzyme labels. The residue number of amino acids flanking the remodeled lids are shown next to the sequence of J3736. The residues in red are not a part of the remodeled lid but were mistakenly allowed to change during the sequence redesign.

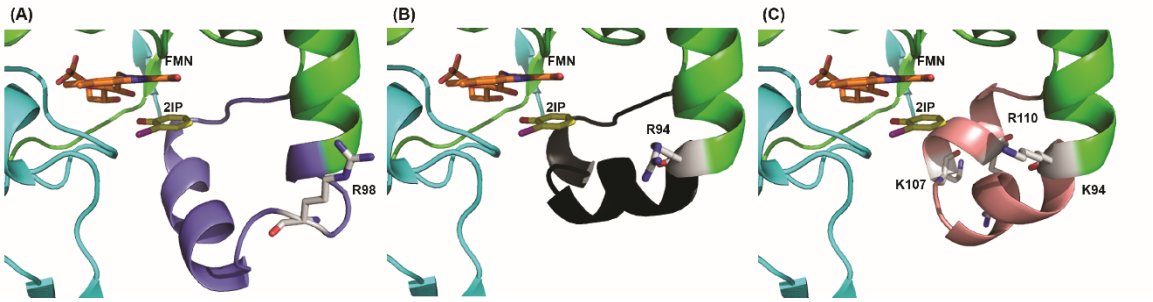

Figure B5 Trypsin digestion sites on the lids of HhIYD and its variants. (A) Rosetta model of HhIYD•2IP. Green and cyan represents two monomeric units of HsIYD. FMN and I-Tyr are shown in orange and yellow, respectively. The active site lid is colored in blue. The only digestion site on the lid is shown in gray. (B) Rosetta model of J3736•2IP. The only digestion site on the lid is shown in gray. (C) Rosetta model of 0039•2IP. The three digestion site on the lid are shown in gray.

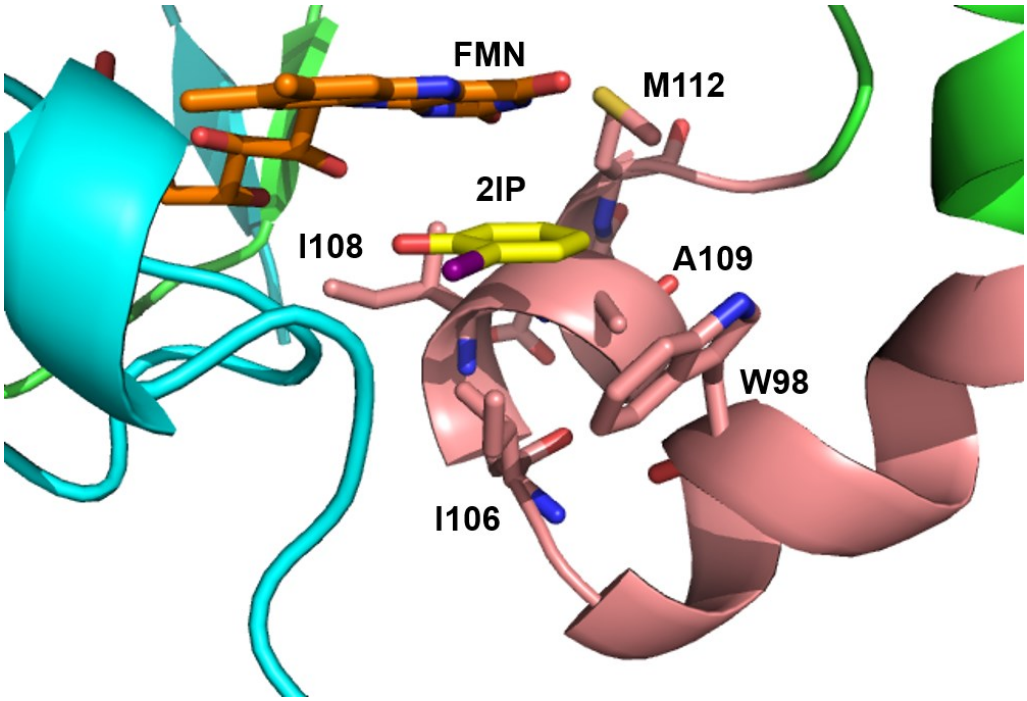

Figure B6 Side chain packing around the hydrophobic edge of 2IP in the Rosetta model of 0039•2IP. Green and cyan represents two monomeric units of HsIYD. FMN and I-Tyr are shown in orange and yellow, respectively. The active site lid is colored in pink. Residues within 5 Å of 2IP's hydrophobic edge were displayed.

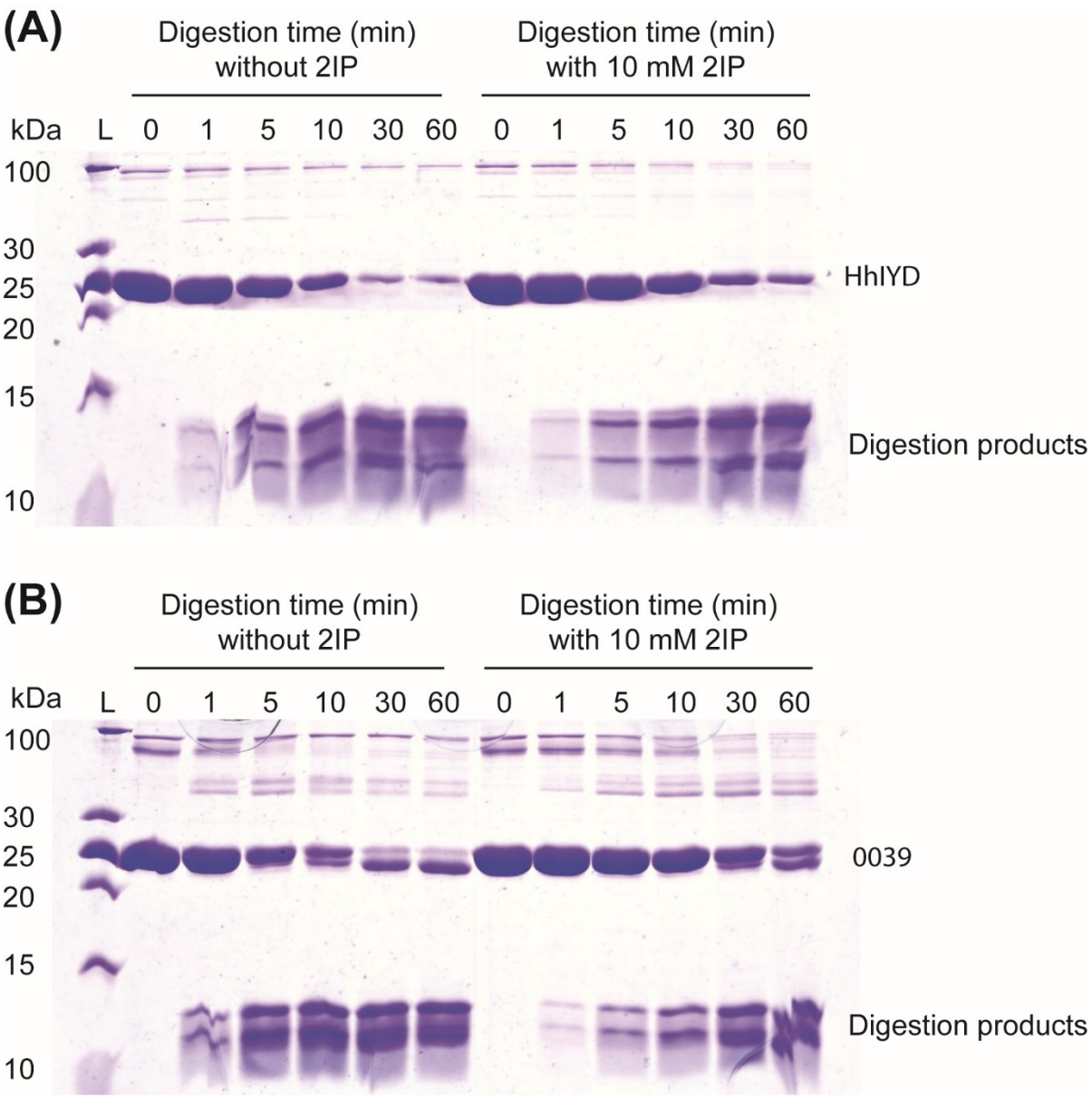

Figure B7 Trypsin digestion of HhIYD and 0039 in the absence and presence of 2IP analyzed by SDS-PAGE. (A) Digestion of HhIYD overtime. (B) Digestion of 0039 overtime. The mass ratio of deiodinase to trypsin in both cases was 50:1.

Appendix C: Supporting information for Chapter 4

Table C1 DNA oligonucleotides used for cloning.

		DNA oligonucleotides[a]	PCR Template
TnIYD restriction sites[c]	F[b]	AAGAAGGAGATATACATATGATGAAAATGCTGTACGACCCTG	TnIYD pET 28[d]
	R[b]	GTGGTGGTGGTGCTCGAGAAAGGTGTTATAGCGC	
TnIYD C-$(His)_6$[e]	F	ATACATATGAAAATGCTGTACGACCTGGCAAAGAAGC	TnIYD pET24a
	R	GTGGTGGTGGTGCTCGAGCTAGTGATGGTGATGGTGATGAAAGGTGTTATAGCGCAC	
Fre OEPCR[f]	F	TTTGTTTAACTTTAAGAAGGAGATATACATATGACAACCTTAAGCTGTAAAGTGAC	*E. coli* genomic DNA
	R	ATCTCAGTGGTGGTGGTGGTGGTGCTCGAGTTAGTGATGGTGATGGTGATGGATAAATGCAAACGCATCGCCAAAC	
TnIYD Y112A SDM[g]	F	TTTTCTCCGAAAAATCCGCGCCGGCGTCTCGTGAATCTGTATG	TnIYD[h]
	R	CGCGGATTTTTCGGAGAAAACCAGCAGCAGGTACGGCGCTTC	

[a]All DNA oligonucleotides are from 5' end to 3' end from left to right. [b]F, forward; R, reverse. [c]This PCR reaction introduced NdeI and XhoI restriction sites flanking the sequence of TnIYD. [d]The template here is the original pET28 plamid carrying TnIYD [e]This PCR reaction is to introduce a C-terminal $(His)_6$ tag to TnIYD after it was subcloned into pET24a vector to facilitate its purification. [f]OEPCR, overlap extension PCR. [g]SDM, site directed mutagenesis. [h]The template here is the final construct of TnIYD in the pET24a vector with a C-terminal $(His)_6$ tag.

Table C2 HPLC solvent gradient for the analysis of the greenish yellow form of TnIYD.

Time (min)	% Solvent B[a]
0	0
10	5
25	60
30	95
41	95
43	0
55	0

[a]Solvent A is 0.44% formic acid in water and solvent B is 0.44% formic acid in acetonitrile.

Table C3 HPLC solvent gradient for the analysis of Tyr under neutral conditions.

Time (min)	% Solvent B[a]	% Solvent C[a]
0	0	0
10	5	0
40	5	0
40.01	5	95
45	80	20
55	80	20
60	0	100
60.01	0	0
70	0	0

[a]Solvent A is 10 mM potassium phosphate pH 6.6, solvent B is acetonitrile, and solvent C is water.

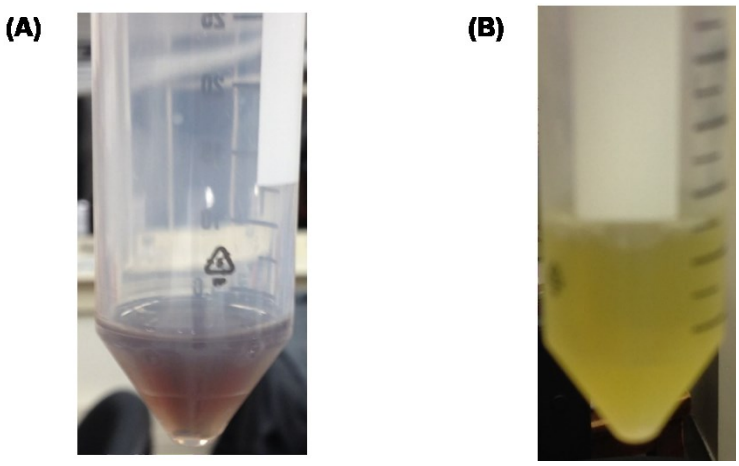

Figure C1 Color of TnIYD during purification. (A) TnIYD eluted from a gravity Ni-NTA column. (B) TnIYD in (A) after incubated on ice overnight.

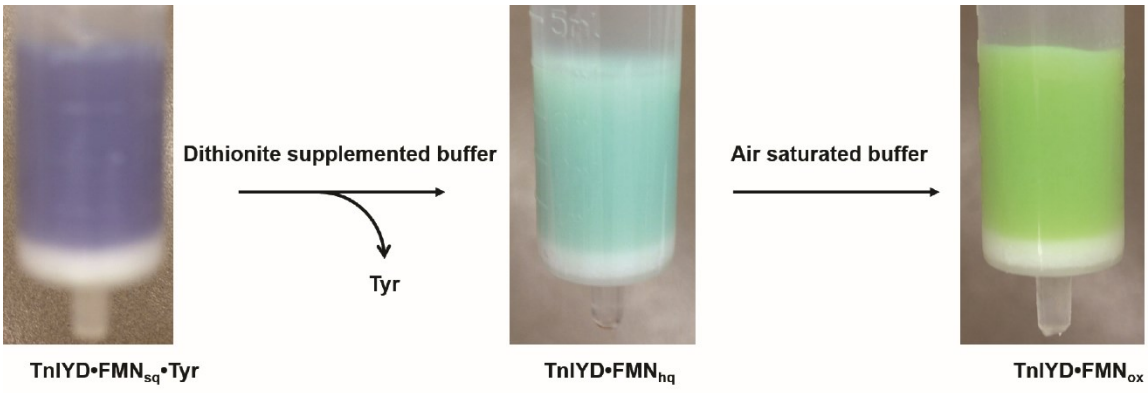

Figure C2 Removal of Tyr from the greenish yellow form of TnIYD via dithionite treatment. TnIYD•FMN$_{sq}$, TnIYD•FMN$_{hq}$, TnIYD•FMN$_{ox}$ represent the semiquinone form, the hydroquinone form (fully reduced), and the fully oxidized form of TnIYD, respectively. The TnIYD•FMN$_{ox}$ is bright yellow without Tyr but shows in the picture as green on top of the blue Ni-NTA resin.

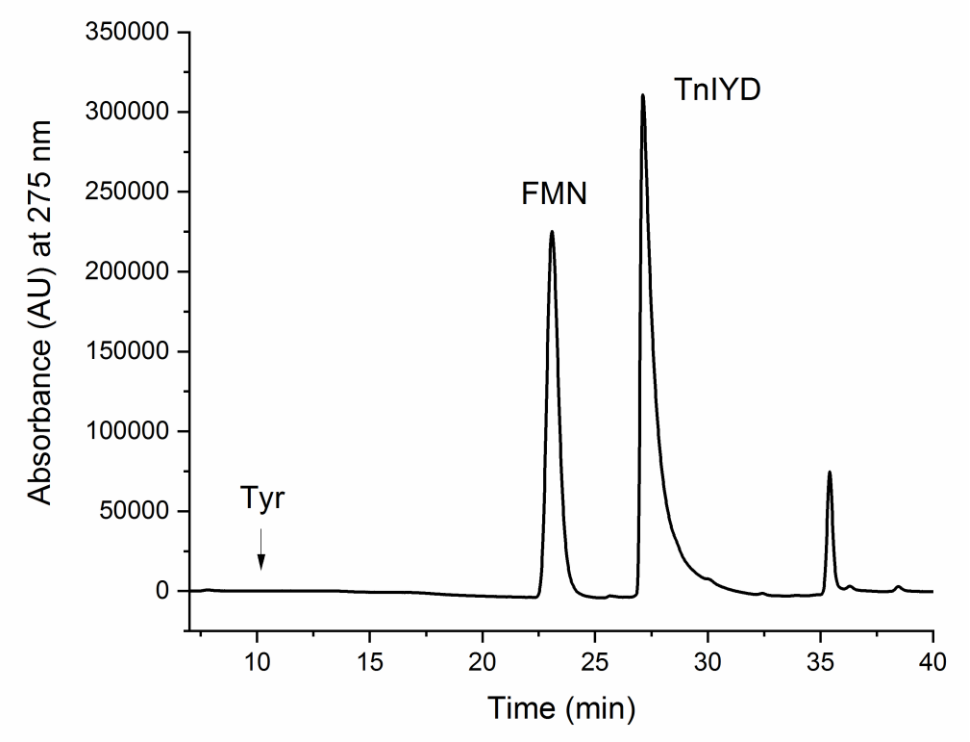

Figure C4 HPLC analysis of 40 μM TnIYD after dithionite treatment. Tyr bound to the greenish yellow form of TnIYD was removed by the dithionite treatment and therefore is absent in the above chromatogram.

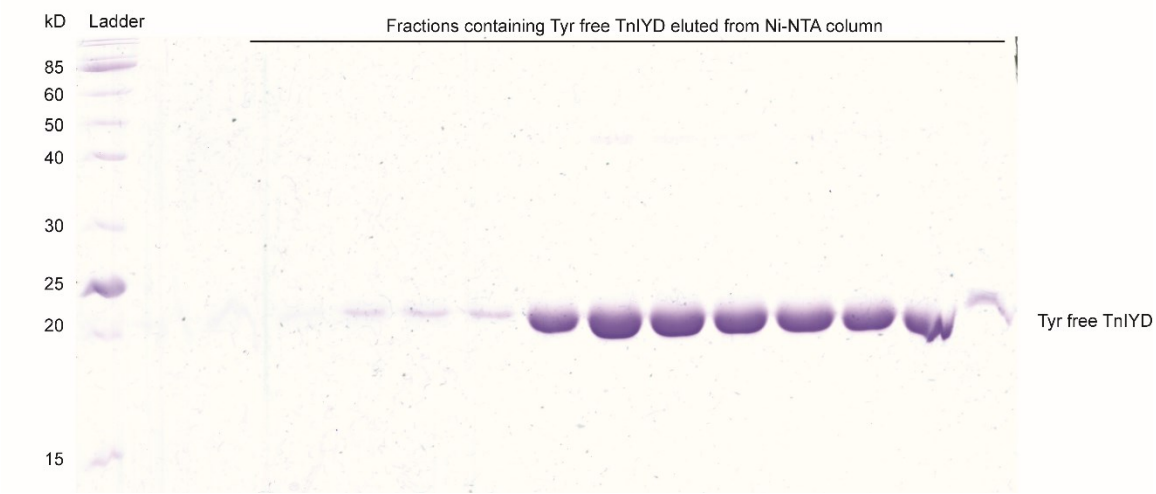

Figure C4 SDS-PAGE (12%) of purified Tyr free TnIYD.

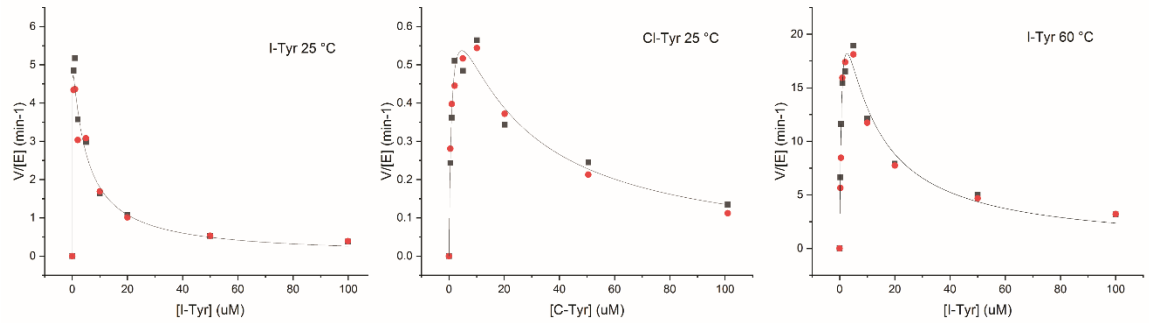

Figure C5 Substrate inhibition kinetics of TnIYD.

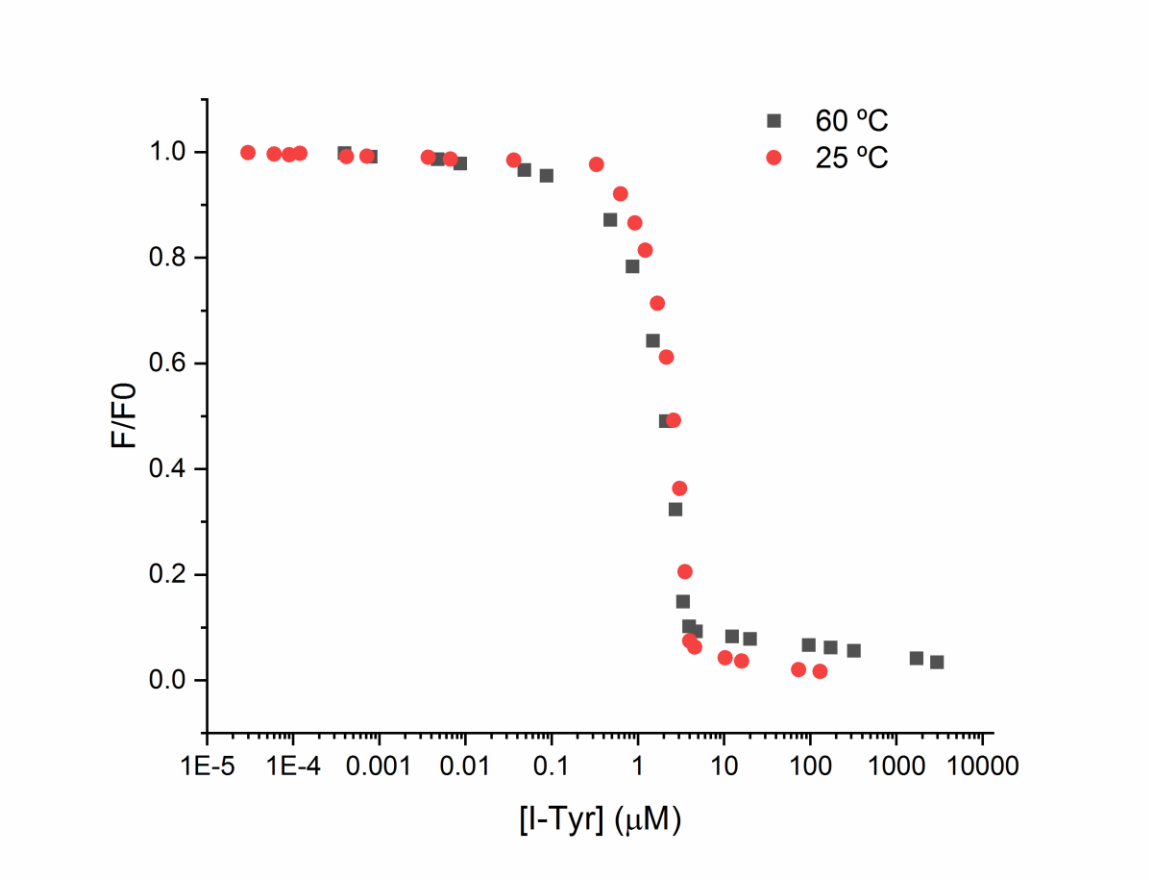

Figure C6 Fluoresence quenching of TnIYD's FMN cofactor upon I-Tyr titration at 25 ºC and 60 ºC. Each data point represents one single determination.

Appendix D: Supporting information for Chapter 5

Table D1 Steady-state kinetics of TnIYD with I-Tyr measured by different reaction initiation methods.[8]

Initiation method	Temperature (°C)	k_{cat} (min^{-1})[a]	K_M (μM)[a]	k_{cat}/K_M ($min^{-1}\times \mu M^{-1}$)	K_i (μM)
TnIYD•FMN_{hq}	25	5.4 ± 0.9	0.02 ± 0.10	270 ± 1000	5 ± 2
Dithionite	25	0.42 ± 0.07	5 ± 2	0.08 ± 0.03	N. D.
TnIYD•FMN_{hq}	60	29 ± 4	0.8 ± 0.2	36 ± 10	9 ± 2
Dithionite	60	15 ± 3	2 ± 1	8 ± 4	N. D.

[a]All the data and error bars were obtained by fitting of two independent measurements as one curve to substrate inhibition kinetics (TnIYD•FMN_{hq} initiation) or Michaelis-Menton kinetics (Dithionite initiation).

[8] The kinetic measurements by the dithionite initiation method were performed by Shaun Spisak (Johns Hopkins University).

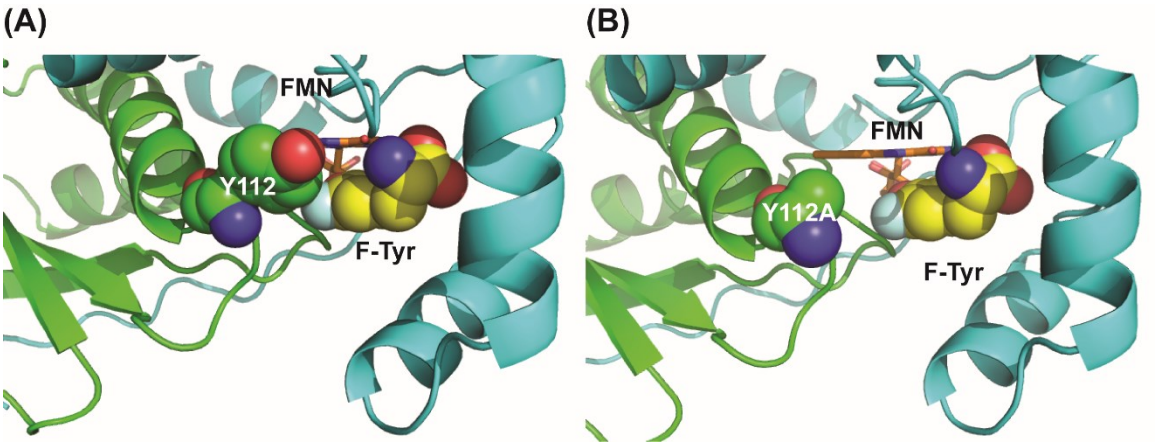

Figure D1 Structural comparison of TnIYD and the Y112A variant with F-Tyr bound. (A) The co-crystal structure of TnIYD•FMN_{ox} and F-Tyr (PDB 6Q1B). The monomeric polypeptides of TnIYD are colored green and cyan, respectively. Y112 and F-Tyr are shown in green and yellow spheres, respectively. FMN is represented by orange sticks. (B) Model structure of TnIYD Y112A with F-Tyr bound generated by Pymol based on PDB 6Q1B. Y112A mutation is shown in green spheres.

Bibliography

(1) National Toxicology Programs. Pentachlorophenol and By-Products of Its Synthesis. In *Report on Carcinogens*; U.S. Department of Health and Human Services, Public Health Service.: Research Triangle Park, NC, 2016; pp 1–7.

(2) Yueh, M.-F.; Tukey, R. H. Triclosan: A Widespread Environmental Toxicant with Many Biological Effects. *Annu. Rev. Pharmacol. Toxicol.* **2016**, *56*, 251–272.

(3) Luo, J.; Hu, J.; Wei, X.; Fu, L.; Li, L. Dehalogenation of Persistent Halogenated Organic Compounds: A Review of Computational Studies and Quantitative Structure–Property Relationships. *Chemosphere* **2015**, *131*, 17–33.

(4) Cupples, A. M.; Sanford, R. A.; Sims, G. K. Dehalogenation of the Herbicides Bromoxynil (3,5-Dibromo-4-Hydroxybenzonitrile) and Ioxynil (3,5-Diiodino-4-Hydroxybenzonitrile) by Desulfitobacterium Chlororespirans. *Appl. Environ. Microbiol.* **2005**, *71*, 3741–3746.

(5) United States Environmental Protection Agency. Priority Pollutant List, 2014.

(6) Miller LL, Ingerman LD, Singh M. Toxicological Profile for Pentachlorophenol. Agency for Toxic Substances and Disease Registry, U.S. Department of Health and Human Services, Atlanta, GA, 2001.

(7) Murray HE, Wond D. Toxicological Profile for Chlorophenols. Agency for Toxic Substances and Disease Registry, U.S Department of Health and Human Services, Atlanta, GA, 1999.

(8) Shimizu, R.; Yamaguchi, M.; Uramaru, N.; Kuroki, H.; Ohta, S.; Kitamura, S.; Sugihara, K. Structure-Activity Relationships of 44 Halogenated Compounds for Iodotyrosine Deiodinase-Inhibitory Activity. *Toxicology* **2013**, *314*, 22–29.

(9) Kitamura, S.; Kato, T.; Iida, M.; Jinno, N.; Suzuki, T.; Ohta, S.; Fujimoto, N.; Hanada, H.; Kashiwagi, K.; Kashiwagi, A. Anti-Thyroid Hormonal Activity of Tetrabromobisphenol A, a Flame Retardant, and Related Compounds: Affinity to the Mammalian Thyroid Hormone

Receptor, and Effect on Tadpole Metamorphosis. *Life Sci.* **2005**, *76*, 1589–1601.

(10) Atlas RM, Philp J (Ed.). Bioremediation: Applied Microbial Solutions for Real-World Environmental Cleanup. ASM Press, Washington DC, 2005.

(11) P., R. T.; W., T. J. Enhancing Bioremediation with Enzymatic Processes: A Review. *Pract. Period. Hazardous, Toxic, Radioact. Waste Manag.* **2006**, *10*, 73–85.

(12) Fetzner, S.; Lingens, F. Bacterial Dehalogenases: Biochemistry, Genetics, and Biotechnological Applications. *Microbiol. Rev.* **1994**, *58*, 641–685.

(13) Chaudhry, G. R.; Chapalamadugu, S. Biodegradation of Halogenated Organic Compounds. *Microbiol. Rev.* **1991**, *55*, 59–79.

(14) Agarwal, V.; Miles, Z. D.; Winter, J. M.; Eustáquio, A. S.; El Gamal, A. A.; Moore, B. S. Enzymatic Halogenation and Dehalogenation Reactions: Pervasive and Mechanistically Diverse. *Chem. Rev.* **2017**, *117*, 5619–5674.

(15) Arora, P. K.; Srivastava, A.; Singh, V. P. Application of Monooxygenases in Dehalogenation, Desulphurization, Denitrification and Hydroxylation of Aromatic Compounds. *J. Bioremediation Biodegrad.* **2010**, *1*, 1000112.

(16) Pimviriyakul, P.; Thotsaporn, K.; Sucharitakul, J.; Chaiyen, P. Kinetic Mechanism of the Dechlorinating Flavin-Dependent Monooxygenase HadA. *J. Biol. Chem.* **2017**, *292*, 4818–4832.

(17) Koudelakova, T.; Bidmanova, S.; Dvorak, P.; Pavelka, A.; Chaloupkova, R.; Prokop, Z.; Damborsky, J. Haloalkane Dehalogenases: Biotechnological Applications. *Biotechnol. J.* **2013**, *8*, 32–45.

(18) Chan, P. W. Y.; Yakunin, A. F.; Edwards, E. A.; Pai, E. F. Mapping the Reaction Coordinates of Enzymatic Defluorination. *J. Am. Chem. Soc.* **2011**, *133*, 7461–7468.

(19) Wang, G.; Li, R.; Li, S.; Jiang, J. A Novel Hydrolytic Dehalogenase for the Chlorinated Aromatic Compound Chlorothalonil. *J. Bacteriol.* **2010**, *192*, 2737–2745.

(20) Wu, R.; Reger, A. S.; Cao, J.; Gulick, A. M.; Dunaway-Mariano, D. Rational Redesign of the 4-Chlorobenzoate Binding Site of 4-Chlorobenzoate: Coenzyme a Ligase for Expanded Substrate Range. *Biochemistry* **2007**, *46*, 14487–14499.

(21) Warner, J. R.; Copley, S. D. Pre-Steady-State Kinetic Studies of the Reductive Dehalogenation Catalyzed by Tetrachlorohydroquinone Dehalogenase. *Biochemistry* **2007**, *46*, 13211–13222.

(22) Jugder, B.-E.; Ertan, H.; Lee, M.; Manefield, M.; Marquis, C. P. Reductive Dehalogenases Come of Age in Biological Destruction of Organohalides. *Trends Biotechnol.* **2015**, *33*, 595–610.

(23) Payne, K. A.; Quezada, C. P.; Fisher, K.; Dunstan, M. S.; Collins, F. A.; Sjuts, H.; Levy, C.; Hay, S.; Rigby, S. E.; Leys, D. Reductive Dehalogenase Structure Suggests a Mechanism for B12-Dependent Dehalogenation. *Nature* **2015**, *517*, 513–516.

(24) Rokita, S. E.; Adler, J. M.; McTamney, P. M.; Watson, J. A. J. Efficient Use and Recycling of the Micronutrient Iodide in Mammals. *Biochimie* **2010**, *92*, 1227–1235.

(25) Phatarphekar, A.; Buss, J. M.; Rokita, S. E. Iodotyrosine Deiodinase: A Unique Flavoprotein Present in Organisms of Diverse Phyla. *Mol. Biosyst.* **2014**, *10*, 86–92.

(26) Bobyk, K. D.; Ballou, D. P.; Rokita, S. E. Rapid Kinetics of Dehalogenation Promoted by Iodotyrosine Deiodinase from Human Thyroid. *Biochemistry* **2015**, *54*, 4487–4494.

(27) McTamney, P. M.; Rokita, S. E. A Mammalian Reductive Deiodinase Has Broad Power to Dehalogenate Chlorinated and Brominated Substrates. *J. Am. Chem. Soc.* **2009**, *131*, 14212–14213.

(28) Phatarphekar, A.; Rokita, S. E. Functional Analysis of Iodotyrosine Deiodinase from Drosophila Melanogaster. *Protein Sci.* **2016**, *25*, 2187–2195.

(29) Sun, Z.; Su, Q.; Rokita, S. E. The Distribution and Mechanism of Iodotyrosine Deiodinase Defied Expectations. *Arch. Biochem. Biophys.* **2017**, *632*.

(30) Tanner, D. D.; Chen, J. J.; Chen, L.; Luelo, C. Fragmentation of Substituted Acetophenones and Halobenzophenone Ketyls. Calibration of a Mechanistic Probe. *J. Am. Chem. Soc.* **1991**, *113*, 8074–8081.

(31) Hu, J.; Chuenchor, W.; Rokita, S. E. A Switch between One- and Two-Electron Chemistry of the Human Flavoprotein Iodotyrosine Deiodinase Is Controlled by Substrate. *J. Biol. Chem.* **2015**, *290*, 590–600.

(32) Ingavat, N.; Kavran, J. M.; Sun, Z.; Rokita, S. E. Active Site Binding Is Not Sufficient for Reductive Deiodination by Iodotyrosine Deiodinase. *Biochemistry* **2017**, *56*.

(33) Thomas, S. R.; McTamney, P. M.; Adler, J. M.; Laronde-Leblanc, N.; Rokita, S. E. Crystal Structure of Iodotyrosine Deiodinase, a Novel Flavoprotein Responsible for Iodide Salvage in Thyroid Glands. *J. Biol. Chem.* **2009**, *284*, 19659–19667.

(34) Akiva, E.; Copp, J. N.; Tokuriki, N.; Babbitt, P. C. Evolutionary and Molecular Foundations of Multiple Contemporary Functions of the Nitroreductase Superfamily. *Proc. Natl. Acad. Sci. U. S. A.* **2017**, *114*, E9549–E9558.

(35) Nestl, B. M.; Hauer, B. Engineering of Flexible Loops in Enzymes. *ACS Catal.* **2014**, *4*, 3201–3211.

(36) Sykora, J.; Brezovsky, J.; Koudelakova, T.; Lahoda, M.; Fortova, A.; Chernovets, T.; Chaloupkova, R.; Stepankova, V.; Prokop, Z.; Smatanova, I. K.; et al. Dynamics and Hydration Explain Failed Functional Transformation in Dehalogenase Design. *Nat. Chem. Biol.* **2014**, *10*, 428–430.

(37) Chen, K.; Arnold, F. H. Tuning the Activity of an Enzyme for Unusual Environments: Sequential Random Mutagenesis of Subtilisin E for Catalysis in Dimethylformamide. *Proc. Natl. Acad. Sci. U. S. A.* **1993**, *90*, 5618–5622.

(38) Zhang, R. K.; Chen, K.; Huang, X.; Wohlschlager, L.; Renata, H.; Arnold, F. H. Enzymatic Assembly of Carbon-Carbon Bonds via Iron-Catalysed Sp(3) C-H Functionalization.

Nature **2019**, *565*, 67–72.

(39) Stemmer, W. P. Rapid Evolution of a Protein in Vitro by DNA Shuffling. *Nature* **1994**, *370*, 389–391.

(40) Tanner, J. J.; Lei, B.; Tu, S. C.; Krause, K. L. Flavin Reductase P: Structure of a Dimeric Enzyme That Reduces Flavin. *Biochemistry* **1996**, *35*, 13531–13539.

(41) Race, P. R.; Lovering, A. L.; Green, R. M.; Ossor, A.; White, S. A.; Searle, P. F.; Wrighton, C. J.; Hyde, E. I. Structural and Mechanistic Studies of Escherichia Coli Nitroreductase with the Antibiotic Nitrofurazone. Reversed Binding Orientations in Different Redox States of the Enzyme. *J. Biol. Chem.* **2005**, *280*, 13256–13264.

(42) Taga, M. E.; Larsen, N. A.; Howard-Jones, A. R.; Walsh, C. T.; Walker, G. C. BluB Cannibalizes Flavin to Form the Lower Ligand of Vitamin B12. *Nature* **2007**, *446*, 449–453.

(43) Wijma, H. J.; Janssen, D. B. Computational Design Gains Momentum in Enzyme Catalysis Engineering. *FEBS J.* **2013**, *280*, 2948–2960.

(44) Richter, F.; Blomberg, R.; Khare, S. D.; Kiss, G.; Kuzin, A. P.; Smith, A. J. T.; Gallaher, J.; Pianowski, Z.; Helgeson, R. C.; Grjasnow, A.; et al. Computational Design of Catalytic Dyads and Oxyanion Holes for Ester Hydrolysis. *J. Am. Chem. Soc.* **2012**, *134*, 16197–16206.

(45) Eiben, C. B.; Siegel, J. B.; Bale, J. B.; Cooper, S.; Khatib, F.; Shen, B. W.; Players, F.; Stoddard, B. L.; Popovic, Z.; Baker, D. Increased Diels-Alderase Activity through Backbone Remodeling Guided by Foldit Players. *Nat. Biotechnol.* **2012**, *30*, 190–192.

(46) Zheng, F.; Yang, W.; Ko, M.-C.; Liu, J.; Cho, H.; Gao, D.; Tong, M.; Tai, H.-H.; Woods, J. H.; Zhan, C.-G. Most Efficient Cocaine Hydrolase Designed by Virtual Screening of Transition States. *J. Am. Chem. Soc.* **2008**, *130*, 12148–12155.

(47) Murphy, P. M.; Bolduc, J. M.; Gallaher, J. L.; Stoddard, B. L.; Baker, D. Alteration of

Enzyme Specificity by Computational Loop Remodeling and Design. *Proc. Natl. Acad. Sci.* **2009**, *106*, 9215–9220.

(48) Siegel, J. B.; Zanghellini, A.; Lovick, H. M.; Kiss, G.; Lambert, A. R.; St.Clair, J. L.; Gallaher, J. L.; Hilvert, D.; Gelb, M. H.; Stoddard, B. L.; et al. Computational Design of an Enzyme Catalyst for a Stereoselective Bimolecular Diels-Alder Reaction. *Science (80-.).* **2010**, *329*, 309–313.

(49) Buss, J. M.; McTamney, P. M.; Rokita, S. E. Expression of a Soluble Form of Iodotyrosine Deiodinase for Active Site Characterization by Engineering the Native Membrane Protein from Mus Musculus. *Protein Sci.* **2012**, *21*, 351–361.

(50) Unpublished Results. Kozyryev, A.; Rokita S. E.

(51) Copeland, R. A. Chemical Mechanisms in Enzyme Catalysis. In *Enzymes: A Practical Introduction to Structure, Mechanism, and Data Analysis*; John Wiley & Sons, Inc.: New York, 2000; pp 146–187.

(52) Pellett, J. D.; Becker, D. F.; Saenger, A. K.; Fuchs, J. A.; Stankovich, M. T. Role of Aromatic Stacking Interactions in the Modulation of the Two-Electron Reduction Potentials of Flavin and Substrate/Product in Megasphaera Elsdenii Short-Chain Acyl-Coenzyme A Dehydrogenase. *Biochemistry* **2001**, *40*, 7720–7728.

(53) Leaver-Fay, A.; Tyka, M.; Lewis, S. M.; Lange, O. F.; Thompson, J.; Jacak, R.; Kaufman, K.; Renfrew, P. D.; Smith, C. A.; Sheffler, W.; et al. ROSETTA3: An Object-Oriented Software Suite for the Simulation and Design of Macromolecules. *Methods Enzymol.* **2011**, *487*, 545–574.

(54) Kaufmann, K. W.; Lemmon, G. H.; Deluca, S. L.; Sheehan, J. H.; Meiler, J. Practically Useful: What the Rosetta Protein Modeling Suite Can Do for You. *Biochemistry* **2010**, *49*, 2987–2998.

(55) Labonte, J. W.; Adolf-Bryfogle, J.; Schief, W. R.; Gray, J. J. Residue-Centric Modeling and

Design of Saccharide and Glycoconjugate Structures. *J. Comput. Chem.* **2017**, *38*, 276–287.

(56) Jiang, L.; Althoff, E. A.; Clemente, F. R.; Doyle, L.; Rothlisberger, D.; Zanghellini, A.; Gallaher, J. L.; Betker, J. L.; Tanaka, F.; Barbas, C. F. 3rd; et al. De Novo Computational Design of Retro-Aldol Enzymes. *Science* **2008**, *319*, 1387–1391.

(57) Röthlisberger, D.; Khersonsky, O.; Wollacott, A. M.; Jiang, L.; DeChancie, J.; Betker, J.; Gallaher, J. L.; Althoff, E. A.; Zanghellini, A.; Dym, O.; et al. Kemp Elimination Catalysts by Computational Enzyme Design. *Nature* **2008**, *453*, 190–195.

(58) Gordon, S. R.; Stanley, E. J.; Wolf, S.; Toland, A.; Wu, S. J.; Hadidi, D.; Mills, J. H.; Baker, D.; Pultz, I. S.; Siegel, J. B. Computational Design of an α-Gliadin Peptidase. *J. Am. Chem. Soc.* **2012**, *134*, 20513–20520.

(59) Chaudhury, S.; Lyskov, S.; Gray, J. J. PyRosetta: A Script-Based Interface for Implementing Molecular Modeling Algorithms Using Rosetta. *Bioinformatics* **2010**, *26*, 689–691.

(60) Sun, Z.; Rokita, S. E. Toward a Halophenol Dehalogenase from Iodotyrosine Deiodinase via Computational Design. *ACS Catal.* **2018**, *8*, 11783–11793.

(61) Gray, J. J.; Moughon, S.; Wang, C.; Schueler-Furman, O.; Kuhlman, B.; Rohl, C. A.; Baker, D. Protein-Protein Docking with Simultaneous Optimization of Rigid-Body Displacement and Side-Chain Conformations. *J. Mol. Biol.* **2003**, *331*, 281–299.

(62) Dunbrack, R. L. J.; Cohen, F. E. Bayesian Statistical Analysis of Protein Side-Chain Rotamer Preferences. *Protein Sci.* **1997**, *6*, 1661–1681.

(63) Li, Z.; Scheraga, H. A. Monte Carlo-Minimization Approach to the Multiple-Minima Problem in Protein Folding. *Proc. Natl. Acad. Sci. U. S. A.* **1987**, *84*, 6611–6615.

(64) PyRosetta: Obtaining and Preparing Ligand PDS FIles; Available via the Internet at: Http://Www.Pyrosetta.Org/Obtaining-and- Preparing-Ligand-Pdb-FIles (Accessed June 2018).

(65) Kuhlman, B.; Baker, D. Native Protein Sequences Are Close to Optimal for Their Structures. *Proc. Natl. Acad. Sci.* **2000**, *97*, 10383–10388.

(66) Fersht, A. R. Protein Stability. In *Structure and Mechanism in Protein Science: A Guide to Enzyme Catalysis and Protein Folding*; W.H. Freeman and Company: New York, 1999; pp 508–536.

(67) Yu, H.; Yan, Y.; Zhang, C.; Dalby, P. A. Two Strategies to Engineer Flexible Loops for Improved Enzyme Thermostability. *Sci. Rep.* **2017**, *7*, 41212.

(68) Mossessova, E.; Lima, C. D. Ulp1-SUMO Crystal Structure and Genetic Analysis Reveal Conserved Interactions and a Regulatory Element Essential for Cell Growth in Yeast. *Mol. Cell* **2000**, *5*, 865–876.

(69) Zheng, L.; Baumann, U.; Reymond, J.-L. An Efficient One-Step Site-Directed and Site-Saturation Mutagenesis Protocol. *Nucleic Acids Res.* **2004**, *32*, e115.

(70) Liu, H.; Naismith, J. H. An Efficient One-Step Site-Directed Deletion, Insertion, Single and Multiple-Site Plasmid Mutagenesis Protocol. *BMC Biotechnol.* **2008**, *8*, 91.

(71) Li, M. Z.; Elledge, S. J. Harnessing Homologous Recombination in Vitro to Generate Recombinant DNA via SLIC. *Nat. Methods* **2007**, *4*, 251–256.

(72) Stemmer, W. P.; Crameri, A.; Ha, K. D.; Brennan, T. M.; Heyneker, H. L. Single-Step Assembly of a Gene and Entire Plasmid from Large Numbers of Oligodeoxyribonucleotides. *Gene* **1995**, *164*, 49–53.

(73) Hoover, D. M.; Lubkowski, J. DNAWorks: An Automated Method for Designing Oligonucleotides for PCR-Based Gene Synthesis. *Nucleic Acids Res.* **2002**, *30*, e43.

(74) Kozioł, J. B. T.-M. in E. Fluorometric Analyses of Riboflavin and Its Coenzymes. In *Vitamins and Coenzymes*; Academic Press, 1971; Vol. 18, pp 253–285.

(75) Gasteiger, E.; Gattiker, A.; Hoogland, C.; Ivanyi, I.; Appel, R. D.; Bairoch, A. ExPASy: The Proteomics Server for in-Depth Protein Knowledge and Analysis. *Nucleic Acids Res.*

2003, *31*, 3784–3788.

(76) Yamaguchi, H.; Miyazaki, M.; Maeda, H. Limited Proteolysis in Proteomics Using Protease-Immobilized Microreactors. *Methods Mol. Biol.* **2012**, *815*, 187–198.

(77) Cohen, S. L.; Chait, B. T. Mass Spectrometry of Whole Proteins Eluted from Sodium Dodecyl Sulfate-Polyacrylamide Gel Electrophoresis Gels. *Anal. Biochem.* **1997**, *247*, 257–267.

(78) Toney, M. D.; Kirsch, J. F. Direct Bronsted Analysis of the Restoration of Activity to a Mutant Enzyme by Exogenous Amines. *Science* **1989**, *243*, 1485–1488.

(79) Qiao, Y.; Molina, H.; Pandey, A.; Zhang, J.; Cole, P. A. Chemical Rescue of a Mutant Enzyme in Living Cells. *Science* **2006**, *311*, 1293–1297.

(80) Dantas, G.; Kuhlman, B.; Callender, D.; Wong, M.; Baker, D. A Large Scale Test of Computational Protein Design: Folding and Stability of Nine Completely Redesigned Globular Proteins. *J. Mol. Biol.* **2003**, *332*, 449–460.

(81) Renfrew, P. D.; Choi, E. J.; Bonneau, R.; Kuhlman, B. Incorporation of Noncanonical Amino Acids into Rosetta and Use in Computational Protein-Peptide Interface Design. *PLoS One* **2012**, *7*, e32637.

(82) Eriksson, A. E.; Baase, W. A.; Zhang, X. J.; Heinz, D. W.; Blaber, M.; Baldwin, E. P.; Matthews, B. W. Response of a Protein Structure to Cavity-Creating Mutations and Its Relation to the Hydrophobic Effect. *Science* **1992**, *255*, 178–183.

(83) Eriksson, A. E.; Baase, W. A.; Wozniak, J. A.; Matthews, B. W. A Cavity-Containing Mutant of T4 Lysozyme Is Stabilized by Buried Benzene. *Nature* **1992**, *355*, 371–373.

(84) Alford, R. F.; Leaver-Fay, A.; Jeliazkov, J. R.; O'Meara, M. J.; DiMaio, F. P.; Park, H.; Shapovalov, M. V; Renfrew, P. D.; Mulligan, V. K.; Kappel, K.; et al. The Rosetta All-Atom Energy Function for Macromolecular Modeling and Design. *J. Chem. Theory Comput.* **2017**, *13*, 3031–3048.

(85) Santiago, G.; de Salas, F.; Lucas, M. F.; Monza, E.; Acebes, S.; Martinez, Á. T.; Camarero, S.; Guallar, V. Computer-Aided Laccase Engineering: Toward Biological Oxidation of Arylamines. *ACS Catal.* **2016**, *6*, 5415–5423.

(86) Currin, A.; Dunstan, M. S.; Johannissen, L. O.; Hollywood, K. A.; Vinaixa, M.; Jervis, A. J.; Swainston, N.; Rattray, N. J. W.; Gardiner, J. M.; Kell, D. B.; et al. Engineering the "Missing Link" in Biosynthetic (-)-Menthol Production: Bacterial Isopulegone Isomerase. *ACS Catal.* **2018**, *8*, 2012–2020.

(87) Hoffmeister, D.; Yang, J.; Liu, L.; Thorson, J. S. Creation of the First Anomeric D/L-Sugar Kinase by Means of Directed Evolution. *Proc. Natl. Acad. Sci.* **2003**, *100*, 13184–13189.

(88) Aharoni, A.; Gaidukov, L.; Yagur, S.; Toker, L.; Silman, I.; Tawfik, D. S. Directed Evolution of Mammalian Paraoxonases PON1 and PON3 for Bacterial Expression and Catalytic Specialization. *Proc. Natl. Acad. Sci. U. S. A.* **2004**, *101*, 482–487.

(89) Romero, P. A.; Arnold, F. H. Exploring Protein Fitness Landscapes by Directed Evolution. *Nat. Rev. Mol. Cell Biol.* **2009**, *10*, 866–876.

(90) Miton, C. M.; Tokuriki, N. How Mutational Epistasis Impairs Predictability in Protein Evolution and Design. *Protein Sci.* **2016**, *25*, 1260–1272.

(91) Voigt, C. A.; Kauffman, S.; Wang, Z. G. Rational Evolutionary Design: The Theory of in Vitro Protein Evolution. *Adv. Protein Chem.* **2000**, *55*, 79–160.

(92) Breen, M. S.; Kemena, C.; Vlasov, P. K.; Notredame, C.; Kondrashov, F. A. Epistasis as the Primary Factor in Molecular Evolution. *Nature* **2012**, *490*, 535–538.

(93) Fontana, A.; de Laureto, P. P.; Spolaore, B.; Frare, E.; Picotti, P.; Zambonin, M. Probing Protein Structure by Limited Proteolysis. *Acta Biochim. Pol.* **2004**, *51*, 299–321.

(94) Newton, M. S.; Arcus, V. L.; Gerth, M. L.; Patrick, W. M. Enzyme Evolution: Innovation Is Easy, Optimization Is Complicated. *Curr. Opin. Struct. Biol.* **2018**, *48*, 110–116.

(95) Kaltenbach, M.; Burke, J. R.; Dindo, M.; Pabis, A.; Munsberg, F. S.; Rabin, A.; Kamerlin,

S. C. L.; Noel, J. P.; Tawfik, D. S. Evolution of Chalcone Isomerase from a Noncatalytic Ancestor. *Nat. Chem. Biol.* **2018**, *14*, 548–555.

(96) Mak, W. S.; Tran, S.; Marcheschi, R.; Bertolani, S.; Thompson, J.; Baker, D.; Liao, J. C.; Siegel, J. B. Integrative Genomic Mining for Enzyme Function to Enable Engineering of a Non-Natural Biosynthetic Pathway. *Nat. Commun.* **2015**, *6*, 10005.

(97) Kotay, S. M.; Datta, T.; Choi, J.; Goel, R. Biocontrol of Biomass Bulking Caused by Haliscomenobacter Hydrossis Using a Newly Isolated Lytic Bacteriophage. *Water Res.* **2011**, *45*, 694–704.

(98) Tyka, M. D.; Jung, K.; Baker, D. Efficient Sampling of Protein Conformational Space Using Fast Loop Building and Batch Minimization on Highly Parallel Computers. *J. Comput. Chem.* **2012**, *33*, 2483–2491.

(99) Rosetta Commons: Preparing Ligands; Available via the Internet at: Https://Www.Rosettacommons.Org/Demos/Latest/Tutorials/Prepare_ligand/Prepare_ligand_tutorial (Accessed September 2019).

(100) Frisch, M. J.; Trucks, G. W.; Schlegel, H. B.; Scuseria, G. E.; Robb, M. A.; Cheeseman, J. R.; Scalmani, G.; Barone, V.; Mennucci, B.; Petersson, G. A.; et al. Gaussian 09 (Gaussian, Inc., Wallingford CT, 2009).

(101) Marenich, A. V; Jerome, S. V; Cramer, C. J.; Truhlar, D. G. Charge Model 5: An Extension of Hirshfeld Population Analysis for the Accurate Description of Molecular Interactions in Gaseous and Condensed Phases. *J. Chem. Theory Comput.* **2012**, *8*, 527–541.

(102) Rohl, C. A.; Strauss, C. E. M.; Chivian, D.; Baker, D. Modeling Structurally Variable Regions in Homologous Proteins with Rosetta. *Proteins* **2004**, *55*, 656–677.

(103) DeLuca, S.; Khar, K.; Meiler, J. Fully Flexible Docking of Medium Sized Ligand Libraries with RosettaLigand. *PLoS One* **2015**, *10*, e0132508.

(104) Le Guilloux, V.; Schmidtke, P.; Tuffery, P. Fpocket: An Open Source Platform for Ligand

Pocket Detection. *BMC Bioinformatics* **2009**, *10*, 168.

(105) Mandell, D. J.; Coutsias, E. A.; Kortemme, T. Sub-Angstrom Accuracy in Protein Loop Reconstruction by Robotics-Inspired Conformational Sampling. *Nature methods*. United States August 2009, pp 551–552.

(106) Bryksin, A. V; Matsumura, I. Overlap Extension PCR Cloning: A Simple and Reliable Way to Create Recombinant Plasmids. *Biotechniques* **2010**, *48*, 463–465.

(107) Setser, J. W.; Heemstra, J. R.; Walsh, C. T.; Drennan, C. L. Crystallographic Evidence of Drastic Conformational Changes in the Active Site of a Flavin-Dependent N-Hydroxylase. *Biochemistry* **2014**, *53*, 6063–6077.

(108) Johansson, R.; Torrents, E.; Lundin, D.; Sprenger, J.; Sahlin, M.; Sjöberg, B.-M.; Logan, D. T. High-Resolution Crystal Structures of the Flavoprotein NrdI in Oxidized and Reduced States – an Unusual Flavodoxin. *FEBS J.* **2010**, *277*, 4265–4277.

(109) Kitzing, K.; Fitzpatrick, T. B.; Wilken, C.; Sawa, J.; Bourenkov, G. P.; Macheroux, P.; Clausen, T. The 1.3 Å Crystal Structure of the Flavoprotein YqjM Reveals a Novel Class of Old Yellow Enzymes. *J. Biol. Chem.* **2005**, *280*, 27904–27913.

(110) Sukumar, N.; Dewanti, A. R.; Mitra, B.; Mathews, F. S. High Resolution Structures of an Oxidized and Reduced Flavoprotein: THE WATER SWITCH IN A SOLUBLE FORM OF (S)-MANDELATE DEHYDROGENASE . *J. Biol. Chem.* **2004**, *279*, 3749–3757.

(111) Derewenda, Z. S. Application of Protein Engineering to Enhance Crystallizability and Improve Crystal Properties. *Acta Crystallogr. D. Biol. Crystallogr.* **2010**, *66*, 604–615.

(112) Ingavat, N. CHARACTERIZATION AND MUTATION OF IODOTYROSINE DEIODINASE FROM Haliscomenobacter Hydrossis FOR DETOXIFICATION OF IODOPHENOLS, The Johns Hopkins University, Baltimore, MD, 2017.

(113) Phatarphekar, A. V. THE UBIQUITY OF IODOTYROSINE DEIODINASE: IDENTIFICATION OF ITS SIGNATURE SEQUENCE AND FUNCTIONAL

ANALYSIS IN A MODEL INVERTEBRATE, The Johns Hopkins University, Baltimore, MD, 2016.

(114) Bloom, J. D.; Labthavikul, S. T.; Otey, C. R.; Arnold, F. H. Protein Stability Promotes Evolvability. *Proc. Natl. Acad. Sci. U. S. A.* **2006**, *103*, 5869–5874.

(115) Littlechild, J. A. Thermophilic Archaeal Enzymes and Applications in Biocatalysis. *Biochem. Soc. Trans.* **2011**, *39*, 155–158.

(116) Münchow, V.; Steudel, R. The Decomposition of Aqueous Dithionite and Its Reactions with Polythionates SnO2−6 (n = 3–5) Studied by Ion-Pair Chromatography. *Zeitschrift für Anorg. und Allg. Chemie* **1994**, *620*, 121–126.

(117) Reed, M. C.; Lieb, A.; Nijhout, H. F. The Biological Significance of Substrate Inhibition: A Mechanism with Diverse Functions. *Bioessays* **2010**, *32*, 422–429.

(118) Kabsch, W. Automatic Processing of Rotation Diffraction Data from Crystals of Initially Unknown Symmetry Land Cell Constants. *J. Appl. Crystallogr.* **1993**, *26*, 795–800.

(119) McCoy, A. J.; Grosse-Kunstleve, R. W.; Adams, P. D.; Winn, M. D.; Storoni, L. C.; Read, R. J. Phaser Crystallographic Software. *J. Appl. Crystallogr.* **2007**, *40*, 658–674.

(120) Terwilliger, T. C. Using Prime-and-Switch Phasing to Reduce Model Bias in Molecular Replacement. *Acta Crystallogr. D. Biol. Crystallogr.* **2004**, *60*, 2144–2149.

(121) Emsley, P.; Cowtan, K. Coot: Model-Building Tools for Molecular Graphics. *Acta Crystallogr. D. Biol. Crystallogr.* **2004**, *60*, 2126–2132.

(122) Adams, P. D.; Afonine, P. V; Bunkoczi, G.; Chen, V. B.; Davis, I. W.; Echols, N.; Headd, J. J.; Hung, L.-W.; Kapral, G. J.; Grosse-Kunstleve, R. W.; et al. PHENIX: A Comprehensive Python-Based System for Macromolecular Structure Solution. *Acta Crystallogr. D. Biol. Crystallogr.* **2010**, *66*, 213–221.

(123) Rosenberg, I. N.; Goswami, A. Iodotyrosine Deiodinase from Bovine Thyroid. *Methods Enzymol.* **1984**, *107*, 488–500.

(124) Matthews, R. G.; Massey, V. Isolation of Old Yellow Enzyme in Free and Complexed Forms. *J. Biol. Chem.* **1969**, *244*, 1779–1786.

(125) Matthews, R. G.; Massey, V.; Sweeley, C. C. Identification of P-Hydroxybenzaldehyde as the Ligand in the Green Form of Old Yellow Enzyme. *J. Biol. Chem.* **1975**, *250*, 9294–9298.

(126) Choi, S.-S.; Song, M. J.; Kim, O.-B.; Kim, Y. Fragmentation Patterns of Protonated Amino Acids Formed by Atmospheric Pressure Chemical Ionization. *Rapid Commun. Mass Spectrom.* **2013**, *27*, 143–151.

(127) Nivière, V.; Fieschi, F.; Décout, J.-L.; Fontecave, M. The NAD(P)H:Flavin Oxidoreductase from Escherichia Coli : EVIDENCE FOR A NEW MODE OF BINDING FOR REDUCED PYRIDINE NUCLEOTIDES. *J. Biol. Chem.* **1999**, *274*, 18252–18260.

(128) Eichhorn, E.; van der Ploeg, J. R.; Leisinger, T. Characterization of a Two-Component Alkanesulfonate Monooxygenase from Escherichia Coli. *J. Biol. Chem.* **1999**, *274*, 26639–26646.

(129) Campbell, Z. T.; Baldwin, T. O. Fre Is the Major Flavin Reductase Supporting Bioluminescence from Vibrio Harveyi Luciferase in Escherichia Coli. *J. Biol. Chem.* **2009**, *284*, 8322–8328.

(130) Tu, S. C. Reduced Flavin: Donor and Acceptor Enzymes and Mechanisms of Channeling. *Antioxid. Redox Signal.* **2001**, *3*, 881–897.

(131) Stradins, J.; Hasanli, B. Anodic Voltammetry of Phenol and Benzenethiol Derivatives.: Part 1. Influence of PH on Electro-Oxidation Potentials of Substituted Phenols and Evaluation of PKa from Anodic Voltammetry Data. *J. Electroanal. Chem.* **1993**, *353*, 57–69.

(132) Vieille, C.; Zeikus, G. J. Hyperthermophilic Enzymes: Sources, Uses, and Molecular Mechanisms for Thermostability. *Microbiol. Mol. Biol. Rev.* **2001**, *65*, 1–43.

(133) Belkin, S.; Wirsen, C. O.; Jannasch, H. W. A New Sulfur-Reducing, Extremely

Thermophilic Eubacterium from a Submarine Thermal Vent. *Appl. Environ. Microbiol.* **1986**, *51*, 1180–1185.

(134) Hu, J.; Su, Q.; Schlessman, J. L.; Rokita, S. E. Redox Control of Iodotyrosine Deiodinase. *Protein Sci.* **2019**, *28*, 68–78.

(135) Rohr, A. K.; Hersleth, H.-P.; Andersson, K. K. Tracking Flavin Conformations in Protein Crystal Structures with Raman Spectroscopy and QM/MM Calculations. *Angew. Chem. Int. Ed. Engl.* **2010**, *49*, 2324–2327.

(136) Ludwig, M. L.; Pattridge, K. A.; Metzger, A. L.; Dixon, M. M.; Eren, M.; Feng, Y.; Swenson, R. P. Control of Oxidation-Reduction Potentials in Flavodoxin from Clostridium Beijerinckii: The Role of Conformation Changes. *Biochemistry* **1997**, *36*, 1259–1280.

(137) Senda, M.; Kishigami, S.; Kimura, S.; Fukuda, M.; Ishida, T.; Senda, T. Molecular Mechanism of the Redox-Dependent Interaction between NADH-Dependent Ferredoxin Reductase and Rieske-Type [2Fe-2S] Ferredoxin. *J. Mol. Biol.* **2007**, *373*, 382–400.

(138) Ulas, G.; Lemmin, T.; Wu, Y.; Gassner, G. T.; DeGrado, W. F. Designed Metalloprotein Stabilizes a Semiquinone Radical. *Nat. Chem.* **2016**, *8*, 354.

(139) Orville, A. M.; Lountos, G. T.; Finnegan, S.; Gadda, G.; Prabhakar, R. Crystallographic, Spectroscopic, and Computational Analysis of a Flavin C4a-Oxygen Adduct in Choline Oxidase. *Biochemistry* **2009**, *48*, 720–728.

(140) Anderson, V. E. Isotope Effects on Enzyme-Catalyzed Reactions. *Curr. Opin. Struct. Biol.* **1992**, *2*, 757–764.

(141) Yorita, K.; Misaki, H.; Palfey, B. A.; Massey, V. On the Interpretation of Quantitative Structure–Function Activity Relationship Data for Lactate Oxidase. *Proc. Natl. Acad. Sci.* **2000**, *97*, 2480–2485.

(142) Mayhew, S. G. The Redox Potential of Dithionite and SO-2 from Equilibrium Reactions with Flavodoxins, Methyl Viologen and Hydrogen plus Hydrogenase. *Eur. J. Biochem.*

1978, *85*, 535–547.

(143) Lambeth, D. O.; Palmer, G. The Kinetics and Mechanism of Reduction of Electron Transfer Proteins and Other Compounds of Biological Interest by Dithionite. *J. Biol. Chem.* **1973**, *248*, 6095–6103.

(144) Ryerson, C. C.; Walsh, C. The Stereochemistry of NADH Utilization by the Flavoenzyme Monooxygenase Orcinol Hydroxylase. *J. Biol. Chem.* **1979**, *254*, 4349–4351.

(145) Sollner, S.; Deller, S.; Macheroux, P.; Palfey, B. A. Mechanism of Flavin Reduction and Oxidation in the Redox-Sensing Quinone Reductase Lot6p from Saccharomyces Cerevisiae. *Biochemistry* **2009**, *48*, 8636–8643.

(146) Janczak, M. W.; Poulter, C. D. Kinetic and Binding Studies of Streptococcus Pneumoniae Type 2 Isopentenyl Diphosphate:Dimethylallyl Diphosphate Isomerase. *Biochemistry* **2016**, *55*, 2260–2268.

(147) Neti, S. S.; Eckert, D. M.; Poulter, C. D. Construction of Functional Monomeric Type 2 Isopentenyl Diphosphate:Dimethylallyl Diphosphate Isomerase. *Biochemistry* **2016**, *55*, 4229–4238.

(148) Mayhew, S. G.; Foust, G. P.; Massey, V. Oxidation-Reduction Properties of Flavodoxin from Peptostreptococcus Elsdenii. *J. Biol. Chem.* **1969**, *244*, 803–810.

(149) Entsch, B.; Ballou, D. P.; Massey, V. Flavin-Oxygen Derivatives Involved in Hydroxylation by p-Hydroxybenzoate Hydroxylase. *J. Biol. Chem.* **1976**, *251*, 2550–2563.

(150) Suske, W. A.; van Berkel, W. J. H.; Kohler, H.-P. E. Catalytic Mechanism of 2-Hydroxybiphenyl 3-Monooxygenase, a Flavoprotein from Pseudomonas Azelaica HBP1 . *J. Biol. Chem.* **1999**, *274*, 33355–33365.

(151) Ballou, D. P.; Massey, V. Flavin Conformational Changes in the Catalytic Cycle of P-Hydroxybenzoate Hydroxylase Substituted with 6-Azido- and 6-Aminoflavin Adenine Dinucleotide. *Biochemistry* **1997**, *36*, 15713–15723.

(152) Ryan, K. S.; Chakraborty, S.; Howard-Jones, A. R.; Walsh, C. T.; Ballou, D. P.; Drennan, C. L. The FAD Cofactor of RebC Shifts to an IN Conformation upon Flavin Reduction. *Biochemistry* **2008**, *47*, 13506–13513.

(153) Renko, K.; Hoefig, C. S.; Dupuy, C.; Harder, L.; Schwiebert, C.; Kohrle, J.; Schomburg, L. A Nonradioactive DEHAL Assay for Testing Substrates, Inhibitors, and Monitoring Endogenous Activity. *Endocrinology* **2016**, *157*, 4516–4525.

(154) Goswami, A.; Rosenberg, I. N. Studies on a Soluble Thyroid Iodotyrosine Deiodinase: Activation by NADPH and Electron Carriers. *Endocrinology* **1977**, *101*, 331–341.

(155) Goswami, A.; Rosenberg, I. N. Ferredoxin and Ferredoxin Reductase Activities in Bovine Thyroid. Possible Relationship to Iodotyrosine Deiodinase. *J. Biol. Chem.* **1981**, *256*, 893–899.

(156) Levitt, M. Conformational Preferences of Amino Acids in Globular Proteins. *Biochemistry* **1978**, *17*, 4277–4285.

(157) Richardson, J. S.; Richardson, D. C. Amino Acid Preferences for Specific Locations at the Ends of Alpha Helices. *Science* **1988**, *240*, 1648–1652.

(158) Swiderek, K. M.; Davis, M. T.; Lee, T. D. The Identification of Peptide Modifications Derived from Gel-Separated Proteins Using Electrospray Triple Quadrupole and Ion Trap Analyses. *Electrophoresis* **1998**, *19*, 989–997.

(159) Sievers, F.; Wilm, A.; Dineen, D.; Gibson, T. J.; Karplus, K.; Li, W.; Lopez, R.; McWilliam, H.; Remmert, M.; Soding, J.; et al. Fast, Scalable Generation of High-Quality Protein Multiple Sequence Alignments Using Clustal Omega. *Mol. Syst. Biol.* **2011**, *7*, 539.

(160) Crooks, G. E.; Hon, G.; Chandonia, J.-M.; Brenner, S. E. WebLogo: A Sequence Logo Generator. *Genome Res.* **2004**, *14*, 1188–1190.

Curriculum Vitae

Zuodong Sun, Ph.D. candidate

Department of Chemistry, Johns Hopkins University

3400 N. Charles Street, Remsen Hall 122, Baltimore, MD, 21218

Date and location of birth:

1990/08/04, Jinchang, China

Education:

2019 Ph.D. Chemistry, Johns Hopkins University, Baltimore, MD

2015 M.A. Chemistry, Johns Hopkins University, Baltimore, MD

2012 B.S. Chemistry, Wuhan University, Wuhan, China

Research Experience:

2014-2019 Ph.D. Thesis Research, Department of Chemistry, Johns Hopkins University

Advisor: Prof. Steven E. Rokita

Project 1: Computational design of iodotyrosine deiodinase toward bioremediation of halophenols.

Project 2: Characterization of the unique structural and redox properties of a thermophilic iodotyrosine deiodinase.

Project 3: Probing the active site conformations of iodotyrosine.deiodinase during catalysis.

2012-2014 Graduate Research, Department of Chemistry, Johns Hopkins University

Advisor: Prof. Justine P. Roth

Project: Metabolism of arachidonoyl ethanolamide by cyclooxygenase-2 and its response to nitric oxide.

2010-2012 Undergraduate Research, College of Chemistry and Molecular Sciences, Wuhan University

Advisor: Prof. Zhiling Zhang

Project: Electrochemical detection of carcinoma embryonic antigen based on microfluidics and magnetic beads.

Publications:

Reviews:

1. **Sun, Z.**; Qi, S.; Rokita, S. E. The distribution and mechanism of iodotyrosine deiodinase defied expectations. *Archives of Biochemistry and Biophysics* **2017**, 632, 77-87.

Research articles:

1. **Sun, Z.**; Kavran, J. M.; Rokita, S. E. In preparation.
2. **Sun, Z**.; Rokita, S. E. Toward a halophenol dehalogenase from iodotyrosine deiodinase via computational design. *ACS Catalysis* **2018**, 8, 11783-11793.
3. Ingavat, N.; Kavran, J. M.; **Sun, Z**.; Rokita, S. E. Active site binding is not sufficient for reductive deiodination by iodotyrosine deiodinase. *Biochemistry* **2017**, 56, 1130-1139.
4. Yu, X.; Xia, H-S.; **Sun, Z-D.**; Lin,Y.; Wang, K.; Yu, J.; Tang, H.; Pang, D-W.; Zhang, Z-L. On-chip dual detection of cancer biomarkers directly in serum based on self-assembled magnetic bead patterns and quantum dots. *Biosensors & Bioelectronics* **2013**, 41, 129-136.

Awards/Honors:

2018-2019	Rudolph Sonneborn Fellowship, Department of Chemistry, Johns Hopkins University
2014	Ernest M. Marks Teaching Award, Department of Chemistry, Johns Hopkins University
2011, 2009	Third-class Scholarship, Wuhan University
2010	Second-class Scholarship, Wuhan University
2009	National Scholarship, the Ministry of Education of China
2009-2011	Merit student in curriculum, morals, and health, Wuhan University

Presentations:

Poster: Towards a halophenol dehalogenase via computational design

Presented at:

2018 Gordon Research Conference, Biocatalysis & Biocatalysis GRS

2018 11th Frontiers in Chemistry & Biology Interface Symposium

2017 10th Frontiers in Chemistry & Biology Interface Symposium

Oral: Selenocysteine: the 21st Amino Acid

Presented at:

2016 Seminar on the Chemical Literature, Department of Chemistry, Johns Hopkins University

Teaching Experience:

2014 Teaching Assistant for Organic Chemistry II and Advanced Inorganic Lab

2013 Teaching Assistant for Introductory Chemistry II (lecture/lab) and Advanced Inorganic Lab

2012 Teaching Assistant for Introductory Chemistry I (lecture/lab)

Mentoring Experience:

2013-present Four graduate students and two undergraduate students

Professional Membership:

2016-present American Chemical Society